Development of a Multi-Cellular Tissue Engineered Model of Oral Lichen Planus

Asma Muftah Mohamed El Howati

A thesis submitted in partial fulfilment of the requirements for the degree of

Doctor of Philosophy

School of Clinical Dentistry

Faculty of Medicine, Dentistry and Health

The University of Sheffield

September 2022

(This page is left blank intentionally)

Declaration

I, the author, confirm that the Thesis is my own work. I am aware of the University's Guidance on the Use of Unfair Means (www.sheffield.ac.uk/ssid/unfair-means). The entirety of the laboratory work and clinical data analysis presented in this thesis, unless otherwise stated, is that of the author. The author has been responsible entirely for writing up and drafting. A thesis editor has not been used. This work has not been previously accepted for any other award at this, or any other, university.

Acknowledgments

Here, a PhD journey comes to an end and here I wish to thank all the people whose assistance was a milestone in the completion of this project.

Foremost, my dear supervisors, Helen and Craig, no words can do you justice. You have been the best supervisors a student could have. Helen, you taught me that it is possible to be a successful female scientist and a mother at the same time. You understood me and believed in my right to be so. Having two children into this PhD was not easy but you never stopped showing support and make me feel on ease which motivated me to give my best. I learnt a lot from your extensive knowledge and expertise and greatly benefited from your time management and organisation skills which were instrumental for my PhD survival. Craig, your infinite wisdom and expertise were inspiring for me to develop and keep up an illuminating discussion with you. You have been a teacher before a supervisor to me and I am most grateful for teaching me how to use my scientific words and how to express my research while embracing its limitations. Helen and Craig, I am thankful for the over fifty supervisory meetings full of constructive, insightful comments, ideas, encouragement and thankful for giving me the space to express my opinions and lead this research under your brilliant supervision. You helped me to develop personally and professionally into an independent confident researcher and I am privileged to have you both as mentors and lucky that I joined your research group.

I would like to recognise the financial support received by the Libyan higher ministry of education. Without their generous support and funding, undertaking this PhD would not be possible. I would like to pay my special regards to the University of Sheffield for being such a scientific light house and providing the supportive climate and environment for science seekers. I would like to express my gratitude for the army behind the scenes supporting with scientific and technical courses that met my needs and helped to develop my skills. I am grateful to the administrative and technical staff in the dental school for coming to the rescue every time a machine breaks down and my heart start racing and for managing access to the labs following the lockdown period. I would like to acknowledge Susan Clark in her help with flow cytometry. I am most grateful for the dental school PGR research committee for providing flexibility and financial support to attend conferences. I would like to recognise the help provided by Dr Ali Khurram in providing patients samples and for his invaluable suggestions. The advice and feedback received by Professor Martin Thornhill and Professor Keith Hunter is whole-heartedly appreciated.

I am thankful to my fellow students in the dental school and in my research group for providing a vibrant, positive atmosphere. Many thanks to my friends who always brought food, chocolate, and coffee with their lovely company when I was recovering (Naeima, Esra, Basma, Maryam, Rawan, Alaa, and Hajer). My gratitude at first and last goes to my parents who supported, trusted, and believed in me and allowed me to travel in the pursuit of my dreams. For my dear sisters who were my companions for a huge part of my life and to my brothers. Huge thanks to my awesome childminders for being so understanding to my circumstances and supporting all the way. My sincere grattitude for Catherine, Karen, Steve, and Aunty Cath for loving and taking care of my children.

To the most magical part of my life, my children, Habiba and Ghaith, without you realising it, you charged me with energy, motivation to continue giving my best and forced me to disconnect when I get home which was what I needed without me realising that. Last but not least, Thanks to my biggest rock, my best friend, and my companion, my husband Ahmed, for your patience, unwavering support, sacrifices, and love. I appreciate how you casually ask me how my cells are doing or if the new “thing” has worked to check if I am doing ok even if that will provoke me to ramble about cells and chemicals for the next two hours. Endeavouring PhD while having kids was not possible if not for you. To you, I owe it all and to you, Ahmed Hussen, I dedicate this thesis.

“He who doesn’t thank people is not thankful to Allah*”*

Prophet Mohammed PBUH

Presentations and awards

Oral presentations:

Development of a multi-cellular tissue engineered model of oral lichen planus. **The University of Sheffield' School of clinical Dentistry PGR day**, Sheffield, 2019.

Development of a Tissue Engineered Model of Oral Lichen Planus. **Biomaterials and tissue engineering group (BiTEG) annual meeting**, Leeds, 2019.

Happy cells. Internal oral presentation, Sheffield, 2019.

Immunity (brief background). Internal oral presentation, Sheffield, 2020.

Development o f a Tissue Engineered Model of Oral Lichen Planus. **Biomaterials and tissue engineering group (BiTEG) annual meeting**, Virtual, 2021.

Development of a Tissue Engineered Model of Oral Lichen Planus. **European Association of Oral Medicine E-conference (EAOM)**, Portugal, Virtual, 2021.

Development of a Tissue Engineered Model of Oral Lichen Planus. **British and Irish Society of Oral Medicine (BISOM)**, Belfast, 2022.

Development of a Multi-cellular Tissue Engineered Model of Oral Lichen Planus. **The Pan European Region of the International Association for Dental Research (PER-IADR Oral Health Research Congress**) Marseille, France, 2022.

Poster presentations:

Developing a 3D tissue engineered model of oral lichen planus. **The University of Sheffield' School of clinical Dentistry PGR day**, Virtual, 2020.

Developing a 3D tissue engineered model of oral lichen planus. **Biomaterials and tissue engineering group (BiTEG) annual meeting**, Virtual, 2020.

Prizes:

Best oral presentation prize; oral presentation for School of clinical Dentistry PGR day' The University of Sheffield, UK, 2019.

Third place "Gone in 60 seconds competition" Video presentation for the faculty of Medicine, Dentistry, and Health' PGR day, Virtual, 2021.

Best research oral presentation prize, European Association of Oral Medicine E-conference (EAOM), 2021.

Best research oral presentation prize, British and Irish Society of Oral Medicine (BISOM), Belfast, UK, 2022.

BSODR Senior Colgate Prize, the Pan European Region of the International Association for Dental Research (PER-IADR Oral Health Research Congress) Marseille, France, 2022.

Publications

El-Howati, A., Thornhill, M.H., Colley, H.E. and Murdoch, C., 2022. Immune mechanisms in oral lichen planus. Oral Diseases. https://doi.org/10.1111/odi.14142

El-Howati, A., Edmans, G.J., Santocildes-Romero, M., Madsen, L.S., Murdoch, and Colley, H.E., 2023. A tissue-engineered model of T cells inflammatory disease. Manuscript for the Journal of dental research.

Abstract

Oral lichen planus (OLP) is an immune-mediated mucocutaneous disease of unknown aetiology. There is no cure for OLP and the main treatment aims to relieve symptoms and control the progression. Despite advances in OLP research, investigations into the condition are hampered by the lack of effective experimental models. Tissue-engineered models have been developed, characterised and used in modelling different diseases to study their pathogenesis and test novel treatments. However, there is no OLP model, nor an oral mucosal model that incorporate polarised T cells. Therefore, this project aims to develop tissue-engineered oral mucosal equivalents (OME) containing polarised T cells to replicate OLP for use in the development of novel treatments.

Initially, cell culture conditions were defined and optimised before being developed and adapted for complex 3D culture. T cells and keratinocytes were adapted to be cultured in Green's medium without hydrocortisone with their proliferation and activation status assessed compared to culture in their original medium. T cell viability in collagen hydrogels was assessed overtime using flow cytometry and a PrestoBlue metabolic assay, revealing an increase in viability 5 days post incorporation into the 3D hydrogel.

CD4+ and CD8+ T cells isolated from buffy coats showed high purity (85-95%) and viability (>90%). Upon activation with CD3/CD28 Dynabeads, CD69 levels were increased when analysed by flow cytometry. T cells were cultured in conditions to polarise naive CD4+ T cells into Th1 or Th17 and CD8+ T cells into cytotoxic T cells. Phenotypes were confirmed using flow cytometry, ELISA, qPCR and western blot. Th1 cells secreted IFN-γ and TNF-α, key cytokines for Th1 and showed a higher expression of Th1 transcriptional factor, T-bet. 92% of CD8+ T cells produced granzyme B.

Full-thickness OME were created by seeding immortalised oral keratinocytes (FNB6) on top of normal oral fibroblast-containing hydrogels before being raised to an air-liquid interface (ALI). H&E staining of the OME revealed a multi-layered stratified squamous epithelium on top of a fibroblast-populated connective tissue. To simulate the inflammatory mucosa as in OLP, OME were cultured with IFN-γ and TNF-α. This led to a hyperproliferative epithelium and an increase in inflammatory markers, mainly chemokines relevant to T cell chemotaxis in OLP. A chemotaxis assay was employed to investigate T cell migration towards a chemoattractant gradient and revealed that conditioned medium from TNF-α and IFN-γ-stimulated OME caused the T cells to migrate towards the chemokine gradient in a directional manner.

Finally, a model of T cell-mediated inflammatory oral mucosal disease was developed *in vitro* by combining OME on top of a T cell-containing hydrogel, followed by stimulation with IFN-γ and TNF-α. Histological staining of the disease model revealed basement membrane destruction and basal cell layer apoptosis. 48 hours after stimulation, the recruitment of T cells towards the epithelium was evident and confirmed by immunohistochemical (IHC) staining for CD4 and CD8. Tissue destruction was shown to progress gradually over time and the OME maintained high levels of CCL5, CXCL9, and CXCL10 secretion until day 25. The disease model was validated against OLP patient biopsies with PAS staining and IHC staining for laminin, and integrin evidencing basement membrane damage and for cleaved-caspase-3 confirming the presence of apoptosis in the basal keratinocytes.

In summary, this study reports the development of a complex T cell-mediated disease model that displayed basal cell apoptosis, T cell infiltration and basement membrane destruction, which are key characteristics of OLP. This novel preclinical disease model has great potential to probe for molecular mechanisms of disease and to be used as a platform to test for novel therapeutics and modes of treatment.

Table of Contents

List of figures:

List of Tables

List of abbreviations

ABC™	Antibody compensation beads
AD	Atopic dermatitis
AI	Artificial intelligence
ALI	Air to liquid interface
ANOVA	Analysis of variance
APC	Allophycocyanin
APC	Antigen presenting cell
AU	Arbitrary units
B2M	Beta 2 microglobulin
BCA	Bicinchoninic acid assay
BCRs	B cell receptors
BDNF	Brain derived neurotrophic factor
BFP	Blue fluorescent protein
BL	Basal layer
BLC	B lymphocyte chemoattractant
BM	Basement membrane
BSA	Bovine serum albumin
BUV	Brilliant ultraviolet
BV	Brilliant violet
CCL	Chemokine (C-C motif) ligand
CCR	Chemokine (C-C motif) receptor
CD	Cluster of differentiation
GM-CFC	Granulocyte-macrophage colony-stimulating factor
CFP	Human complement factor protein
CFSE	Carboxy fluorescein N-succinimidyl ester
CO2	Carbon dioxide
G-CSF	granulocyte-colony stimulating factor
CT	Connective tissue
CTLA	Cytotoxic T lymphocyte-associated antigen
CXCL	Chemokine (C–X–C motif) ligand
CXCR	Chemokine (C–X–C motif) receptor
ArC™	Amine reactive compensation beads
DAB	3,3’-diaminobenzidine
DAMP	Damage-associated molecular patterns
DAPI	4′,6-diamidino-2-phenylindole
DC	Dendritic cell
DED	De-cellularised dermis
DMEM	Dulbecco's Modified Eagle Medium
DMSO	Dimethyl sulfoxide
d-NTP	Deoxyribonucleotide triphosphate
EBV	Epstein-Barr virus
ECACC	European Collection of Authenticated Cell Cultures
ECM	Extracellular matrix
EDTA	Ethylenediaminetetraacetic acid

EGF	Epidermal growth factor
ELISA	Enzyme-linked immunosorbent assay
ENA-78	Epithelial-derived neutrophil-activating peptide-78/ CXCL5
FACS	Fluorescence-activated cell sorting
FBS	Foetal bovine serum
FCS	Foetal calf serum
FGF	Fibroblast growth factor
FITC	Fluorescein isothiocyanate
FMO	Fluorescence minus one
FOXP3	Forkhead box P3 protein
FSC	Forward scatter
GATA3	GATA Binding Protein 3
GCP-2	Granulocyte chemotactic protein 2/ CXCL6
GDNF	Glial cell line-derived neurotrophic factor
GFP	Green fluorescent protein
GIT	Gastrointestinal tract
GRO	Growth-related oncogene
GvHD	Graft versus host disease
H_2SO_4	Sulphuric acid
HBSS	Hank's balanced salt solution
HC	Hydrocortisone
HCL	Hydrochloric acid
HCO_3	Bicarbonate
HCV	Hepatitis C virus
HEPES	4-(2-hydroxyethyl)-1-piperazinethanesulfonic acid
HGF	Hepatocyte growth factor
h-TERT	Human telomerase reverse transcriptase
HLA	Human leukocyte antigen
HRP	Horseradish peroxidase
ICAM	Intercellular adhesion molecule
IGFBP	Insulin-like growth factor binding protein
IHC	Immunohistochemistry
IL	Interleukins
IMS	Industrial methylated spirits
INF-γ	Interferon gamma
IP10	Interferon gamma-induced protein 10/ CXCL10
I-TAC	inducible T cell alpha chemoattractant/ CXCL11
IU	International units
JAK	Janus kinase
KL	Keratinised layer
KBM	Keratinocyte basal medium
KCL	Potassium chloride
KGF	Keratinocyte growth factor
KL	Keratin layer
LC	Langerhans cell
LFA	Lymphocyte function associated antigen

LP	Lichen planus
LPS	Lipopolysaccharide
LTR	Lichenoid tissue reaction
MALT	Mucous associated lymphoid tissue
MBP	Major basic protein
MCG	Membrane coating granules
MCP	Monocyte chemoattractant protein
MDM	Monocyte derived macrophages
MEM,	Minimum essential medium
MFI	Median fluorescence intensity
MHC	Major histocompatibility complex
MIF	Migration inhibitory factor
MIG	Monokine induced by gamma interferon/ CXCL9
MIP	Macrophage inflammatory protein
MMP	Matrix metalloproteinase
MNC	Monocytes
NAP	Neutrophil attractant/activation protein
NaOH	Sodium hydroxide
NET	Neutrophil extracellular trap
NFκB	Nuclear factor kappa- B
NK	Normal keratinocytes
NOF	Normal oral fibroblast
OD	Optical density
OLP	Oral lichen planus
OME,	Oral mucosa equivalent
OPN	Osteopontin
PAMP	Pathogen-associated molecular patterns
PARC	Pulmonary activation-regulated chemokine/ CCL18
PAS	Periodic acid-Schiff
PBMC	Peripheral blood mononuclear cells
PBS,	Phosphate buffered saline
q-PCR	Quantitative polymerase chain reaction
PDC	Plasmacytoid dendritic cells
PDGF	Platelet-derived growth factor
PE	Phycoerythrin
PECAM	Platelet endothelial cell adhesion molecule
PC	Polycarbonate
PET	Polyethylene terephthalate
PH	Potentiometric hydrogen ion concentration
PHA	Phytohemagglutinin
PI	Propidium iodide
PIGF	Placental growth factor
PKC	Protein kinase C
PLGA	Polylactic glycolic acid
PMA	Phorbol 12-myristate-13-acetate
PMN	Polymorphonuclear leukocytes

PRR	Pattern recognition receptor
PSC	Pluripotent stem cells
PVDF	Polyvinylidene difluoride
RA	Retinoic acid
RANTES	Regulated upon Activation, Normal T Cell Expressed and Secreted
RHG	Reconstructed human gingiva
RHS	Reconstructed human skin
RIPA	Radioimmunoprecipitation assay
RNA	Ribonucleic Acid
RORC	Retinoic acid-related orphan receptor
RPMI	Roswell Park Memorial Institute 1640 medium
RT	Room temperature
SCF	Stem cell factor
SD	Standard deviation
SDF	Stromal cell-derived factor
SDS	Sodium dodecyl sulphate
SKDM	Supplemented keratinocyte defined medium
SL	Superficial layer
SLE	Systemic lupus erythematosus
SLS	Sodium lauryl sulphate
SPL	Spinous/prickle layer
SSC	Side scatter
STAT	Signal transducer and activator of transcription
TAM	Tumour associated macrophages
TARC	Thymus- and activation-regulated chemokine/ CCL17
TBS	Tris-buffered saline
TBST	Tris-buffered saline- Tween
TCR	T cell receptor
TEMED	Tetramethyl ethylenediamine
TGF	Transforming growth factor
TIMP	Tissue inhibitor of metalloproteinases
TLR	Toll like receptors
TMP	3,3',5,5'-tetramethylbenzidine
TNF-α	Tumour necrosis factor-alpha
TNFR	Tumour necrosis factor receptor
TPO	Thrombopoietin
TUNEL	Terminal deoxynucleotidyl transferase biotin-dUTP nick end labelling
UV	Ultraviolet
VCAM	Vascular cell adhesion molecule
VEA	Very early activation
VEGF	Vascular endothelial growth factor
VLA-4	Very late antigen 4
WHO	World health organisation
YFP	Yellow fluorescent protein

1 Chapter one: Introduction

1.1 The oral mucosa

The oral cavity is the first part of the alimentary tract and is lined with an oral mucosa that is composed of two distinctive layers; a stratified squamous epithelium supported by a connective tissue. Depending on the location, it can be categorised into three types: masticatory, lining, or specialised mucosa. The masticatory mucosa covers about 25% of the surface lining of the mouth and includes the gingiva and the hard palate. Like the skin, it is composed of a keratinised epithelium where the epithelium is tightly attached to an underlying lamina propria. The dorsum surface of the tongue represents the specialised mucosa that covers 15% of the surface area of the oral cavity (Collins and Dawes, 1987). It is covered by mosaic mixed pattern of keratinised and non-keratinised mucosa with special regional distribution of taste buds and papillae. The lining mucosa covers about 60% of the oral surface area (Collins and Dawes, 1987). It forms a non-keratinised mucosa that covers all the other surfaces such as buccal mucosa, floor of the mouth, labial mucosa, the vestibule, ventral surface of the tongue, and soft palate. The lining mucosa is attached by elastic, loose connective tissue to underlying tissues which allow for the functional movements of the lining mucosa (Squier, 1991).

The outer stratified squamous layer epithelium and lamina propria are attached to each other by a thin layer of specialised extracellular matrix called the basement membrane. The lamina propria is separated from the underlying muscles by a fatty or collagenous layer that is rich in blood vessels and nerves known as the submucosa and is important in determining the flexibility of the tissue. In some regions of masticatory mucosa like the gingiva, the submucosa is absent leaving the lamina propria directly attached to the bone (mucoperiosteum) (Nanci, 2013).

1.1.1 Oral epithelium

The oral epithelium is the outer most layer in the oral mucosa and is composed of tightly attached stratified squamous epithelial cells. The epithelium, from basal to apical, consists of the following distinct layers: basal layer (stratum basale), spinous/prickle layer (stratum spinosum), granular layer (stratum granulosum) and a cornified layer (stratum corneum). Two types of keratinisations exist in the oral epithelium; orthokeratinisation, if the surface layer does not contain nuclei, or parakeratinisation/non-keratinised, if the surface keratinised layer retains small pyknotic nuclei (Nanci, 2013). As the cells pass from the basal to the apical direction, they differentiate and mature. Basal cells produce cytokeratins 5, 14 and as cells mature, they get larger and display more desmosomes and keratin filaments. Polyhedral cells in the spinous layer produce cytokeratins 1, 6, 10 and 16. As the keratinocytes move to the granular layer they

produce more membrane coating granules (MCG) which contribute to membrane thickening and the permeability barrier in the keratinised layer resulting in cells with thick plasma membrane, densely packed keratin filaments, few desmosomes, and no organelles (Winning and Townsend, 2000) (**Figure 1.1**).

The granular and cornified layers are present in the keratinised mucosa while absent in the non-keratinised mucosa. Instead, cells above the prickle cell layer are divided into intermediate (stratum intermedium) and superficial layer (stratum superficiale) (Winning and Townsend, 2000). In non-keratinised mucosa, as cells mature and differentiate, they produce cytokeratins 4 and 13. As cells move to the intermediate and superficial layers, they display increased keratin filament condensation and MCG that contributes to the permeability barrier. However, non-keratinised mucosa shows greater permeability than keratinised mucosa and the latter is considered ten times more permeable than the skin (Winning and Townsend, 2000).

Other types of cells that reside within the epithelium include melanocytes, Langerhans, and Merkel cells. Melanocytes are present in the basal layer and are commonly known as pigment cells as they produce melanin that contributes to the colour of the skin and mucosa. The melanin is formed inside small vesicles called melanosomes that are transferred to surrounding keratinocytes through melanocyte dendritic processes. Different skin colours are generated by amount of melanin produced and degraded by melanocytes as the numbers of melanocytes remain unchanged. Macrophages that have engulfed melanosomes can be detected under microscopic sections as pigmented cells in the connective tissue . Langerhans cells are dendritic cells originated from the bone marrow and situated in the supra-basal layer of the epithelium. Langerhans cells are characterised by the presence of small rod-shaped granules called Birkbeck granules. They interlink through their dendritic processes forming a net called the reticulo-epithelial trap, which traps antigens. After they bind with an antigen, they migrate to the regional lymph node to initiate a primary immune response. In histological section stained with haematoxylin and eosin (H&E) they appear as clear cells like other non-keratinocytes (Barrett, Cruchley and Williams, 1996). Unlike melanocytes and Langerhans, Merkel cells are not dendritic and do not have desmosomes and tonofilaments attaching it to the surrounding cells. Hence, merkel cells under microscopic examination may not resemble other non-keratinocytes. However, these cells can be characterised by the presence of membrane bound vesicles adjacent to nerve fibres. Merkel cells are thought to play a role in triggering and transmitting sensory impulses (Hashimoto, 1972; Nanci, 2013). Inflammatory cells can be detected in the basal layer of epithelium in clinically normal sections. Lymphocytes are the most common leukocyte that are present in the epithelium. Though the presence of inflammatory cells is transient, they play a role in the stability of the epithelium mainly through the action of cytokines. Keratinocytes produce cytokines that cause Langerhans cells to produce

IL-1 that in turn stimulate T lymphocytes to produce IL-2 to generate an immune response to antigenic challenge. IL-1 also increases expression of receptors to melanocyte-stimulating hormone on melanocytes, which affect the pigmentation of the mucosa (Squier and Kremer, 2001).

1.1.1.1 Basement membrane and connective tissue

The basement membrane forms the junction between the epithelium and the lamina propria. It is composed of three layers: lamina lucida, lamina densa and lamina fibroreticularis. The lamina densa consists of a net of polymers such as type IV collagen and laminin. The lamina lucida contains proteins that connect cells to the basal lamina including collagen VII, integrins and laminin. Oral keratinocytes play an important role in maintaining the basement membrane through the production of collagen IV and laminin 5. The lamina fibroreticularis is discontinuous layer that is thought to be associated with the reticular fibers of the connective tissue(Nanci, 2013) (**Figure 1.1**).

Underlying the basement membrane, the connective tissue is composed of cells, fibres, blood vessels, nerves, and matrix. The connective tissue is divided into a superficial papillary layer that runs under epithelial rete ridges and a deeper reticular layer which separates the papillary layer from deeper structures. The most abundant cell in the connective tissue is the fibroblast. However, other cells like macrophages, mast cells, and inflammatory cells are present. Fibroblasts are responsible for the production of the extracellular matrix. They are stellate or spindle-shaped and have abundant endoplasmic reticulum. They have a low proliferation rate, can be contractile and help in wound contraction due to their content of actin. The extracellular matrix of the lamina propria is composed of collagen and elastin fibres and matrix. The collagen types mainly present in the lamina propria are collagen types I and III, with types IV and VII present as part of the basal lamina. The elastic fibres are dispersed throughout the lamina propria, but they are found in abundance in the connective tissue of lining mucosa as they support that function with their ability to deform and restore the tissue shape. The ground substance of extracellular matrix is an amorphous gel-like material. It is transparent and fills the spaces between fibres and cells and is mainly composed of large carbohydrate molecules supplied by the tissue fluid. These include proteoglycan that is formed of a polypeptide core with glycosaminoglycan attached to it, and glycoprotein, which is composed of a polypeptide chain with hexoses attached (Squier and Kremer, 2001) (**Figure 1.1**).

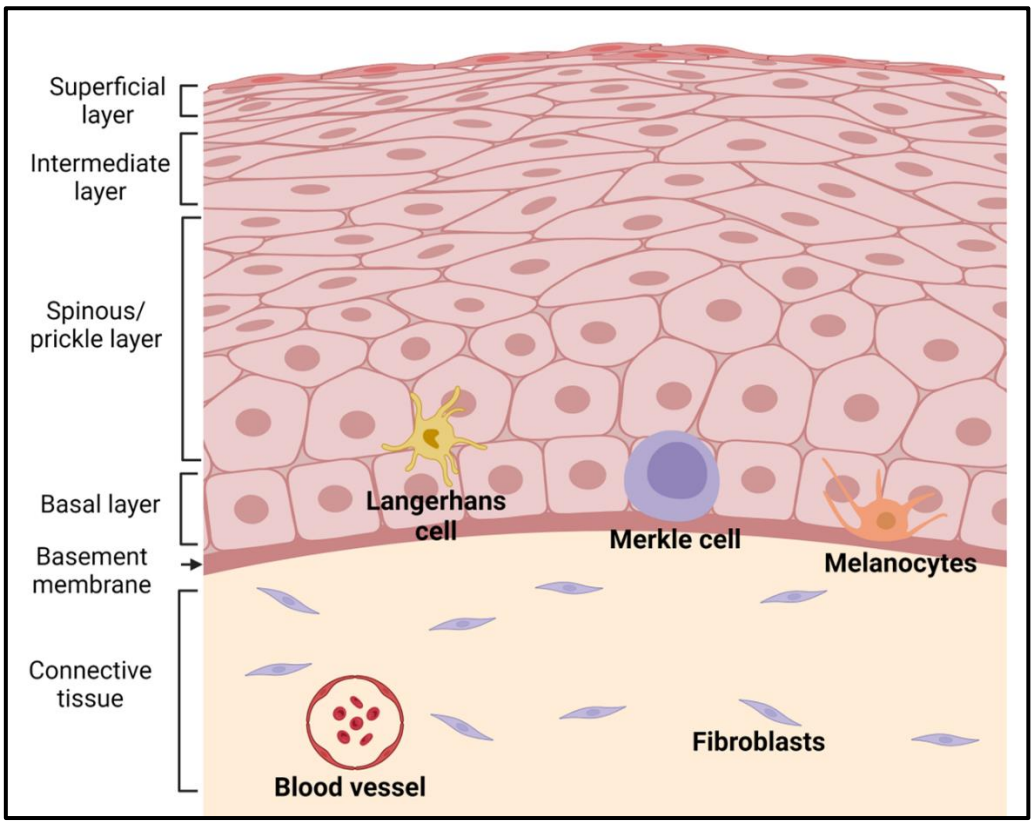

Figure 1.1: An illustration of the morphology of normal buccal normal oral mucosa. Normal oral mucosa composed of an epithelium and connective tissue joined by a basement membrane. The epithelium constitutes a basal layer, spinous/prickle layer, intermediate, and superficial layer. Other cells reside in the epithelium include melanocytes, Merkel cells, and Langerhans cells. Connective tissue contains fibroblasts, blood vessels, and extracellular matrix. Created in BioRender.com.

1.2 The immune system

The human body is surrounded by a heavily populated environment comprised of microbes and substances that threaten normal homeostasis, a state of balance between appropriate immune activation and suppression that is maintained by a highly sophisticated immune system. Depending on the virulence and hostility of the offending microbe on one side and the health and competence of the body at that time, the result of this confrontation varies between asymptomatic events, mild symptoms, to severe symptoms and debilitating illness. When the immune response is not sufficient, infections and inflammations may occur, whereas, if it is overactivated, hypersensitivity or autoimmune diseases may occur. Also, the dysregulated function of these cells may produce immune mediated diseases. Hence, it is fundamentally important that the immune system keeps a state of balance. The immune system has traditionally been divided into innate and adaptive arms. The innate immunity including the physical and chemical barriers on one side is considered the first line of defence as it produces a quick non-specific response against antigens and accordingly does not produce memory for this antigen attack, if it occurred in the future. Adaptive immunity on the other side is an antigen-specific response that requires some time from the first exposure to an antigen to provide

maximum response against that antigen. Memory cells are formed that can mount quick and efficient attacks if the body encounters the same antigen in the future. The two arms are complementary to each other to produce an appropriate immune response (Marshall *et al.*, 2018; Nicholson, 2016).

1.2.1 Components of the immune system

All the cellular elements of the blood including the erythrocytes, the platelets, and the leukocytes are derived from the same precursor cell in the bone marrow, the pluripotent hematopoietic stem cell. Initially, these stem cells give rise to two types of cells: the common myeloid progenitors and the common lymphoid progenitors. The common myeloid progenitors give rise to the megakaryocyte–erythroid progenitors which in turn develop into erythrocytes and platelets (Sola-Visner and Ramsey, 2017). The myeloid progenitors also give rise to most cells of the innate immunity including mast cells, neutrophils, basophils, eosinophils and monocytes, whereas the common lymphoid progenitors give rise to the cells of the adaptive immune system including T lymphocytes and B lymphocytes (**Figure 1.2**) (Janeway Jr *et al.*, 2001b).

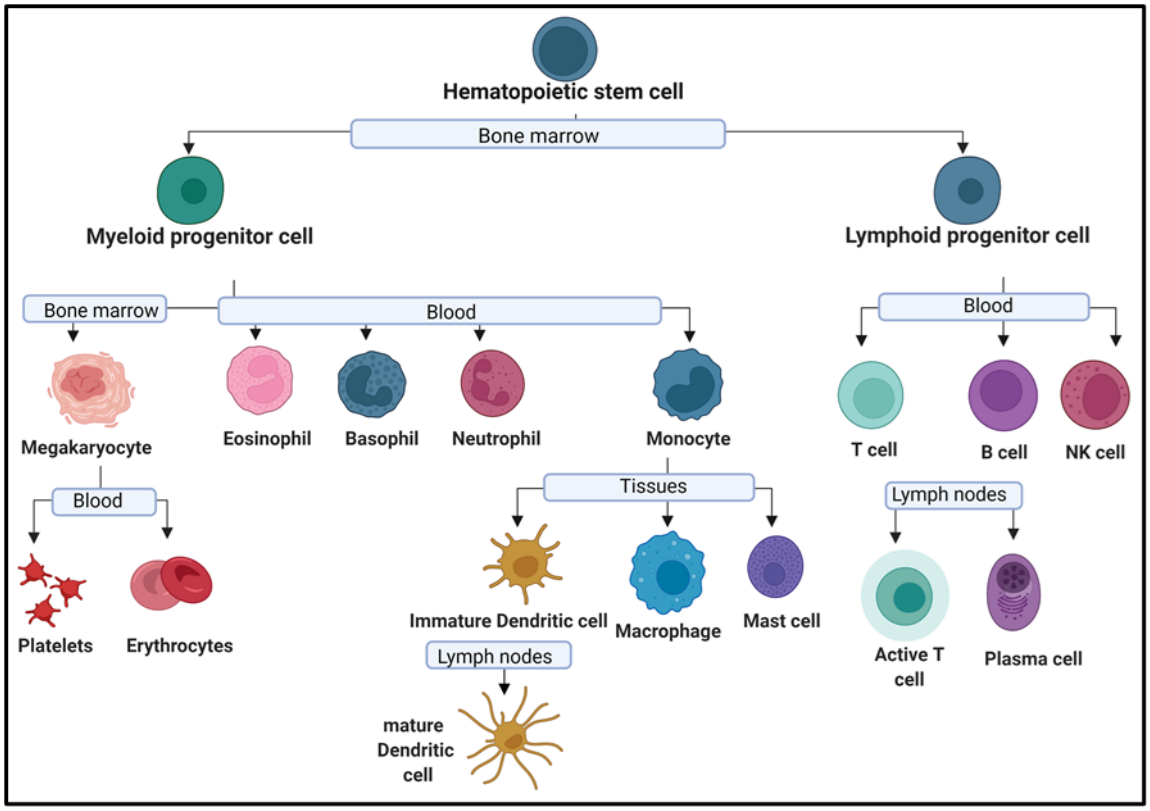

Figure 1.2: A schematic diagram of the cellular immune components. All immune cells are produced from the pluripotent hematopoietic stem cell in the bone marrow which give rise to the common myeloid and lymphoid progenitors. The common myeloid progenitors give rise to the erythrocytes, platelets, mast cells, neutrophils, basophils, eosinophils, and monocytes, whereas the common lymphoid progenitors give rise to the cells of the adaptive immune system including T lymphocytes and B lymphocytes. These cells mainly circulate in the blood and further mature in the tissues or lymph nodes. Created in BioRender.com.

1.2.2 Innate immunity

Innate immunity is the major contributor of protection, acting through the inflammatory response and plays a role in stimulating the adaptive immune arm. Innate immunity can be categorised into four types of defensive barriers: physical such as the skin, physiologic such as temperature and pH, endocytic or phagocytic and finally inflammatory. Cells of the innate immune system recognise pathogens or tissue damage through pattern recognition receptors (PRRs). These structures are able to recognise non-self-pathogens that display pathogen-associated molecular patterns (PAMPs) or recognise endogenous molecules produced by damaged tissue displaying damage-associated molecular patterns (DAMPs) (Takeuchi and Akira, 2010). Upon engagement with the pathogen, a non-specific process is activated that includes phagocytosis, cell locomotion and cytokine production.

1.2.2.1 Monocytes

Monocytes descend from the common myeloid progenitors in the bone marrow before entering the circulation, spleen, and bone marrow. These cells are effective in defending the body through production of inflammatory cytokines and performing phagocytosis. Through

expression of cell surface chemokine receptors and adhesion molecules, they are able to migrate from the blood to tissues where they differentiate into more specialised cells in the tissues such as macrophages and dendritic cells under the influence of the cytokine milieu in the local environment (Geissmann *et al.*, 2010).

1.2.2.2 Macrophages

Macrophages are found as either prenatal tissue resident macrophages or postnatal monocyte-derived macrophages and as one of the three main phagocytes in the immune system, they have an important role in defending the body against non-self agents. They are equipped with a wide spectrum of PRRs to recognise different antigens and are broadly distributed through the body's tissues. They act to engulf and destroy particles or damaged cells then present foreign antigen in complex with major histocompatibility complex (MHC) class II to T helper cells. Beyond innate immunity, macrophages have an essential role in homeostasis through clearing tissue debris and secreting growth hormones, cytokines, and chemokines (Janeway Jr *et al.*, 2001b). Macrophages are not terminally polarised as they are plastic throughout their life and depending on their origin and the microenvironment, can be polarised into M1 (pro-inflammatory) or M2 (anti-inflammatory) phenotypes and demonstrate distinct functions. Similar to the Th1 and Th2 paradigm in T cells differentiation (see section 1.3.8), a similar paradigm exists between M1/M2 (Zhang, Yang and Ericsson, 2021). A distinct type of macrophages termed, tumour associated macrophages (TAMs) are recruited to tumour areas and believed to have a role in the immune regulation of tumour cells by either producing killing factors or promoting factors (Zhou *et al.*, 2020).

1.2.2.3 Dendritic cells

Dendritic cells (DCs) are highly specialised antigen presenting cells (APC), derived from circulating monocytes. Immature dendritic cells are found in the circulation as highly mobile cells that can migrate to tissues throughout the body and mature into dendritic cells upon activation by appropriate combinations of cytokines or recognition of an antigen (Geissmann *et al.*, 2010). DCs can move from tissues to the T cell and B cell zones of lymphoid organs to present antigen to T cells through their MHC molecules. They express both class I and class II MHC molecules on their surface that permit the recognition of an antigen or part of it by the T cells receptors (TCR) on the surface of T cells. These are usually known as the classical dendritic cells (cDCs) (Chaplin, 2010). Another type of DCs are Langerhans cells (LCs) that reside in the skin epidermis. They are situated at the suprabasal layer of the epithelium and are considered the first line of defence since they produce a primary immune response (Geissmann *et al.*, 2010). It is proposed that the population of LCs precursors residing in the skin during embryonic life, rely

on their proliferation independent from circulating DCs to compensate for the low LCs loss that occurs during steady-state turnover and minor injuries. Yet, LCs progenitors may be recruited from circulation in events of severe loss during inflammation (Merad *et al.*, 2002). Plasmacytoid DCs (PDCs) are another subtype of DCs that are relatively long-lived and are present in the bone marrow and all peripheral organs. PDCs can act as antigen presenting cells but their main role is fighting viral infection through producing type I interferons (IFNs) (Geissmann *et al.*, 2010).

1.2.2.4 Mast cells

Mast cells are derived from myeloid stem cells and found in an immature form in the circulation before they migrate to local tissues, particularly to the skin, airways and intestine, where they mature under the influence of the microenvironment (Janeway Jr *et al.*, 2001b). Once inflammation occurs, local mediators may cause degranulation of mast cells and the release of its cytoplasmic granules, including histamine, proteases such as tryptase and chymase, tumour necrosis factor-a (TNF-α), prostaglandins and leukotrienes. Being rich in multi-potent molecules, mast cells can regulate the function of other leukocytes such as DCs, macrophages, T and B cells, fibroblasts, eosinophils, endothelial and epithelial cells (Krystel-Whittemore, Dileepan and Wood, 2016). Moreover, mast cells have a role in regulating physiological functions including vasodilation, angiogenesis, and microbial clearance. These cells are important for wound healing, clot formation and through activating fibroblasts and keratinocytes by releasing growth factors (Komi, Khomtchouk and Santa Maria, 2020). However, mast cells are chiefly known for their role in allergic reactions through the binding of an antigen to IgE, which is mostly found bound to the high affinity IgE receptor (FcεRI) expressed on the mast cell surface. This binding along with receptor clustering stimulates mast cell degranulation, releasing its inflammatory mediators that result in an immune response and hypersensitivity reactions such as vasodilation, tissue oedema, leukocyte extravasation and skin reactions, etc (Krystel-Whittemore, Dileepan and Wood, 2016).

1.2.2.5 Granulocytes

Granulocytes are also known as polymorphonuclear leukocytes because of the variable shapes of their nuclei or granulocytes due to the densely stained granules in their cytoplasm. There are three types of granulocytes: neutrophils, basophils and eosinophils (Marshall *et al.*, 2018).

Neutrophils are the most abundant granulocytes in the body and have a prominent role as phagocytes to clear infections and control other immune cell responses. The bone marrow produces millions of neutrophils every day to circulate in the blood. Their production increases

in response to increased secretion of colony stimulating factors such as G-CSF due to infection (Stark *et al.*, 2005). In response to a foreign antigen, local tissue macrophages release TNFα, IL-1β and other cytokines that stimulate endothelial cells to capture circulating neutrophils (Nauseef and Borregaard, 2014). Neutrophils then cross the vasculature by extravasation and migrate to the infected site along chemokine gradients. The role of neutrophils in inflammation is believed to be more than the antimicrobial functions and includes phagocytosis, degranulation and the release of nuclear material in the form of neutrophil extracellular traps (NETs). They are able to respond to numerous signals by producing cytokines and inflammatory factors that effect and control inflammation and the immune response (Rosales, 2018).

Basophils and eosinophils are granulocytes that exhibit similarities with mast cells. Basophils exhibit FcεRI expression, Th2 cytokine secretion, and histamine release but they differ markedly in their ability to either react to other stimuli, generate inflammatory eicosanoids or release immunomodulating cytokines and chemokines. Basophils can be identified through metachromatic staining and through their segmented nucleus. Eosinophils exhibit highly condensed chromatin and cytoplasm and have bilobed nuclei. Basophils act through production of histamine, leukotrienes, IL-4 and IL-13 to participate in allergic reactions and in the defence against parasitic infection, whereas eosinophils, play a role in allergy and defence against parasitic infection through their degranulation of major basic protein (MBP) and release of cysteinyl leukotrienes (Prussin and Metcalfe, 2003).

While Mast cells are tissue resident cells, basophils are largely circulating cells that migrate to local tissue in allergic responses. Circulating hematopoietic stem cells may also serve as a source of recruited mast cell precursors in infection or other settings. Interestingly, a bipotent progenitor for the basophil and mast cell lineages have been identified in mice spleen (Okayama and Kawakami, 2006). There is a strong indication that basophils and mast cells can play relevant and complementary pro-inflammatory roles in several allergic disorders and that basophils can produce anti-inflammatory properties (Varricchi *et al.*, 2018).

1.2.3 Adaptive immunity

Lymphocytes are divided into three types: bursa-or bone marrow-derived lymphocytes (B cells), thymus-derived lymphocytes (T cells), and natural killer (NK) cells. The B and T lymphocytes are the main cells responsible for adaptive immune responses. B cells form the humoral immune response while T cells form the cellular immune response, which are slower to develop but are antigen-specific and lead to long-term immunological memory. Unlike the innate system, adaptive immunity manifests specificity towards a target antigen (Marshall *et al.*, 2018). While innate immune cells recognise non-self through PRRs that recognise a wide and

diverse array of foreign molecules, the antigen-specific receptors on the surface of lymphocytes are encoded by genes that undergo rearrangement in the bone marrow or thymus to form a specialised receptor on each lymphocyte. This antigen recognition receptor on each lymphocytic cell can bind with only one foreign molecule or antigen, thus, creating a heterogeneous repertoire of antigen receptors (Janeway Jr *et al.*, 2001c). Both B and T lymphocytes develop from their lymphoid precursor in the bone marrow and while B cells continue their development and maturation in the bone marrow, T cells travel to the thymus where they continue their development. Both cells, however, undergo two stages of development. In the first stage, they develop their antigen specificity through the rearrangement of gene segments on their immunoglobulin receptor, for B cells, or T cell receptor (TCR) for T cells. In the next stage, these cells undergo a training period to distinguish self from nonself-antigens before being permitted to the circulation. During this training period, lymphocytes are confronted with different antigens and molecules from their environment, if they interact with any of the self-antigens, they will receive signals that lead to their apoptosis. Hence, any self-reacting lymphocytes are removed from the repertoire before being able to mount a damaging autoimmune reaction (Janeway, Travers and Walport, 2001). In response to the appropriate antigen/MHC combination, specific T or B cells become activated, recruited to target organs, and undergo clonal expansion creating an army of the same specific cell to fight a specific antigen (Janeway Jr *et al.*, 2001c).

1.2.3.1 B lymphocytes

Following production and rearrangement of the immunoglobulin gene segment, immature B cells express monomeric IgM on their surface and migrate to the spleen where they differentiate through distinct transitional B cell stages termed T1 and T2, before differentiating into either long-lived mature follicular (FO) or marginal zone (MZ) B cells which are mature but naïve B cells. These mature or naïve B cells recirculate between secondary lymphoid organs searching for an antigen (Nutt *et al.*, 2015). Unlike T cells, B cells can bind and recognise an antigen without the need for APCs as they can directly identify an antigen. The MZ B cells are activated through T cell-independent activation and additional signals for activation are either received from toll like receptors (TLR) or crosslinking of B cell receptors (BCRs) to repeated epitopes on the foreign antigen. However, FO B cells may require stimulation by T helper cells as some antigen can only be recognised by T cells in a process known as T cell-dependant activation. Once internalised, B cells process the antigen and display epitopes in association with MHC II which are recognised by T helper cells via their TCR complex. This binding leads T cells to increased expression of CD40L surface protein and cytokines that are responsible for activating both B and T cells (Nutt *et al.*, 2015; Parker, 1993).

Once activated, B cells go through short and long-term paths of differentiation. In the short-term, B cells differentiate quickly into short-lived plasma cells that are mostly IgM secreting plasma cells which are able to secrete an initial response but with low affinity antibodies (MacLennan *et al.*, 2003). In the long-term path, B cells create a germinal centre through rounds of proliferation, affinity maturation, and class switch into IgG, IgA and IgE providing long-lived immune cells with higher diversity and affinity in plasma cells to meet the immunity challenge. Furthermore, some B cells differentiate into long-lived memory cells equipped to mount quick and efficient responses if the same antigen was to be encountered again in the future (LeBien and Tedder, 2008; Shlomchik and Weisel, 2012; Marshall *et al.*, 2018).

1.2.3.2 T lymphocytes

T cells recognise antigens only if they are presented on the surface of APCs in conjunction with a MHC, which in turn binds to the TCR. CD8 binds to MHC class I and CD4 binds to MHC class II.

CD4+ T cells recognise the antigen presented by class II MHC molecules. TCR engagement with a specific antigen is accompanied by a specific cytokine environment (cytokine milieu),whereby antigen-stimulated T cells are genetically programmed into a variety of potential subsets that possess effector mechanisms appropriate for eliminating the pathogen (Pennock *et al.*, 2013). Their main function is to help and regulate other immune cells in their function, for example, CD4 T cells are capable of activating B cells, macrophages, and CD8+ T cells, hence the name “helper cells”. Helper cells are categorised mainly into three groups: Th1, Th2 and Th17. Th1 can produce cytokines such as INF-γ, IL-2, and TNF-α, which activate macrophages and cytotoxic T-cells. Th2 cells produce IL-4, IL-5, IL-10, and IL-13 and these activate B cells. Th17 induce IL-26, IL-22, and IL-17 secretion and these promote an inflammatory response in autoimmune disease. Another T cell subtype is the regulatory T cells (Tregs) which are believed to have an important role in the regulatory control over immune responses, suppressing autoimmune disease while maintaining immune homeostasis.

CD8+ T cells are the corner stone of the adaptive immune response against viral infections. They respond to the cytokine milieu and antigenic stimuli and divide into distinct subtypes with characteristic functional criteria. This includes the development of the terminally differentiated short-lived effector/ cytotoxic T cells which migrate from lymph organs toward infection area. Effector CD8 T cells can also preferentially mature in response to cytokines to long-lived memory T cells (Kaech and Wherry, 2007). Antigen detection alone is not sufficient to activate CD8+ T cells as they need a costimulatory signal for a successful activation and specific cytokines to modulate the immune response. Local inflammatory cells participate in

creating a proper cytokine milieu for CD8+ T cells activation mainly Th1 and their related cytokines; IL-2, IL-12 and IFN-γ. These serve as checkpoints to prevent improper immune responses. Similar to CD4+ differentiation, IL-12 promotes T-bet transcriptional factor of which high expression was related to short-lived effector cells and low expression connected to long-lived memory cells differentiation (Joshi *et al.*, 2007). Other cytokines such as IL-6 and IL-1 family members including IL-18 andIL-33 able to promote and potentiate the cytotoxic potential of CD8+ T cells and controlling the viral infection. Nonetheless, cytokines such as IL-10 and TGF-β were reported to supress CD8 activity (Cox, Kahan and Zajac, 2013). Upon contact with target cells, cytotoxic CD8+ T cells can trigger programmed cell death of the target cells and intracellular pathogen leading to DNA fragmentation and apoptosis. Once CD8 T cells recognise an antigen on the surface of host cells, they release lytic granules that contain at least two cytotoxic proteins, perforin and Granzyme. While perforin compromise the integrity of the cell membrane by creating pores, Granzyme can enter the cell through these pores and induce apoptosis through cleaving Caspase which activate nucleases that are believed to be responsible for DNA degradation. Another perforin independent killing mechanism exist through the binding of Fas on the target cell membrane with the Fas-ligand on cytotoxic and Th1 cell membrane. This binding provide alternative signal to activate nuclease and induce apoptosis in the Fas bearing cells (Janeway Jr *et al.*, 2001a).

1.3 Oral lichen planus

1.3.1 Background to oral lichen planus

Lichen Planus (LP) is a relatively common mucocutaneous inflammatory disease of unknown aetiology (Odell, 2017). It was first described by William Erasmus Wilson in 1869 with the name based on the appearance of the skin lesion. Similar to the appearance of the lichen found growing in forests on trees, the Greek word “leichen” means tree moss and the Latin word “planus” means flat-topped (Gupta and Jawanda, 2015; Wilson, 1869; Neville *et al.*, 2002). LP is characterised by a clinical presentation of variable patterns and can be categorised into two types; cutaneous lichen planus, affecting the skin, nails, hair and the scalp and mucosal lichen planus, which commonly occurs in the mouth and hence is referred to as oral lichen planus (OLP). LP can to a lesser extent affect other mucosae, including the gastrointestinal tract (GIT), genital areas, nasal mucosa, larynx and the conjunctiva of the eye (Nico, Fernandes and Lourenco, 2011; Tyldesley, 1974).

OLP is considered the most common non-infectious oral disease with a global prevalence of around 1%, although there are marked geographical differences, and it is usually a long-lasting condition compared to the skin lesions (González‐Moles *et al.*, 2020). OLP occurs most frequently in isolation. However, it can occur with involvement of other mucosal surfaces, particularly genital (20%) or the skin (15%). In contrast, OLP is found in approximately 70% of patients with a history of cutaneous LP (Farhi and Dupin, 2010). The condition ranges in severity from asymptomatic, mild, moderate to severe forms and commonly undergoes periods of quiescence and exacerbations that often coincide with such factors as stress, anxiety, trauma, or exposure to a low chronic irritant, for example dental plaque, tobacco use or dental filling (Scully and Carrozzo, 2008; Kurago, 2016).

The effect of smoking in aggravating symptomatic OLP has been related to the direct thermal and chemical irritaion and to a lesser extent to the indirect vasoconstriction effect of nicotine and its metabolites which contribute to delayed wound healing (Benowitz and Burbank, 2016). Smoking has also been associated with enhanced TLR-2 and CD34 expression in OLP which are considered as inflammatory mediators and are contributing factors in the pathogenesis of OLP (Amin, Yussif and Ahmed, 2020). However, there might be a protective role associated with mucosal hyperkeratosis and the decreseased cytokine production mediated by nicotine related steroid release. This might cause aggravation of the condition upon smoking cessation as in aphthous stomatitis (Unal, Yalcin and Ozturk, 2014).

Classically, OLP presents with reticular white lesions that are bilaterally and symmetrically distributed on the oral mucosa, particularly the buccal mucosa and sides of the

tongue, gingiva, followed by labial mucosa and lower lip. The floor of the mouth and upper lips are considered as less-common sites. Sometimes these white patches are more plaque-like in appearance. In both cases, the thickening of the mucosa may be relatively asymptomatic apart from feeling rough. However, with increasing disease activity there is mucosal thinning that produces erosive (atrophic) lesions that are erythematous in appearance, often with surrounding reticular or striated areas. Erosive areas are often painful and particularly sensitive to strong flavours, acids, spirits etc., probably due to loss of the mucosal permeability barrier. As disease activity increases further, there is complete loss of epithelium and the development of ulcerative lesions. Like erosive lesions these may be surrounded by reticular or straited lesions and are extremely sensitive (Al-Hashimi *et al.*, 2007; Carrozzo *et al.*, 2019) (**Figure 1.3**). Hence, it is the erosive/ulcerative form that is considered the more clinically significant, causing symptoms of discomfort, burning and pain (Scully and Carrozzo, 2008; Park, Hurwitz and Woo, 2012).

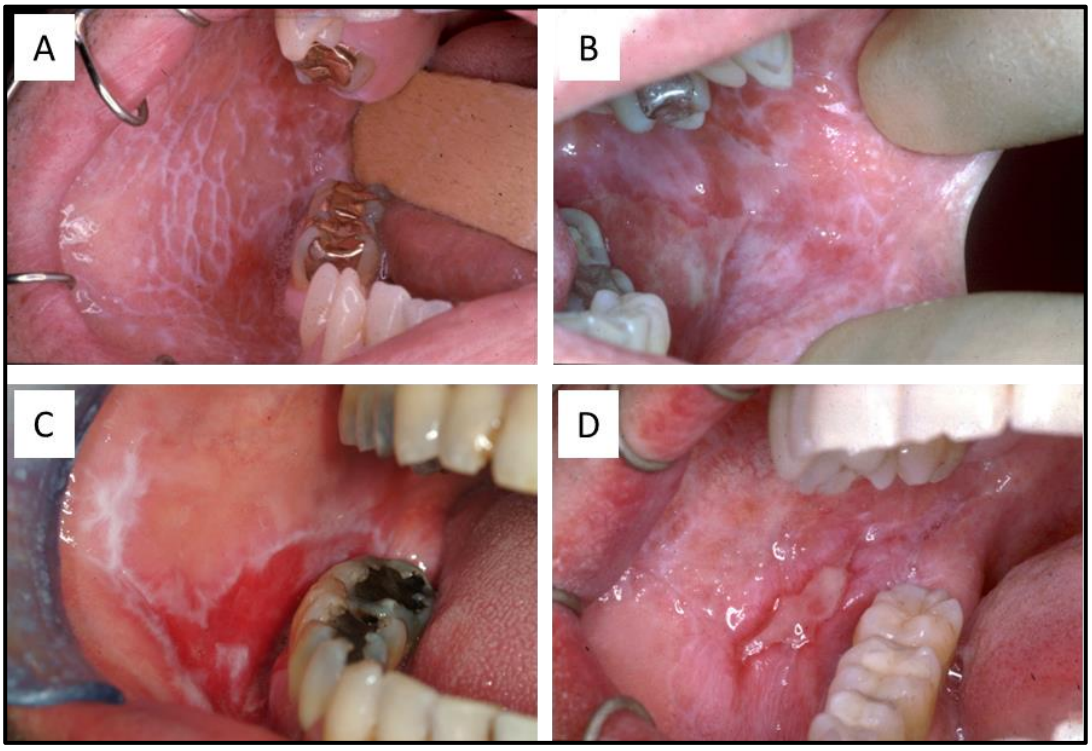

Figure 1.3: Clinical presentations of the different forms of oral lichen planus presented on the buccal mucosa: (A) reticular, (B) plaque (C) erosive, and (D) ulcerative. Images provided by Prof Thornhill, Sheffield Teaching Hospitals NHS Foundation Trust, Sheffield, UK. (Images were taken with written, informed consent under ethical approval).

Ten per cent of OLP patients have gingival involvement that commonly occurs in erosive and atrophic forms leading to a clinical condition termed "desquamative gingivitis". Differentiation from other conditions with a similar presentation is needed such as pemphigus, mucous membrane pemphigoid, graft versus host disease, dermatitis herpetiform, and lupus erythematosus (Ebrahimi *et al.*, 2012; Odell, 2017). A triad of gingival, vulvar and vaginal lesions has been reported called vulvovaginal-gingival syndrome. Hence, other reports suggested the

use of the term "mucosal LP" instead of using ‘‘oral lichen planus" and "vulvovaginal LP (Sousa and Rosa, 2008; Canto *et al.*, 2010).

The classical histopathological features of OLP include a dense sub-epithelial band of inflammatory T-cells, along with intra-epithelial lymphocytic cell infiltration, liquefaction degeneration of the basement membrane and apoptosis of basal keratinocytes to form colloid bodies (also termed cytoid, hyaline, keratin or Civatte bodies) (Matthews, Scully and Potts, 1984) (**Figure 1.4**).

Other histological features include surface hyper-parakeratosis, irregular acanthosis with occasional areas of atrophic epithelium where the rete pegs may be pointed (saw-tooth), and the presence of a fibrinous precipitate at the epithelial-connective tissue junction (Müller, 2017). Classical features of OLP can be altered by candida infection (Hiremath, Kale and Charantimath, 2011), and some features such as the absence of liquefactive degeneration of the basal cells, a heterogeneous cell infiltrate, abnormal cell morphology and maturation might exclude the diagnosis of OLP (Canto *et al.*, 2010).

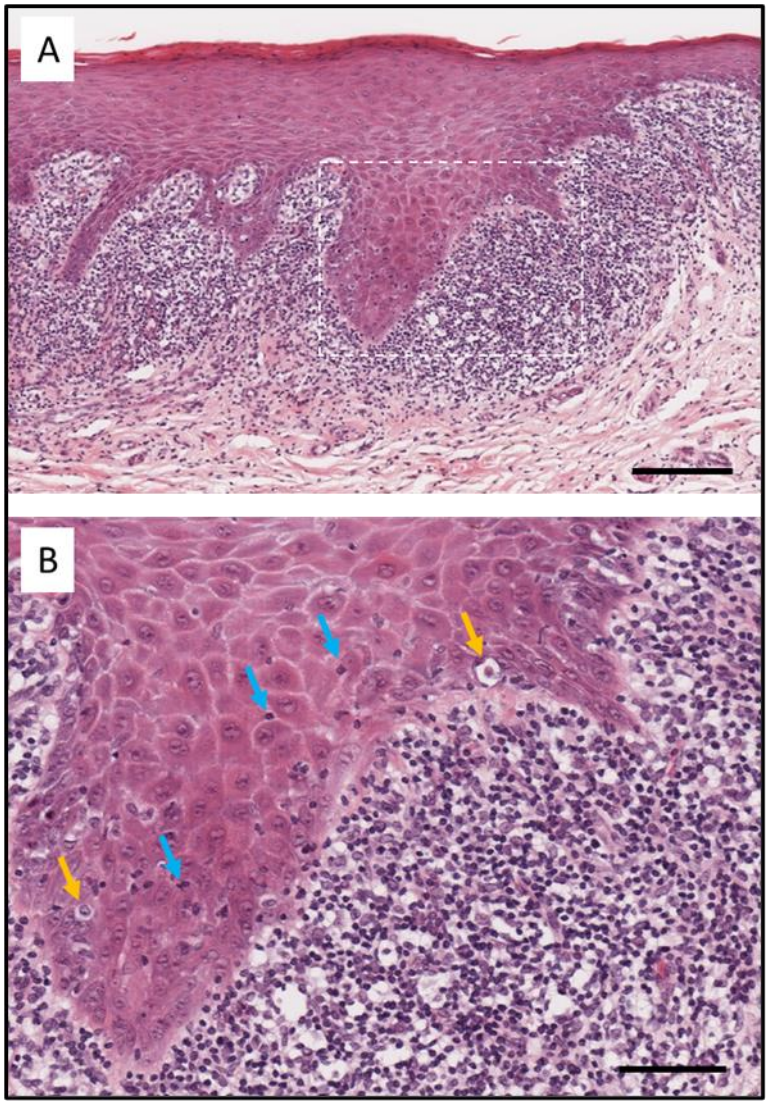

Figure 1.4: Histopathological features of oral lichen planus. (A) Haematoxylin and eosin-stained section of an OLP lesion showing the oral mucosa composed of a stratified squamous epithelium and underlying connective tissue containing a dense band of inflammatory T cells in the subepithelial compartment. (B) Magnified image of area depicted in A (white dotted outline box) showing the presence of colloid bodies within the epithelium (yellow arrows) and infiltration of intra-epithelial T cells (blue arrows). Scale bar in A = 200 μm and in B = 50 μm. Images provided by Prof Thornhill, Sheffield Teaching Hospitals NHS Foundation Trust, Sheffield, UK.

Oral lichenoid reactions (OLR) are regarded as either a distinct variant of OLP or an OLP-like lesion and are similar in clinical and histopathological appearance to OLP. In contrast to OLP, OLR tends to present clinically as a unilateral lesion that is not accompanied by extraoral lesions (Thornhill *et al.*, 2003). Moreover, histologically, the lymphocytic band tends to be more diffuse, containing more eosinophils, plasma cells and colloid bodies than in OLP (Thornhill *et al.*, 2006; Müller, 2017). However, some cases of OLR can be difficult to distinguish from OLP. Unlike the idiopathic nature of OLP, OLR is often associated with an identifiable factor such as a specific dental material (e.g., amalgam or nickel), chemical or medication and so is considered to occur as a result of a delayed hypersensitivity reaction (Thornhill *et al.*, 2006). Diagnosis can often be made on clinical presentation alone, although a correlation between

both clinical and histopathological criteria are required to prova definitive diagnosis. The World Health Organization (WHO) has proposed a set of modified diagnostic criteria to reach a diagnosis and differentiate between OLP and OLR (Rad *et al.*, 2009). Since other conditions resemble OLP, complementary investigations are needed to exclude them, and a second biopsy may be ordered to perform a direct immunofluorescence test, especially if another autoimmune condition is suspected such as pemphigus or mucous membrane pemphigoid (Sousa and Rosa, 2008; van der Meij and van der Waal, 2003).

There is a long history concerning the proposed cellular and molecular pathogenic mechanisms in OLP, starting with Walsh and colleagues in 1990 (Walsh *et al.*, 1990), further developed by Sugerman et al., in 2002 (Sugerman *et al.*, 2002) and more recently extended by others to take into account new data (Khan *et al.*, 2003; DeAngelis, Cirillo and McCullough, 2019; Lu *et al.*, 2015). The overall consensus is that the pathogenesis of OLP is initially driven by the recognition of a non-self-antigen that evokes an intricate and complex interplay between immune and non-immune cells, cytokines and adhesion molecules, culminating in a dysregulated cell-mediated immune reaction. This leads to proteolytic-mediated basement membrane destruction and an inappropriate and harmful immune response, mainly by T cell subsets, directed against oral keratinocytes leading to keratinocyte apoptosis. Despite much advancement in the knowledge of OLP pathophysiology, the dysregulated immune response that governs the disease is still not completely understood. The next section provides an overview of the accumulated knowledge and current understanding of the specific and non-specific immune responses in OLP and reflects on areas of research that may lead to the development of new, targeted therapies.

1.3.2 Which antigens drive OLP pathogenesis?

The specific etiologic factors driving OLP are still unknown, although several lines of evidence point to the presentation of a foreign or altered antigen by basal keratinocytes that induce a T cell-mediated autoimmune response against these cells as the root cause. Each T cell expresses a specific cell surface TCR that is composed of α and β chains which contain variable (V) regions with unique amino acid sequences that mediate binding to a specific antigenic determinant. Rearrangements in the genes that encode the α and β proteins during T cell development create an extensive antigen specific TCR repertoire. In response to an OLP-mediating antigen presented in association with the MHC, the corresponding antigen-specific T cell becomes activated, recruited to the target oral mucosa where it undergoes clonal expansion and directs a deleterious immune response against target oral keratinocytes resulting in keratinocyte cell death.

In order to identify the specific antigens that instigate OLP, studies have attempted to characterise the TCRs expressed by T cells in OLP lesions. The over-representation of specific Va and Vb TCR families expressed by OLP lesional T cells indicate the selective recruitment and expansion of particular T cells at lesional sites. However, the overall heterogeneous nature of these Va and Vb sub-family suggests that several antigens rather than one distinct antigen are responsible for provoking disease progression. Moreover, since superantigens (i.e., antigens that mediate non-specific excessive T cell activation) can bind to multiple types of Vβ regions irrespective of TCR specificity, it has been proposed that superantigens are also involved in driving OLP (Simark‐Mattsson *et al.*, 1994; Thomas *et al.*, 1997; Zhou *et al.*, 1996).

At present no single antigenic determinant has been shown to specifically trigger OLP pathogenesis. Although still highly debated, current data points to the involvement of a number of exogenous viral or microbial antigens in driving the cell-mediated host response. Three independent systematic reviews with meta-analysis have shown an association between presence of hepatitis C virus (HCV) and OLP, although this association showed regional differences, with increased association observed in areas with higher prevalence of HCV infection (Lodi, Pellicano and Carrozzo, 2010; Petti *et al.*, 2011; Alaizari *et al.*, 2016). Another systematic review identified that human papillomavirus (HPV) may also play a causal role in OLP, but once again the strength of this association varied across geographic populations, clinical types of OLP and HPV genotypes (Ma *et al.*, 2016). An association of OLP with presence of Epstein-Barr virus is less convincing (Ashraf *et al.*, 2020). The commensal fungus, *Candida albicans* has also been studied as a potential instigator for OLP, but there is difficultly in establishing a causal relationship, even where high prevalence was reported because oral candidiasis is an opportunistic infection or can occur as a side-effect of corticosteroid and other treatments for oral diseases including OLP (Baek and Choi, 2018). Several periodontal pathogenic bacteria (*Porphyromonas gingivalis*, *Tannerella forsythia, Prevotella denticola*) have been detected in OLP lesions and direct or indirect roles of these microbes, along with superantigens derived from *Staphylococcal* and *Streptococcal* bacteria and even *Escherichia coli* have been proposed in the aetiology of OLP (Zhong *et al.*, 2020; Baek and Choi, 2018; Ertugrul *et al.*, 2013; Bornstein, Hakimi and Persson, 2008), although their role in disease pathogenesis is still contentious (Villa, Sánchez-Pérez and Sieiro, 2021). The detection of intracellular bacteria within oral keratinocytes and their close association with intra-epithelial T cells suggests a route for microbial antigen presentation by oral keratinocytes, and it has been proposed that individual bacterial species are responsible for the presentation of different OLP types (Choi *et al.*, 2016). Sequencing of 16S rRNA from healthy oral mucosa compared to OLP lesion shows that the OLP-associated microbiota is significantly different (Baek *et al.*, 2020). However, in all instances, it has proven difficult to establish a direct causal relationship between

microbe and OLP pathogenesis. Also, the fact that OLP is responsive to steroids which represent the first line of treatment contradicts the potential for a microbial causative factor. Otherwise, steroid treatment would have caused deterioration of OLP as the microbe would take advantage of the suppressed immune system.

Other predisposing factors have been related to OLP onset such as stress, hypothyroidism, nutrient deficiency and food allergy. It has been postulated that these factors as well as others such as drugs or mercury salts may cause the unmasking or alteration of endogenously expressed self-antigens that in turn stimulate a dysregulated T cell immune response in OLP (Sugerman *et al.*, 2002; Payeras *et al.*, 2013). Despite this research, the precise nature of the antigen(s) that instigate OLP remain elusive and so the initial events driving OLP are still ambiguous.

1.3.3 Antigen presentation and initiating events in OLP pathogenesis

The initiating events in OLP pathogenesis not only revolve around acquisition of exogenous or endogenous antigens but importantly production of pro-inflammatory cytokines and response to these. Upon stimulation, oral keratinocytes release a multitude of pro-inflammatory cytokines that significantly contribute at different stages to OLP pathogenesis. Keratinocytes from OLP lesions have been reported to produce TNF-a, IL-1b, G-CSF, IL-12 and IL-6 with many at levels 10- to 20-fold greater than from healthy oral mucosa (Yamamoto and Osaki, 1995; Khan et al., 2003; Aragane et al., 1994). In addition, TNF-a, IL-1b and IL-6 were detected at high levels in the supernatant of OLP keratinocytes, tissue-infiltrated mononuclear cells and in the saliva of OLP patients (Yamamoto et al., 1994; Yamamoto and Osaki, 1995; Rhodus et al., 2005; Rhodus, Cheng and Ondrey, 2007). Gene polymorphisms in TNF-a and IL-6 have been associated with increased risk of OLP whilst no association was found for the IL-1 cluster or IL-10 (Xavier et al., 2007). The activated keratinocytes act in concert with Langerhans cells, which are APCs that reside within the oral epithelium and are found in increased numbers in OLP lesions (Rich and Reade, 1989). These DCs mature by capturing, processing, and presenting OLP-mediating antigens in association with MHC class II on their cell surface. The key pro-inflammatory molecules at this stage appear to be TNF-α and IFN-g. Increased levels of IFN-g up-regulates the expression of MHC class II by DC enhancing antigen presentation and at the same time stimulates oral keratinocytes to express human leukocyte antigen (HLA)-DR and -DQ MHC class II, enabling them to also act as APCs (Takeuchi *et al.*, 1988; Li *et al.*, 1996a; Farthing and Cruchley, 1989). Increased levels of TNF-α, due to both DC and keratinocyte activation, cause activation of the key intracellular pro-inflammatory transcription factor, nuclear factor kappa B (NFkB) in the surrounding cells and, in combination with the effects of IFN-g, lead to increased expression of numerous chemokines that drives

immune cell recruitment as the disease progresses (Li *et al.*, 1996a; Zhao *et al.*, 2002; Marshall *et al.*, 2017b; Orlando, Bragazzi and Nicolini, 2013). Importantly, activated DC migrate to the local lymph node where they interact with antigen specific T cells to produce a primary (often termed the specific) OLP immune response.

1.3.4 T cell activation

T cells with an OLP-mediating antigen-specific TCR can be activated either at distal lymph nodes sites or at the lesional site by APCs. The activation of naïve T-cells in the lymph nodes follows the physical interaction between T cells and DC. The primary signal in T cell activation is the binding of the TCR-CD3 complex and either CD4 or CD8 co-receptor with MHC class I or II, respectively (**Figure 1.5**).

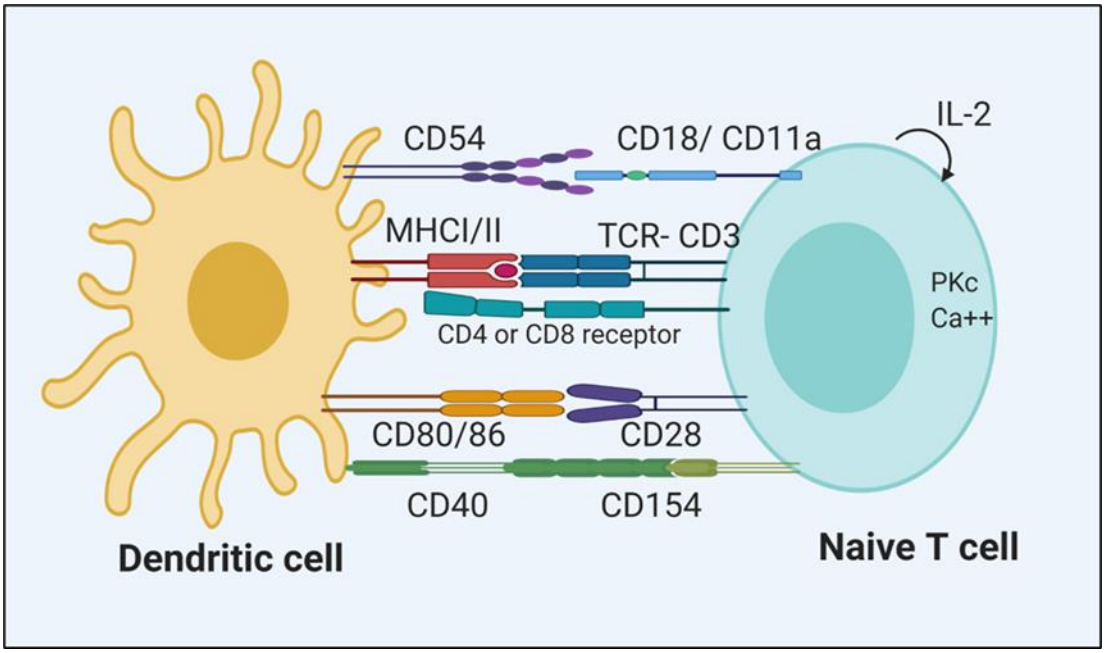

Figure 1.5: Schematic diagram illustrating the interaction of an antigen presenting dendritic cell with a naive T-cell. and the binding of the primary (MHC and TCR-CD3 complex with either CD4 or CD8) and costimulatory signals responsible for T cell activation. Created in BioRender.com.

This interaction stimulates a cascade of intracellular signalling that results in the initial activation of T cells. However, other co-stimulatory events are essential for T cell proliferation and cytokine secretion. The primary co-stimulatory signal for T cell activation is the binding of CD28 and the integrin CD18/CD11a (LFA-1) expressed on the T cell surface with their counter-receptors, CD80 (B7-1)/CD86 (B7-2) and CD54 (ICAM-1) respectively, expressed by DC (Wingren *et al.*, 2017) (**Figure 1.5**). Ligation of CD28 augments T cell immune responses by inducing enhanced secretion of IL-2 that then acts in an autocrine manner to stimulate T cell proliferation (Thompson *et al.*, 1989; Lindstein *et al.*, 1989). Indeed, the expression of IL-2 has been consistently found at elevated levels in OLP lesions (Yamamoto and Osaki, 1995; Orlando,

Bragazzi and Nicolini, 2013). DC constitutively express moderate levels of CD80 and CD86, however, these levels increase 100-fold upon activation. To modulate this immune response, CD80/CD86 also bind cytotoxic T-lymphocyte-associated protein 4 (CTLA-4) but with higher affinity than CD28, blocking CD28-medaited T cell activation and dampening intracellular signalling (Krummel and Allison, 1995). In addition to CD28, binding of CD40 with CD154 (also termed CD40-ligand), also induces the expression of CD80/CD86 as well as the secretion of pro-inflammatory cytokines such as IL-6 and IL-12, which can influence T cell differentiation into different T cell subsets (Mackey, Barth and Noelle, 1998) (**Figure 1.5**).

Activated antigen-specific T cells then enter the bloodstream and are recruited to the OLP lesional site by chemokines and adhesion molecules (see section 1.3.5). Interestingly, non-activated T cells are also recruited to lesional sites where they are activated by tissue APCs including DC, macrophages and IFN-γ-activated oral keratinocytes that are stimulated to express MHC class II, CD40, CD54 and CD86 (Zhou *et al.*, 1996; Marshall *et al.*, 2017b). Moreover, OLP lesional mast cells can also activate T cells through the expression of MHC class II, CD80/86 and CD11a (Kambayashi *et al.*, 2009). Hence, both the chance encounter and the attracted migration hypothesis have been suggested for T cell activation and recruitment in OLP.

1.3.5 T cell recruitment to the OLP lesion sites

In OLP, the lesional cell population is predominantly made up of variable levels of CD4+ and CD8+ T cell subpopulations. The crucial role of T cells in OLP pathogenesis was first established after an oral lesion was induced following local transfer of CD4+ T cell clones with a cytotoxic ability into mice recipients (Shiohara *et al.*, 1986). Immunostaining analysis shows that the majority of T cells within the epithelium and adjacent to apoptotic keratinocytes are activated CD8+ cells, while most T cells in the lamina propria are CD4+ T cells (JUNGELL *et al.*, 1989; Matthews, Scully and Potts, 1984), providing an early indication that cytotoxic CD8+ T cells are largely responsible for driving keratinocyte apoptosis (Sugerman *et al.*, 2000).

Recruitment of T cells from the circulation to OLP lesions is mediated by adhesion molecules that are expressed on the surface of activated endothelium with their cognate receptors on T cells. Endothelial adhesion molecules such as CD31 (PECAM-1), CD106 (VCAM-1), CD54 (ICAM-1) and CD62E (E-selectin) are expressed at very low levels in quiescent endothelium but stimulation by pro-inflammatory cytokines such as TNF-α and IFN-γ released from OLP lesional sites dramatically up-regulates their expression on nearby blood vessels (Little *et al.*, 2003b; Meager, 1999). For example, endothelial CD31 was found to be overexpressed in OLP compared to normal mucosa with higher expression in erosive than

reticular forms (Lavanya *et al.*, 2020). Circulating T cells, under the influence of specific chemokines, then bind to the activated vascular endothelium via multiple receptor/ligand interactions including CD18/CD11a with CD54, integrin CD49d/CD29 (VLA-4) with CD106 and CD62L (L-selectin) with CD62E (Meager, 1999).

T cell migration from the endothelial surface into lesional tissue is directed by chemokine gradients produced by IFN-γ and TNF-α-activated immune and non-immune lesional cells and increased expression of CD54 on the surface of oral keratinocytes that facilitate leukocyte locomotion through the epithelium (Little *et al.*, 2003b). CCL5 (RANTES) is a potent T-cell chemoattractant that also causes degranulation of mast cells. *In vitro*-cultured oral keratinocytes increase gene and protein expression of CCL5 in response to IFN-γ and TNF-α (Little *et al.*, 2003b; Li *et al.*, 1996a) and high levels of CCL5 have been detected in the epithelium, lamina propria and serum of OLP patients (Ichimura *et al.*, 2006; Shan *et al.*, 2019; Hu *et al.*, 2013). Moreover, CCL5 was found to be expressed by oral keratinocytes in the majority of OLP and OLR biopsies analysed (Little *et al.*, 2003b) and CCR1 and CCR5, which are cell surface receptors for CCL5 as well as other T cell chemokines, have also been identified in OLP lesions (Zhao *et al.*, 2002; Hu *et al.*, 2013). Recently, Shan *et al*., highlighted the importance of the CCL5-CCR5 axis in OLP. The authors reported that as well as acting as a potent chemoattractant, CCL5 inhibited T cell apoptosis, increased T cell longevity whilst simultaneously inducing expression of CCL5 and CCR5 in an autocrine manner to form a positive feedback loop to establish chronicity of OLP (Shan *et al.*, 2019). As well as CCL5 other T cell chemokines such as CXCL9, CXCL10, CXCL11 and CCL20 as well as their receptors have also found to be upregulated in OLP (Ichimura *et al.*, 2006; Fang *et al.*, 2019). It is plausible that these chemokines may mediate the recruitment of specific T cell subsets in lesional sites or direct their migration to specific locations within the oral mucosa such as to the lamina propria or intra-epithelial sites, although the precise role of each specific chemokine is yet to be determined.

1.3.6 The role of mast cells and macrophages in OLP

Mast cells act in concert with T cells in the pathogenesis of OLP and are found in higher numbers in the lamina propria, near blood vessels and adjacent areas of basement membrane destruction (Sharma *et al.*, 2011; Zhao *et al.*, 1997). Elevated degranulation of mast cells has been reported when compared to normal mucosa via detection with electron microscopy, through the loss of metachromasia following toluidine blue staining or via immunohistochemistry (Jontell, Hansson and Nygren, 1986; Zhao *et al.*, 2001). Upon degranulation, mast cells release TNF-α, chymase, tryptase and the T cell chemo-attractants IL-16 and CCL4 as well as CCL5 (Zhao *et al.*, 2002; Rumsaeng *et al.*, 1997). These mast cell-derived chemo-attractants act in

concert with the keratinocyte-derived chemokines to perpetuate T cell recruitment to the lesional site. CCL5 and CCL3 can also act in a paracrine manner by binding to CCR1 on nearby mast cells driving their degranulation with further release of TNF-α, histamine and other pro-inflammatory molecules culminating in a positive feedback loop (**Figure 1.5**) (Zhao *et al.*, 2001; Miyazaki *et al.*, 2005).

Mast cell-derived tryptase and chymase are potent activators of matrix metalloproteinases MMP-2 or -9, by proteolytic cleavage (Takai and Jin, 2022). Culture supernatants from OLP lesional T cells contained higher levels of MMP-9 than those from healthy control peripheral blood T cells suggesting T cell-mediated secretion of MMP-9 at lesional sites (Zhou *et al.*, 2001). Moreover, increased levels of MMP-2 and the broad-spectrum protease MMP-7 have been observed in OLP tissue compared to controls (Li and Cui, 2013; Rubaci *et al.*, 2012). This increased proteolytic activity facilitates the migration of T cells through the extracellular matrix of the lamina propria whilst also cleaving collagen IV and V to cause direct proteolytic destruction of the basement membrane that has two consequences: firstly, allowing CD8+ T-cells greater access to the oral epithelium and secondly detaching basal cells from the basement membrane thereby depriving these cells of basolateral attachment survival signals, driving apoptosis. Along with mast cells, inflammatory macrophages are also found in increased numbers in OLP lesions (Ferrisse *et al.*, 2021) where they likely exacerbate inflammation by OLP antigen presentation and further secretion of TNF-α, IL-1β, MMPs and CCL5 (**Figure 1.6**). Besides their pathogenic role in OLP and other autoimmune diseases, they are best known for their role in allergic conditions including Asthma. To limit the detrimental effect of MCs in disease, several therapeutic approaches were developed including inhibiting MC related mediators such as protease inhibitors (Sommerhoff and Schaschke, 2007), inhibiting MC activation such as omalizumab, anti-IgE antibody (Sheinkopf *et al.*, 2008), or reduce their numbers by reduce survival by targeting stem cell factor (SCF) or induce MC apoptosis (Finotto, Mekori and Metcalfe, 1997). These strategies to target MCs can potentially be adopted for the treatment of OLP and similar conditions. However, further investigation into the applicability of such regeims is needed.

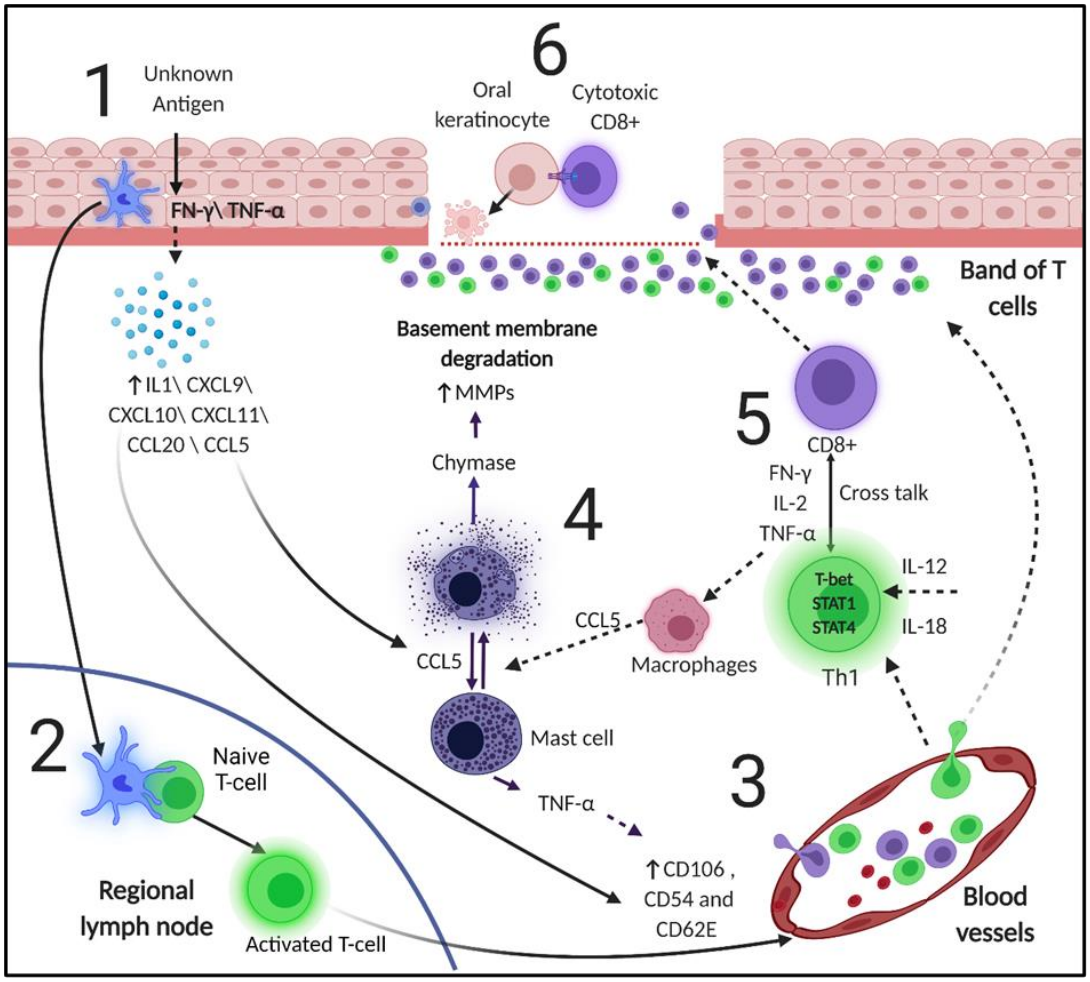

Figure 1.6: A schematic illustration of the immune process in OLP. (1) An as yet unknown antigenic stimulus activates keratinocytes and APCs to release pro-inflammatory cytokines and chemokines that up-regulate keratinocyte and endothelium adhesion molecule. (2) Activated APC migrate to a lesional lymph node and bind to the antigen specific T cells via cognate surface receptors and molecules leading to activation of signalling pathways that activate CD8+ cytotoxic cells and differentiate CD4+ into Th1 subset. (3) T cells migrate to the OLP lesion through blood vessels. (4) The cytokine milieu further enhances the Th1 differentiation, and their secreted cytokines propagate the inflammatory response. In addition, CCL5 mediates mast cell degranulation releasing molecules such as TNF-α, chymase, tryptase, histamine as well as further CCL5 to create a positive feedback loop increasing the chronicity of OLP. TNF-α and IL-1 up-regulate adhesion molecules expression while chymase and tryptase activate MMPs that degrade the oral mucosal basement membrane. (5) Cross talk between CD4+ and CD8+ occurs to enable CD8+ cell functions. (6) CD8+ cells infiltrate the epithelium through the disrupted basement membrane and cause keratinocytes apoptosis by a number of mechanisms. Created in BioRender.com.

1.3.7 CD8+ T-cell activation and keratinocyte apoptosis

Keratinocyte apoptosis, based on the detection of the colloid bodies in histological sections of OLP lesions, is a major outcome of the dysregulated immune response, where CD8+ T cells are consistently reported to be the principal cell type responsible for keratinocyte death (Sugerman *et al.*, 2002). There are two hypotheses for the OLP site infiltration by CD8+ T cells. First, the chance encounter hypothesis, where T cells encounter the altered epithelium through its random surveillance. This hypothesis is supported by the fact that the disease occurs in adult life because it takes time for chance finding of the aetiological antigen. Second, the attracted

migration hypothesis, where the T cells are attracted to the site of the antigen through chemokines secreted by the altered keratinocytes and the Langerhans cells. This hypothesis could be supported by the expression of chemokine receptors on T cells and the fact that T cells infiltrate the lamina propria prior to the intra-epithelial infiltration. Hence, CD8+ T cells infiltrate the mucosal epithelium along a T cell-specific chemokine gradient, which is often enhanced by a disrupted basement membrane. These intra-epithelial T cells are activated by two means; stimulation from IL-2, TNF-α, and IFN-γ produced by various cell types including Th1 CD4+ cells, and by direct binding to MHC class I-presented antigen on immune cells or keratinocytes (Sugerman *et al.*, 2000). Crosstalk between CD8+ and CD4+ T cells is essential, as CD8+ cells require an antigen-specific confirmation from CD4+ cells to enable them to proceed and eliminate target cells (**Figure 1.6**).

Current evidence suggests that CD8+ T cells trigger keratinocyte apoptosis by several mechanisms including the interaction of CD8+ T cell-expressed CD95L (FasL) with CD95 (FasR) on the cell surface of keratinocytes and apoptosis by caspase activation, T cell-secreted granzyme-B entering the keratinocyte cytoplasm through perforin-induced membrane pores, the action of CD8+ T cell-secreted TNF-α binding to TNFR1 that is up-regulated on the keratinocyte plasma membrane in OLP (Tobón‐Arroyave *et al.*, 2004; Khan *et al.*, 2003; Neppelberg, Johannessen and Jonsson, 2001; Shimizu *et al.*, 1997; Dekker *et al.*, 1997). In addition, the interaction of CD40 and CD40L expressed by keratinocytes and cytotoxic T cells, respectively, along with TNFR2 activation enhance TNFR1-induced apoptosis, suggesting other mechanisms may be at play (Grell *et al.*, 1999). T cell independent mechanisms also regulate apoptosis. E-cadherin and integrins are epithelial adhesion molecules involved with cell-cell contacts and contacts with the basement membrane, respectively, and both are essential for cell survival (Grossmann, 2002). Loss of keratinocyte E-cadherin expression has been reported in OLP, and this along with degradation of the basement membrane may also induce keratinocyte apoptosis via anoikis, as well as further facilitating the migration of CD8+ T cells into the epithelium (Neppelberg *et al.*, 2007; Grossmann, 2002).

1.3.8 Th1/Th2 paradigm and other T-cell subsets

For CD8+ T cells to enact their specific cell targeting and destructive behaviour in OLP they must interact and receive signals from Th cells. It is now appreciated that upon appropriate cytokine stimulation naïve Th cells are programmed to differentiate into several different Th cell subsets, each with distinct receptor expression and cytokine-secretion profiles and immune modulatory functions (**Figure 1.7**).

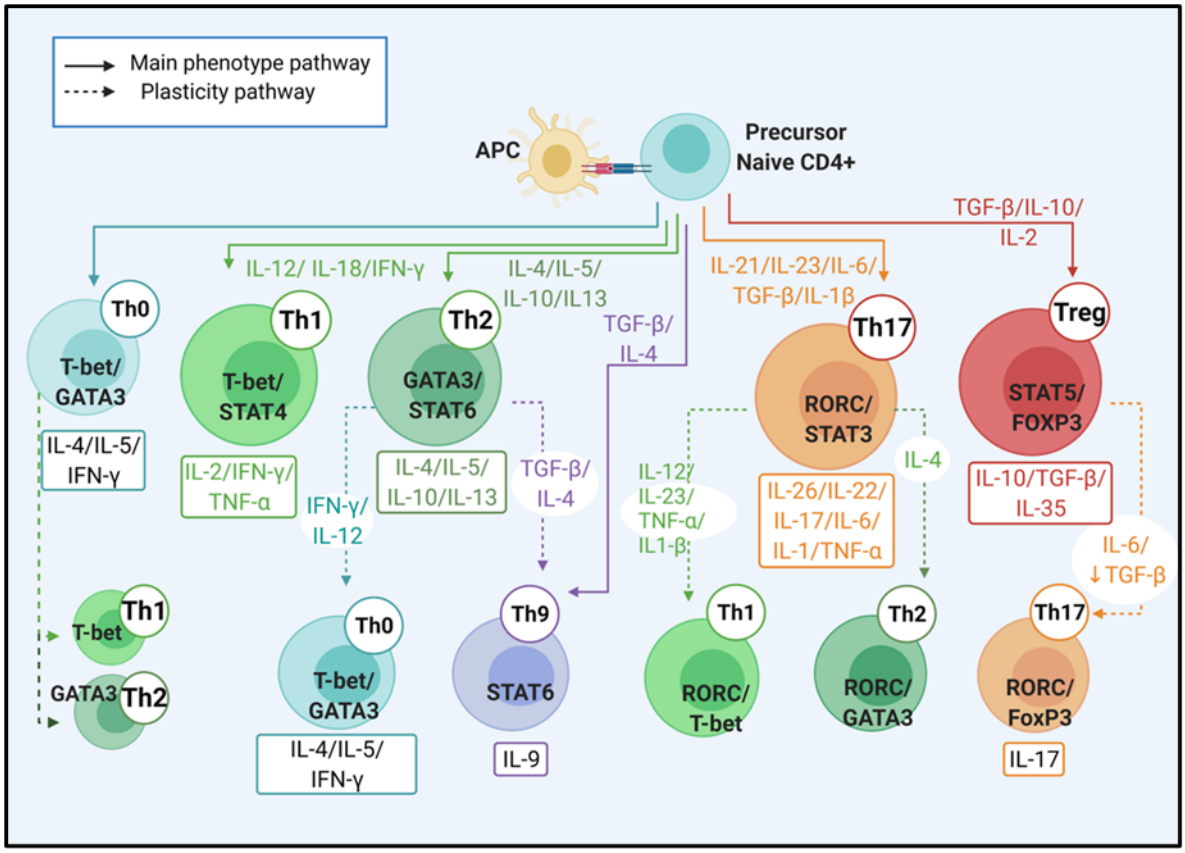

Figure 1.7: Schematic illustration of CD4+ naïve Th subset differentiation and plasticity. Upon appropriate cytokine stimulation naïve Th cells are programmed to differentiate into several different T cell subsets, each with a distinct transcriptional factor, receptor expression and cytokine secretion profile and immune modulatory function. Some subsets show different levels of plasticity in response to changes in the cytokine milieu. Th0 is a mixed phenotype but under abundance of either IFN-γ or IL-4 may switch into either Th1 or Th2 phenotypes respectively. Th2 under influence of high levels of TGF-b or IFN-γ/ IL-12 have the ability to transform to Th0 or Th9, respectively. Th17 under high levels of IL-12 or IL-4 can switch to Th1 or Th2 subsets, and Treg cells may switch to the Th17 subset under high levels of IL-6 combined with a reduction in TGF-b levels. Created in BioRender.com.

Given that many of these Th cell phenotypes have been examined using *in vitro* cultures under defined cytokine conditions it is currently uncertain as to whether these T cell subsets are distinct or form a continuum, with their exact phenotype dependent on the local micro-environmental cytokine milieu they experience *in vivo*.

In response to IL-12 and through the activation of transcription factors STAT4 and T-bet, naïve Th cells are programmed to differentiate into a Th1 phenotype that secrete high levels of IL-2, IFN-γ, TNF-α, express cell surface IL-12R, and are involved in cell-mediated immunity by modulating the activity of macrophages and cytotoxic T cells. In contrast, under the influence of IL-4, STAT6 and GATA-3 transcription factor activation, naïve T cells polarise to a Th2 phenotype that express high levels of IL-4, IL-5, IL-10, IL-13 and tend to be involved in humoral immunity where they interact with B cells (Crane and Forrester, 2005) (**Figure 1.7**).

These two Th subsets regulate each other's function through the antagonistic activity of their related cytokines. The secretion of IFN-γ by Th1 cells supresses Th2 cell formation by inhibiting the actions of IL-4 and silencing GATA-3 whilst increasing expression of T-bet. In contrast, IL-4 and IL-10 secretion by Th2 cells inhibit Th1 formation (Luckheeram *et al.*, 2012). Thus, a dichotomistic relationship exists between Th1 and Th2 cells. Abundant evidence suggests that the cytokine milieu in OLP skews CD4+ T cell differentiation toward the Th1 phenotype that then drives the activation of cytotoxic CD8+ T cells. This was confirmed by the findings of elevated IL-12 and IFN-γ gene expression and secretion by keratinocytes and cells present in the superficial lamina propria and high levels of TNF-α adjacent to basal keratinocytes of OLP lesions (Aragane *et al.*, 1994; Mattsson *et al.*, 1998; Wang *et al.*, 2015).

Several studies have recorded high IFN-γ to IL-4 ratios, inferring Th1 dominance with higher IFN-γ expression purportedly related to the presence of erythematous or ulcerated OLP lesions (Tao *et al.*, 2008; Hu *et al.*, 2015; Wang *et al.*, 2015; Wei *et al.*, 2018). Moreover, Rui Lu *et al*., examined mRNA expression of T-bet and GATA-3 in peripheral blood mononuclear cells isolated from patients with OLP. Their results supported the Th1-bias pattern observed in OLP patients with significantly higher expression of T-bet compared to GATA-3 detected. However, they indicated that different clinical forms of OLP might have different Th1/Th2 imbalanced status with different T-bet/GATA-3 ratios detected (Lu *et al.*, 2011). TNF-α produced by Th1 synergistically works with IL-1 to increase expression of MHC classes I and II antigens, adhesion molecules and chemokines further driving OLP chronicity. In addition, IL-18 functions as a cofactor rather than as an initiator for Th1 development. IL-12 and IL-18 synergistically enhance IFN-γ mRNA transcription by activating the transcription factors STAT4 and AP-1, whilst inhibiting the synthesis of IL-10, a Th2-associated cytokine (Nakahira *et al.*, 2002). In support of this, IL-18 serum levels are elevated in OLP patients and an IL-18 genetic polymorphism has been associated with OLP susceptibility (Negi *et al.*, 2019), although more studies are needed to investigate the role of IL-18 in regulating Th1 differentiation in OLP.

Conversely, a lower IFN-γ to IL-4 ratio and high IL-10 levels have been reported (Zhang *et al.*, 2018; Pekiner *et al.*, 2012; Piccinni *et al.*, 2014). Elevated levels of the Th2 cytokine, IL-5 and IL-6 have been observed in the saliva and serum of OLP patients compared to healthy controls (Wei *et al.*, 2018; Yamamoto and Osaki, 1995). IL-6 can promote IL-4 expression and render CD4+ T-cells unresponsive to IFN-γ signals leading to Th2 differentiation, suggesting that Th1 prominence in OLP may not be as straightforward as it seems. In particular, the protective role of Th2 cells and its related cytokines in controlling or even suppressing Th1 development and connection to the reticular form of OLP has been proposed (Zhang *et al.*, 2018; Pekiner *et al.*, 2012; Piccinni *et al.*, 2014).

Research into OLP has had a tendency toward investigating individual T cell subsets and their associated cytokines to understand the pathogenic mechanism. These criteria may be a too simplistic approach to fully understand the complex pathogenic processes where it is likely that the actions of one cytokine may not be exclusive to only one T cell phenotype. Moreover, there is a need to correlate research results with the clinical type/severity of OLP to uncover their clinical importance. Additional studies are warranted with increased sample size to cover, age, gender, genetic polymorphisms, and disease severity to resolve this issue.

1.3.9 Th17 and the non-classical Th1 phenotype

Th17 cells have been defined through their expression of retinoic acid-related orphan receptor (RORC) transcriptional factor and secretion of IL-17A, which is involved in the recruitment, activation and migration of neutrophils by inducing the production of colony-stimulatory factors (CSF) and CXCL8 by both macrophages and tissue-resident cells (Annunziato *et al.*, 2012). The actions of Th17 cells were initially described in their function to clear extracellular pathogens such as fungi but recently their role in inflammatory and autoimmune diseases through secretion of potent pro-inflammatory cytokines such as IL-26, IL-22, IL-6, IL-1 and TNFα have been uncovered (Wang *et al.*, 2016) (**Figure 1.7**).

Th1 and Th2 show some plasticity when they are partially differentiated but they seem to be more stable when fully differentiated and in a state of dichotomy to each other where, if one is predominant, the signalling pathway for the other is downregulated. In contrast to Th1 and Th2, Th17 cells are highly plastic throughout their entire differentiation and are able to switch into either Th1 or Th2 under the induction of IL-12 or IL-4 respectively (**Figure 1.7**) (Peck and Mellins, 2010). Th1/Th2 phenotypes derived from naïve CD4+ are often described as ‘classic’ whilst Th1/Th2 phenotypes derived from Th17 cells are described as ‘non-classic’ (Maggi *et al.*, 2012). Factors such as IL-12, IL-23, TNF-α and IL1-β activate T-bet transcriptional factor in Th17 cells, stimulating them to produce IL-17, IFN-γ and GM-CSF and acquire features of Th1 cells but retaining the Th17-cell surface marker CD161, and as such are termed Th17/Th1 cells (**Figure 1.7**). To complicate matters further, longer induction with IL-12, IL-23, TNF-α or IL-1β may lead to the loss of IL-17, GM-CSF and IFN-γ secretion but increased expression of IL-23R whilst maintaining CD161, forming what is known as the ‘non-classical Th1’ phenotype (Annunziato *et al.*, 2007b; Mazzoni *et al.*, 2019) (**Figure 1.7**).

Th17/Th1 and non-classical Th1 cells have been detected increasingly in different inflammatory and autoimmune diseases such as rheumatoid arthritis, multiple sclerosis, Crohn’s disease and psoriasis (Kamali *et al.*, 2019). They have important roles in many processes that were previously thought to reflect the activities of Th1 cells. Xie *et al.*, investigated the presence

of Th1 and Th17 cells through their expression signature cytokines IFN-γ and IL-17, respectively, in the tissue of 40 OLP patients and 15 healthy controls using double immunofluorescence staining of leukocytes by flow cytometry and in serum by ELISA. Their findings showed an overabundance of both Th1 and Th17 phenotypes in OLP, suggesting the presence of a mixed Th population. These authors also observed higher IL-17 secretion in the erosive compared to reticular form of OLP (Xie *et al.*, 2012). Indeed, elevated secretion of IL-17 by Th-17 cells has been observed in several oral diseases where it is thought to play a key role in oral immunity (Abusleme and Moutsopoulos, 2017).

Piccinni *et al*., investigated the role of Th17, classical Th1, non-classical Th1, Th2, in patients with OLP and showed that IL-17 was specifically expressed by Th17 cells in OLP lesions with particularly high levels observed in erosive forms, while gene expression of the Th2-related molecules, GATA3 and IL-13, were more associated with the reticular form (Piccinni *et al.*, 2014). Further immunohistochemical studies by Monteiro *et al*., also found increased IL-23 (a cytokine known to aid transcriptional expression of IL-17 by Th17 cells) and IL-17 expressing lymphocytes in OLP lesions compared to controls, with significantly higher levels of IL-23 in erosive compared to reticular forms (Monteiro *et al.*, 2015). Similarly, Lu *et al*., also observed elevated levels of IL-17 and IL-23 in OLP lesions compared to control mucosa, but with predominance this time in the reticular form (Lu *et al.*, 2015). More studies examining the recruitment and cellular interactions of Th-17 cells in OLP are required to fully understand the importance of this Th subtype in disease pathogenesis.

1.3.10 Other T cell phenotypes in OLP

In addition to Th1, Th2 and Th17, evidence is now emerging that other Th subsets have an involvement in OLP pathogenesis. For instance, CD4+ T cells secreting IL-4, IL-5 and IFN-γ have been recognised and are referred to as Th0 cells (Firestein *et al.*, 1989) (**Figure 1.7**). These cells synthesize multiple cytokines and are responsible for effects intermediate between those of Th1 and Th2 cells, or even a precursor of Th1 and Th2 cells. Using co-expression of IL-4, IL-5 and IFN-γ as a cytokine signature, Piccinni *et al*., observed the presence of Th0 cells in OLP lesions, where, like Th-17 cells, their increased numbers were associated with the erosive rather than reticular form (Piccinni *et al.*, 2014).

Th9 cells are reprogrammed from Th2 following induction with TGF-b and IL-4 (**Figure 1.7**). Th9 cells produce IL-9 and, similar to Th2, can be inhibited by Th1-related cytokines (Veldhoen *et al.*, 2008). Wang *et al*., measured intracellular IL-9 and IL-17 by flow cytometry following isolation of CD4+ lymphocytes from peripheral blood mononuclear cells of OLP patients. They reported significantly elevated numbers of Th9 cells (CD4+/IL-9+/IL-17-) in the

peripheral blood from patients with reticular OLP, while elevated numbers of Th17 cells (CD4+/IL-9-/IL-17+) were observed in erosive types (Wang *et al.*, 2017). In a more recent study, gene expression of IL-9 was found to be increased in OLP lesions compared to healthy controls, and interestingly was more abundant in erosive compared to reticular OLP lesions. Co-culture of peripheral blood CD4+ cells with keratinocytes isolated form OLP patients *in vitro* increased the proportion of both Th9 and Th17 cells within the T cell population, suggesting that OLP keratinocytes can support the differentiation of both cell types simultaneously. Moreover, culture of CD4+ cells with recombinant IL-9 increased the levels of Th17 cells in the T-cell population and increased secretion of both IL-17 and MMP-9, indicating a direct effect of Th9 cytokines on Th17 activation. IL-17 was also shown to induce mRNA and protein production of MMP-9 by keratinocytes isolated from OLP patients (Wang *et al.*, 2018). These data suggest an interplay between Th9 and Th17 cells that may drive OLP pathogenesis to more aggressive and chronic forms of the disease via basement membrane destruction, but more data is required to test this hypothesis, indeed, as yet there is no direct evidence for the presence of Th9 cells in OLP tissue.

Th22, an IL-22 cytokine-producing Th cell, have been detected in some inflammatory and autoimmune diseases but their exact role in the immune pathogenesis is not yet fully understood (Hofmann, Kiecker and Zuberbier, 2016). Elevated levels of IL-22 have been detected in OLP lesions compared to heathy controls (Chen *et al.*, 2013; Shen *et al.*, 2016). There is scarcity in the literature regarding the role of Th22 in OLP, however, IL-22 has been shown to induce secretion of several pro-inflammatory molecules by keratinocytes in a STAT3-dependent mechanism and also inhibit keratinocyte differentiation whilst inducing cell migration and hyperplasia (Boniface *et al.*, 2005). Therefore, IL-22 secretion by Th22 cells may play a role in pathogenesis in terms of hyperkeratosis or the remission phases of OLP where erosive lesions undergo wound healing (Wang *et al.*, 2016).

1.3.11 Tregs roles in exacerbation and remission

Tregs differentiate from naïve T cells under the influence of IL-2, TGF-ß, and IL-10 whereupon they express transcription factor forkhead box P3 (FoxP3) and release anti-inflammatory cytokines such as TGF-b, IL-10, and IL-35 to suppress T cell activation (Gouirand, Habrylo and Rosenblum, 2021) (**Figure 1.7**). Increased numbers of FoxP3+ cells in OLP lesions inversely correlated with OLP severity, with highest numbers found in reticular than erosive forms (Tao *et al.*, 2010). The low number of Tregs in the chronic, erosive phase of OLP indicate that a high ratio of activated T cells to Tregs as well as the high levels of pro-inflammatory cytokines may alter Tregs function, prevent T cell resistance to apoptosis and cause T cell accumulation in the tissue (Lei *et al.*, 2014; Tao *et al.*, 2010). In contrast, Pereira *et al*., reported

no significant difference in the numbers of FoxP3+ cells between reticular or erosive OLP lesions (Pereira *et al.*, 2012). The opposing role of Th17 and Tregs to each other besides their close relationship to different Th subsets in terms of plasticity, differentiation and function has led to the hypothesis that Tregs and Th17, along with Th1 cells, may play a pivotal role in regulating the immune response in OLP (**Figure 1.8**). Different environmental factors may cause fluctuations in cytokine levels that can lead to periods of T cell-mediated mucosal damage, which could be reflected clinically as periods of remission and exacerbation of the disease. Current knowledge supports the likely hypothesis that the strong inflammatory process in the acute phase of OLP is promoted by Th17/Th1, or non-classical Th1, while a change in the microenvironment may promote Tregs or even the Th2 to suppress the actions of Th17 or Th1 respectively (**Figure 1.8**). More studies are needed to phenotype CD4+ subsets at different stages of the disease. Investigating the role of these lineages and how they are activated or supressed might provide an understanding of the immune mechanism in OLP and facilitate the development of therapeutic strategies to interpose the deleterious T cell responses.

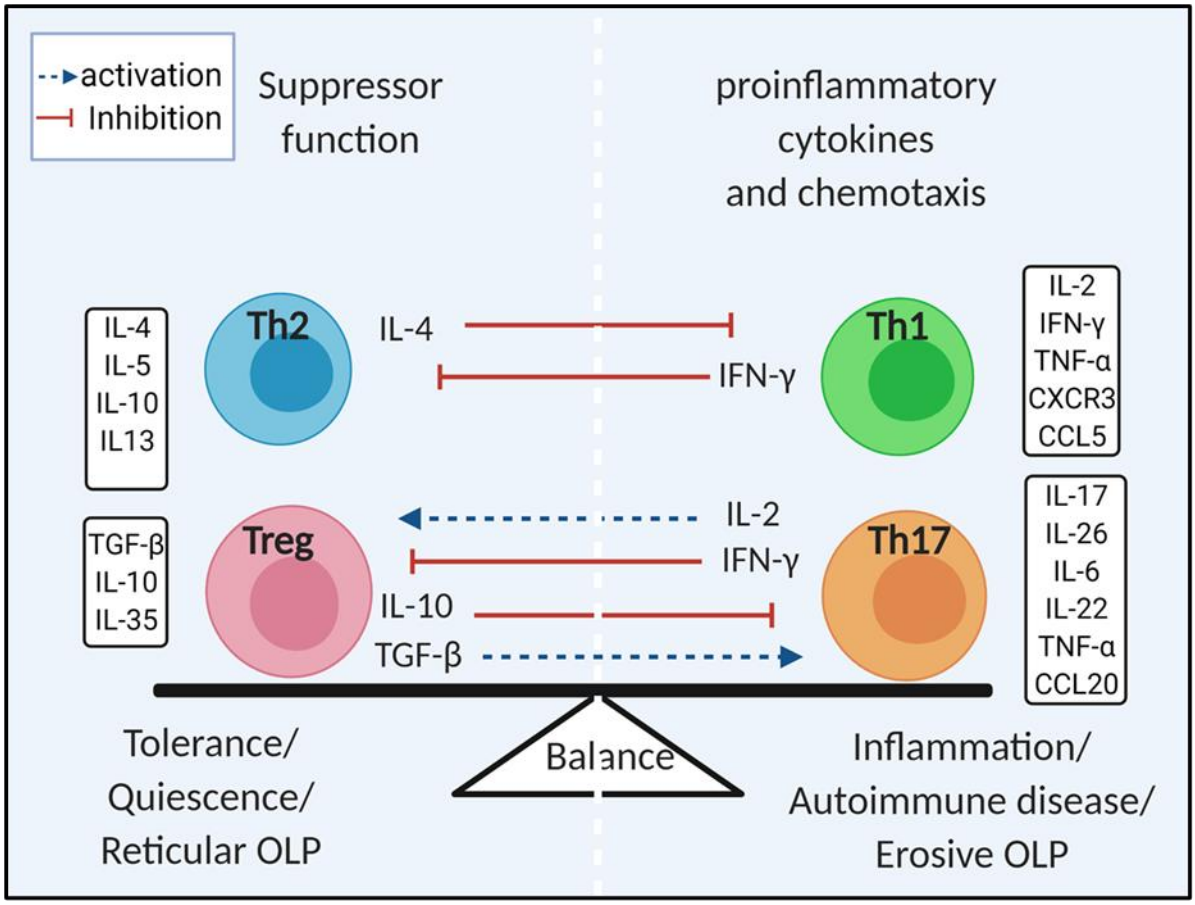

Figure 1.8: A schematic diagram illustrating the conceptualised role of Th17, Th1, non- classical Th1, Th2, and Treg subsets in the pathogenesis of erosive and reticular types of OLP. The make-up of cytokines within the local microenvironment regulates the type T cell phenotype and their number in OLP lesional sites. Th1/Th17 favouring microenvironments tip the balance in favour of chronic inflammation and erosive lesion whilst cytokines that favour Tregs and possibly Th2 T cells favour regression or less aggressive reticular forms. Created in BioRender.com.

Experimental data thus far suggests a complex interplay between non-immune cells at the oral mucosal lesional site and an array of predominantly T cell infiltrates of various subtypes that may fluctuate in number and spatial location (sub/intra-epithelial) as the disease progresses. It is likely that some of the identified Th cell subtypes display plasticity and can respond to changing micro-environmental cues at lesional sites by secreting cytokines and changing cell surface receptor profile, thereby moving from one phenotype to another. It is also likely that the proportion of T cell subtypes and levels of cytokines may tip the balance in favour or against pathogenesis or the type or chronicity of the OLP lesion. To gain a greater understanding of the role of different Th subsets in OLP it would be invaluable to identify distinct Th subsets using standardised antibody panels for each phenotype with multichromatic immunostaining utilising WHO diagnostic criteria defined OLP lesional tissue to examine pathogenesis more directly as opposed to examination of serum or peripheral blood leukocytes that could be subject to the influence of inflammatory lesions elsewhere in the body. Development of advanced tissue engineered oral mucosal models to include T cell subsets would aid in delineating the molecular mechanism that drives pathological outcomes.

1.3.12 Management of OLP

OLP has variable clinical presentations and different natural courses and may require different treatments. There is no definitive cure for OLP, and the main aim in management is to relieve symptoms, control exacerbation and reduce the risk of malignant transformation. The treatment should be personalised to each patient depending on the status, age, pattern, and symptoms. Asymptomatic patients do not generally require treatment. Patients with the atrophic, ulcerative, or bullous type of OLP may experience symptoms ranging from burning sensation and discomfort to severe pain and they require treatment (Odell, 2017; Scully and Carrozzo, 2008). Because of the chronic nature of the disease, patients should be monitored and their medical history, psychological status, treatment compliance should be regularly evaluated. Possible drug interaction should be evaluated. However, spontaneous remission or quiescent phase has been reported in 40% of patients with reticular type.

It is important to advise patients to keep high standards of oral hygiene to enhance healing. Calculus and plaque are associated with high rates of inflamed gingival lesions in OLP. Also, it is essential to instruct the patient to avoid any irritant or potential exacerbating factors, such as acidic, spicy, crunchy, or hot food. They should be advised to use sodium lauryl sulphate (SLS)-free toothpaste and alcohol-free chlorhexidine mouthwash. Any causes of mucosal trauma or injury should be treated such as a sharp tooth cusp. Moreover, OLP patients should be informed on the very small risk of malignant change that OLP may undergo and hence, they

should be encouraged to moderate alcohol intake, smoking cessation, and avoid any other carcinogens (Scully and Carrozzo, 2008; Field and Longman, 2003).

Topical analgesic can be used to relieve pain and discomfort associated with erosive and ulcerative OLP such as Benzydamine mouthwash or spray (Difflam). Topical steroids are the mainstream for treating mild to moderate OLP. For patients who fail to respond to topical steroids or can not tolerate steroid sparers, use of systemic steroids is considered. Usually, therapy is effective in the first two weeks duration and then a gradual tapering is recommended to avoid adrenal crises. Azathioprine is prefeered to cyclosporin as a third line of treatment if steroids failed or were contraindicated (Scully, 2008a). Supportive psychological care is required for some patients, because of the chronic nature of the disease and treatment. Also, due to the unpredictable prognosis and exacerbations increased the vulnerability of these patients to depression, anxiety and psychological disorders (Lodi *et al.*, 2005; Scully, 2008b).

1.3.12.1 Corticosteroids

Glucocorticoids are the first line treatment of OLP as they reduce pain and inflammation by reducing lymphocytic exudate and stabilizing lysosomal membrane, but the response varies from one person to another. Topical steroids are preferable because the location of OLP lesion is accessible for topical application and due to the fact that systemic use of steroids carries the risk of developing steroid-induced side effects (Lavanya *et al.*, 2011). Corticosteroids are well known for their high risk of adrenal suppression (Stanbury and Graham, 1998). Even though topical steroids are considered safe, adrenal suppression has been reported in long-term use of potent corticosteroids (Decani *et al.*, 2014; Levin and Maibach, 2002). Reports of minor side effects of topical steroid are attributed to either direct absorption of potent steroid through the oral mucosa or by ingestion after incorrect use. The following side effects have been reported with a topical corticosteroid such as moon face and hirsutism, nausea, dry mouth, sore throat, oral candidiasis, bad taste and smell with clobetasol propionate 0.05% mouthwash or fluticasone propionate spray (Gonzalez-Moles *et al.*, 2002; Hegarty *et al.*, 2002). Oral candidiasis can be treated by the use of antifungal treatment in conjunction with corticosteroid therapy (Thongprasom and Dhanuthai, 2008). However, many studies and clinical trials reported that topical steroids are unlikely to cause serious side effects when treating oral lesions (Al-Hashimi *et al.*, 2007).

1.3.12.2 Topical Corticosteroids:

Different formulations of drugs and protocols have been used and investigated, but there is no consensus on one formula to be more effective than the other. Topical steroids have been prepared in a variety of formulations such as solution, adhesive paste, base, ointment, gel, and

intra-lesional injection. Ointments and gels have been used for lip lesions and accessible areas within the oral mucosa. An adhesive paste was used for localised lesions in the oral mucosa (Lavanya *et al.*, 2011). Adhesive paste applied using a custom-made tray was used to treat gingival and palatal lesions and proved to be effective and safe (Thongprasom and Dhanuthai, 2008). There is no evidence to confer whether adhesive vehicles are better than mouth rinses, but empirical evidence shows that mouth rinses are beneficial in patients with widespread symptomatic OLP, or when the lesions are not easily accessible to apply ointments or gels (Al-Hashimi *et al.*, 2007). An intralesional injection was associated with pain during injection and mucosal atrophy, however, they were beneficial in treating localized recalcitrant lesions (Farhi and Dupin, 2010). Adhesive forms were preferred to keep the drug in contact with oral mucosa for a longer period before it is washed away with saliva or absorbed. However, there is no clear evidence to show higher efficacy with adhesive base form when compared with other forms (Thongprasom and Dhanuthai, 2008; Lavanya *et al.*, 2011).

Different potencies of drugs have been used, from moderate to super-potent formulas. The choice of level of potency and concentration depends mainly on the severity of the lesion and experience/ preference of the clinician. Drugs range from mid-potency corticosteroids such as triamcinolone acetonide, to high potent such as fluocinonide acetonide, disodium betamethasone phosphate, and super-potent such as clobetasol propionate (Lavanya *et al.*, 2011).

Commonly used drugs in term of decreasing potency include 0.05% clobetasol propionate gel, 0.1% or 0.05% betamethasone valerate gel, 0.05% fluocinonide gel, 0.05% clobetasol butyrate ointment or cream, and 0.1% triamcinolone acetonide ointment. For more widespread severe cases application of topical gel or base could be very uncomfortable and hence, solution drugs are recommended as 1.0 mg/mL aqueous triamcinolone acetonide or 0.1 mg/mL dexamethasone elixir to be used as a rinse for 2-3 minutes and to be expectorated. For more extensive or recalcitrant cases intralesional corticosteroid injection is considered as 0.2–0.4 mL of a 10 mg/mL solution of triamcinolone acetonide (Edwards and Kelsch, 2002). Evidence also suggests that higher potency corticosteroids, such as clobetasol are probably more effective. Another protocol of treatment was recommended by Sugerman *et al* and includes the use of betamethasone propionate ointment 0.05% 3-4 times a day for the treatment of localized oral lesions, 0.25 mg dexamethasone mouth rinse twice daily for generalized oral lesions, and the use of 10 mg/ml triamcinolone acetonide intralesional for persistent localized erosive OLP lesions (Sugerman *et al.*, 2000). Two forms of triamcinolone acetonide 0.1% (mixed with Orabase and as a mouthwash) were categorized as class I (useful and effective). Other topical steroids (clobetasol propionate ointment, fluocinonide acetonide 0.1% in Orabase or

0.05%) were categorized as class IIA (evidence and opinion in favour of usefulness) (Al-Hashimi *et al.*, 2007).

The current mainstay OLP treatment is the use of topically applied corticosteroids such as mouthwashes. These application forms suffer from short mucosal contact times and inadvertent contact with the surrounding healthy mucosa. New drugs dosage forms include mucoadhesive polymer-based patches pre-loaded with corticosteroid (Edmans *et al.*, 2020). These patches adhere for long periods to the oral mucosa and offer drug delivery directly to the lesion over a number of hours. Colley et al, incorporated Clobetasol-17-propionate into the novel mucoadhesive electro-spun patches and performed pre-clinical studies which showed that Clobetasol-17-propionate was released in a sustained manner in both tissue-engineered oral mucosa and ex vivo porcine mucosa. They further demonstrated prolonged adhesion and drug release at therapeutic-relevant doses and time points *in in vivo* animal models (Colley *et al.*, 2018). Clobetasol in these electro-spun patches has been shown to traverse the epithelium and inhibit T cell cytokine production in a rudimentary model of OLP using tissue engineered oral mucosa and activated T cells and so are an improvement on current treatments (Said *et al.*, 2021; Colley *et al.*, 2018). Recently, these patches which are now produced by the AFYX therapeutic and commercially known as Rivelin® -CLO patch have met their primary end point in a randomised double-blind, placebo controlled, phase 2 clinical trials in 138 symptomatic erosive OLP patients. The treatment with 20 µg Rivelin® -CLO has produced significant improvement in the ulcer area, disease activity, and quality of life (Brennan *et al.*, 2022).

1.3.12.3 New molecular targets for OLP therapy

Understanding immune dysregulation in OLP will inevitably highlight molecules that can in turn be targeted by new therapeutics. One approach is using specific small molecule antagonists or humanised monoclonal antibodies to inhibit the actions of cytokines such as IL-1, IFN-γ and TNF-α. For example, TNF-α inhibitors such as etanercept, infliximab and adalimumab, all of which are FDA approved for treating psoriasis and work by blocking TNF-α binding to the cell surface receptor TNFR1 (Zhang *et al.*, 2011). Hence, TNF-α inhibitors constitute a promising therapeutic for OLP. However, this may not be straightforward as there is evidence of development of an OLP-like lesion in patients treated with infliximab for psoriasis and other inflammatory diseases (Asarch *et al.*, 2009). Blockade of T cell costimulatory molecules may also present a potential target for treatment. Inhibition of CD40-CD40L interactions using an anti-CD40L monoclonal antibody was shown to prevent secretion of IFNg, IL2 and IL-12 by Th1 cells in favour of the Th2 cytokines IL-4 and IL-10 in a murine model of allograft rejection (Hancock *et al.*, 1996). A similar approach for OLP may counter-balance T cell phenotype against lesion development. Since adhesion molecules are involved in immune

cell recruitment to lesional sites, antibodies targeting these molecules may unlock new treatment strategies. Likewise, inhibiting the CCL5-CCR5 axis by blocking CCR5 using Maraviroc could provide therapeutic potential in OLP treatment. Here, Shan *et al.*, showed that T cell proliferation and migration were suppressed while T cell apoptosis was enhanced (Shan *et al.*, 2019). Similar therapies may also work for other chemokines, such as interruption of the CXCL10/CXCL9-CXCR3 axis, although the effects of this type of therapy on leukocyte recruitment in homeostasis or infection may be problematic.

CD8+ T cells are critical perpetrators of inflammatory diseases that have been largely overlooked as most biological therapies target pathways of CD4+ T cell subsets. For instance, the selective expansion and targeting CD4+FOXP3+ Tregs has shown effective therapy or retro-conversion in experimental models of several inflammatory/autoimmune-related disorders (Beyersdorf *et al.*, 2005). However, emerging evidence shows that different subsets of CD8+ T cells exist including suppressor or regulator CD8+ T cells that are able to reset an autoimmune response and protect the host (Xu *et al.*, 2016). There is uncertainty regarding the mechanism by which they control immunity but they constitute a promising therapeutic target that could be approached through T cell transfer therapy or modulating their numbers and activity with novel immune modulators (Konya, Goronzy and Weyand, 2009).

The use of recombinant cytokines (IL-4, IL-10, and TGF-ß) that down-regulate the immune response may also be useful. Enhancing IL-4 production to suppress IFN-γ secretion and Th1 development supports the notion that skewing the T cell response towards the Th2 lineage may be a candidate for autoimmune therapy by suppressing the excessive immune response mediated by IFN-γ in erythematous/ulcerated OLP lesions (Tao *et al.*, 2008). On a similar note, the anti-inflammatory IL-10 is considered to play a role in controlling the progression of OLP by blocking pro-inflammatory cytokine synthesis and inhibiting both the proliferation and cytokine secretion of Th1 cells and so this cytokine may be a promising therapeutic target. Weak expression of the immune suppressive cytokine TGF-b has been reported in OLP; since TGF-b negatively modulates IFN-γ and favours phenotyping toward FoxP3+ Tregs use of exogenous recombinant TGF-b may favour disease regression. On a similar notion, preventing the actions of IFN-γ and its ability to increase MHC expression on keratinocytes might be targeted through inhibition of STAT1 and Janus kinase 2 (JAK2) transcriptional factors. Indeed, results of a recent *in vitro* study support targeting downstream IFN-γ signalling through STAT1/JAK2 inhibition using JAK inhibitors as a therapeutic approach in OLP (Shao *et al.*, 2019). Further studies are required to show the possibility of targeting different transcriptional factors involved in OLP pathogenesis. Selective and targeted biologics may provide a new therapeutic perspective in the management of OLP, but the immune regulation is very complex so blocking a specific receptor/signalling pathway or cytokine may

not be enough in this multifactorial pathogenesis. Also, one cytokine may have several roles and so there may be off-target effects that may enhance disease progression rather than hinder it.

Research over many years has increased our knowledge of OLP, yet new research continues to develop our understanding, especially with regards to identification of OLP-promoting antigens and specific T cell subsets that act in a dynamic and complex manner. Future research to define these mechanisms in more detail will lead to the repurposing of drugs or the development of new therapeutics aimed at inhibiting the disease process. However, the use of animals to model OLP in research is limited by ethical concerns and the scientific concern of the relevance of these models to replicate human OLP given the disparity between the immune systems of humans and rodents. These restrictions and the lack of effective *in vitro* models for OLP have highlighted the importance of developing novel *in vitro* tissue-engineered human oral mucosal equivalents containing immune cells that accurately replicate *in vivo* OLP tissue.

1.4 Experimental models

1.4.1 Animal models

Animals can closely represent the complex physiological interactions needed in experimental models, but they are still different from human tissue, and they are expensive. Moreover, public concerns over animal rights and extensive and sometimes unnecessary animal experimentation call into question the ethical justification for over-use of these animal systems (Freshney, 2015). Hence, *in vitro* models represent an alternative option that is human and aligns to the 3R's (reduction, refinement, and replacement of animal in research).

1.4.2 Two-dimensional culture (monolayer)

In 2D culture, cells grow as a single monolayer attached to a coated substrate (adherent monolayer) or in suspension. An adherent monolayer is common to most cell types while suspension cultures are used for cells that can grow and proliferate without the need for attachment and includes many hematopoietic cells.

1.4.2.1 Advantages of 2D tissue culture

2D cultures are generally well-established *in vitro* systems for culturing cells. They are typically less expensive to perform than in vivo research, easier to manipulate and analyse, and the richness of data in the field make it easy to compare new experimental data with the existing literature. Moreover, this system is efficient for studying numerous types of cell behaviour

including proliferation, respiration, signal transduction or the transcription of genes and secretion of proteins (Freshney, 2015).

Most human cell types can be cultured in 2D. Cells isolated directly from patients (primary cells, e.g., oral keratinocytes) are often most problematical as they usually have a short lifespan and often require complex defined medium. Therefore, regular collection of human tissue is required, and this is often in short supply. Primary cells can be immortalised by ectopic expression of human telomerase reverse transcriptase (hTERT) (for example primary buccal keratinocytes to form the FNB6 cell line) (Dickson *et al.*, 2000). Immortalised cells closely mimic primary cells but their lifespan is substantially extended facilitating prolonged culture, increasing their usefulness. Most laboratories use immortal cells in the form of cancer cells. These are initially patient-derived, but their oncogenic phenotype and DNA mutations means that they can grow continuously in culture for many, many generations and their growth often require less stringent medium formulations. Consequently, cancer cells have been the mainstay cell type for most *in vitro* experiments

1.4.2.2 Limitations of 2D tissue culture

Many differences exist between 2D cultured cells and cells *in vivo*, mostly because cells that have been dissociated from a 3D configuration *in vivo* into a 2D structure lose important cell to cell contacts, interactions and stimulation as cells cultured in isolation in static conditions. Systemic regulations are lost in cell culture including the nervous and endocrine systems (Castells-Sala *et al.*, 2013), although these differences are recognised and replaced by the addition of growth factors and hormones to culture media, to represent more native environments (Freshney, 2015).

1.4.3 Three-dimensional tissue culture

Recognising the differences between *in vivo* and *in vitro* cultured cells has driven increasing efforts for the reconstruction of 3D structures that mimic human tissue. Maintaining a physical geometry for the cells that resemble the *in vivo* structure has been shown to enhance their function, structure and make extrapolation to *in vivo* results more accurate and relevant (Freshney, 2015).

1.4.3.1 Advantages of 3D tissue culture

For cells cultured in 3D, cell-cell contact, and signalling enhances cell growth and differentiation; for example, in the skin, the epidermal proliferation depends on KGF and EGF signals coming from the dermal fibroblasts which in turn respond to signals from the epidermal

keratinocytes. Moreover, this paracrine signalling stimulates the release of extracellular matrix components that, in turn, aid epithelial differentiation (Maas-Szabowski, Stark and Fusenig, 2002). 3D geometry facilitates diffusion gradients of oxygen and nutrients that are required to maintain mature cell populations (Castells-Sala *et al.*, 2013). Thus, 3D cultures achieve the requirement for *in vitro* methods that permit a precise study of the molecular mechanisms underlying human diseases and enable better extrapolation of drug and therapeutic assessment.

1.4.3.2 Limitations of 3D tissue culture

There are certain limitations in using 3D models. One very well-known problem is the lack of a circulatory system which limits growth of cells to a few hundred microns, attributed to the limited diffusion of nutrients, oxygen, and removal of waste product from and to the cells via culture medium. Cells *in vivo* have overcome a similar diffusion capacity by the presence of the dense capillary network. Hence, efforts are being made to employ a sophisticated 3D scaffold technique with culture under flow conditions that overcome these diffusion limitations (Dunn *et al.*, 2006). Another limitation of using 3D models is the difficulty of analysing and monitoring such a complex model throughout the culture period. Setting up 3D model is also considered more expensive and technically challenging when compared to 2D culture (Freshney, 2015).

1.4.4 Scaffolds in tissue engineering:

A scaffold to replicate connective tissue is an important and critical component in constructing a 3D model as it is needed to recreate a similar physical, chemical, and mechanical features to that *in vivo*. Two main types of scaffolds have been categorised according to their origin; natural and synthetic scaffolds (Castells-Sala *et al.*, 2013). Natural scaffolds are preferred for their biocompatibility and biodegradability (Berthiaume, Maguire and Yarmush, 2011) and many have been used for the construction of tissue-engineered *in vitro* oral mucosal including de-epidermalised and de-cellularised dermis (DED)(Izumi *et al.*, 1999; Ponec, 1991), purified type I collagen-based scaffold (Isaac *et al.*, 2012), gelatine (Hoque *et al.*, 2015; Paguirigan and Beebe, 2006), and Fibrin-based scaffolds (Del Rio *et al.*, 2002).

Collagen is considered a naturally acquired matrix in which cells have been seen to grow and penetrate and it is the most common protein in connective tissues. Although there are about 30 types of collagens, type I collagen is the main type produced by the fibroblast to support fibroblast growth and function and their tensile strength is mainly responsible for physical characteristics and support of tissues (Harkness, 1961). Hence, collagen has been used to provide a similar framework for cells *in vitro.* Collagen is biocompatible and remodelled by fibroblasts causing its contraction. However, the level of contraction depends on factors like the

number of seeded cells and collagen concentration and therefore, can be modified. Different types of collagens have been used in tissue engineering. Fibrillar and non-fibrillar collagen can be isolated from animals including bovine and rat tail collagen (Isaac *et al.*, 2012; Szot *et al.*, 2011) in the forms of hydrogels, sponges, and lattices. Hydrogels, in particular, are advantageous as they can be easily populated with cells and moulded into a required tissue shape (Freshney, 2015; Wolf *et al.*, 2009).

Synthetic materials used in tissue engineering include polystyrene (Alvetex) include polyethylene terephthalate membranes (PET membranes), polycarbonate-permeable membranes (PC membranes), and porous polylactic glycolic acid (PLGA) (Moharamzadeh *et al.*, 2007). However, they are far from ideal for many tissue engineering applications, mainly because the hydrolytic biodegradation process releases acid, which can be toxic to cells (Berthiaume, Maguire and Yarmush, 2011).

1.4.5 The development of tissue engineered models

Over the last few decades tissue engineering has developed as a new discipline and has offered promise for its principles and techniques to be applied to *in vitro* 3D models. Escalating ethical and legal regulations for using human tissue led to the increasing demand for *in vitro* models, in particular for drug/chemical permeation and penetration studies and to improve wound and burn healing strategies. In an attempt to study cells in a more *in vivo*-like environment, Ehrmann and Gey, described the mechanism of reconstituting rat-tail collagen into a transparent gel to be used as the stratum for cell growth and study (Ehrmann and Gey, 1956). In 1972, Elsdale and Bar described the use of a collagen lattice as a three-dimensional substrate for culturing fibroblasts to study their behaviour (Elsdale and Bard, 1972). Moreover, in 1979 Bell *et al*., introduced the fibroblast-populated collagen lattice as a dermal equivalent model and reported the phenomena of *in vitro* collagen contraction that resembles *in vivo* wound contraction. They examined the *in vitro* contraction and suggested that the lattice can serve as substrate for epidermal cells and the contraction can be regulated by the protein content, cell numbers and by adding inhibitors like colcemid (Bell, Ivarsson and Merrill, 1979).

Further efforts were made to develop an epidermal equivalent. A cultured graft of epithelial sheet was developed to be used as an alternative to skin and oral mucosal autografts (Lauer, 1994; Madden *et al.*, 1986). Although, the use of epithelial sheets in clinical applications suffered problems such as being thin, fragile and hence, difficult to handle, they were widely used for clinical applications (Moharamzadeh *et al.*, 2007). The use of *in vitro* skin equivalent models for clinical applications like burn repair has been investigated and enhanced by different studies (Gobet *et al.*, 1997; Limat *et al.*, 1989; Markeson *et al.*, 2015).

The work towards an equivalent full thickness skin/oral model was an inevitable chronological scientific evolution. After the keratinocyte and fibroblast crosstalk and reciprocal activation was demonstrated by Maas-Szabowski et al (2000) and Werner and Smola (2001), the important role of the fibroblast for the morphogenesis, adhesion, proliferation of the epithelium, ECM formation, basement membrane formation, and keratin expression was established (Maas-Szabowski, Shimotoyodome and Fusenig, 1999; Maas-Szabowski, Stark and Fusenig, 2000; Werner and Smola, 2001). Organotypic cultures were developed as *in vitro* models to study the molecular mechanism of the underlying dermal-epidermal interactions in a collagen matrix (Maas-Szabowski, Stark and Fusenig, 2000). A simple 3D model was first reported by Rheinwald and Green in 1975 by co-culturing mouse teratoma with lethally irradiated murine fibroblasts (a conventional feeder layer of 3T3 fibroblasts) to establish the first differentiated keratinised stratified squamous cell model. These studies also suggested that the interaction between the epithelium and feeder fibroblast was essential for developing a stratified and differentiated epithelium (Rheinwatd and Green, 1975). This approach has since been utilised by many groups in numerous studies.

The effectiveness of fibroblasts in supporting the growth of keratinocytes was investigated by Limat et al in 1989 by using post-mitotic human dermal fibroblast to support the growth of human follicular keratinocytes. Limat *et al.*, discussed problems associated with 3T3 murine fibroblasts including poor reproducibility mainly due to degeneration and detachment after growth-arrest. Hence, post-mitotic human dermal fibroblasts prepared by irradiation or mitomycin C treatment were used to obtain reproducible results. Also, this method, which used a feeder layer of the same species had advantaged over Rheinwald and Green's method which used a mouse cell line (Limat *et al.*, 1989).

The unavailability of human tissue led to the use of animal cultures at that time (Hoogstraate and Bodde, 1993). Another example was the use of primary cell culture derived from the hamster cheek pouch mucosa that was developed to study drug transport and metabolism (Tavakoli-Saberi and Audus, 1989). In an attempt to produce reproducible and easily accessible human mucosal 3D models, human TR146 keratinocytes, which are non-keratinised epithelium cell line derived from oral buccal squamous cell carcinoma metastasis, were used. The potential usefulness of such a cell line in modelling the human buccal epithelium permeation of drugs was investigated by Jacobsen *et al*., who reported that TR146 represented a valuable model for studying transport of drugs across the human buccal epithelium (Jacobsen *et al.*, 1995). However, it is commonly acknowledged that, when using cancer cell lines, the outcomes should be confirmed with multiple other cell lines as they may not precisely represent normal epithelial cells.

Since then, diverse developments have been made to produce skin or oral equivalent models *in vitro* by co-culturing dermal and epidermal cells, mimicking the natural tissue architecture (Limat *et al.*, 1989; Simonetti *et al.*, 1995). Stark *et al.,* suggested the use of defined medium conditions by excluding ill-defined supplements that contained variable factors and unknown compositions that interfere with physiologic interactions and compromise the clinical application of skin graft. They developed a comparable organotypic keratinocyte culture using a keratinocyte defined medium without pituitary extract and called it the supplemented keratinocyte defined medium (SKDM) (Stark *et al.*, 1999). More in-depth investigations have also been performed in three-dimensional cultures to further improve the models. For example, work towards improving the weak barrier function in the *in vitro* skin model has been attempted using a microfluidic device (organ on chip) that enhances the dynamic perfusion of nutrients and products. This has been utilised by the use of non-contracting fibrin-based dermal matrix (Sriram *et al.*, 2018).

Currently, *in vitro* reconstructed skin models are used worldwide in industrial and academic research (Netzlaff *et al.*, 2005). One of the earliest models produced were in 1991, the Testskin I and II from organogenesis, USA. It consisted of an epidermal tissue produced on a collagen lattice populated with human fibroblasts. The company then concentrated on the clinical application of the model to develop the Apligraf® which is a bi-layered bioengineered skin substitute composed of human keratinocytes and human fibroblasts in a bovine type I collagen matrix. This tissue substitute has been FDA approved and is used for the treatment of venous leg ulcers and diabetic foot ulcers. Advanced Tissue Sciences: USA, launched *in vitro* reconstructed full-thickness human skin models called Skin^{2TM}. The company stopped working on the model to concentrate on its clinical counterpart, the Dermagraft-TC.

At present, several different skin equivalents are commercially available including EpiSkin™ from Imedex (Lyon, France) that was acquired by L'Oréal in 1997. EpiSkin™ is made of a collagen hydrogel containing human fibroblasts, surfaced with a film of type IV collagen, overlaid with a fully differentiated human epidermis that, like all skin and oral models, are cultured at an air-to-liquid interface. SkinEthic Reconstituted Human Epithelium™ (also acquired by L'Oréal in 2006) are generated by seeding human keratinocytes directly onto inert synthetic filters and have no dermal component. The EpiDerm™ reconstructed skin model, was produced by MatTek Corporation, USA. This model is composed of human epidermal keratinocytes that develop a fully differentiated epidermal tissue. A full-thickness model called EpiDerm-FT™ that included both epidermal and dermal layers was alos developed by MatTek. Afterwards, a melanocyte containing epidermal model was developed and called the MelanoDerm™. In recent years a number of other commercially available models have been developed including the EST1000® skin model, the Phenion® Full-Thickness Skin Model and

the OS-Rep model, the StratiCELL® skin model, the StrataTest® skin model, the LabCyte™ skin model, and the Vitrolife-SKIN™ skin model (De Wever, Petersohn and Mewes, 2013). These models were found to reproduce many of the characteristics of normal human epidermis. However, commercially available models still have relatively weak barrier function compared to *in vivo* skin (Boelsma *et al.*, 2000; Ponec *et al.*, 2002; Netzlaff *et al.*, 2005).

1.4.6 Oral mucosal models

Similar to their skin models, SkinEthic developed oral epithelium only models, to be used in different *in vitro* toxicity tests and assays (De Brugerolle, 2007). However, several groups have now successfully created full thickness oral mucosal model composed of oral keratinocytes and fibroblasts (Masuda, 1996; Tomakidi *et al.*, 1998; Lauer and Schimming, 2001). An oral mucosal model utilising different matrix material including collagen matrix, human dermal matrix, and dermal regeneration template were developed and investigated for clinical application as intra-oral graft substitutes (Moriyama *et al.*, 2001; Kriegebaum *et al.*, 2012; Izumi *et al.*, 1999). To obtain an optimum oral mucosal model, standard characteristic criteria need to be defined, although few studies have characterised an ideal model of the oral mucosa (Rouabhia and Deslauriers, 2002). A reproducible characterised tissue engineered oral mucosa was developed by A Dongari-Bagtzoglou & H Kashleva using hTERT-2 immortalized human oral keratinocytes derived from the floor of the mouth (OKF6/TERT-2) that were cultured on a fibroblast-populated collagen scaffold. The resultant epithelial layer looked like the commercially obtainable epithelial model of the TR146 cell line (SkinEthic). However, this model does not produce dyskeratotic changes and unlike TR146 model it is composed of a submucosa which makes it more representative to *in vivo* tissue (Dongari-Bagtzoglou and Kashleva, 2006a).

1.4.6.1 Characterisation of oral mucosal model

The following criteria were suggested to reflect an optimum model of the oral mucosa. First, the oral epithelium should reflect orderly stratified densely packed layers of differentiated epithelium with a polarised basal layer (Moharamzadeh *et al.*, 2007). Ultrastructure analysis by transmission electron microscopy should reveal the presence of tonofilaments network, desmosomes, hemidesmosomes and membrane coating granules (Selvaratnam *et al.*, 2001). Immunohistochemical analysis should demonstrate that epithelial cells express proliferation markers (Ki-67) and differentiation markers including cytokeratin such as K14, K19 and K10 (Rouabhia and Deslauriers, 2002). Furthermore, transmission electron microscopy of the basement membrane should demonstrate a lamina lucida, lamina densa, and anchoring fibres while immunostaining confirms the presence of collagen IV, laminin, fibronectin, and integrin (Rouabhia and Deslauriers, 2002; Moharamzadeh *et al.*, 2007). A three-dimensional model of

extracellular matrix with infiltrating fibroblast should be present in the lamina propria of 3D tissue engineered equivalents (Moharamzadeh *et al.*, 2007). Cytokine analyses using cultured supernatants showed that cells in oral mucosa equivalent (OME) secrete interleukins (IL) including IL-1β, as well as CXCL8 and TNF-α. Additionally, several metalloproteinases such as MMP-2 and MMP-9 have been identified (Rouabhia and Deslauriers, 2002). Furthermore, Selvaratnam L *et al.*, investigated whether *in vitro* models of human oral mucosa could be established with structural and functional permeability criteria parallel to the undamaged oral mucosa. They cultured normal oral buccal and palatal epithelium in the presence of Ɣ-irradiated Swiss 3T3 mouse fibroblast on collagen discs and on dead de-epidermalised dermis using Green's medium. They tested the models for morphology, permeability properties, and lipid analysis. Their overall results demonstrated that normal human oral epithelium grown in 3D *in vitro* developed criteria similar to that of the *in vivo* tissue counterpart (Selvaratnam *et al.*, 2001).

1.4.7 Tissue engineered *in vitro* disease models

There is an increasing need for better models to investigate mechanisms of pathogenesis and novel therapeutics. There is a broad spectrum of models of variable complexity consisting of multiple cell types, reconstructed human epidermis (RHS), to full thickness models composed of dermis and epidermis, and to more sophisticated skin models containing melanocytes (Hedley *et al.*, 2002), Langerhans cells (Ouwehand *et al.*, 2012), hair follicle (Krugluger *et al.*, 2005), endothelial (Black *et al.*, 1998) and other cells responding to the demands of different research or industry. Different *in vitro* models of several stages of oral cancer and dysplasia have been developed (Costea, Johannessen and Vintermyr, 2005; Gaballah *et al.*, 2008; Colley *et al.*, 2011; Wolf *et al.*, 2009). These models of oral dysplasia and carcinogenesis aided the study of the molecular mechanisms and the role of fibroblast and basement membrane in malignant transformation, tumour progression and invasion. Also, *in vitro* cancer models aided the experimentation of new diagnostic and therapeutic agents and procedures (Kulasekara *et al.*, 2009; Gaggioli *et al.*, 2007; Gaballah *et al.*, 2008). Moreover, *in vitro* oral mucosal models were used to study the pathogenesis of oral candidiasis (Dongari-Bagtzoglou and Kashleva, 2006b).

There is a general interest to incorporate immune cells within a 3D model aimed to study mechanisms involved in local inflammatory processes. Although significant advances have been made in the development of tissue engineered model, there are relatively few studies that have reported development of immune models in the literature. One such study cocultured peripheral blood mononuclear cells (PBMCs) in a mucosal model showed increased inflammatory markers when compared to models without PBMCs following irradiation with X-rays or 12C heavy ions to investigate the risk of developing radiation-induced mucositis

(Tschachojan *et al.*, 2014). Polymorphonuclear leukocytes have also been incorporated in reconstructed human oral epithelium only model to assess defence against *Candida albicans* infection (Schaller *et al.*, 2004).

Monocyte-derived-macrophages have been incorporated into 3D dermal scaffold with fibroblasts alone (no epithelium) (Bechetoille *et al.*, 2011; Smith *et al.*, 2021) and another study used these cells in a vaginal mucosal model (Saba *et al.*, 2021). Recently, an immune-responsive oral mucosal model containing primary monocyte-derived-macrophages was reported where these cells were shown to respond to lipopolysaccharide in situ and secrete inflammatory markers such as TNFa (Ollington, Colley and Murdoch, 2021). The promonocytic cancer cell line, THP-1 cells, were polarised into M1 and M2 phenotype and incorporated into a 3D model of oral carcinoma to assess the effect of tumour associated macrophages on tongue cancer (Pirilä *et al.*, 2015; Tedesco *et al.*, 2018). Other monocytic cell lines such as U937 and MM6 were differentiated into MDM and incorporated in 3D gingival model to investigate their responsiveness to external bacterial stimuli (Morin and Grenier, 2017; Bao *et al.*, 2015).

Regarding dendritic cells, oral mucosa and skin equivalents constructed on fibroblast populated collagen gels and co-seeded with MUTZ-3, Langerhans-derived cell line, were compared regarding secretion of cytokines and chemokines involved in LC migration and general inflammation (Kosten *et al.*, 2015). Moreover, MUTZ-3-derived Langerhans cells were incorporated in Reconstructed human gingiva (RHG) and reconstructed human skin which were incorporated into organ-on-chip to investigate metal systemic toxicity and dendritic cells activation (Koning *et al.*, 2022). A reconstructed skin with MUTZ-3 was also used to investigate the effect titanium salts (Rodrigues Neves *et al.*, 2020). Langerhans cells were added into pigmented reconstructed human epidermis (Régnier *et al.*, 1997) and added to skin equivalent with DCs to assess UV associated damage (Bechetoille *et al.*, 2007).

The research described in this thesis is focussed on the development of novel tissue engineered models of OLP. Although there are no reports of *in vitro* or animal models of OLP, a murine model of lichenoid tissue reaction (LTR), an inflammatory mucocutaneous diseases that shares characteristic histopathological features of OLP, has been established. For example, injection of heterologous CD8+ T cells induced a LTR in human skin xenografted into immunodeficient (Christofidou-Solomidou *et al.*, 1997) and in naïve mice (Mehling *et al.*, 2001). Also, transgenic mice have developed a LTR reaction after CD8+ T cell transfer (Azukizawa *et al.*, 2003). There is a wide range of diseases with LTR features such as systemic lupus dermatitis, mixed connective tissue disease, Steven Johnson syndrome/toxic epidermal necrosis, acute graft versus host disease, and LP which is considered a typical mucocutaneous disease with LTR features. Moreover, OLP is mainly a T cell-mediated inflammatory disease.

Hence, unlike other T cell mediated diseases as type I diabetes, or multiple sclerosis, OLP is considered an ideal model to study T cell-mediated inflammatory disease. Also, it is easily accessible through the oral mucosa for diagnosis, investigations, treatment, and disease status follow-up.

Although there is scarcity of studies involving T cells in a complex 3D construct, attempts have been made to involve T cells within skin equivalents. Only a few studies have developed T cell-mediated skin diseases by addition of a cytokine cocktail instead of T cells. For instance, *in vitro* equivalent disease model of atopic dermatitis (AD), a chronic inflammatory multifactorial skin disease, was developed through culturing normal human fibroblast and keratinocyte using a fibrin-based dermal matrix with serum-free culture conditions. The disease was recreated by supplementing the cultures with IL-4 to recapitulate the epithelial hyperplasia and impaired differentiation of basal keratinocyte *in vivo* AD. Also, Tjabringa *et al*, developed psoriasis *in vitro* skin model by the addition of relevant pro-inflammatory cytokines into culture medium (Tjabringa *et al.*, 2008). However, the lack of direct effect of Th2 cells and proper characteristic replication of the disease-like spongiotic dermatitis renders this very simple AD-like *in vitro* model (Sriram, Bigliardi and Bigliardi-Qi, 2018). Eczematous dermatitis was reproduced *in vitro* by combining CD45+ T cells with organotypic skin equivalent (Engelhart *et al.*, 2005).

These models were developed further by Bogaard *et al*, by seeding activated CD4+ T cells, Th1, Th2, and Th17 between a transwell membrane and a 3D skin equivalent (Van Den Bogaard *et al.*, 2014). Building upon this model, further improvement was made through incorporating *in vitro* polarised Th1 and Th17 cells acquired from psoriatic patients in a 3D collagen hydrogel to better recapitulate psoriasis immune mechanism and it was used to evaluate the migration of T cells and drug responsiveness (Lorthois *et al.*, 2019; Shin *et al.*, 2020). Despite that, this model represents an advancement in psoriasis modelling, other immune cells relevant to psoriasis pathogenesis were missing such as macrophages and dendritic cells. Moreover, CD8+ T cells, an important immune component for Th1 related responses, was not investigated.

Al-Samadi et al, explored the effect of peripheral blood MNCs on the proliferation and invasion of oral tongue squamous cell carcinoma cell lines and the ability of cancer cells to attract MNCs, by coculturing primary monocytes, CD8+ T cells, and natural killers with tongue cancer cells in *in vitro* model using human uterine myoma discs (Al-Samadi *et al.*, 2017). Although this was an informative study, the immune cells were not embedded into a 3D construct and the interplay of the CD8 T cells and cancer microenvironment with other immune cells such as Th1 or Th2 was missing.

Kühbacher et al, added either the Jurkat cells, T cell line (Kühbacher *et al.*, 2017b), or primary CD4+ T cells (Kühbacher *et al.*, 2017a) in a 3D collagen hydrogel to a skin model to investigate dermal protection against *Candida albicans* invasion. The downside of this model system was that the T cells were not adapted to the culture medium before being combined with skin model nor their viability assessed following incorporation in a 3D construct which undermine further analysis. Moreover, neither the phenotype nor the activation status of the T cells was defined (Kühbacher *et al.*, 2017b).

Except for Said *et al*, who added activated Jurkat cells to the recipient medium of an full thickness oral mucosal equivalent (Said *et al.*, 2021), no other studies have explored adding immune T cells to oral mucosal equivalent or tried to replicate T cell disease in a 3D *in vitro* model. More advanced T cell inflammatory tissue-engineered models containing appropriately primed T cells hold great potential in replacing experiments performed on animals and provide in-depth read out for novel drug delivery systems. To the best of our knowledge, *in vitro* 3D model of OLP have not yet been developed. Therefore, it is the aim of this project to develop full-thickness mucosal models that utilise oral keratinocytes, oral fibroblasts and activated T cells using tissue-engineering techniques to replicate OLP.

1.5 Hypothesis

Full thickness tissue-engineered models can be developed to replicate disease pathogenesis of OLP to dissect the molecular mechanism and identify novel treatment strategies.

1.5.1 Aim

The overall aim of this study was to develop full-thickness oral mucosal models that employ oral keratinocytes, oral fibroblasts and activated T cells using tissue-engineering techniques to replicate OLP T cell-mediated epithelial damage.

1.5.2 Objectives

To address the overall aim of this thesis, the project was conducted over three main stages following specific objectives:

1. Optimisation of cell culture methods:

- Assess Jurkat T cell morphology, proliferation and activation in suspension cultures using microscopy, CellTrace™ proliferation assay, cell surface marker staining by flow cytometry and cytokine release by ELISA.

- Standardise the culture media for both T cells and oral keratinocytes in an adenine and flavin-enriched keratinocyte medium (Green's media) without hydrocortisone using a CellTrace™ proliferation assay.

- Optimise the number of T cells incorporated within collagen hydrogels and assess proliferation and viability using a PrestoBlue™ metabolic assay.

2. Isolation, activation and polarisation of naïve CD4+ and CD8+ T cells from peripheral blood:

    - Optimise the isolation of PBMC from peripheral blood buffy coats using gradient separation Ficoll medium.

    - Investigate the purification of CD4+ and CD8+ T cells from PBMC using magnetic negative selection.

    - Investigate successful activation of naïve CD4+ with PMA and CD3/CD28 Dynabeads by measuring key activation markers by flow cytometry.

    - Polarise CD4+ into Th1 and confirm phenotype using flow cytometry, q-PCR, western blot and ELISA.

    - Polarise naïve CD4+ into Th17 and confirm phenotype and plasticity with multicolour flow cytometry and ELISA.

    - Activate CD8+ into cytotoxic CD8+ T cells and confirm phenotype using multicolour flow cytometry.

3. Development of a full thickness tissue engineered model of OLP, validated against patient biopsies:

    - Create tissue engineered normal oral mucosal equivalent (OME) composed of FNB6 immortalised oral keratinocytes and normal oral fibroblasts (NOF).

    - Incorporate Th1 into collagen hydrogels and assess their viability overtime with PrestoBlue™ assay and flow cytometry.

- Assess the morphology of Th1 and NOF incorporated into collagen hydrogels over 14 days.

- Stimulate OME model and evaluate cytokines/chemokine release using a protein array.

- Assess T cell chemoattraction towards a chemokine gradient using a live imaging chemotaxis assay.

- Incorporate CD8+ T cells and Th1 within an oral mucosal equivalent using a layering strategy and assess the histology of full thickness tissue-engineered oral mucosal equivalent T cell inflammatory model.

- Validate the full thickness tissue-engineered oral mucosal equivalent inflammatory model against OLP patient's biopsies using immunohistochemistry.

2 Chapter two: Materials and methods

All materials used in this research including reagents, consumables, kits and equipment were from Sigma-Aldrich (Dorset, UK) unless stated otherwise.

2.1 Cell culture

2.1.1 Cell lines

2.1.1.1 FNB6 oral keratinocytes

FNB6, an immortalised oral keratinocyte cell line, (a kind gift from Professor Keith Hunter), was originally isolated from the buccal mucosa of a healthy female and immortalised by ectopic expression of human telomerase reverse transcriptase (hTERT) (McGregor *et al.*, 2002). FNB6 cells were cultured in Green's medium (Table 1) and passaged when 80% confluent.

Table 2.1: Components of Green's medium

Component	Final concentration
3, 3, 5-Tri-iodothyronine (T3)	1.36 ng/ml
Apo-Transferrin	5 µg/ml
Adenine	0.025 µg/ml
Amphotericin B	0.625 µg/ml
Dulbecco's modification of Eagle medium (DMEM)	66% v/v
Epidermal Growth Factor (EGF)	5 ng/ml
Foetal Bovine Serum (FBS)	10% v/v
Hydrocortisone	0.4 µg/ml
Insulin	5 µg/ml
Nutrient mix F12	21.60% v/v
Penicillin/Streptomycin	100 IU/ml Penicillin and 100 µg/ml Streptomycin

2.1.1.2 Jurkat E6.1

Jurkat E6.1 (European Collection of Authenticated Cell Cultures (ECACC) 88042803) cells are a T cell line derived from the Jurkat FHCRC cell line. Jurkat FHCRC cells were originally isolated from a human leukemic T cell lymphoblast. These cells produce IL-2 and were derived by incubating the cells at 41°C for 48 hours followed by limiting dilution cloning over macrophages (Schneider and Schwenk, 1977). Jurkat E6.1 cells were maintained in RPMI-1640 at a density of 3-9 x 10^5 cells/ml.

2.1.2 Isolation and culture of primary cells

2.1.2.1 Normal oral fibroblasts

Normal oral fibroblasts (NOF343 & 359) were isolated from oral biopsies of the buccal mucosa from patients undergoing routine dental procedures under ethical approval with informed consent (09/H1308/66) as previously described (Colley *et al.*, 2011). Briefly, the epithelium was removed, and the connective tissue minced, suspended in 10 ml of 0.5% collagenase A and incubated at 37°C in a 5% CO_2 humidified incubator overnight. Following centrifugation at 200 g for 10 minutes, NOF were cultured in DMEM supplemented with 10% FBS, 100 IU/ml penicillin, 100 µg/ml streptomycin and 0.625µg/ml amphotericin B and used until passage 9.

2.1.2.2 Peripheral blood monocyte cells

T cells were isolated from human PBMCs which were in turn isolated from buffy coats under local ethical review (approval reference 012597) by density gradient centrifugation using the Ficoll-hypaque (Ficoll® Paque Plus, Merck, Germany) density gradient centrifugation. Blood cells were mixed 1:1 with Hank's balanced salt solution (HBSS, modified with sodium bicarbonate, without phenol red, calcium chloride and magnesium sulphate). 30 ml of the diluted buffy coat was carefully overlaid onto 20 ml of Ficoll-hypaque and centrifuged at 400 g for 40 minutes at room temperature with zero deceleration. The blood was separated into three layers and the monocyte layer (between the upper serum and lower Ficoll layers containing red blood cells) was collected by aspiration using a sterile Pasteur pipette and washed several times in HBSS (**Figure 2.1**). The isolated PBMCs were counted and used for further purification of T cells.

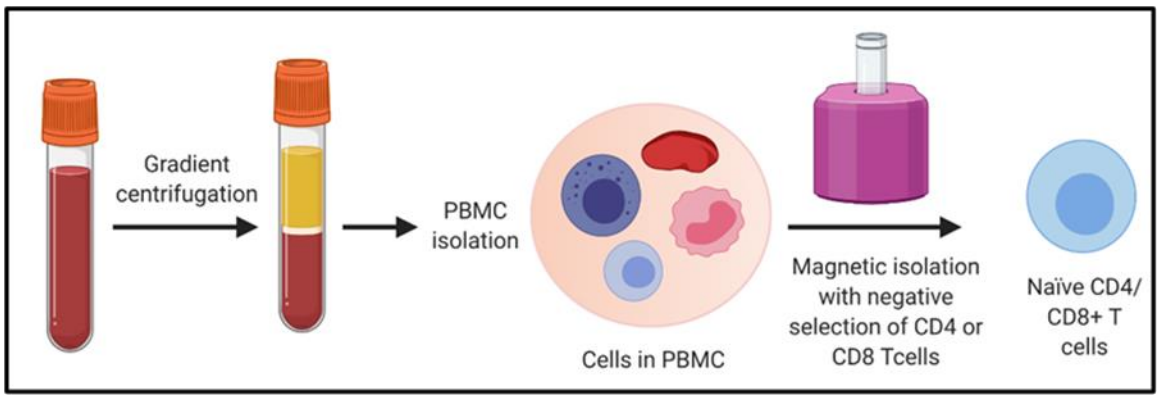

Figure 2.1: A schematic diagram to illustrate the isolation of T cells from a buffy coat. Created in BioRender.com.

2.1.2.3 Naïve CD4+ T cells

Primary CD4+T cells were further isolated from the PBMC using either the Naive CD4+ T Cell Isolation Kit II, human (Miltenyi Biotics, Germany) or the EasySep™ Human Naïve CD4+ T Cell Isolation Kit II (STEMCELL™, UK). The isolation was performed in two steps following negative selection for CD4+. First, CD4- cells were removed using negative selection with a cocktail of biotin-conjugated monoclonal antibodies against CD8, CD14, CD15, CD16, CD19, CD25, CD34, CD36, CD45RO, CD56, CD123, TCRγ/δ, HLA-DR, and CD235a followed by magnetic separation using streptavidin-conjugated iron beads. The Miltneyi kit separates the cells using the MAC's column system (Miltenyi Biotics, Germany) where the iron-labelled CD4- T cells are retained within the column whilst the flow through which contains the enriched naïve CD4+ T Cells (CD3+CD4+CD45RA+CD45R0-) was collected. The STEMCELL kit (STEMCELL™, UK) follows the same principle, however, the cells were separated without the use of a column. Here, Samples were placed in a Falcon® 5 mL or 15 mL round bottom polystyrene test tube (Fischer Scientific, UK) which was placed inside a magnetic field. The iron labelled cells are drawn to the magnet and held within the tube while the unlabelled naïve CD4+ T cell fraction was poured into a new tube (**Figure 2.2B**). The purity of isolation was assessed by staining the collected cells for CD4 surface marker and viability assessed using fixable blue live dead stain (ThermoFisher Scientific, UK) and analysis performed with flow cytometry (Section 2.6.3).

2.1.2.4 Naïve CD8+ T cells

CD8+ naïve cells were isolated using the EasySep™ Human Naïve CD8+ T Cell Isolation Kit (EasySep™, STEMCELL™, UK) that isolates naïve CD8+ T cells from PBMCs by negative selection. Unwanted cells were targeted with a cocktail of antibodies that bind CD4, CD14, CD16, CD19, CD20, CD36, CD45RO, CD56, CD57, CD94, CD123, CD244, TCRγ/δ, and glycophorin A. The labelled cells are separated using an EasySep™ magnet as described above in section 2.1.1.5. The purity of isolation was assessed by staining for CD8 surface marker and viability assessed using fixable blue live dead stain using flow cytometry.

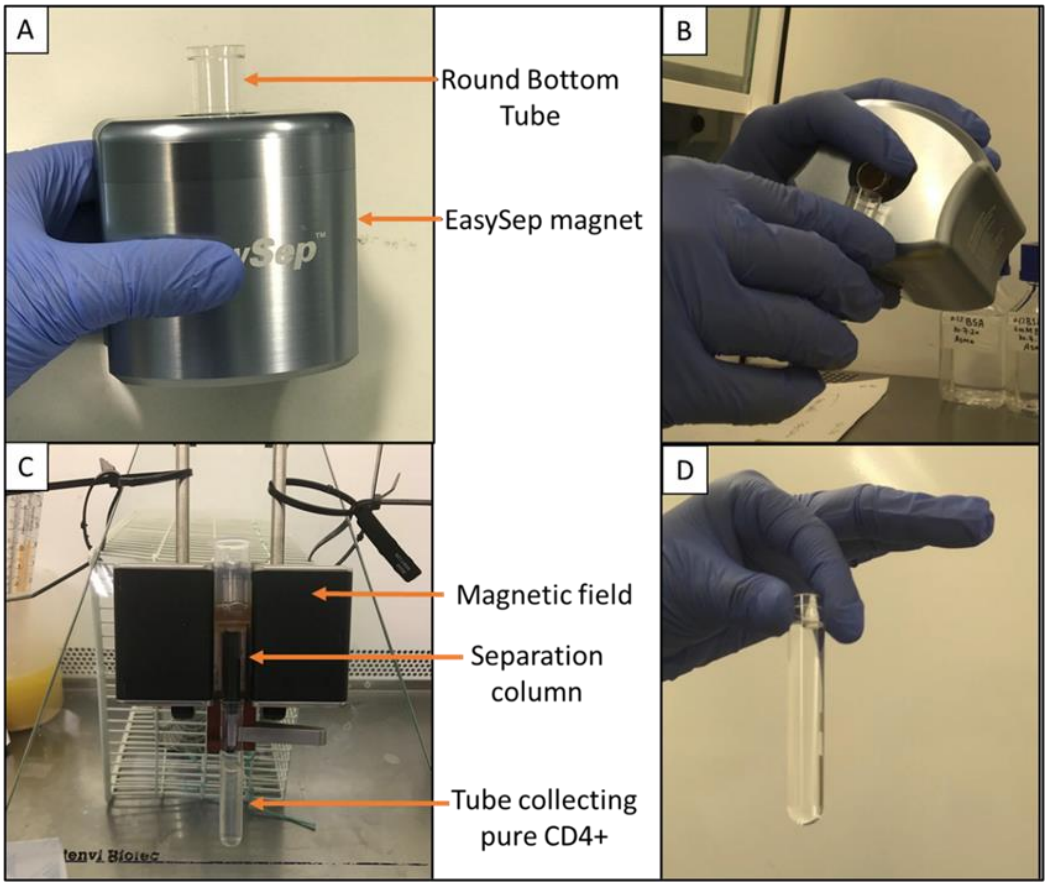

Figure 2.2: Negative selection of naive T cells from PBMCs using magnetic isolation with the (A) Stemcell's kit and the EasySep™ magnet where (B) the enriched unbound naive T cells can be poured off into another tube, or (C) using the Miltenyi kit and the MACs separator where the PBMCs sample is placed in a separation column placed in a magnetic field where (D) both methods result in the isolation of naïve T cells. Image is own work.

2.1.3 Routine cell culture

All cell culture work was carried out in Class II laminar flow hoods (Walker Safety Cabinets, Glossop, Derbyshire, UK) with all equipment sterilised before use 70% (v/v) industrial methylated spirits (IMS) (ThermoFisher Scientific, UK) or by autoclave sterilisation. Cell cultures were examined regularly for evidence of bacterial or fungal contamination. Cells were tested for the presence of mycoplasma on a regular basis. All cells were incubated in a humidified incubator at 37°C with 5% CO_2 (Scientific-Lab Supplies).

2.1.3.1 Passaging of cells

Upon reaching 70-80% confluence, adherent cells (FNB6 and NOF) were transferred into a new cell culture flask with a lower cell number to enable cell proliferation to continue. To passage adherent cells, the culture medium was removed and cells washed twice with 10 ml of phosphate buffered saline (PBS, Oxoid Ltd, UK) to remove any serum proteins in the residual cell culture medium. Cells were then incubated with 5 ml of pre-warmed 0.05% trypsin/0.02%

EDTA solution for 5 minutes or until all cells had detached, monitored using a light microscope. After cell detachment, the trypsin/EDTA was neutralised with cell culture medium (5-8 ml) containing FBS and transferred to a 20 ml centrifuge tube (Becton Dickinson, UK). The cell suspension was centrifuged at 200 g for 5 minutes using a benchtop centrifuge. Finally, the supernatant was discarded, and the cellular pellet re-suspended in the desired volume of fresh cell culture medium and transferred to a new tissue culture flask (Greiner Bio-One GmbH, Germany).

To passage Jurkat cells as a suspension culture, cells were resuspended to a single cell suspension and centrifuged for 5 minutes at 200 g. After centrifugation, the supernatant was discarded, and the cell pellet resuspended in fresh medium at a density of 3-9 x 10^5 cells/ml.

Unlike Jurkat, primary T cells have a limited life span and need extrinsic stimuli (activation) to maintain their proliferative state. To expand primary T cells, they were activated as described in section 2.1.4 and the cell density determined by counting at regular intervals, whilst noting cell morphology by light microscopy. Cell shrinkage, reduced proliferation rates or reduced clumping is typically observed in exhausted cell cultures and indicates that re-stimulation is required. Cells were maintained at density of 5 × 10^5 cells/ml in culture medium containing 30 U/mL recombinant (r) IL-2 (Aksoy *et al.*, 2018).

2.1.3.2 Counting cells

Once cells were in suspension, cell counts were performed using a modified Neubauer haemocytometer (Weber Scientific international, UK) under a light microscope. Ten µL of cell suspension was removed and added to the haemocytometer and at least three 1 mm^2 squares counted, and their average taken. Cell numbers were then calculated as follows:

Average number of cells counted per 1 mm^2 square x 10^4 x dilution factor, e.g., average cell count of 100 in 10 ml total = 100 x 10^4 x 10 = 1 x 10^7 cells in total.

2.1.3.3 Imaging of cell monolayers and suspensions

Cells were examined under an inverted phase contrast light microscope (Nikon, ECLIPSE TS100) and images were taken using a Spot Idea CMOS microscope camera with associated Spot 5.1 software (SPOT IMAGING™, US).

2.1.3.4 Cryopreservation of cells

For cryopreservation cells were treated as described for passaging (section 2.1.3.1). However, after centrifugation cells were resuspended into cryopreservation media composed of

FBS containing 10% v/v dimethyl sulfoxide (DMSO) for FNB6, NOF or Jurkat cells, and 5% DMSO for primary CD4+ or CD8+ T cells. The pellet was resuspended to give a cell density of between 1-4 x 10^6 cells per ml, depending on the cell type. PBMC were resuspended at higher cell densities of 100-200 x 10^6 cells per ml. One ml of cell suspension was added to each cryovial (Greiner Bio-One, GmbH, Germany) and placed in a Nalgene™ Cryo 1°C freezing container (Nalgene Co., New York, USA). This freezing container, which contains 250 ml of isopropanol, controls the rate of cooling to 1°C per minute in a -80°C freezer. After a minimum of 24 hours the vials were transferred into a liquid nitrogen dewar (-196°C) for long-term storage (Yokoyama, Thompson and Ehrhardt, 2012).

2.1.3.5 Thawing of cells

To thaw cells, cryovials were removed from the liquid nitrogen using appropriate safety precautions and the vial quickly thawed in a 37°C water bath. Once thawed, the cell solution was diluted in cell culture medium and centrifuged for 5 minutes 200 g. The supernatant was discarded, and the cellular pellet resuspended in the appropriate cell culture medium.

2.1.4 T cells activation, expansion, and polarisation

2.1.4.1 CD4+ T cell activation with CD3/CD28

Primary T cells express CD3/CD28 surface receptors that engage with CD80/86 and MHC class II on antigen presenting cells for T cell activation (**Figure 2.3A**). In this study T cells were activated using Dynabeads™ Human T-Activator CD3/CD28 according to manufacturers instructions (ThermoFisher Scientific, UK) which provides a more physiologically relevant activation pathway through engagement with CD3 and CD28 receptors on T cells surface (**Figure 2.3B**). T cells were activated at a 1:1 cell to Dynabeads ratio. First, the Dynabeads vial was vortexed for 30 seconds, then the desired volume was transferred to a 0.5 ml micro centrifuge tube (Greiner Bio-One, GmbH, Germany) and washed with an equal volume or at least 1 ml of FACS Buffer (PBS with 0.1% BSA and 2 mM EDTA, pH 7.4) and vortexed for 5 seconds. T cells binding to the CD3/CD28 Dynabeads were isolated via magnetic column separation and the supernatant aspirated and discarded. Then, the washed Dynabeads were resuspended in the same volume of culture medium as the initial volume of Dynabeads that was taken from the vial. T cells were seeded to 3-5 x 10^5/mL and Dynabeads were added to obtain a bead-to-cell ratio of 1:1. A 30 IU/ml of rIL-2 (Peprotech, UK) was added to the culture and cells incubated in a humidified CO_2 incubator at 37°C until analysis.

2.1.4.2 *Jurkat activation with phorbol 12-myristate 13-acetate and ionomycin*

Jurkat were activated by incubation with phorbol 12-myristate 13-acetate (PMA) and ionomycin (**Figure 2.3C**) at a final concentration of 50 and 500 ng/ml, respectively, to $1x10^6$/ml Jurkat cells then incubated for 4, 6 and 24 hours. Cells were centrifuged at 1800 g for 2-3 minutes, then cell culture conditioned medium stored at -80°C and the cells collected for CD69 surface marker staining by flow cytometry (Section 2.6.3).

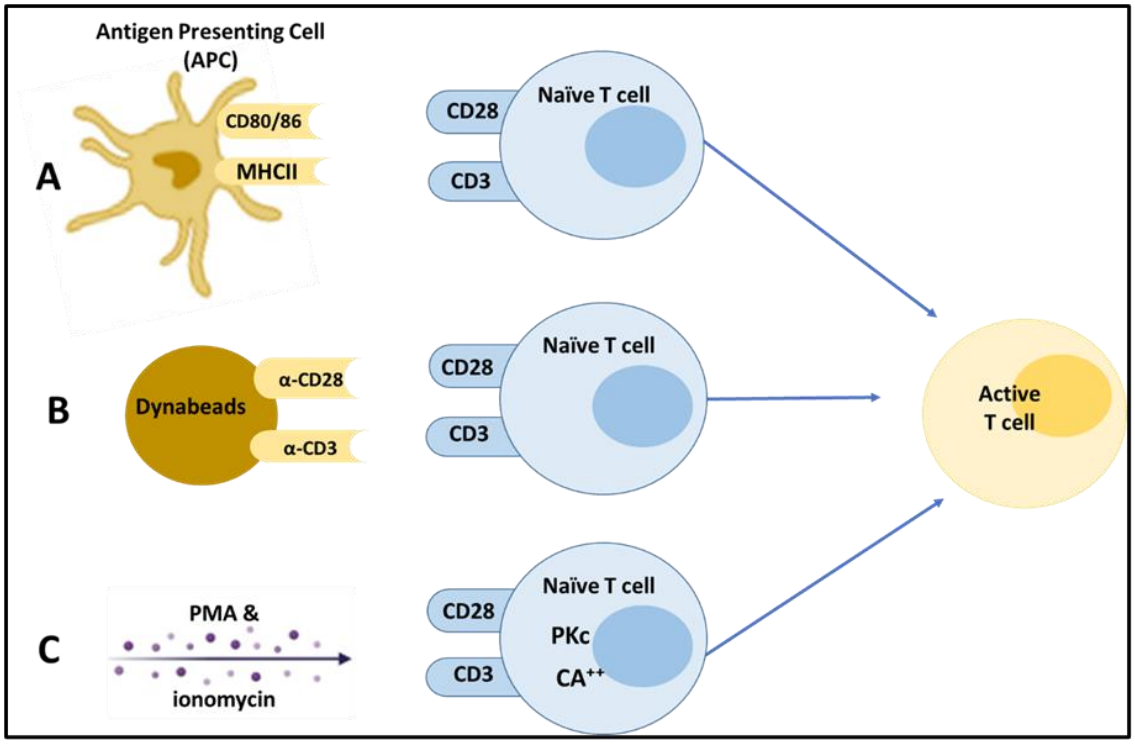

Figure 2.3: An illustration of T cells activation. (A) In vivo, the binding of the TCR-CD3 complex on T cells with the antigen-MHC molecule on the APC surface, augmented by CD28 stimulation starts a cascade of intracellular signalling system resulting in the activation of T cells. (B) *In vitro*, activation can be mimicked directly using CD3/CD28 Dynabeads that follow the same interaction seen *in vivo* but without the need for APC or (C) indirectly, using mitogenic molecules such as PMA and ionomycin which trigger protein kinase C (PKC) activation and Ca^{++} release and mobilization, resulting in a cascade of additional cellular responses mediating T-cell activation. Created for this research in BioRender.com.

To investigate different activation conditions, CD4+ T cells were isolated from PBMCs, and activated with either PMA, Ionomycin, and IL-2 or with CD3/CD28 Dynabeads and IL-2 or with IL-2 alone. Then, cells were either cultured in Green's medium without hydrocortisone or RPMI medium for 24 hours. Cells were collected for viability and CD69 surface activation marker abundance using flow cytometric analysis.

2.1.4.3 *CD8+ T cell activation*

Naïve CD8+ cells were isolated from PBMC as described in section 2.1.2.4. To identify the best method to activate and transform naïve CD8+ T cells into cytotoxic T cells, cells were

cultured in Green's medium without hydrocortisone in the presence of either IL-2 alone, IL-2 with CD3/CD28 Dynabeads, or with IL-2 and CD3/CD28 Dynabeads in the presence of CD4+ T cells. To assess cell proliferation, CD8+ cells were cultured for 7 days and counted using a haemocytometer on days 0, 3, 5, and 7. Media was changed every two to three days, noting to leave about 20% of existing conditioned media and topping this up with new fresh medium. On day seven, cells were centrifuged and separated into further two groups. One group was re-stimulated with eBioscience™ Cell Stimulation Cocktail (ThermoFisher, UK) whilst the other was left unstimulated. Thirty minutes following restimulation, protein secretion from the Golgi apparatus was inhibited using eBioscience™ Protein Transport Inhibitor Cocktail (ThermoFisher, UK) and cells incubated at 37°C for 4 hours before analysis with flow cytometry. For the analysis, multicolour flow cytometry staining was performed to simultaneously detect the cell surface marker CD8+, CD4+, and cell viability (live/dead stain), the cell activation marker CD69, and intracellular Granzyme B levels (in section 2.6.4).

2.1.4.4 CD4+ T cell polarisation to Th1 cells

Th1 polarising medium was prepared by adding 20 ng/ml of human rIL-12 p70 (Peprotech, UK), 20 ng/ml of human rIL-18 (R&D Systems, USA), and 2.5 µg/ml purified anti-human IL-4 antibody (Biolegend, UK) to Green's medium (without hydrocortisone).

CD4+ T cells were isolated from PBMCs then cultured in Greens medium (without hydrocortisone) supplemented with either rIL-2 alone, rIL-2 and CD3/CD28 Dynabeads or cultured in Th1 polarising medium (as described in 2.1.4.1) along with rIL-2 and CD3/CD28 Dynabeads.

Cells were counted on days 0, 3, 5 and 7 with 80% of the media refreshed every 2-3 days. Analysis was performed on day 7 where cells were centrifuged at 200 g for 5 minutes and separated into two groups for either treatment with Cell Stimulation Cocktail (eBioscience™, ThermoFisher, UK) for 're-stimulation' or left without further treatment i.e., 'not re-stimulated'. Following restimulation, protein secretion from Golgi apparatus was inhibited using eBioscience™ Protein Transport Inhibitor Cocktail (Thermo Fischer, UK) and incubated at 37°C for 4-5 hours before analysis using flow cytometry. Both stimulation cocktail and protein transport inhibitors were used following manuacturer's instructions. For the analysis, multicolour flow cytometry staining was performed to determine CD4 surface marker expression, intracellular IFN-γ abundance and nuclear T-bet transcription factor expression along with viability (Section 2.6.4).

2.1.4.5 Polarisation to Th17 cells

Th17 polarising medium was prepared by adding 30 ng/ml human rIL-6, 20 ng/ml human rIL-1β and 2 ng/ml human rTGFβ (Peprotech, UK) along with 2.5 µg/mL each of anti-IL-2, anti-IL-4 and anti-IFN-γ antibody (Biolegend, UK) to Greens medium (without hydrocortisone). To prepare polarising conditions towards a Th17/Th1 mixed phenotype, the above Th17 polarising medium was prepared without the addition of anti-IFN-γ antibody to avoid blocking the Th1 pathway while 20 ng/ml of human r IL-12 p70 (Peprotech, UK) was added to encourage Th17 plasticity towards Th1.

CD4+ T cells were isolated from PBMCs and cultured in Green's medium (without hydrocortisone) with the addition of either IL-2, Th17 polarising medium with the addition of CD3/CD28 or Th17/Th1 polarising media supplemented with CD3/CD28 in 1:1 bead-to-cell ratio.

Th17 cells do not undergo rapid expansion compared to Th1, because the IL-2 pathway was blocked to support Th17 differentiation. Hence, the cells were seeded at a higher density of 1 x 10^6 per sample to account for any loss of cells. 60% of the media was refreshed every 3-4 days, depending on cell density. Analysis was performed on day 7 where cells were centrifuged at 200 g for 5 minutes and separated into two groups as described above for Th1 analysis regarding re-stimulation and protein secretion inhibition (Section 2.1.4.4). Multicolour flow cytometry staining was performed to detect the presence of CD4 and CCR6 cell surface markers, intracellular IL-17 and IFN-γ, nuclear FOXP3 and RORC transcription factors (in section 2.6.4).

2.1.5 Proliferation profile tracing

Jurkat and FNB6 proliferation profiles were measured using CellTrace™ Far Red Cell Proliferation Kit (Fischer Scientific, UK) according to manufacturer's instructions and under different growth media conditions. The lyophilised dye was dissolved in DMSO to a final concentration of 1 mM then diluted in PBS to a working concentration of 1 µM. Jurkat cells at 2.5 x 10^6 cells per sample were collected and centrifuged at 200 g for 5 minutes, re-suspended in 2 ml Far-Red dye (1 µM) or PBS (as a control) and incubated at 37°C for 20 minutes whilst protected from light. After 20 minutes the samples were diluted (5x) with fresh complete growth media and incubated for a further 5 minutes and subsequently centrifuged 200 g for 5 minutes and the pellet resuspended in 5 ml fresh, pre-warmed complete RPMI-1640 medium and cultured under normal conditions. FNB6 cells were trypsinised and stained with Far Red CellTrace following the same steps detailed above, however, following staining, 5 x 10^4 cells were seeded into each well of 6 well plate for analysis. For Jurkat cells 400 µl samples were

collected over five consecutive days whilst for FNB6 a separate well of monolayer cells was detached each day. For both cell types, cells were counted, washed in FACs buffer (0.1% BSA in PBS), resuspended in 4% paraformaldehyde and stored at +4°C, protected from light for analyses. Fluorescence intensity was acquired using flow cytometry LSRII (BD Biosciences, California, US) with 638 nm excitation and a 660/20 nm bandwidth emission filter. Unlabelled cells were analysed to establish background fluorescent levels. Analysis was performed using FlowJo software (BD Biosciences, California, US).

The doubling time calculation of the cell specific growth rate (μ) was determined from the slope of the natural logarithm of cell count or MFI as a function of time and doubling time (DT) using the formula [$DT = \ln 2/\mu$].

2.1.6 Trypan blue viability assay

Jurkat cells were seeded at 4 x 10^5 cells/ml in two T75 flasks. One flask continued to be cultured in RPMI and served as a control, while the media in the other flask was changed with increasing concentration of Green's medium (25%, 50%, 75%, and finally 100%; v/v). Media was changed every two days and the viability of the cells was determined.

The trypan blue (ThermoFisher Scientific, UK) exclusion test was used to determine the number of viable cells present in a cell suspension. Live cells possess intact cell membranes that exclude certain dyes, such as trypan blue, whereas dead cells do not. A cell suspension is simply mixed with the dye and visually examined under a microscope to determine whether the cells take up or exclude Trypan blue. A viable cell will have a clear cytoplasm whereas a non-viable cell will have a blue cytoplasm. Cell viability was calculated using the following formula:

Viability % = Viable cells/ Total cells ×100%. *Total cells = viable + dead cells

2.2 3D tissue culture

2.2.1 Rat tail collagen type I extraction

Collagen was isolated from rat tail tendons following our research group standard protocol. Rat tails were collected following Home Office guidelines and stored at -20 °C and thawed overnight prior to use. The rat tail skin was sliced at about a third length of the tail with a surgical blade (Swann-Morton, UK) around the circumference without going too deep into the tendons. The tail bone was broken by folding it at the cutting point and then twisted in one direction until the tendons, string-like white fibres, came out smoothly as the skin and bone were separated. The tendons then were cut with a blade and washed in sterile PBS twice and transferred to a bottle of 0.1 M acetic acid. The collagen was mixed at 4°C on a stirrer until

completely dissolved which took approximately 1-2 weeks. Once dissolved, the collagen suspension was filtered and aliquoted into 15 ml tubes and lyophilised using a freeze-dryer (VirTis Benchtop K Manifold freeze drier, SP Scientific, Suffolk, UK). The lyophilised collagen was weighed and stored at -20°C for long term storage or dissolved in 0.1 M acetic acid to a final concentration of 5 mg/ml and stored at 4ºC ready for use.

2.2.2 Collagen hydrogel preparation

The collagen hydrogel was prepared by adding DMEM (10X), reconstitution buffer (10X), FBS, L-glutamine, and collagen. The reconstitution buffer consisted of 2.2 g sodium bicarbonate, 4.8 g HEPES, 0.238 g NaOH, dissolved in 100 ml distilled H_20, sterile filtered, aliquoted and stored at -20°C until use. Volume and final concentrations of the reagents used in the preparation of the collagen hydrogels are detailed in (**Table 2.2**). All the components were kept on ice and mixed gently by inverting the tube. After the collagen had been added, the pH was adjusted to 7.4 using 2 M NaOH with a pH meter (HANNA Instrument, UK), after which the cells were added.

Table 2.2: Components of collagen hydrogel

Items	Volume per model (µL)	Final concentration
DMEM (10X)	100	13.8 mg/ml
Reconstitution buffer (10X)	100	$NaHCO_3$ (2.25 mg/ml), HEPES (2 mM), NaOH (6.3 mM)
Foetal bovine serum	83	8.5% v/v
L-glutamine	10	2.1 mM
Collagen	673	3.37 mg/ml

2.2.3 Extraction of cells from collagen hydrogels

Collagen hydrogels were cut into small pieces using a sterile blade (company) and incubated in 2 ml of 0.5 mg/ml collagenase I (ThermoFisher, UK) in Green's medium in a microcentrifuge tube and incubated on for 1-2 hours at 37°C. Once the hydrogel was dissolved, the cell suspension was filtered to remove any residual collagen fibres using a Falcon® 5 ml round bottom polystyrene test tube, with a 35 µm mesh size cell strainer snap cap attached (Fischer Scientific, UK). The cell suspension was centrifuged 3000 g for 3 minutes and the cell pellet resuspended in fresh Green's medium or in FACS buffer for immediate analysis.

2.2.4 Construction of hydrogel embedded with Jurkat cells of different densities

To investigate T cell viability inside collagen hydrogels, Jurkat cells were seeded inside a hydrogel at different densities and cultured for 14 days. Jurkat cells were prepared as previously described (Section 2.1.3.1). Cells were counted and resuspended in Green's medium (without hydrocortisone) to give a final density of 0.5, 1 or 2 x 10^6 cells per 1 ml collagen or with no cells added, to act as a negative control. Each cell suspension was added to the neutralised collagen solution and mixed thoroughly to ensure uniform distribution. One ml of collagen hydrogel was added to each well of 12 well inserts (Greiner-Bio-One, Germany) and the hydrogels incubated in a humidified atmosphere of 5% CO_2 at 37°C for 30 minutes or until completely set, before adding medium. The PrestoBlue viability test was performed on days 1, 3, 7, 10 and 14 as described in section 2.2.6.

2.2.5 Construction of hydrogel embedded with primary T cells of different activation conditions

To investigate the viability of primary T cells inside collagen hydrogel, this primary T cells were isolated from blood and prepared as naïve, activated or polarised cells as previously described (Section 2.1.2.2 & 2.1.4) and incorporated within a collagen hydrogel according to the protocol designed in this research. T cells were counted and added to a collagen hydrogel to reach a final concentration of 1 x 10^6 cells per 0.5 ml collagen. For Th1 polarisation, the cells were either cultured in polarised conditioned for 5 days in 2D before adding them to the hydrogel or were freshly isolated, activated, and then added to a hydrogel and cultured in polarising conditions. Hence, polarisation was either established in 2D or 3D. The hydrogel/cell suspension was mixed thoroughly and each 0.5 ml (containing 1 x 10^6 cells) was added to a 12 well insert and incubated from 30-60 minutes or until the hydrogel set. The naïve T cell hydrogels were treated with rIL-2 only and cultured in Greens medium without hydrocortisone. The activated T cell hydrogels were treated with rIL-2, CD3/CD28, and cultured in Greens medium without hydrocortisone and the Th1 T cell hydrogels were treated with rIL-2, CD3/CD28, and cultured in Th1 polarising medium. A control hydrogel containing no cells were made to account for any background fluorescence when performing the viability test. T cell viability in a hydrogel was assessed using PrestoBlue assay at days 1, 3, 5, 7 and 10 as described in section 2.2.6.

2.2.6 PrestoBlue assay to assess T cell viability within a hydrogel

PrestoBlue® reagent (Invitrogen, UK) contains resazurin, a blue compound with no intrinsic fluorescence that is reduced by metabolising viable cells to resorufin, which is pink in colour and fluorescent. This conversion is proportional to the number of metabolically active cells and therefore can be measured quantitatively. Furthermore, PrestoBlue® is non-toxic and

non-destructive hence, assayed cells can be recovered for further culturing or use in a subsequent assay.

PrestoBlue reagent (10x) was added directly to the medium (1:10 dilution) in light-protected conditions and incubated for 6 hours at 37°C according to the manufacturer's instructions. Each condition was measured in triplicate and a control hydrogel with no cells was used as a control to account for background fluorescence. A 100 µl sample was taken from the conditioned medium of each sample and transferred to a 96-well plate, then the hydrogels were washed with PBS and medium was refreshed. The fluorescence readings were taken by spectrometry at excitation of 535 nm and 615 nm emission at the time points 1, 5 and 14 days. All values were normalised to the control readings and analysed.

2.2.7 The use of LIVE/DEAD™ fixable dead cell stain to assess T cells viability following extraction from hydrogel

Primary T cells were incorporated into a hydrogel as described in section 2.2.5, then, cells were extracted from collagen on days 1, 7 and 14 (Section 2.2.3) and stained for viability using a Fixable Blue Live/Dead dye.

The LIVE/DEAD™ Fixable Dead Cell Stain (ThermoFisher Scientific, UK) was used to evaluate the viability of cells by flow cytometry according to the manufacturer's instructions. This assay is based on the reaction of a fluorescent reactive dye with cellular amines. The reactive dye can permeate the compromised membranes of necrotic cells and react with free amines both in the interior and on the cell surface, resulting in intense fluorescent staining. In contrast, only the cell-surface amines of viable cells are available to react with the dye, resulting in relatively dim staining. The discrimination between live and dead cells is completely preserved following fixation of the sample by formaldehyde. Moreover, these single colour assays use only one channel of a flow cytometer, leaving the other channels available for multicolour experiments.

T cells were washed and resuspended with 1 ml PBS. Two µl of blue live dead reactive dye was added to the cell suspension and incubated on ice for 30 minutes, protected from light. If fixation was not required and analysis was planned on the same day, then cells were washed with 1 ml of 1% BSA/PBS buffer and resuspended in 300-500 µL of 1% BSA. However, if fixation was required, then the cells were washed once with 1 ml of PBS and resuspended in 4% formaldehyde for 15 minutes at room temperature. After fixation, cells were washed with 1% BSA and resuspended in 300-500 µl of 1% BSA. The fixed cell suspension was analysed by flow cytometry using a LSRII Flow Cytometer (BD Biosciences, California, US) with 350–360 nm excitation and 450 nm emission.

2.2.8 The construction of an oral mucosa equivalent

An oral mucosal equivalent (OME) was fabricated utilising NOF359 or 343 and FNB6 cells following protocol developed by our research group (Jennings *et al.*, 2016). NOF cells were prepared and counted as described in section 2.1.3.1. The medium was discarded, and the cell pellet resuspended in DMEM to give a final cell density of 0.25 x 10^6 cells per 40 µl of medium (2.5 x 10^5 per model). Collagen hydrogels were prepared as described (see **Table 2.2**) in an appropriate volume to the number of models desired for each experiment. Once the hydrogel pH was neutralised, the prepared NOF suspension was added to the collagen solution and mixed gently. One ml of the mixture was then transferred into each 12 well cell culture inserts fitted in a standard 12-well plate. The hydrogels populated with NOF were incubated for 1-2 hours or until it had solidified in a humidified atmosphere of 5% CO_2 at 37°C. Once the hydrogels had set, DMEM culture medium was added to the wells, 1 ml to the bottom well and 0.5 ml to the top of each insert then incubated for 48 hours.

Following incubation, FNB6 cells were prepared as described in section 2.1.3.1 and the cell pellet was resuspended in Green's medium to give a final concentration of 0.25 or 0.5 x 10^6 cells per 0.5 ml (per model). Cell culture medium was carefully removed from the top and bottom of each insert and the inserts transferred into a deep 12-well plate (Greiner Bio-One, GmbH, Germany). FNB6 cells (0.25 or 0.5 x 10^6 cells in 0.5 ml medium) were seeded on top of each collagen gel and 4.5 ml of Green's medium added to the bottom of each well and incubated from 2-5 days. Following incubation, the medium on top and bottom of the models was carefully removed, and 4.5 ml of fresh Green's medium added to the bottom only, raising the model to an air-to-liquid interface (ALI). The models were further cultured for 10 or 14 days, and the medium changed every two days (**Figure 2.4**). Finally, models were fixed in 10% formalin and stored at room temperature for histological assessment.

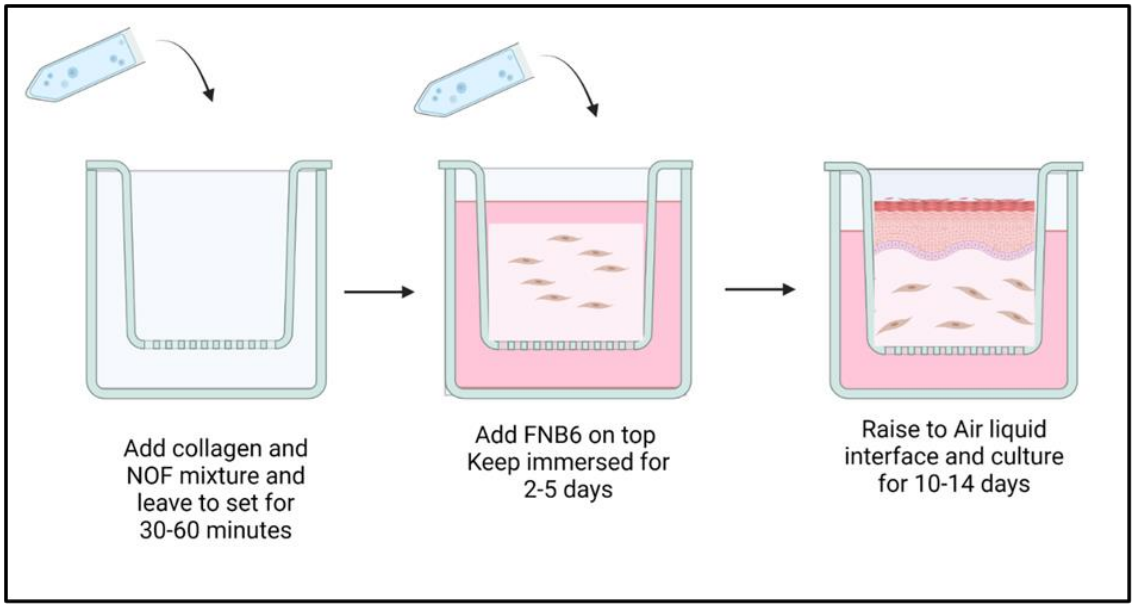

Figure 2.4: An illustration of the main steps in the fabrication of normal oral mucosal equivalent. Collagen hydrogels embedded with NOF cells were prepared and incubated until the collagen was set. Then, FNB6 were seeded on top and immersed in media for 2-4 days. Finally, hydrogel was raised to an air-to-liquid interface for a further 10-14 days while media was changed every two days. Created using BioRender.com.

2.2.9 Stimulation of oral mucosa equivalents

OME were stimulated with different conditions to determine which produces the most relevant inflammatory response to OLP. OME were fabricated as described in section 2.2.8 and raised to ALI for 10 days. At day 10, the medium was removed and one of the following conditions were added in duplicate: Green's medium as control (unstimulated), Green's medium supplemented with 1000 IU/ ml IFN-γ (equivalent to 50 ng/ml) and 1000 IU/ml TNF-α (equivalent to 20 ng/ml), conditioned medium obtained from Th1 polarised T cells, and finally, Th1 differentiation medium containing human rIL-12 p70 (20 ng/ml), rIL-18 (20 ng/ml), and anti-human IL-4 antibody (2.5 µg/ml).

After 48 hours of incubation, medium was collected and centrifuged at 200 g, 4°C for 5 minutes. The supernatant was stored at -80°C for cytokine quantification. The OME were fixed in 10% formalin and stored at room temperature for histological assessment.

2.2.10 3D chemotaxis assay

To investigate the potential of activated T cells to migrate towards a chemoattractant gradient produced by stimulated OME in a 3D environment, a chemotaxis assay was performed using chemotaxis µ-slides (Ibidi, GmbH, Germany). Each slide of the µ-slide includes three chambers for three parallel assays where each chamber is composed of two large reservoirs that are connected by a narrow observation area that harbours the cells (**Figure 2.5**). Each slide

received three different conditions as follow: A negative control consisting of serum free medium in the reservoir chambers on both sides of the viewing chamber with no chemoattractant, a positive control with one reservoir containing CCL5 (Peprotech, UK) at a final concentration of 100 ng/ml, and an experimental group where one reservoir was filled with conditioned media from OME stimulated with IFN-γ and TNF-α.

The assay was performed in accordance with the manufacturer's instructions. In summary, the µ-slide was placed into a 10 cm petri dish with a sterile wet tissue around the slide and incubated in a humidified atmosphere of 5% CO_2 at 37°C overnight before use. Primary T cells were isolated from buffy coat and activated as previously described (Section 2.1.2.3, 2.1.2.4 and 2.1.4) and cultured in a serum-free Green's medium without hydrocortisone.

The collagen hydrogel was prepared to yield a final concentration of 2.5 mg/ml and T cells were seeded in the hydrogel to a final cell density of 3-9 x 10^6 cells/ml then loaded into the µ-slide. During the hydrogel gelation process, the migration chamber was incubated in a humid Petri dish at 37°C and 5% CO_2 for 35 minutes. To prevent sedimentation of the cells and attachment to the bottom of the microslide, the Petri dish was turned upside down after 15 minutes and again after another 10 minutes. After gelation, the reservoirs were filled with the test medium.

The chemotaxis slide was incubated directly in the incubation chamber of the live imaging system to allow for gradual stabilisation of temperature and CO_2 at 37°C and 5%, respectively. The inverted transmitted-light microscope in the live imaging system (Microscope Leica DM18 inverted light microscope, Leica Microsystems, UK) was set for phase-contrast microscopy and a time-lapse experiment performed with an interval set time of 10 minutes over a period of 24 hours. Cell tracking and analysis was performed using the FastTrack AI Automated Image Analysis software (Ibidi, GmbH, Germany).

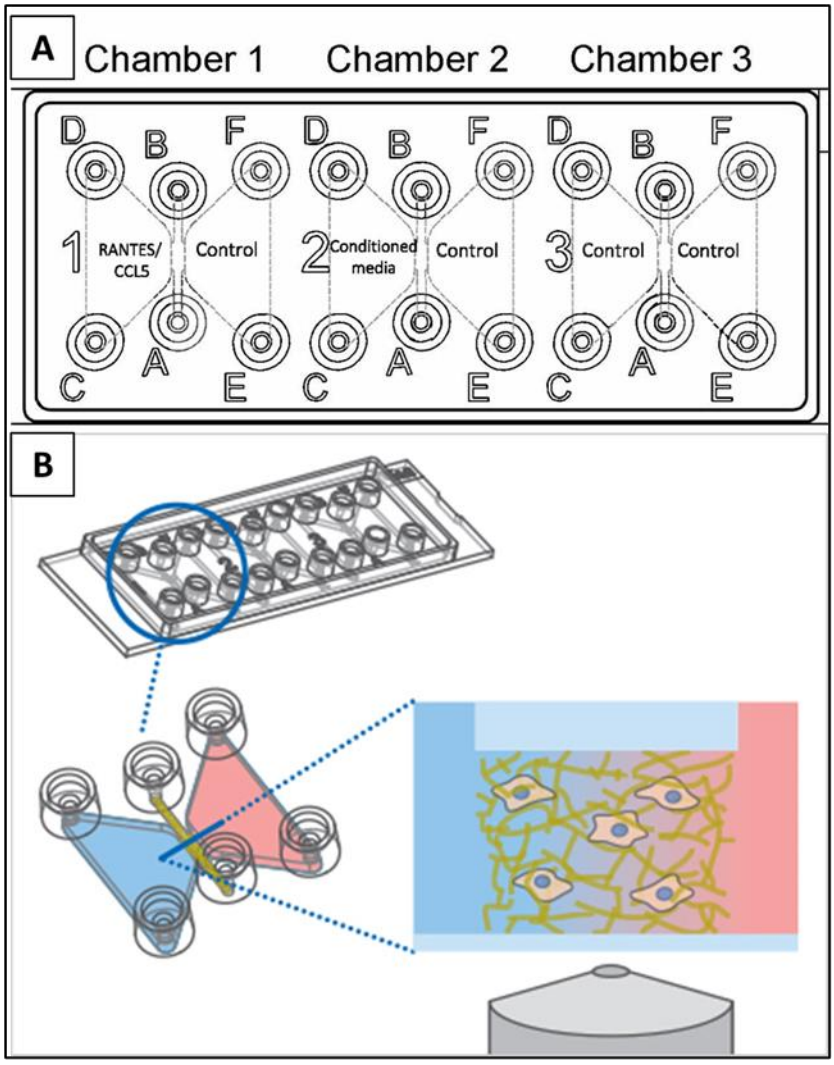

Figure 2.5: Chemotaxis assay µ-slide. (A) An illustration of the design of the µ-slide chemotaxis and the conditions used for the chemotaxis assay. (B) An illustration of how cells distributed inside the observation area in a 3D environment with established chemotactic gradient. Copy rights to ibidi.com.

2.2.11 Fabrication of a full thickness inflammatory oral mucosal model

Two different methodologies were tested for successful establishment of a full thickness T cell inflammatory model. The first method incorporated NOF359, CD4 and CD8 T cells together into a collagen hydrogel at day 0 and will from herein be referred to as the '*all in one technique*'. Primary CD4+ and CD8+ T cells were isolated from buffy coat and primed into Th1 or cytotoxic CD8 as previously described (Section 2.1.2.3, 2.1.2.4 and 2.1.4). A final seeding density of 1.5 x 10^6 T cells per model was used. NOF359 were prepared as previously described (Section 2.1.3.1) to give a final concentration of 0.25 x 10^6 cells per model. Both the T cells and NOF359 were added to the collagen hydrogel and mixed gently. One ml of the resultant hydrogel mixture was added to each of a 12-well insert. Once the hydrogel had set, they were immersed in Th1 differentiation medium and after 48 hours incubation FNB6 (0.25 X 10^6) were seeded on top of each hydrogel. The FNB6 reach confluence within 2-5 days, when the models were raised

to ALI and cultured for a further 10 days. After day 10 at ALI, the models were stimulated with IFN-γ (1000 IU/ml) and TNF-α (1000 IU/ml) and fixed on day 10, 12, 16, 20 and 25.

The second approach combined a previously prepared OME (Section 2.2.8) to a previously prepared T cell hydrogel (Section 2.2.5) and will from herein be referred to as the '*layering technique*' (**Figure 2.6**). One ml or 2 ml of the NOF/hydrogel mixture was added to each well of a 12-well or 6-well insert, respectively. Following 48 hours of incubation, 0.5 or 1ml of FNB6 cells (0.5x 10^6 cells/ ml) were prepared and seeded on top of the models in the 12 and 6 well inserts, respectively. On the same day of seeding FNB6, T cells (CD4 and CD8) were isolated from blood and primed into Th1 and cytotoxic CD8 T cells. After 5 days of incubation, the OME model were raised to an ALI interface and cultured in full Green's medium whereas the primed T cells were incorporated into a collagen hydrogel. T cells hydrogel (0.5 ml) was added into each 12-well inserts with a final seeding density of 1.5 x 10^6 cells per model and cultured in Th1 medium. At day 7 of culture at an ALI, the OME was combined with the T cells hydrogel (OME top layer/T cells bottom layer) using 100-150 µL of 3 mg/ml collagen solution to sandwich the layers together. The OME constructed in a 12-well insert did not need cutting and was transferred directly and gently using small lab spoon and spatula to the top of a T cell hydrogel after wetting its surface with a collagen solution, an illustration of this step is presented in (**Figure 2.7**). If the OME was constructed in a 6-well insert it was cut to fit into the smaller 12 well insert. Here, the OME was transferred gently into a sterile petri dish with medium and cut with a sharp blade to fit the 12-well inserts. The cut was made in one stroke to avoid tearing the mucosa and transferred carefully to the top of a T cell hydrogel. From this point, the full model continued to be cultured in Th1 medium for 2-3 days then stimulated with IFN-γ (1000 IU/ml) and TNF-α (1000 IU/ml) and fixed in 10% formalin on day 10, 12, 16, 20 and 25 of ALI (**Figure 2.7**). Since models stimulated at day 10 of ALI, this is also Day 0, 2, 6, 10, and 15 of stimulation.

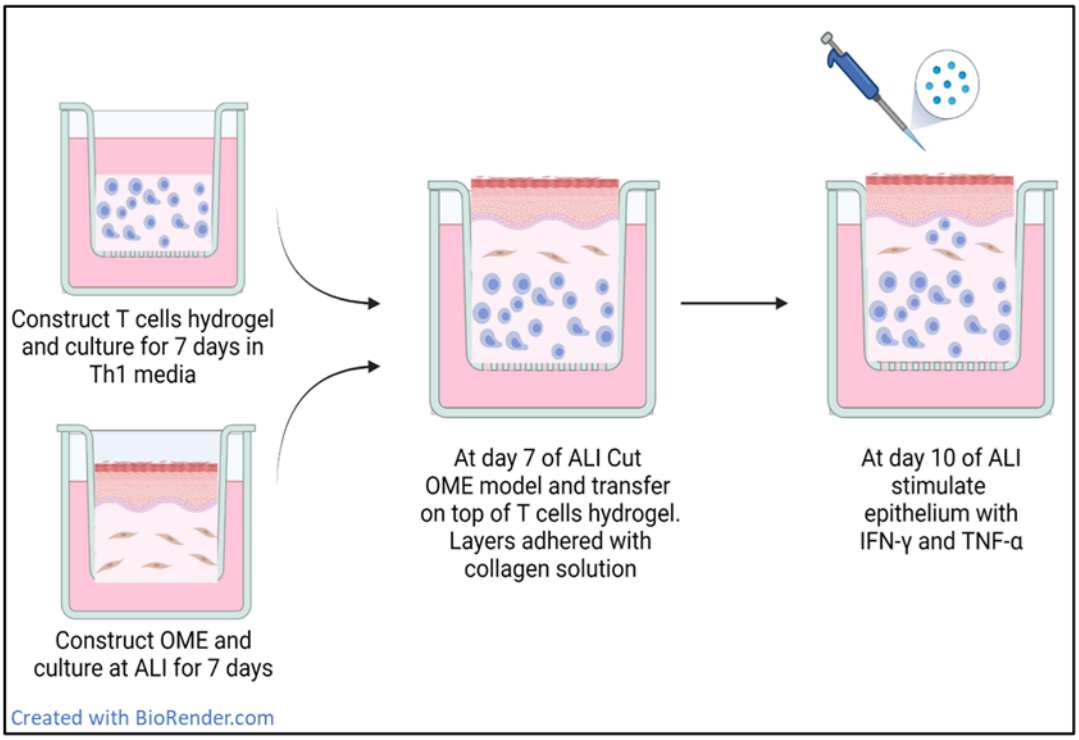

Figure 2.6: An illustration of the main steps involved in the construction of a full T cell inflammatory model using the layering technique. OME at day 7 of ALI was transferred to the top of T cell hydrogel at day 7 of culture and combined with collagen solution. The combined full model was stimulated at day 10 of ALI while media collected and model fixed at day 10, 12, 16, and 20 of culture. Created using BioRender.com.

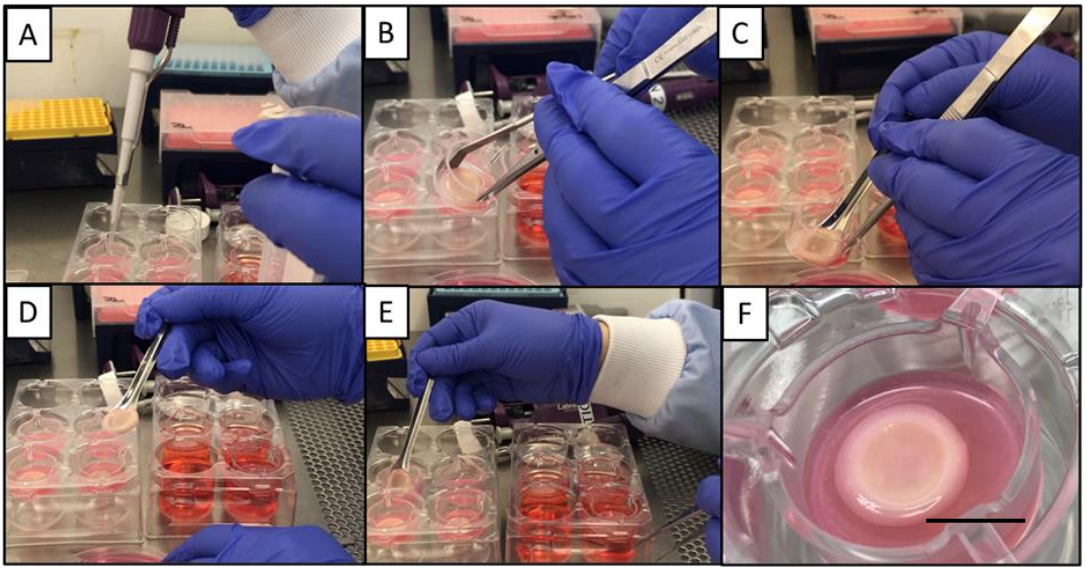

Figure 2.7: Images illustrate the steps of combining two independent models into one full inflammatory model, described as the layering technique. (A) a collagen suspension was used to wet the T cells hydrogel model before (B) the edges of the OME model were detached gently from the membrane underneath using a micro spatula, (C) then the OME model was gently removed using a micro lab spoon and (D) transferred to the top of the T cell hydrogel. (F) A combined full layered model of the contracted OME on top of uncontracted T cell hydrogel. Scale bar =10mm.

2.3 Histological assessment

2.3.1 Haematoxylin and eosin staining

Normal oral mucosa (ethical approval 09-H1308-66) and OLP (ethical approval 22-SC-0111) tissue blocks were ready for cutting. All collagen hydrogels and tissue-engineered models were fixed with 10% PBS-buffered formalin for at least 24- 48 hours to allow complete crosslinking that will preserve the cellular morphology. Then, tissues were processed overnight using a Shandon Citadel 2000 tissue processor using the steps outlined in (**Table 2.3**). Dehydration performed using alcohol in certain order to alllow for removal of free water while maintaining the bound water. The xylene, clearing agent, removes the alcohol to allow complete infiltration of wax. Finally, wax infiltration to support the tissue structure. After processing, the tissue samples were bisected then embedded in molten paraffin wax using a Leica EG1160 Embedding Centre (Leica Microsystems, Germany).

Table 2.3: Processing schedule for formalin-fixed tissues.

Histological processing steps	Time
10% neutral buffered formalin	60 minutes
70% alcohol	60 minutes
70% alcohol	60 minutes
90% alcohol	60 minutes
90% alcohol	60 minutes
Absolute alcohol	60 minutes
Absolute alcohol	60 minutes
Absolute alcohol	60 minutes
Xylene	90 minutes
Xylene	90 minutes
Paraffin wax I	120 minutes
Paraffin wax II	120 minutes

Cooled wax blocks were sectioned (5 µm) using a microtome (Leica RM2235 microtome, Leica Microsystems, Germany) with microtome blade S35 type (Feather, Japan) and transferred

onto SuperFrost plus slides (ThermoFisher Scientific, UK) after being floated on a water bath set at 35°C (Barnstead Electrothermal, Staffordshire, UK). The tissue sections were warmed for at least 30 minutes in an oven set at 60°C before staining to ensure adherence of the sections to the slides. Haematoxylin and eosin (H&E) staining was performed using a Leica ST4040 linear Stainer (Leica Microsystems, Germany) (**Table 2.4**) and sections then mounted with dibutyl phthalate polystyrene xylene (DPX) and covered with a coverslip (VWR International, UK). Stained tissue sections were examined under upright brightfield microscope and images captured with an Olympus BX51 Colour view IIIu camera and associated Cell^D software (Olympus soft imaging solutions, GmbH, Münster, Germany).

Table 2.4: Staining schedule for H&E staining using the Leica linear auto-Stainer

Solutions	Repeats
Xylene	3
Absolute alcohol	3
Distilled water	2
Harris's Haematoxylin	4
Running tap water	1
0.1% HCL in 70% alcohol	1
Running tap water	1
Scott's water substittute	1
Running tap water	1
Eosin	3
Running tap water	1
Absolute alcohol	3
Xylene	4

2.3.2 Immunohistochemistry staining

Five µm sections were deparaffinised in two xylene baths, for 5 minutes each, then rehydrated in two 100% ethanol baths, each for 5 minutes. Endogenous peroxidases were quenched with 3% hydrogen peroxide in methanol for 20 minutes. Antigens are usually obscured in the specimen by the formalin fixation and paraffin embedding processes, hence, an antigen retrieval step is required either by heat or enzymatic treatment. Heat treatment was performed using TRIS/EDTA buffer (10 mM Tris Base, 1.2 mM EDTA, 0.05% v/v Tween20 in ddH_2O, pH 9). All antibodies (**Table 2.5**) showed best performance when heat-treated using TRIS/EDTA Buffer carried out in a 2100 antigen retriever pressure cooker (Aptum Biologics,

UK) for a full cycle of 20 minutes. The tissue samples in the slides were bordered with a wax pen and blocked with normal horse or goat serum for 30 minutes. Sections were incubated with primary antibody diluted in normal serum or EnVision FLEX Antibody Diluent (Agilent, UK) overnight at 4°C in a humidified chamber. Next day, sections were washed twice for 5 minutes in PBS and incubated with anti-mouse or anti-rabbit IgG secondary antibody (Vector laboratories, Ca, US) for 30 minutes. Following a further two 5 minute washes with PBS, ABC reagent (Vectastain Elite ABC-HRP kit, Vector laboratories, Ca, US) was applied for 30 minutes, then washed twice with PBS. 3,3'-diaminobenzidine (DAB) stain (Vector laboratories, Ca, US) was applied and after 5 minutes or once the brown colour had started to develop, slides were immersed in dH_2O to stop the colour development reaction. Sections were then counterstained with haematoxylin and mounted as described (Section 2.3.1).

Table 2.5: Antibodies used for immunohistochemistry.

Antibody	Clone	Dilution	Supplier
Monoclonal mouse anti-human CD4	4B12	1:10	Agilent, UK
Monoclonal rabbit anti-human CD4	SP35	1:50	ThermoFisher Scientific, UK
Monoclonal mouse anti-human CD8	C8/144B	1:25	Bethyl Laboratories, US
Vimentin mouse anti-human	RV202	1:25	Santa Cruz Biotechnology, US
Mouse IgG1	DAK-GO1		Agilent, UK

2.4 Gene analysis

2.4.1 RNA extraction and reverse transcription

Total RNA was extracted from prepared samples using the Monarch® Total RNA Miniprep Kit (New England BioLabs, UK) or Direct-zolTM RNA MicroPrep (ZYMO Research, USA) following the manufacturer's instructions. First, to create a lysate, T cells were collected through centrifugation and pellet resuspended in 500 µl lysis buffer then stored in -80°C until use. For 3D models, collagen was incubated with 300 ul of RNA protect for half an hour or until dissolved, centrifuged to pellet debris, then supernatant added to an equal volume of lysis buffer. To extract RNA from lysate, samples were passed through gDNA removal columns to discard any genomic DNA contamination, then an equal volume of ethanol ≥95% was mixed with the flow through and passed though RNA purification columns. Another optional step to discard

remnant gDNA by DNAse enzymatic removal was carried out. The collected RNA was primed, washed, then eluted in nuclease-free water. RNA was quantified using a Nanodrop 1000 spectrophotometer (ThermoFisher Scientific, UK).

2.4.2 Complementary DNA generation

Total RNA was reverse transcribed to generate complementary DNA (cDNA) using high-capacity cDNA reverse transcription kit (ThermoFisher Scientific, UK) following the manufacturer's instructions. In brief, 10 µL of an equal concentration of RNA diluted in nuclease-free water was added to a 10 µL master mix consisted of RT buffer, d-NTP, random primer, reverse transcriptase, and nuclease-free water. The 20 µL mix was transcribed using a Peltier Thermal cycler (MJ Research, UK). The thermal cycler was set to run at 25°C for 10 minutes, followed by 2 h at 37°C, and finally at 85°C for 5 minutes. cDNA was then stored at -20˚C.

2.4.3 Quantitative PCR

Quantitative RT-PCR (qRT-PCR) was carried out using Rotor-Gene Q (Qiagen, Manchester, UK) using TaqMan chemistry. One µL of the prepared cDNA was added to 9 µL master mix consisting of TaqMan target probe (FAM-labelled), water, and a reference gene probe (VIC-labelled) which was β2-microglobulin (B2M control mix; Applied biosystems, Life Technologies, UK). The reference gene was used to normalise gene expression and all assays were performed in triplicate. The standard thermal cycle consisted of 95°C for 10 s, 60°C for 15 s and 72°C for 20 s. All primers used are indicated in **Table 2.6**.

Table 2.6: TaqMan primers used for Th1 phenotyping. All primers were purchased from (ThermoFisher Scientific, Leicestershire, UK).

Name	Assay ID
TBX21	Hs00894392_m1
STAT1	Hs01013996_m1
STAT4	Hs01028017_m1

Quantification of gene expression was calculated using the delta-delta CT (2-ΔΔCT) method (Livak and Schmittgen, 2001). The cycle threshold (CT) represents the number of cycles that causes the fluorescent signal to reach a fixed threshold. The ΔCT value represents the difference in CT values between target genes and reference control. The calculated 2-ΔΔCT values represent the relative fold change in gene expression between samples. Data will be presented as fold-change in target gene expression compared to the reference controls.

2.5 Protein analysis

2.5.1 Enzyme-linked immunosorbent assay

Conditioned media was collected and stored in -80°C until analysis. Cytokine released in media was measured by sandwich Enzyme-linked Immunosorbent Assay (ELISA) assay using DuoSet ELISA kits specific for IL-2, IL-4, IFN-γ, TNF-α, CCL5, CXCL9, CXCL10, and IL-17 (R&D systems, Abingdon, UK) (**Table 2.7**) as per manufacturer's instructions. Briefly, high binding 96-well microplates (Greiner, Gloucestershire, UK) were incubated overnight with 100 µl of diluted capture antibody and covered with a plate sealer. Next day, plates were blocked for 1 hour with 300 µL of blocking reagent, washed and samples and standards added at 100 µl per well. After a two-hour incubation, the plates were washed and incubated with 100 µl detection antibody for two hours before washing and 100 µl of streptavidin-HRP added for 20 minutes. Finally, plates were washed and 100 µl of TMP (3,3',5,5'-tetramethylbenzidine) substrate solution (KPL SureBlue™, SeraCare, Massachusetts, US) added. After 30 minutes or once a dark blue colour had developed in the wells with highest standard concentration, the reaction was stopped with 2N H_2SO_4 and the optical density determined using a Tecan Infinite M200 spectrophotometer and associated Magellan software, version 7.2, (Tecan lifeSience, Switzerland) using a 450 nm wavelength filter with correction at 570 nm. A standard curve was plotted from the standard's concentrations and the concentration of the samples determined.

Table 2.7: Reagents and antibodies specification for each ELISA kit.

Cytokine	Capture antibody (µg/mL)	Blocking reagent	Reagent diluent	Standard (pg/mL)	Detection antibody (ng/mL)
IL-2	4	1% BSA in PBS	0.1% BSA, 0.05% Tween 20 in Tris-buffered saline	15.6-1000	100
IL-4	4	1% BSA in PBS	0.1% BSA, 0.05% Tween 20 in Tris-buffered saline	31.2-2000	25
IFN-γ	2	1% BSA in PBS	1% BSA in PBS	9.38-600	200
TNF-α	4	1% BSA in PBS	1% BSA in PBS	15.6-1000	50

2.5.2 Cytokine array

Cytokines were detected in conditioned media using a RayBio® C-Series Human Cytokine Antibody Array C5 (Ray Biotech, Georgia, US) for the semi-quantitative detection of 80 human proteins (**Table 2.8**). The assay was performed following the manufacturer's instruction. In short, each of the antibody array membrane was placed into a well of the incubation tray and blocked for 30 minutes before the samples were added and incubated for two hours. Membranes were then washed and incubated with the biotinylated antibody cocktail for two hours, washed again and incubated with horse radish peroxidase (HRP)-streptavidin for another two hours. After a final wash, a detection buffer mixture was added for 2-5 minutes to the membranes before being exposed and images were taken with a C-DiGit blot scanner (Li-cor, Cambridge, UK) with the associated software. Densitometry data were extracted from images using the array analyser plug-in in ImageJ software. To normalise data, the background was subtracted then, the control (unstimulated media) array was used as a reference array to which the other arrays were normalised.

Table 2.8: Array map of 80 proteins in the human cytokine antibody array C5.

	A	B	C	D	E	F	G	H	I	K	L
1	Pos	Pos	Pos	Pos	Neg	Neg	ENA-78	G-CSF	GM-CSF	GRO	GRO-α
2	I-309	IL-1alpha	IL-1beta	IL-2	IL-3	IL-4	IL-5	IL-6	IL-7	IL-8	IL-10
3	IL12-p40	IL-13	IL-15	IFN-gamma	MCP-1	MCP-2	MCP-3	M-CSF	MDC	MIG	MIP-1 β
4	MIP-1-δ	RANTES	SCF	SDF-1	TARC	TGF-β1	TNF-α	TNF-β	EGF	IGF-1	Angio-genin
5	Oncostatin M	TPO	VEGF	PDGF-BB	Leptin	BDNF	BLC	CK beta 8-1	Eotaxin	Eotaxin-2	Eotaxin-3
6	FGF-4	FGF-6	FGF-7	FGF-9	Flt-3 Ligand	Fractalkine	GCP-2	GDNF	HGF	IGFBP-1	IGFBP-2
7	IGFBP-3	IGFBP-4	IL-16	IP-10	LIF	LIGHT	MCP-4	MIF	MIP-3α	NAP-2	NT-3
8	NT-4	Osteopontin	Osteoprotegerin	PARC	PIGF	TGF- b2	TGF-b3	TIMP-1	TIMP-2	Pos	Pos

2.5.3 Western blot

2.5.3.1 Protein extraction and quantification

Ten ml of radioimmunoprecipitation assay buffer (RIPA buffer) with complete mini-EDTA free protease inhibitor cocktail and phosphatase inhibitors (Roche, Basel, Switzerland) was used to lyse cells, solubilise proteins, and to ensure protein stability. Each sample pellet was mixed with 150-300 µl of the lysis buffer and incubated for 30 minutes at 4°C or on ice before being centrifuged at 18,000 g for 20 minutes at 4°C to avoid protein denaturation. The supernatant containing the soluble proteins was gently aspirated into a fresh tube and stored at -80°C.

The bicinchoninic acid assay (BCA) (Pierce BCA protein assay Kit, Fisher-Scientific, UK) was used to quantify protein concentration following the manufacturer's instructions and BSA (Thermo Fisher Scientific) was used to produce a standard curve. The absorbance values were measured using a spectrophotometer plate reader at 562 nm and the concentrations extrapolated from the standard curve.

2.5.3.2 Protein separation and transfer to a nitrocellulose membrane

This step was performed following standard operating procedure in the molecular biology lab. The acrylamide gel concentration is selected according to the protein molecular weight. For instance, if the target protein molecular weight is smaller than 100 kDa usually a 12% concentration is selected (**Table 2.9**).

Table 2.9: Components of the acrylamide gel.

Gel	Acrylamide (ml)	Lower Tris (ml)	TEME (µl)	Ammonium Persulfate (APS) (µl)	H_2O (ml)
Resolving gel (12%)	1.2	2.5	5	350	6.1
Resolving gel (15%)	1.9	2.5	5	350	5.4
Stacking gel	1	2.1	17	100	7.4

The protein lysate (20 µg) was mixed with 5 x SDS lysis buffer 1:5 (v/v) and heated for 5 minutes at 95°C in a heat block. The gel was placed into the XCell SureLock Mini Cell electrophoresis system (Invitrogen Ltd, UK) following the manufacturer's instructions and filled with 1 x SDS running buffer (0.025M Tris-base, 0.032M glycine, 1% SDS in ddH_2O). The protein ladder (Ez run protein ladder) and the protein samples were loaded into gel wells and the gel run for 15 minutes at 70-90 V to allow slow movement of the sample through the gel then the voltage was increased to 100-120 V for 1 hour or until good separation between the molecular weight bands could be observed.

Proteins in the gel were transferred onto a nitrocellulose or polyvinylidene difluoride (PVDF) membrane using the Trans-Blot Turbo™ transfer system (Bio-Rad, Hertfordshire, UK) in semi-dry transfer buffer (0.05 M Tris-base, 0.025 M glycine, 0.4% SDS and 20%

methanol in ddH_2O). Protein transfer was confirmed by Ponceau S stain, then the membrane washed in TBST solution (8 g NaCl, 0.2g KCl, 3 g Tris-base in ddH_2O).

2.5.3.3 Target protein detection

Membranes were cut, separating the β-actin protein from the target protein and blocked with 5% skim milk powder in TBST for 1 hour at room temperature, then washed and incubated overnight at 4°C with either the target protein (anti-STAT1 antibody [EPRR21057-168], Abcam, Cambridge, UK) at 1:1000 dilution in 5% TBS-T milk or with β-actin primary antibody (A1978, Sigma Aldrich, UK) at 1:3000 dilution. Next day, membranes were washed with TBS-Tween and incubated with secondary anti-rabbit antibody at 1:3000 dilution (7074S-Cell Signalling, UK) or secondary anti-mouse antibody at 1:5000 (GTX22166701, Genetex, US) for 1 hour at room temperature. The membranes were washed, developed using chemiluminescence (Clarity™ Western ECL Substrate, Bio-Rad, Hertfordshire, UK) and imaged using a C-DiGit blot scanner (Li-cor, Cambridge, UK) with the associated software then analysed with ImageJ.

To detect the phosphorylated form of the STAT1, membrane was stripped of antibodies using Restore Western Blot Stripping Buffer as per the manufacturer's instructions (ThermoFisher Scientific, Leicestershire, UK), re-blocked in blocking solution, and then re-probed with a primary antibody specific for the phosphorylated STAT1 (Anti-STAT1 (phospho Y701 antibody [EPR3147], Abcam) at 1:1000 dilution overnight at 4°C. Next day, membranes were incubated with anti-rabbit secondary antibody, washed, and re-developed as described previously.

2.6 Flow cytometry

Flow cytometry can be used to assess cells according to their size, granularity or fluorescence, or it can be used to analyse cell cycle, assess viability, amongst other uses. A flow cytometer consists mainly of a fluidic system, optical system and the electronic system. The fluidic system is the heart of flow cytometry because the faster moving fluid sheath creates a channel in centre that directs the cells in a stream where they can be analysed in a line one by one in the same axis and velocity. The optical system consists of lasers to illuminate the cells in the sample stream and optical filters to direct the resulting light signals to the appropriate detectors. Finally, the electronics system converts the detected light into electronic signals that can be processed by the computer.

Once the laser hits the cell, a light is scattered at a low angle which is collected through the forward scatter detector (FSC) and this is proportional to the size of the cells. When the light

faces obstructions when passing through the cells, it produces scattering at higher angles which is called side scatter (SSC) and this is proportional to the granularity and complexity of the cells. The number of cells passing through the laser can be recorded, also, the FSC and the SSC can be combined into a scatter blot where populations of different physical characteristics can be identified. A popular example for this is the identification of different cells in a blood sample including lymphocyte (smaller cells with low granularity), monocyte (slightly larger with more granularity), and neutrophils and granulocytes (larger cells with dense granularity) (**Figure 2.8**).

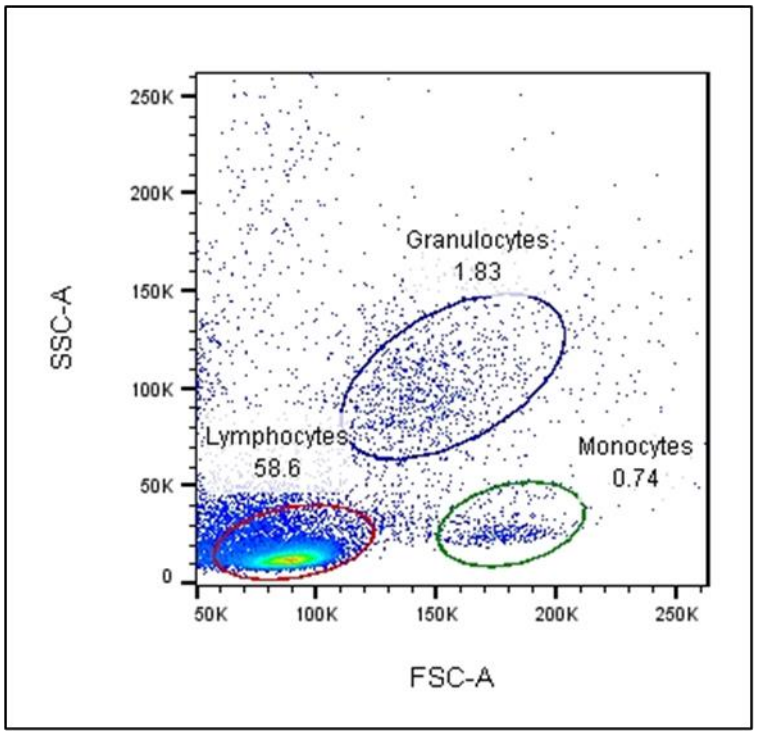

Figure 2.8: Dot plot with cell subpopulations based on SSC vs FSC. Sample of PBMCs shows three subpopulations of different size and granularity. The lymphocyte (smaller cells with low granularity), monocyte (slightly larger with more granularity), and neutrophils and granulocytes (larger cells with dense granularity). Image is own work.

Antibodies can be conjugated with a fluorochrome that can be excited through the flow cytometry laser and emit light of specific wavelength that can be collected through specific detectors. The intensity of the fluorescent signals detected are proportional to the number of fluorochrome molecules on the particle. More than one fluorochrome can be used simultaneously if they can be excited with the same laser and their peak emission is not close and hence can be detected by separate detectors. An example is the combination of fluorescein isothiocyanate (FITC) and phycoerythrin (PE) conjugated antibodies. All flow experiments in this work were analysed with LSRII (BD Biosciences, California, US) with 4 lasers and the configurations are presented in **Table 2.10**.

Table 2.10: List of the lasers and filters available in the customised BD LSRII and the compatible fluorochromes.

Laser	Bandpass filter	Viability	Reporter protein	Fluorochrome
355nm UV laser	450/50	LIVE/DEAD Blue Zombie UV		BUV 496
	530/50	Zombie Aqua		
405nm Violet laser	450/50	LIVE/DEAD Violet Zombie violet DAPI	BFP CFP	Alexa Fluor 405 BD-Horizon V450 BV 421 Pacific Blue eFluor 450
	525/50	LIVE/DEAD Aqua Or Yellow Zombie Aqua		AmCyan BD-Horizon V500 BV510 Cascade Yellow Pacific Orange
488nm Blue laser	530/30	LIVE/DEAD Green Zombie Green	GFP YFP CFSE	Alexa Fluor 488 FITC
	575/26	PI	mOrange	PE Ds Red
	610/20	LIVE/DEAD Red PI		Alexa Fluor 594 PE-Alexa Fluor 610 PE-CF594 PE-Texas Red
	660/20	PI 7AAD		PE-Cy5 PerCp
	695/45			PerCp-Cy5.5 PerCp-eFluor 710
	780/60			PE-Cy7
633nm laser	660/20	LIVE/DEAD Far Red TOPRO3	DID	APC Alexa Fluor 647
	730/45			Alexa Fluor 700 APC-Cy5.5
	780/60	LIVE/DEAD Near-IR Zombie NIR		APC-Cy7 APC-H7 APC-eFluor780 APC-FIRE

2.6.1 Sample preparation

Adherent and suspension cells were prepared as described (Section 2.1.2.1) and resuspended to give a final cell density of 1 x 10^6 cells/ml in an appropriate volume of FACS buffer. The 3D collagen hydrogel was enzymatically digested (Section 2.2.1), and the residual cells pellet resuspended in FACS buffer. If the cells need blocking for non-specific Fc-mediated

interactions, then cell were incubated with 10 µl of human Fc Receptor Binding Inhibitor per 100 µL sample for 20 minutes at 4°C before staining.

2.6.2 Validating the LIVE/DEAD™ fixable dead cell stain

Propidium iodide (PI) (ThermoFisher Scientific, UK) is a popular red-fluorescent counterstain and since PI does not permeate through the living cell's membrane, it is also commonly used to detect dead cells in a population. To compare the functionality of fixable blue dye to the PI dye, Primary T cells were freshly isolated from blood then sorted into a live sample, treated with DMSO for 2 minutes to create a dead population of cells or mixed (live and dead population). Then, samples were either unstained, stained with fixable blue live/dead dye (Section 2.2.5), or resuspended in 300-500 µL FACs buffer with 1 µL of PI. The samples were analysed using a LSRII flow cytometry and using an excitation at 488 nm and emitting wavelength of 575/26 nm.

2.6.3 Surface staining of proteins for analysis by flow cytometry

Samples were centrifuged at 1800 g for 3 minutes and the cellular pellet resuspended in 95 µL FACS buffer containing 5 µL of a conjugated fluorescence antibody (**Table 2.11**). The samples were incubated for 20 minutes on ice protected from light, washed with 1 ml FACS buffer before staining with a live/dead stain (2 µL) and incubated for further 30 minutes. The samples were then washed and fixed in 10% formalin for 15 minutes and re-suspended in 300-500 µl FACS buffer. Unstained control sample to account for background fluorescence and an IgG isotype control-stained sample to account for non-specific staining were prepared.

The FCS data for the single colour samples were collected with LSRII flow cytometry. 10^3 events stored and threshold for FSC, SSC and fluorochrome were adjusted before recording using the unstained and a stained sample. Then a gating strategy was performed by gating for the parent cell population in the FSC and SSC light beam (**Figure 2.9**). Then, the parent population gate was blotted against UV450-40 channel to exclude dead cells and gate for the viable cell population. Finally, the fluorochrome was blotted from the viable population and gate adjusted with the isotype control sample. Both median fluorescence and percentage cell population from parent data were recorded and analysed with FlowJo software (BD Life Sciences, US). Normalised median fluorescence (nMFI) was calculated as follow: nMFI = positive MFI/ negative MFI.

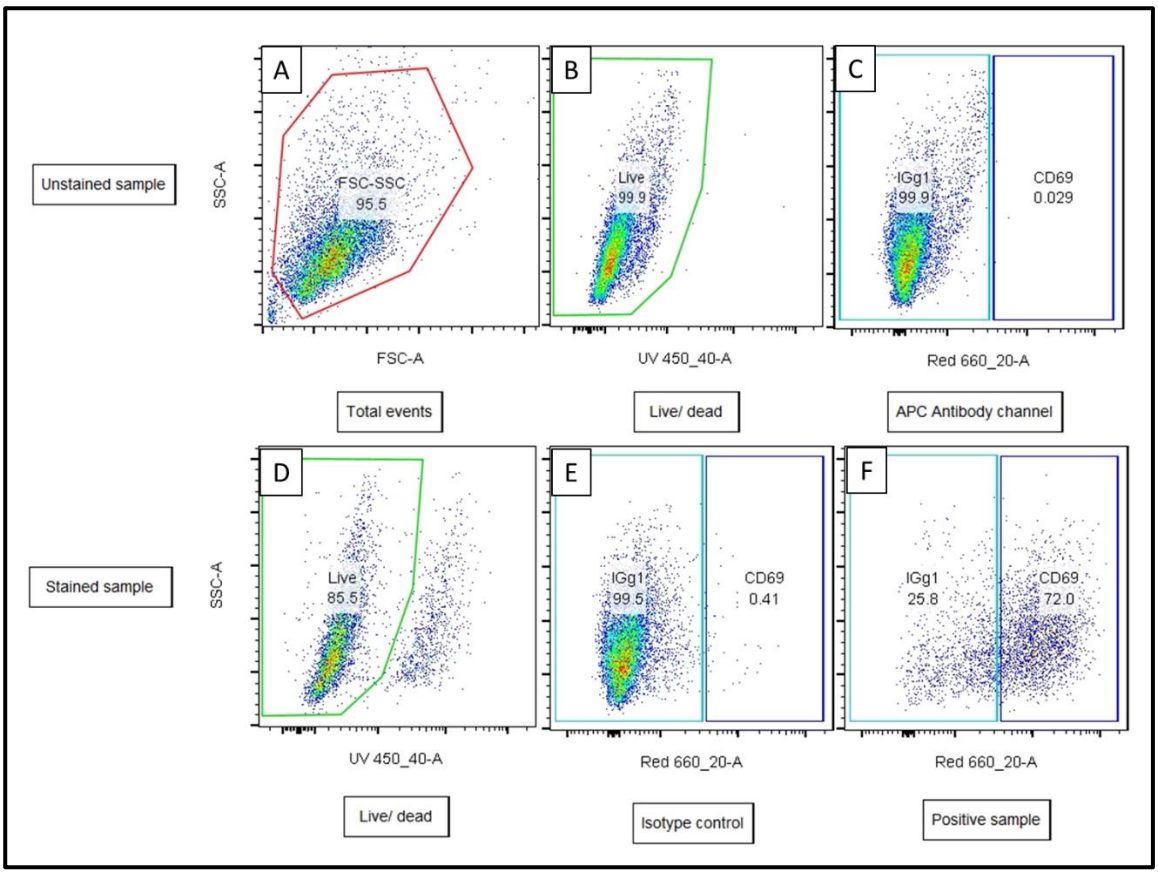

Figure 2.9: Dot plots presents the gating strategy for the single colour flow cytometry. The unstained sample was used to set voltages for (A) the main population on the FSC/SSC blot and to exclude background fluorescence (B) UV channel, and (C) the APC antibody detecting channel. Then, (D) The viability was gated from main population in a stained sample to exclude dead cells from analysis. (E) an isotype control was used to account for non-specific staining and the fluorescent channel (APC) voltages adjusted with a (F) positively stained sample. Image from gating for T cell activation experiment.

2.6.4 Multicolour surface, intracellular, and nuclear flow cytometry staining to phenotype Th1, Th17, and cytotoxic CD8 T cells

Although the ability of flow cytometry to stain for different targets simultaneously is very important for applications such as phenotyping cells, care must be taken to employ the correct controls and colour panel design. One consideration when performing multicolour fluorescence is the possibility of spectral overlap between different fluorophores. For instance, one fluorochrome, FITC, may emit light in the green detector but some light may spill into other detectors such as the PE or yellow detector which is not an issue with single colour experiment but may produce false positive results when performing multicolour experiment (**Figure 2.10**). Therefore, compensation, which is a mathematical measurement to subtract each fluorochrome spillage from the other detectors, must be performed.

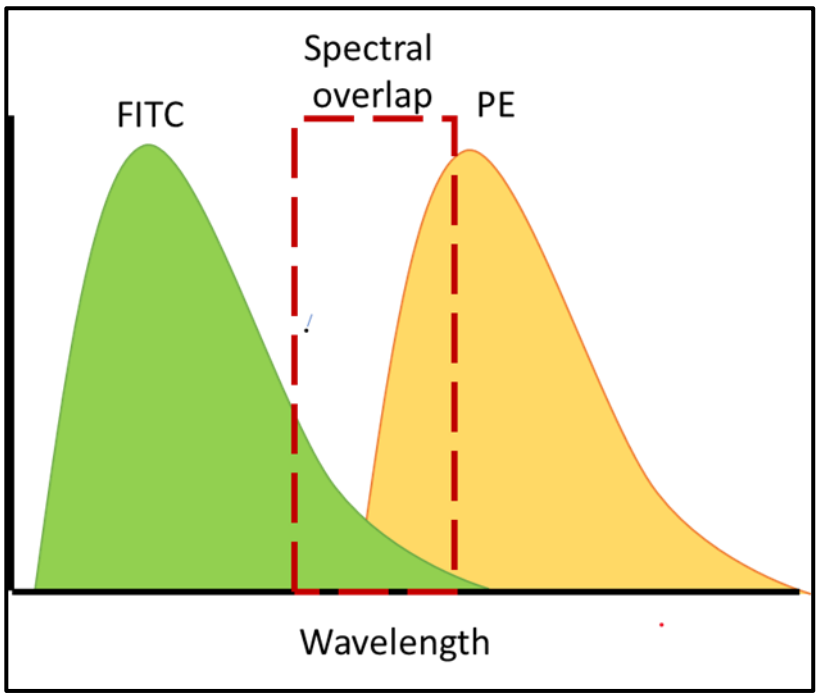

Figure 2.10: An illustration of the spectral overlap between two colours excited through the same laser. Image is own work created by PowerPoint.

To apply and calculate compensation, the following conditions must be fulfilled: first, colour selection is very important as colour overlap cannot always be compensated. For example, if two fluorochromes with very close emission were used, there will be a large spill over especially into a dimly expressed marker and even a good compensation can still lead to a lowered resolution and inaccurate population detection. On the other hand, correct panel design may reduce the need for compensation, for instance, if fluorochromes are excited by different laser beams, there is low, or no compensation needed even if their emission is close. Similarly, if fluorochromes are excited by the same laser but their emission is distant, their compensation is very low. Second, it is important for the bright colours to be matched to less expressed markers in the panel whereas dim colours selected to a highly expressed popular marker. Third, appropriate controls should be used, and they should include at least the followings; unstained sample to account for background fluorescence, a single stained sample to calculate compensation, in which there is a separate sample for each colour in the panel stained with only that colour, and a fluorescence minus one (FMO) control to adjust gating and exclude non-specific fluorescence. The FMO consist of a sample stained with all the colours in the panel except the one its gating for and hence, any fluorescence detected in this sample represents a spillage from the other colours and should be excluded in gating. It is also important that the control used to calculate compensation be brighter than the experimental samples for accurate compensation and to reduce false positive associated with colour spillage and this can be done by using compensation beads, the ABC™ Total Antibody Compensation bead kit, and

the ArC™ Amine Reactive Compensation Bead Kit (Life Technologies, UK) (Cossarizza *et al.*, 2017; Maecker and Trotter, 2009).

Multicolour staining consists of different steps including viability staining, surface staining, fixation and permeabilization, intracellular and nuclear staining, single colour beads control staining, and FMO control staining. The cells were prepared and both viability and surface markers stained as previously described.

2.6.4.1 Staining of Intracellular and nuclear proteins

Cells were fixed with eBioscience™ fixation buffer to stabilise the cell membrane, and then permeabilised by creating pores with detergent or alcohol to allow antibodies access to stain intracellular targets. If intracellular staining alone was required, the eBioscience™ Intracellular Fixation & Permeabilisation buffer set was used whereas if intracellular and nuclear proteins were targeted, the eBioscience™ Foxp3 Transcription Factor staining buffer set was used (ThermoFisher Scientific, UK). Briefly, after surface staining, pellets were resuspended in 1 ml 1 x fixation buffer, pulse vortexed, and incubated, protected from light, for 30-60 minutes at 4°C or room temperature. 0.5 ml 1 x permeabilisation buffer was added to each tube and centrifuged at 400-600 g for 5 minutes then supernatant discarded. The pellet was washed again in permeabilisation buffer then resuspended in 100 µL permeabilisation buffer. The recommended amount of the directly conjugated antibodies directed to intracellular or nuclear target (**Table 2.11**) were added and incubated for 30 minutes at room temperature. Samples then were washed twice with 1 ml of permeabilisation buffer and resuspended in 300-500 µL 1% BSA ready for analysis by flow cytometry.

Table 2.11: Flow cytometry antibodies. List of the conjugated antibodies used for single and multicolour flow cytometry and the designed fluorochromes panel for each experiment.

Fluorophore	Laser	Target	Filter	Clone	Vendor	Category
Single colour antibodies						
LIVE/DEAD™ Fixable Blue Dead Cell Stain	UV 355nm	Viability	450/50	-	ThermoFisher	Viability
PE	Blue 488nm	CD4+	575/26	RPA-T4	eBioscience	Lineage

APC	Red 633	CD4+	660/20	PRA-T4	ThermoFisher	Lineage
APC	Red 633	CD69	660/20	FN50	ThermoFisher	Surface marker
APC	Red 633	Mouse IgG1 Isotype Control	660/20	P3.6.2.8.1	eBioscience	
APC-CY7 or H7	Red 633nm	IL-17	780/60			Intracellular cytokine
First Th1 Panel						
LIVE/DEAD™ Fixable Blue Dead Cell Stain	UV laser 355nm	Viability	450/50	N/A	ThermoFisher	Viability
BD Horizon V500	Violet 405nm	CD4+	525/50	RPA-T4	BD Bioscience	Lineage
APC	Red 633nm	CXCR3	660/20	CEW33D	eBioscience	Surface receptor
PE	Blue 488nm	RANTES/ CCL5	575/26	NP-6G4	eBioscience	Surface marker
PE-Cy7	Blue 488nm	CCR6	780/60	R6H1	eBioscience	Surface receptor
Alex Fluor 700	Red 633	IL12-R-Beta1	730/45	69310	R&D System	Surface
FITC	Blue 488	IFN-γ	530/30	4S B3	Biolegend	Surface
Second Th1 Panel						
LIVE/DEAD™ Fixable Blue Dead Cell Stain	UV 355nm	Viability	450/50		ThermoFisher	Viability
PE	Blue 488nm	CD4+	575/26	RPA-T4	eBioscience	Lineage
FITC	Blue 488nm	IFN-g	530/30	4S.B3	eBioscience	Intracellular cytokine

PE-CY7	Blue 488nm	T-bet	780/60	4B10	eBioscience	Transcriptional factor
Th17 Panel						
LIVE/DEAD™ Fixable Blue Dead Cell Stain	UV 355nm	Viability	450/50		ThermoFisher	Viability
PE	Blue laser 488nm	CD4+	575/26	RPA-T4	eBioscience	Lineage
FITC	Blue 488nm	IFN-g	530/30	4S.B3	eBioscience	Intracellular cytokine
APC-CY7	Red 633nm	IL-17	780/60	BL168	Biolegend	Intracellular cytokine
PE CF594	Blue laser 488nm	FOXP3	660/20	236A/E7	BD Bioscience	Transcriptional factor
APC	Red 633	RORC2	660/20	600380	R&D System	Transcriptional factor
Cytotoxic CD8 Panel						
LIVE/DEAD™ Fixable Blue Dead Cell Stain	UV 355nm	Viability	450/50		ThermoFisher	Viability
APC	Red 633nm	CD8+	660/20	RPA-T8	ThermoFisher	Lineage
PE	Blue laser 488nm	CD4+	575/26	RPA-T4	eBioscience	Lineage
Alexa Fluor 700	Red 633nm	Granzyme B	730/45	GB11	BD Bioscience	Intracellular cytokine
APC	Red laser 633nm	CD69	660-20	FN50	eBioscience	Surface marker

2.6.4.2 Single stained controls

Each kit of the ABC™ Total Antibody Compensation bead kit contains two types of modified polystyrene microspheres, the total compensation capture beads that bind to all antibodies and the negative beads which have no antibody binding capacity. Following incubation with conjugated antibody, the two beads will provide distinct positive and negative populations that can be used to set compensation (**Figure 2.11**). For any amine reactive dyes such as the fixable blue live dead dye, the ArC™ Amine Reactive Compensation Bead Kit was used. This kit works similarly to the ABC kit but it is compatible with amino reactive dyes.

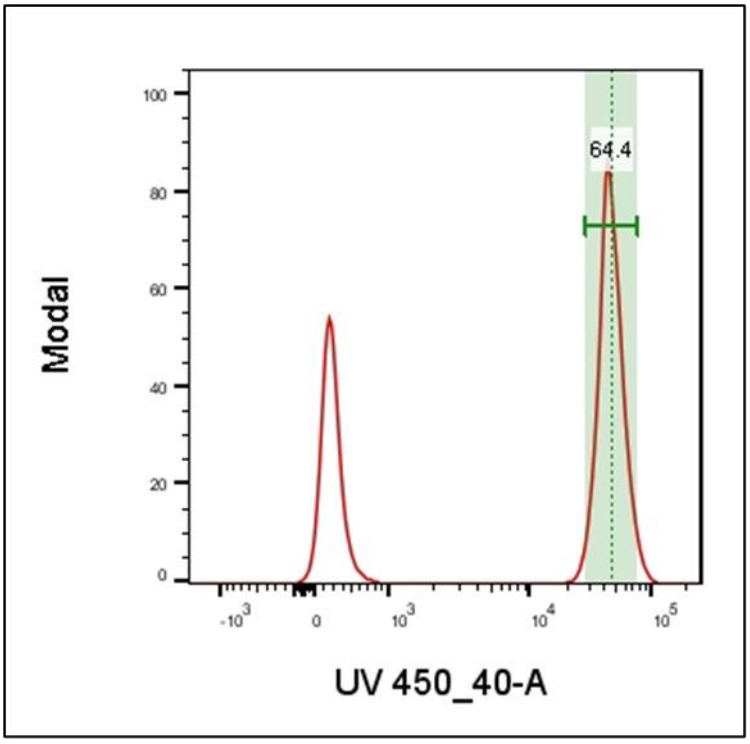

Figure 2.11: A histogram illustrates distinct positive (far right) and negative populations (far left) using the ArC beads that can be used to set compensation. Image is own work created by FlowJo.

The ABC and the ArC beads were vortexed for 10 seconds and one drop from component A (positive beads) of the ArC kit was added to one tube labelled for live/dead which was mixed with 2 µl of the fixable blue viability. Similarly, one drop from component A of the ABC kit was added to the tubes corresponding to the other conjugated antibodies and a relevant amount of the antibody was added to each designated tube. All tubes were incubated for 30 minutes, protected from light then washed with PBS and resuspended in 300-500 µL 1% BSA before a drop of component B (negative beads) was added. An example of calculated compensation values for the first Th1 panel shown in (**Table 2.12**).

Table 2.12: Compensation matrix. The Compensation matrix applied by BD LSRII using ABC™ and ArC™ compensation beads for a panel of fluorochromes. This is a representative example shows the average compensation for the first Th1 panel.

Average Compensation values	Blue 530_30-A	Blue 575_26-A	Blue 780_60-A	Red 660_20-A	Red 730_45-A	UV 450_40-A	Violet 450_50-A
Blue 530_30-A	100%	28%	1%	0%	0%	0%	3%
Blue 575_26-A	1%	100%	2%	0%	0%	0%	0%
Blue 780_60-A	0%	2%	100%	0%	11%	0%	0%
Red 660_20-A	0%	0%	0%	100%	28%	0%	0%
Red 730_45-A	1%	0%	2%	1%	100%	0%	0%
UV 450_40-A	2%	1%	1%	1%	1%	100%	21%
Violet 450_50-A	15%	9%	-2%	-2%	0%	1%	100%

2.6.4.3 Fluorescence minus one control

1 x 10^6 cells per sample were composed of cells most positive for the antigen. The microtubes were labelled by the missing fluorochrome then the staining steps described before (Sections 2.6.4) were followed except for that, each sample composed of all the conjugated antibodies except for one antibody, hence, one of the antibodies will not be used for each sample.

2.6.4.4 LSRII setting and gating strategy

The flow cytometry FSC and SSC thresholds first adjust using an unstained sample to minimise the background signals and then by a positively stained sample to adjust fluorescence threshold for each parameter used. The gating strategy followed a hierarchy starting by gating for total events in the sample using the FSC/SSC plot, to which a stopping gate was set at $1x10^4$ events for all samples but increased to $1x20^4$ when acquiring the FMO samples. Then, FSC-H/FSC-A plot was set to gate for single cells and exclude cell doublet events, followed by a viable cell gating using the UV450-40 parameter (live/dead dye). Finally, the parent population

was gated from viable cells using cell surface marker, CD4 or CD8, from which all other the parameters were separately gated (**Figure 2.12**).

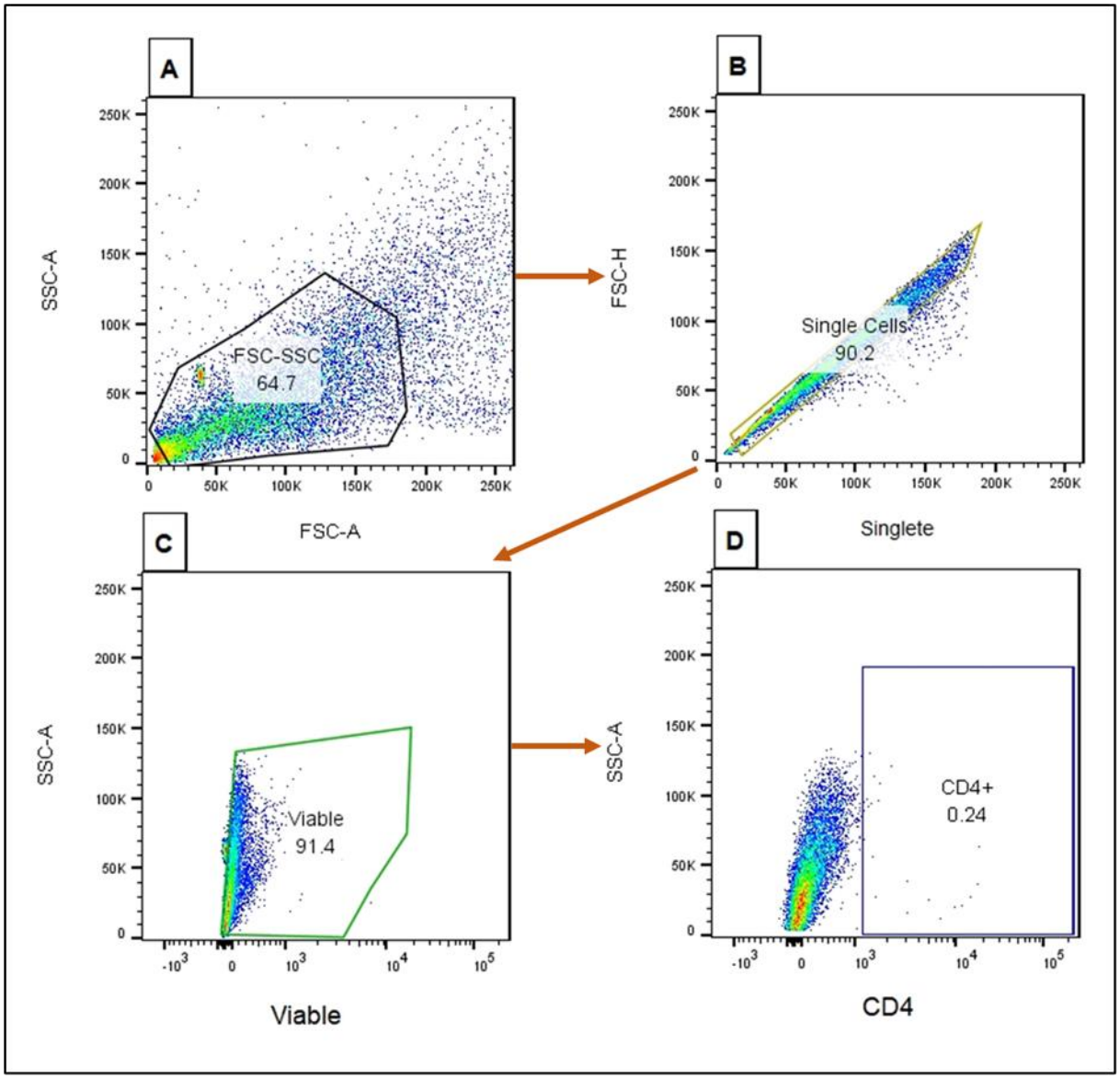

Figure 2.12: An example of the gating strategy for the multicolour flow cytometry using unstained sample that was adjusted with FMO sample. (A) the total events collected, then (B) doublet events and (C) dead cells were excluded, before (D) gating for the CD4+ (or CD8 population) which was used for further analysis. This is a representative example used the second Th1 panel experiment.

The gates for all targets were adjusted using an FMO samples. An example using the second Th1 panel is illustrated in (**Figure 2.13**). After setting all parameters, a compensation group was created and for each bead tube run, negative and positive populations were identified. The compensation was calculated and applied, then all samples recorded by the LSRII and further analysed using FlowJo.

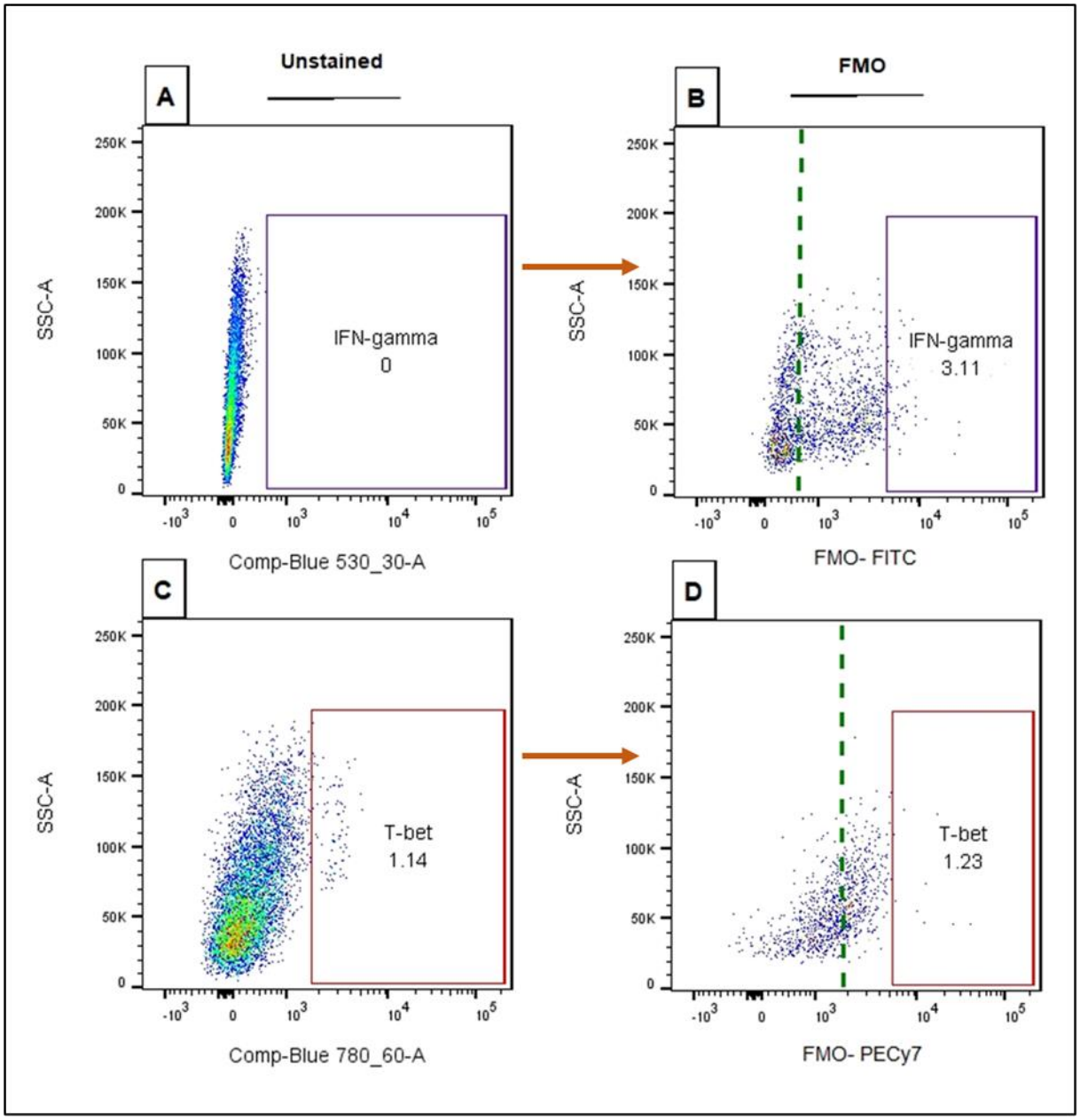

Figure 2.13: Target gating adjustment in multicolour flow cytometry using FMO samples. Dot plots in (A) and (C) show gating for IFN-γ-FITC and T-bet-PE-CY5 using an unstained sample whereas (B) and (D) show corrective gating using the FMO sample that reflects any spillage from the other colours. The area between the FMO gate and the unstained gate (in green dotted line) represents a false positive result. This is a representative example used the second Th1 panel experiment.

2.7 Statistical analysis

Unless otherwise stated, statistical analysis was performed using Graph-Pad Prism software (GraphPad, US). Data are presented as mean ± standard deviation (SD) and the number of biological repeats is shown as n=. Analysis of variance, unpaired T test was used to determine if there is a difference between two different groups, one-way and two-way (ANOVA) was carried out to compare the differences between more than two means and differences

between individual means were performed using a post-hoc test as stated. Significant difference was determined when *$p < 0.05$, **$p < 0.01$ and ***$p < 0.001$ compared to control.

3 Chapter three: Optimisation of culture methods

3.1 Introduction

A breakdown in immune tolerance and an autoreactive T cell response may cause immune mediated diseases such as diabetes mellitus (DM), rheumatoid arthritis (RA), systemic lupus erythematosus (SLE), oral lichen planus (OLP), amongst others (Skapenko *et al.*, 2005; Schwartz *et al.*, 2020). A large body of murine and human studies have utilised whole tissue or peripheral blood to establish different mechanisms of T cells dysfunction. Although monocytes and T cells can be obtained from other sources, peripheral blood and buffy coats are considered the most common source of peripheral blood mononuclear cells (PBMCs) for *in vitro* studies (Raulf, 2019). Primary T cell isolation from blood requires the use of specialist reagents and kits that are expensive and often produce a low yield of cells. Moreover, these cells have a finite lifespan, limited expansion capacity and inter-donor variability. Hence, their use to establish experimental standardisation may be considered limited, expensive and time-consuming (Pan *et al.*, 2009). Cell lines are generally highly proliferative and easier to culture. Therefore, in this chapter, Jurkat cells, an established T-cell cell line, were used to optimise cell culture techniques in 2D and 3D. Although major advances in our understanding of T cell receptors and signalling pathways has stemmed from the use of different T cell lines such as human MALT, HL60, HuT-78, and mouse EL4 and LBRM-3, debatably, the Jurkat T cell line has been the most popular, most characterised, and historically the most utilised of this T cell line collection (Abraham and Weiss, 2004). Jurkat T cells are an immortalised human T lymphocyte cell line that were established in the late 1970s from the peripheral blood of a 14-year-old boy with T cell leukaemia (Schneider and Schwenk, 1977; Schneider, Schwenk and Bornkamm, 1977). These cells have often been used as a classical T cell line to study multiple events in T cell biology, besides, many of the signalling proteins were first identified and characterised *in vitro* using long-term cultured T cell lines (Abraham and Weiss, 2004). On a similar note, FNB6 which are normal oral keratinocytes obtained from a healthy volunteer and immortalised by ectopic overexpression of human telomerase reverse transcriptase (hTERT), were used to establish methods and to contribute to the epithelium formation in oral mucosal equivalents (OME) in this study. Since hTERT has been reported to be able to immortalise cells without causing cancer-associated changes or altering phenotypic properties, FNB6 came into popular use to overcome the limitation of using primary oral keratinocytes or cancer cells (Lee, Choi and Ouellette, 2004; Dickson *et al.*, 2000).

The dense sub-epithelial band of inflammatory T lymphocyte in OLP is an essential criterion to be reproduced in *in vitro* OME by involving activated and polarised T cells and has not been achieved to date. There are a few attempts in the literature to involve T cells in oral

disease models but none of these have used polarised T cells or included these cells in complex 3D oral mucosal models (Sriram, Bigliardi and Bigliardi-Qi, 2018; Kühbacher *et al.*, 2017b). Hence, it is the aim of this study to incorporate activated T cells into OME composed of fibroblast-populated connective tissue topped by a stratified epithelium. However, these different cell types are usually cultured in different media suitable for their biological and cellular needs. As a result, one of the challenges that needs to be overcome is the fact that different cell types need to be cultured in one mutual medium when combined in 3D. While T cells require RPMI medium, optimal conditions for tissue-engineered OME and epithelial differentiation requires adenine and flavin-enriched Green's medium. Moreover, hydrocortisone, which is one of the components of Green's medium and commonly used as a supplement for endothelium, epithelial or mesenchymal cell culture media (as it supports long term growth and differentiation) (Jung *et al.*, 2012), is a glucocorticoid hormone with anti-inflammatory and immunosuppressive effects and, hence, inhibitory for activated T cells (PALACIOS and Sugawara, 1982). Therefore, in this chapter, both FNB6 and T cells were adapted to grow in Green's medium without hydrocortisone supplementation and their proliferation status determined using a cell proliferation assay. These assays are extensively used in tissue culture to measure the growth rate of a cell population not only to provide valuable information about basic health and cell maintenance, but accurate measurement of cell proliferation allows for a better understanding of the dynamics of cellular responses to extracellular stimuli, such as immune responses.

This chapter also provides a learning process through the main concepts of this research, handling T cells. For this purpose, the morphology and activation of T cells were investigated in suspension cultures. However, since 3D cultures achieve the requirement for *in vitro* methods that permit a precise study of the molecular mechanisms underlying human diseases (Freshney, 2015), Jurkat cells proliferation and viability in collagen hydrogel were assessed using the PrestoBlue™ assay.

3.2 Aim and objectives:

This chapter aims to optimise the medium and cell culture methods for T cells using Jurkat cells as a model cell line.

3.2.1 Objectives:

- Assess Jurkat T cell morphology, proliferation and activation in suspension cultures using microscopy, CellTrace™ Far Red, and flow cytometry.

- Standardise the culture media for both T cells and oral keratinocytes in Green's medium without hydrocortisone using the cell trace proliferation assay.

- Optimise the number of T cells and assess proliferation and viability within a collagen hydrogel using a PrestoBlue™ assay.

3.2.2 Materials and methods

Please refer to chapter 2 for all materials and methods.

3.3 Results:

3.3.1 Morphology and proliferation characteristics of Jurkat T cells

Jurkat cells were maintained in RPMI-1640 media at a density of 3-9x10^5 cells/ml. Cells were examined by light microscopy to monitor cell morphology. After passaging, cells appear as small round shiny spheres dispersed in a suspension culture. Following 2-3 days of incubation, healthy cells were observed to proliferate and clump together forming shiny aggregates indicative of cell proliferation (**Figure 3.1**)

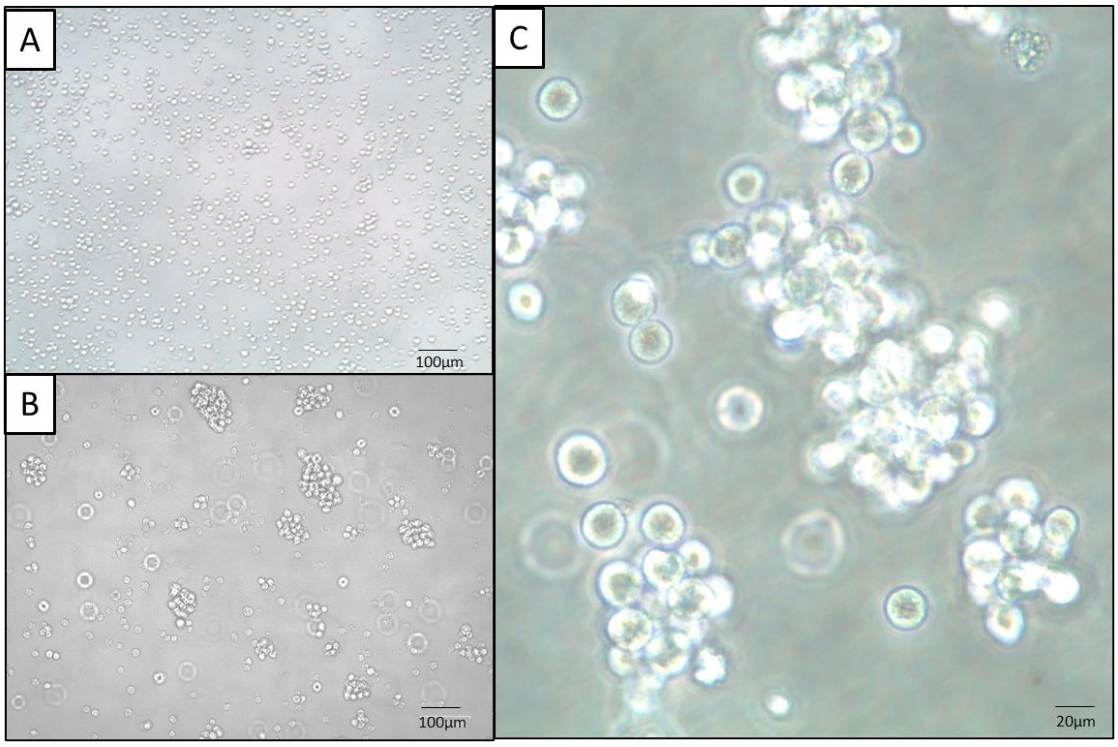

Figure 3.1: Morphology of Jurkat T cells in suspension culture over-time. Jurkat cells were examined in suspension culture by inverted light microscopy (A) Jurkat cells form small transparent spheres of cells dispersed in cell suspension. (B) Once proliferating, cells tend to aggregate together forming (C) shiny transparent clusters of active T cells. Images are representative. Scale bar for A & B= 100 µm and C= 20 µm.

The cell proliferation profile of Jurkat cells was followed for five days using CellTrace Far Red. An optimal cell trace dye dilution should stain cells brightly, uniformly and with no cytotoxicity. The discrete peaks in the histograms represent successive generations of Jurkat

cells with the peak of the highest median fluorescence (day 0; on the far right of the histogram) representing the parent population while the other peaks are the successive daughter generations (**Figure 3.2**). Generally, there is an overall uniformity of peaks as the CellTrace Far Red is distributed equally into daughter cells upon mitosis with the quantified median fluorescent intensity decreasing overtime from 2139± 794 MFI at day 0 to 18.5± 1.6 MFI at day 6 (**Figure 3.2A&B**). Doubling time (dt) is the time it takes for a population to double in number (Pereira *et al.*, 2020). The doubling time of Jurkat T cells was (17.6 ± 0.9 hours).

Jurkat cells were directly counted under an inverted light microscope daily over 6 days of culture to confirm their growth profile. The number of live cells increased gradually from 2.5 $x10^6$ for both stained and unstained control at day 0 to 16.9 ± $4x10^6$ and 17.7 ± $4.7x10^6$ at day 6 for stained and unstained control, respectively (**Figure 3.2C**).

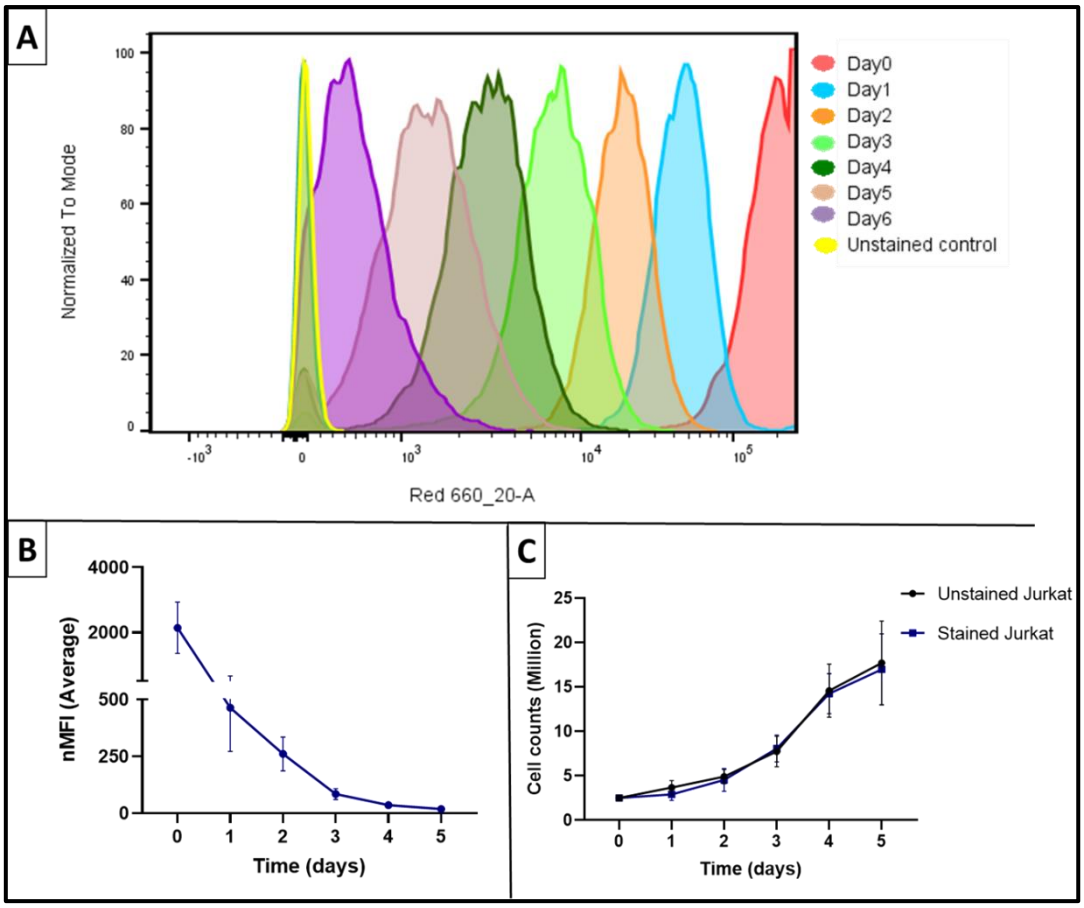

Figure 3.2: Jurkat cell population proliferation profile. (A) Jurkat cells were stained with CellTrace™ Far Red and cell proliferation determined over 6 days using flow cytometry. The discrete peaks in the histogram represent successive generations of daughter cells. The parent generation is indicated as day 0 (dark red, far right peak). (B) Normalised median fluorescent intensity (nMFI) decreased overtime as the dye was distributed into daughter cells following mitosis. (C) Direct cell counting to determine cell growth over 6 days in culture. The histogram in (A) is representative and both line graph data are expressed as the mean ± SD; n=3.

3.3.2 Jurkat cell activation status determined by CD69 surface protein levels and secreted IL-2

Jurkat cells were activated by incubation with PMA and ionomycin at a final concentration of 50 and 500 ng/mL, respectively, for 4, 6, and 24 hours. Cell surface protein levels of the activation marker CD69, also known as very early activation antigen (VEA), was determined by staining with a fluorescently conjugated anti-CD69 antibody and subsequent analysis by flow cytometry. An anti-mouse IgG1 antibody was used as an isotype control to identify any non-specific staining. The increased cell surface abundance of CD69 showed successful activation of Jurkat cells with an average of 90 ± 5.9% of the cells expressing the marker after 24 hours (**Figure 3.3**), compared to the inactivated control (4.4 ± 7%, $p<0.0001$). Cell activation was time-dependent with an average of 60 ± 18, 74 ± 13 and 90 ± 5.9% of cells positively stained after 4-, 6- and 24-hours activation, respectively (**Figure 3.3A-D**). There was no significant difference in levels of CD69 between 4 and 6 hours or 6 and 24 hours but the expression after 24 hours CD69 showed a significant 30% increase over that observed at 4 hours ($p <0.001$) (**Figure 3.3E**).

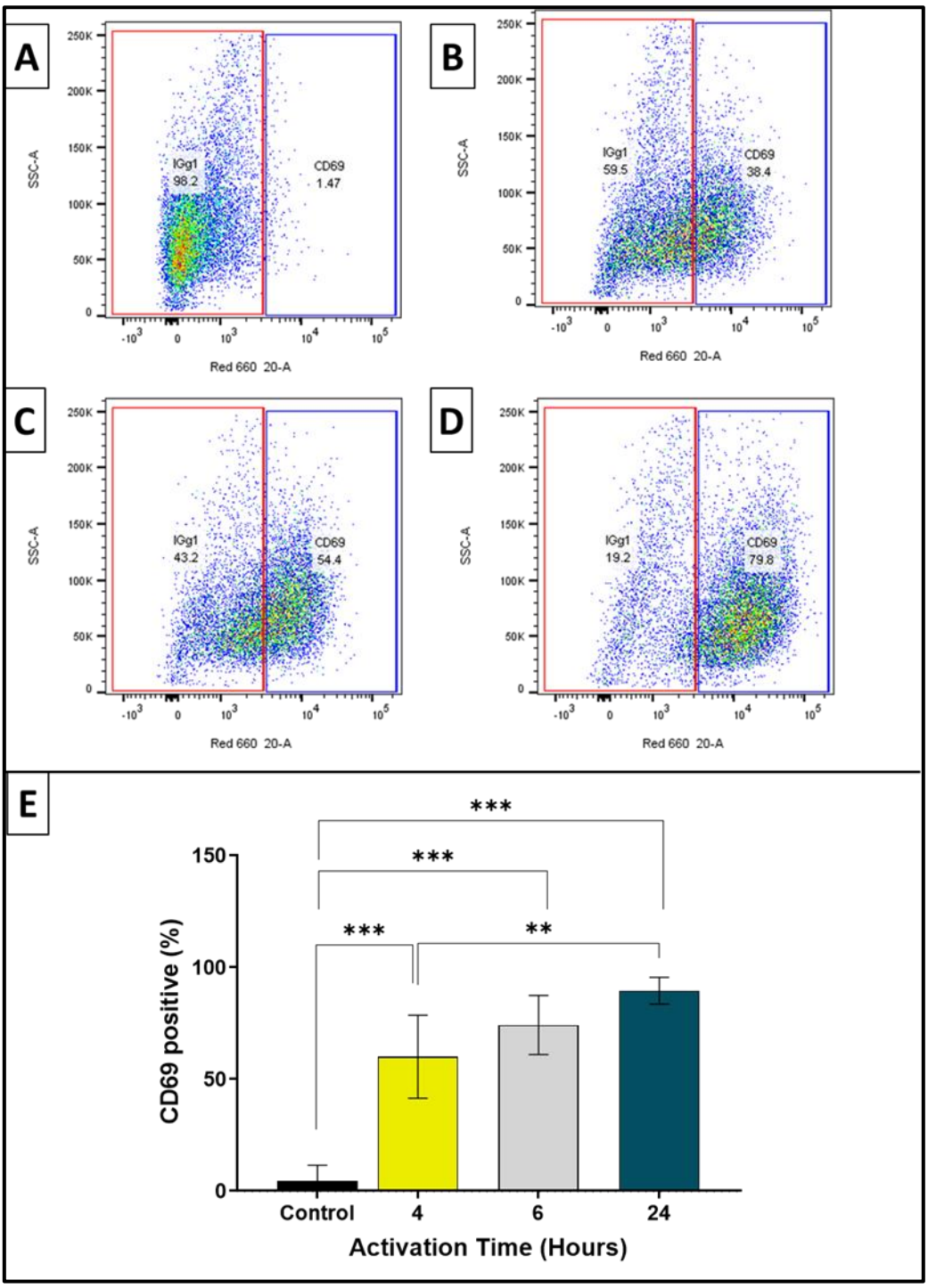

Figure 3.3: Abundance of cell surface marker CD69 following Jurkat cell activation. Jurkat cells were left untreated (A) or treated with PMA and ionomycin for either (B) 4, (C) 6 or (D) 24 hours before being stained with anti-CD69. Viable cells were gated using Live/Dead stain and the CD69-positive cells detected by flow cytometry. Data are presented as representative dot plots. (E) Data are presented as the mean ± SD. A mean difference was considered significant when *p < 0.05, **p <0.001, and ***p <0.0001, using one-way ANOVA with Tukey's post-hoc multiple comparison tests to detect difference between groups. Main ANOVA reported ***p <0.0001; n=5.

An ELISA was performed on the conditioned medium collected following Jurkat T cell activation to detect the secretion of IL-2 after 4, 6 and 24 hours. A significant increase in IL-2 levels was observed in a time-dependent manner. All samples collected from activated Jurkat

T cells had detectable levels of IL-2 secreted in the media. Four hours after activation 72.4 ± 28.4 pg/ml of IL-2 was detected but this was not significantly different from the non-activated control. IL-2 levels increased to 225.3 ± 104 pg/ml and 321 ± 113 pg/ml after 6 and 24 hours of activation, respectively. The levels of IL-2 secreted after 24 hours activation was approximately 4-fold higher ($p < 0.001$) than at 4 hours, but no significant difference was observed between 6 and 24 hours (**Figure 3.4**).

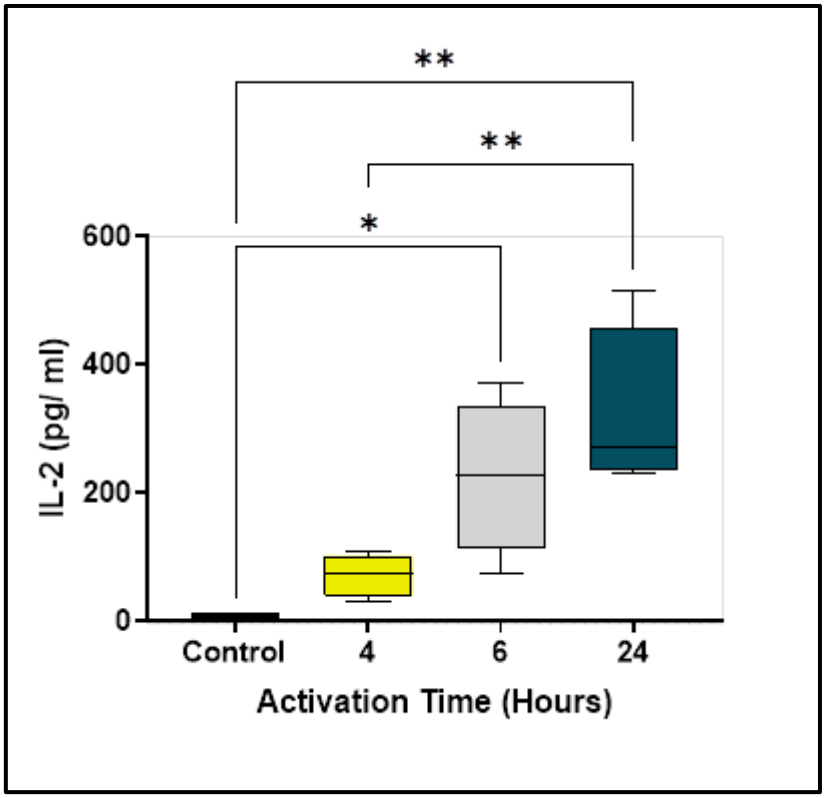

Figure 3.4: Secretion of IL-2 following activation of Jurkat cells. The levels of IL-2 secreted in the medium of activated Jurkat T cells were detected by ELISA. The IL-2 secretion was increasing in time dependant manner. OD was acquired at 450 nm with a wavelength correction at 570 nm. Data are expressed as the mean ± SD. A mean difference was considered significant when *$p < 0.05$ and **$p < 0.001$ using one-way ANOVA with Tukey's post-hoc multiple comparison tests to detect difference between groups. Main ANOVA reported *$p < 0.0012$. n=4

3.3.3 Growth of Jurkat T cells in different culture medium

Jurkat T cells were transferred gradually in incremental steps from culture in 100% RPMI to 100% Green's medium (without hydrocortisone). As cells were transferred into higher concentrations of Green's medium during passaging, the cell viability was assessed using the trypan blue exclusion dye assay. Once the cells had been transferred into 100% Green's medium for continued growth, a proliferation profile was completed over 5 days using the Far Red Cell Trace assay.

Jurkat cells were successfully transferred and adapted for culture in 100% Green's medium without hydrocortisone. The mean viability over a 10-day transfer period is presented in (**Table 3.1**). All cells cultured in the different concentrations of media; 100% RPMI, 25%, 50%, 75% and 100% Green's medium, maintained viability at or above 89.3 ± 7%. Following transfer to 100% Green's media, cells cultured in different concentrations showed no significant difference in cell viability from those cultured in 100% RPMI medium.

Table 3.1: Viability of Jurkat T cells during transfer from 100% RPMI to 100% Green's media. The viability of Jurkat T cells whilst being gradually transferred from 100% RPMI into 100% Green's media over 10 days was assessed using the trypan blue viability assay. Data were expressed as the mean ± SD; n=3.

Days	100% RPMI	25% Green's	50% Green's	75% Green's	100% Green's
0	96.3 ±2				
3	95.4 ±2	92.4 ±3			
5	92.4 ±6	91.7 ±7	92 ±7		
7	91.6 ±5	92.2 ±4	89 ±7	90.6 ±6	
10	95 ±3	94.3 ±3	90.6 ±8	91.6 ±5	89.3 ±7

3.3.4 Jurkat T cell proliferation profile and activation in Green's medium compared to RPMI

The proliferation profile of Jurkat T cells was followed over 6 days in cells grown in either 100% RPMI (**Figure 3.5A**) or 100% Green's medium (**Figure 3.5B**) using a Far Red CellTrace assay. Both cultures showed a comparable proliferation profile with distinctive peaks, each representing a new daughter cell generation. The red peak on the far right of the graphs represents the parent population that was labelled with the fluorescent dye at day 0. At days 3, 4, and 5 peaks in both media became broader and had larger overlap reflecting heterogeneity of daughter populations. Moreover, the reduction in fluorescence was less compared to the sharp drop witnessed in the first two days (**Figure 3.5B**) reflecting reduced proliferation. Both cultures lost fluorescence and hence no further division rounds could be detected after day 5. Doubling time of Jurkat in RPMI (18.6 ± 1.6 hours) was not statistically different to Dt of Jurkat in Green's (20 ± 1.4 hours, $p < 0.4$). A two-way ANOVA test concluded no significant difference between the means of the two groups at each time points, indicating that Jurkat T cells proliferated at similar levels in both RPMI and Green's medium.

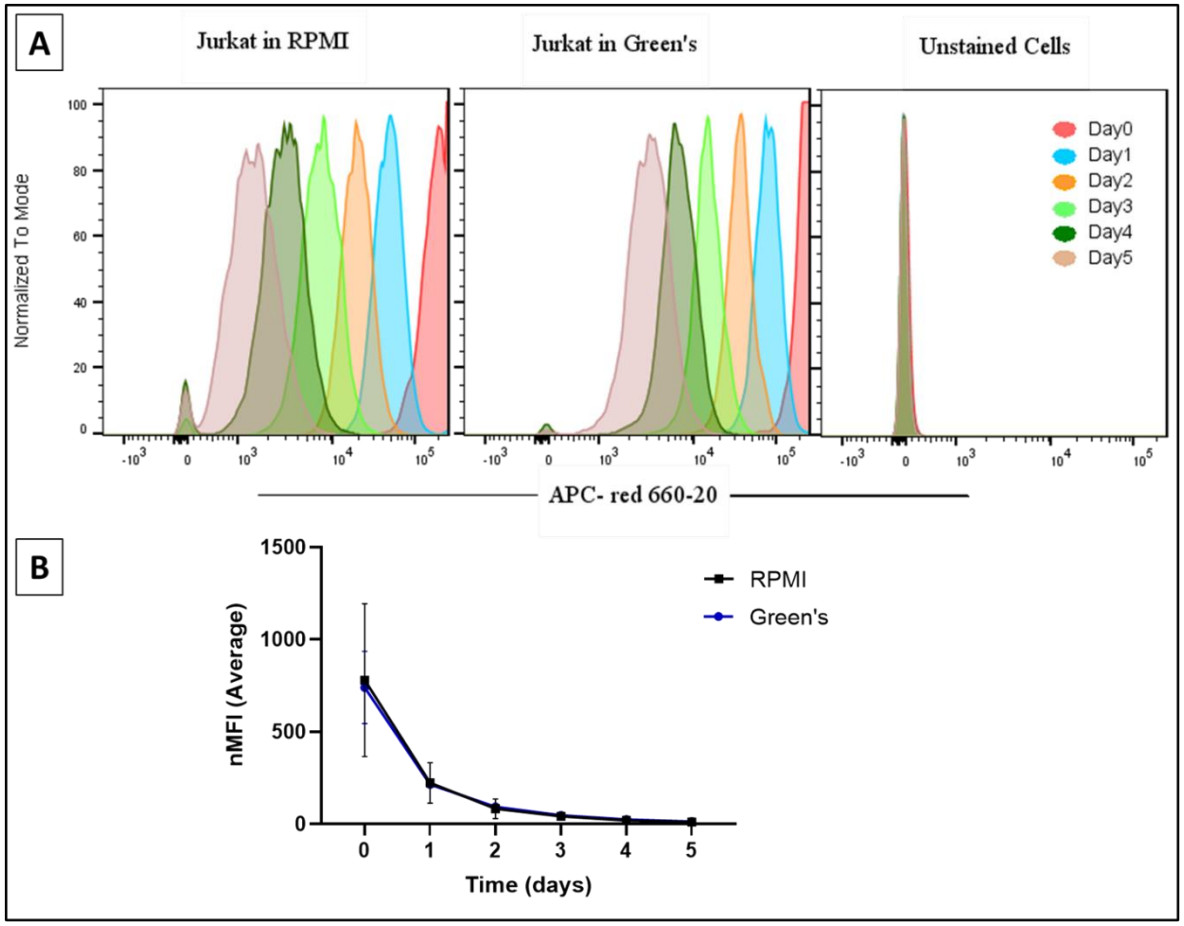

Figure 3.5: Jurkat T cell proliferation profiles in RPMI compared to Green's medium. Jurkat T cells were stained with CellTrace™ Far Red and cell proliferation traced over 6 days in 100% RPMI and Green's medium. (A) Representative histograms and (B) normalised median fluorescent intensity (nMFI) reveals that cells cultured in Green's and RPMI show similar proliferation profiles over time. Data is presented as mean ± SD. ANOVA reported statistically significant effect of time but there was no effect of media or of the interaction between the two. n=3

3.3.5 Jurkat T cell activation in different culture medium

Jurkat T cells were activated by incubating with PMA and ionomycin for 24 hours, as previously described, but this time in different culture media; 100% RPMI, 100% Green's medium (without hydrocortisone) or in mixture of 75%/25% Green's to RPMI, respectively. The levels of the cell surface activation marker CD69 was analysed by flow cytometry. CD69 was significantly increased (p= 0.0012) when compared to non-activated controls in all media investigated but were not significantly different from each other (**Figure 3.6**).

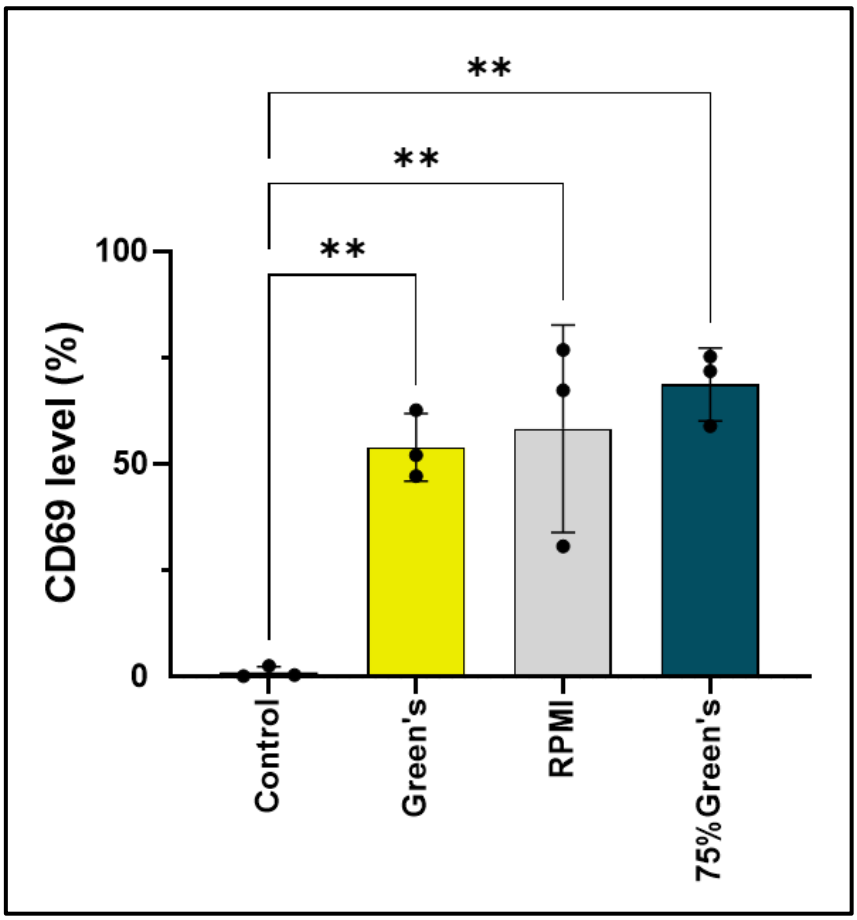

Figure 3.6: Abundance of the cell surface marker CD69 following Jurkat T cell activation in different medium. Untreated Jurkat T cells or cells treated with PMA and ionomycin were cultured in either 100% RPMI, 100% Green's medium, or 75%/25% of Green's: RPMI medium for 24 hours before being stained with anti-CD69. Viable cells were gated using Live/Dead stain and the CD69 positive cells detected by flow cytometry. Data presented as the mean ± SD. A mean difference was considered significant when *p < 0.05 with **p <0.001 using one-way ANOVA with Tukey's post-hoc multiple comparison tests to detect difference between groups. Main ANOVA reported *p <0.001 n=3.

3.3.6 Incorporation of Jurkat T cells into collagen hydrogels

Haematoxylin and eosin (H&E)-stained histological sections showed well-distributed Jurkat T cells within the collagen hydrogel. The cells were typical of lymphocytic cells in appearance in that they were small, with a large nucleus and were observed to exist in aggregates. Cells were distributed throughout the collagen scaffold, however, more cells existed solo or in clusters at the medium/scaffold interface (**Figure 3.7A**).

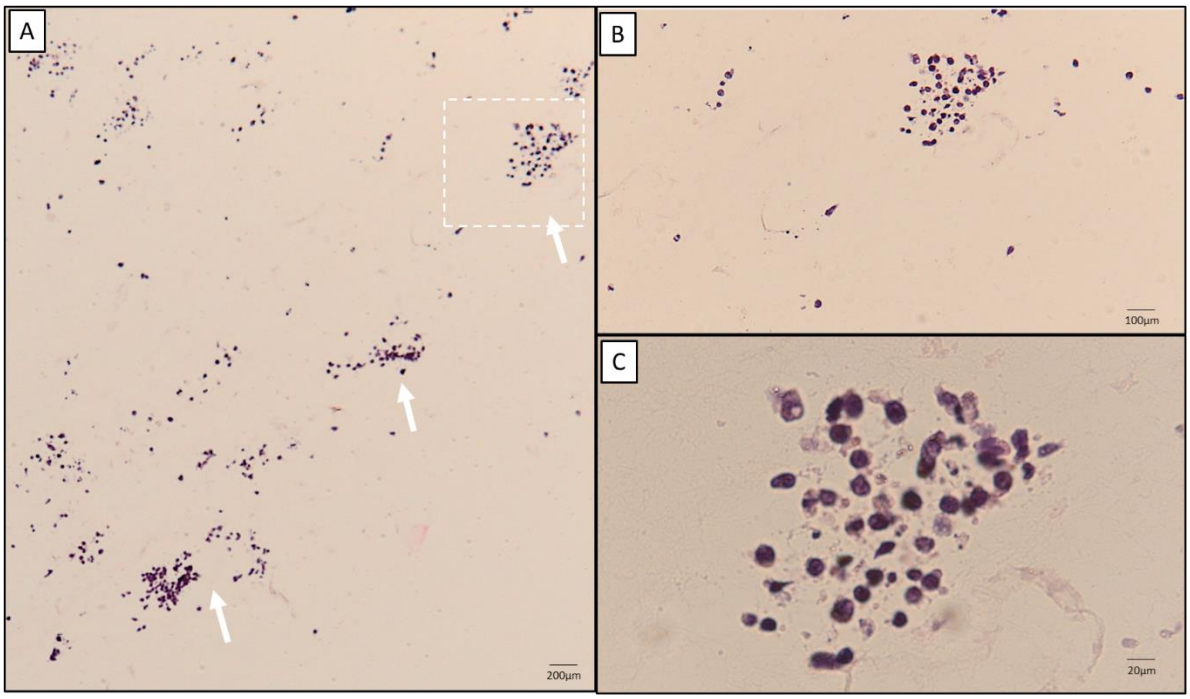

Figure 3.7: Morphology of Jurkat T cells in 3D collagen hydrogels. Representative H&E-stained sections of Jurkat T cells cultured in collagen hydrogels were examined using light microscopy. Sections displayed (A) well distributed cells within the hydrogel with more aggregates were noticed at the liquid-scaffold interface (white arrows). (B&C) Evidence of cell clusters, indicative of proliferating cells. (C) Higher magnification shows typical lymphocytic cells appearance, small, with large pyknotic nucleus. Scale bar: A= 200 µm, B= 100 µm and C= 20 µm.

To assess if Jurkat T cells could be incorporated into collagen hydrogels, survive, and proliferate, cells were seeded at three different densities $0.5x10^6$, $1x10^6$ and $2x10^6$ and cultured for 14 days. Resazurin, a compound with no intrinsic fluorescence that is present in PrestoBlue® reagent, is reduced upon metabolism by viable cells to form resorufin, which is pink in colour and fluorescent. This conversion is proportional to the number of metabolically active cells and therefore can indirectly infer the number of viable cells in a population. The metabolic rate was assessed on days 1, 3, 7, 10 and 14 post-seeding. There was a general trend for the three cell densities to increase and reach a maximum at day 7 and though their metabolic rate declined slightly afterwards, fluorescence was maintained at or above 21106 ± 5027 AU by day 14 for all densities reflecting continued metabolic activity (**Figure 3.8**).

The metabolic activity of of $0.5x10^6$ per collagen model at day 1 was the lowest, 8703 ± 4356 AU, and had a significantly less metabolic rate than the cells seeded at 1 $x10^6$ and $2x10^6$ in the collagen gels. Cells seeded at $0.5x\ 10^6$ continued to show increased metabolic activity in a time-dependent manner until day 7, 26685 ± 7305 AU, whereupon the fluorescence levels plateau to day 14. Cells seeded at 1 $x10^6$ had an initial fluorescence intensity of 24141 ± 7864 AU at day 1 that increased gradually to reach a maximum metabolic rate of 31894± 6276 AU by

day 7, before gradually declining by day 14 to 21975 ± 6574 AU . In contrast, cells seeded at $2x10^6$ had a high initial fluorescence value at day 1, 30167 ± 5101 AU, that remained stable until day 7 (31508± 3090 AU). At day 7, all densities metabolic levels were roughly similar (**Figure 3.8A**). Moreover, the three cell densities displayed similar fluorescence values; 23271 ± 5199, 21975 ± 6574, and 21107 ± 5027, respectively at day 14 (**Figure 3.8A**). Although, the three cell densities showed slightly decreased metabolic activity on day 14 than day 7, they maintained their metabolic activity reflected by their continual ability to transform resazurin (blue) to resorufin (Pink) when compared to the control hydrogel with no cells (**Figure 3.8B**). These data suggest that while $2x10^6$ might represent maximum capacity for the experimental conditions since the added dye was saturated by $2x10^6$, the $0.5X10^6$ density required cells to adapt and proliferate to be able to produce a colour change by day 7. Regardless, the three densities seem to find their optimal density at day 7.

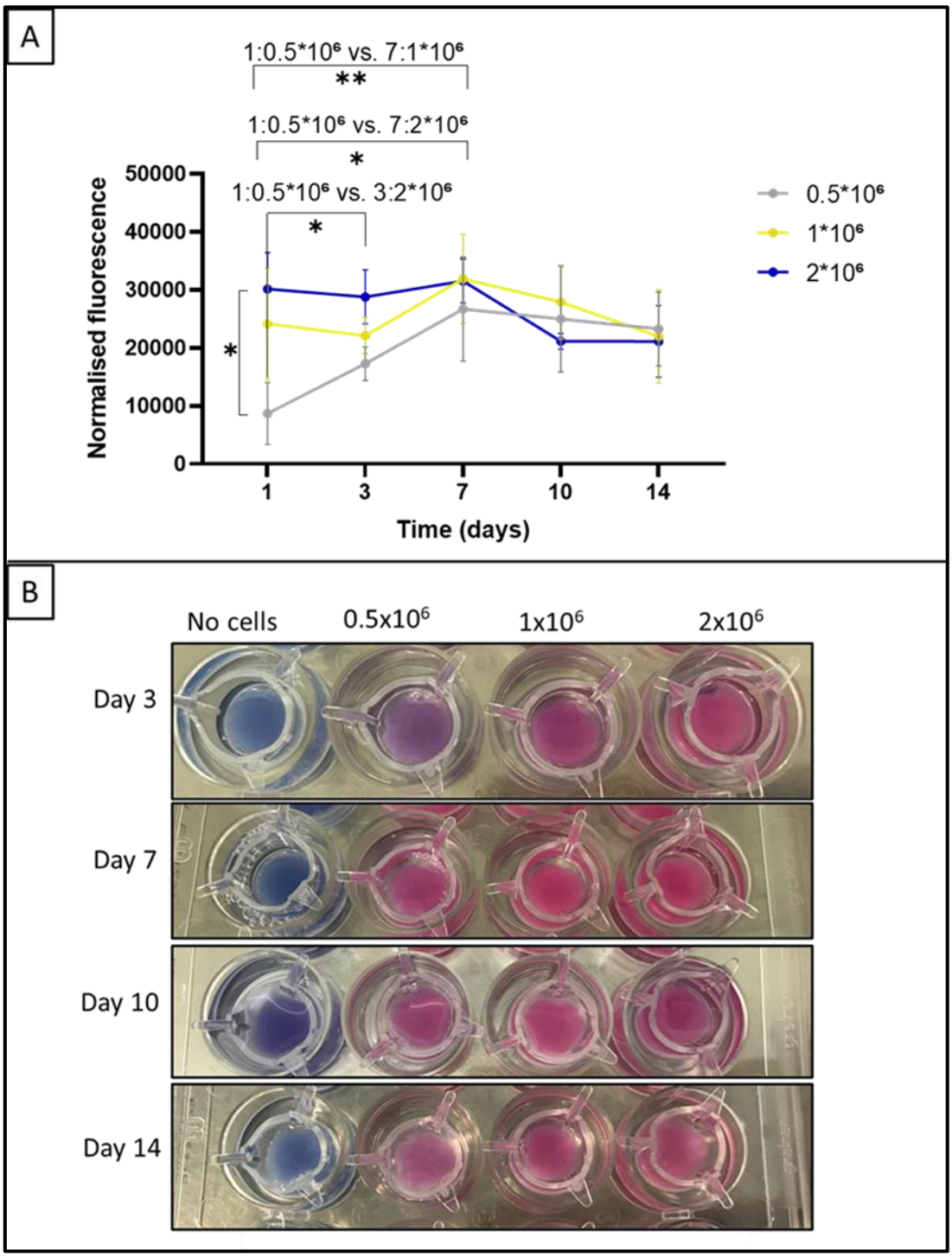

Figure 3.8: Jurkat cell metabolic rate in 3D collagen hydrogels. Viability of cells seeded at different densities (0.5, 1 and 2 x10^6 cells) in collagen hydrogels were assessed overtime using a PrestoBlue® assay and (A) fluorescence measured using a fluorescent plate reader. (B) Representative images of colour change in Jurkat hydrogels over time. Data are expressed as mean ± SD. A mean difference was considered significant when *p < 0.05 and **p <0.001 using two-way ANOVA with Tukey's post-hoc multiple comparison tests to detect difference between and among groups. ANOVA reported statistically significant effect of time and cell number's but there was no effect of the interaction between the two.; n=3.

3.3.7 Proliferation profile of FNB6 in Green's medium with or without hydrocortisone

FNB6 were cultured in Green's medium with or without hydrocortisone supplementation and their proliferation traced over 4 days. The proliferation profile in both types of medium produced uniform and distinct peaks of daughter cells. On the first day of staining (day 0), cells showed the maximum fluorescence intensity which reduced rapidly as the cells divided. This is illustrated with distinct peaks of reduced fluorescence in the histogram (**Figure 3.9B**) or with shift in population to zero fluorescence in the dot plots (**Figure 3.9A**). Average nMFI decreased from 1920 ± 1113 and 1556 ± 595 at day 0 to 14 ±13 and 12 ± 12 at day 4 for FNB6 in Green's medium with or without hydrocortisone, respectively. Using two-way ANOVA test to detect difference between two or more groups, no significant difference was detected between the two conditions (**Figure 3.9C**). Doubling time for FNB6 cultured in Green's with hydrocortison was 12.6 ± 2.6 hours which was not significantly different from those cultured in Green's without hydrocortisone (12 ± 2.9 hours) using unpaired T test. These data show that FNB6 cells proliferate equally as well in the absence of hydrocortisone as in its presence.

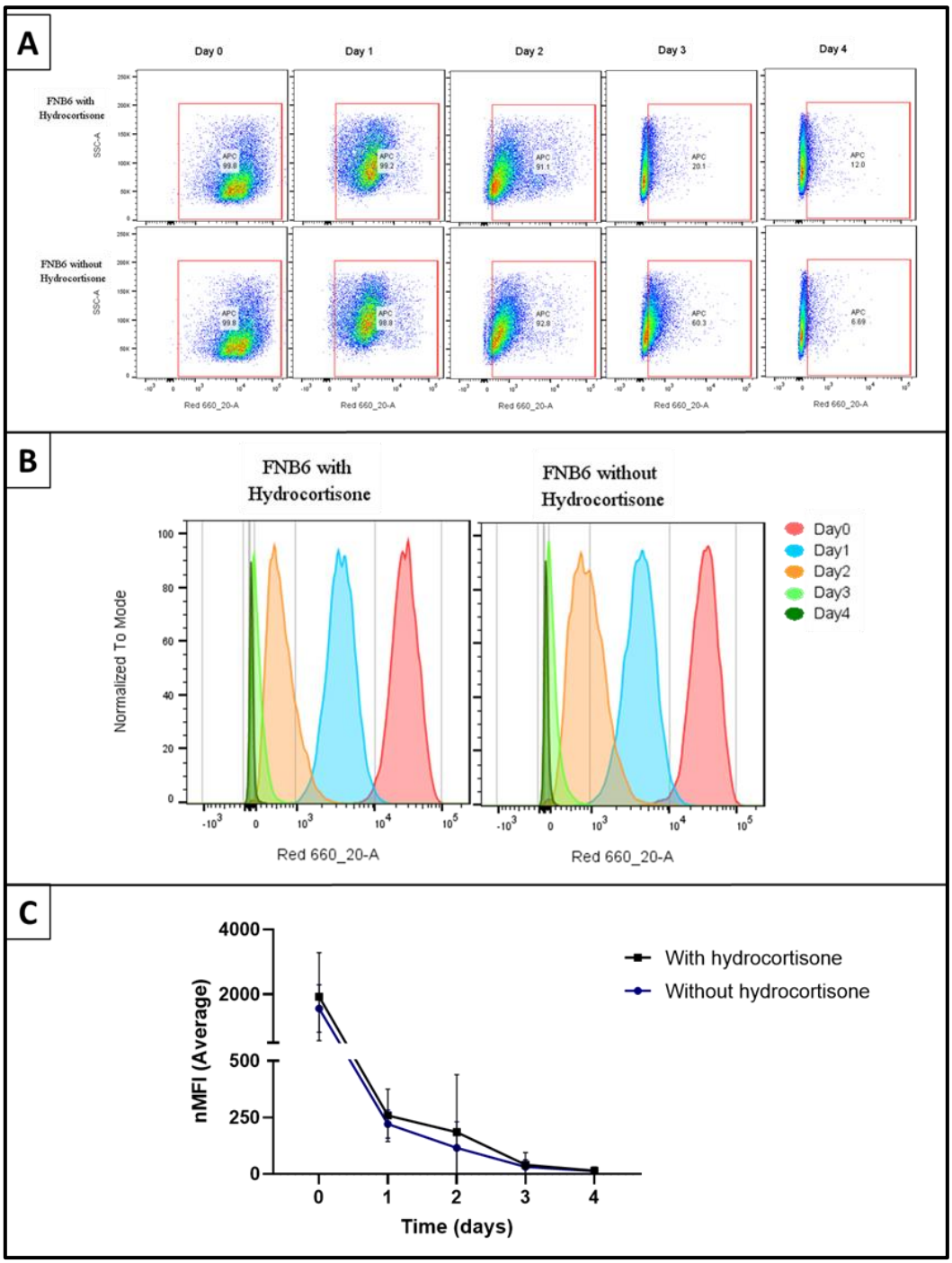

Figure 3.9: FNB6 cell proliferation profiles in Green's medium with or without hydrocortisone. FNB6 cells were stained with CellTrace™ Far Red and cell proliferation traced over 5 days in Green's medium with or without hydrocortisone supplementation using flow cytometry. (A) dot blots, (B) Histogram and (C) normalised median fluorescent intensity (nMFI) normalised to control revealed that the absence of hydrocortisone did not affect the proliferation pattern of the cells. Data presented as representative dot blots and histogram. Line graph data expressed as the mean ± SD; n=3.

3.4 Discussion

A cell proliferation assay should give a direct and accurate indication of the number of cells actively dividing in a population. There are a number of different assays that directly or indirectly measure cell proliferation, and each comes with its advantages and disadvantages

(Adan, Kiraz and Baran, 2016). The use of the non-toxic intracellular fluorescent dyes has become popular since this allows for cell population analysis whilst being able to simultaneously measure other parameters such as mitochondrial function or morphological markers by flow cytometry. In these assays the fluorescently labelled parent population divides and in doing so the levels of fluorescence is divided equally to its two daughter populations upon mitosis, so that each cycle of cell division is represented in the histogram by distinct peaks of populations with decreasing fluorescence, thereby facilitating the tracking of cell division over time (Filby *et al.*, 2015).

Overloading of cells with dye may cause cell toxicity, while under labelling may produce poorly resolved peaks. Dye concentrations of 1 μM proved to be optimal for Jurkat T cells as observed by other investigators (Lim, Berger and Su, 2016; Chung *et al.*, 2017).

Jurkat T cells in this study produced very similar mitotic proliferation peaks over 6 days to those observed by Filby *et al* (Filby *et al.*, 2011). Although Jurkat is a leukemic cell line, they are expected to be a heterogeneous population producing a histogram with broad peaks, representing cells in different stages of the cell cycle (Chung *et al.*, 2017). The cells in this study displayed identical width at days 0, 1, and 2, which is indicative of homogeneity and synchronized cell divisions. However, the peaks broadened and overlap as the population continues to divide and produced cells in different stages of the cell cycle, attributable to heterogeneity at days 3, 4, and 5 similar to those observed by Chung *et al* (Chung *et al.*, 2017).

3.4.1 Jurkat T cell activation

T cells are activated in response to specific antigen presented by appropriate antigen-presenting cells (APCs). The primary signal in T cell activation is the interaction of the T cell receptor (TCR)-CD3 complex with major histocompatibility complex (MHC) on the APCs surface. This interaction starts a cascade of intracellular signalling including activation of protein kinase C signalling pathways leading to the activation of T cells. However, co-stimulation by CD28 is essential for proliferation and lymphokine secretion by activated T cells (Thompson *et al.*, 1989; McLeod *et al.*, 1998). CD28 stimulation augments T-cell immune responses by inducing the expression and secretion of IL-2 in an autocrine manner, increasing T cell proliferation (Thompson *et al.*, 1989; Kay, 1991).

In vitro, different techniques have been developed to activate T cells either by direct antigen stimulation using monoclonal antibodies directed against the TCR-CD3 complex which provides initial activation signals via activation of protein kinase C signalling, but co-stimulation is necessary to provide proliferation, and this is usually achieved by activation of CD28 (Trickett and Kwan, 2003; McLeod *et al.*, 1998).

Activation of T cells can also be mimicked indirectly by the combination of the phorbol ester PMA or phytohemagglutinin (PHA) in conjunction with a Ca^{2+} ionophore (*i.e*., ionomycin) (Kay, 1991; Tanaka *et al.*, 2005). Changes induced by ligation of CD3 along with CD28 co-stimulation and those induced by ionomycin and PMA were reported to be similar (Diehn *et al.*, 2002; Weiss *et al.*, 1986; Weiss and Imboden, 1987). PMA has a structure analogous to diacylglycerol which is an allosteric activator of protein kinase C (PKC) activation and inositol triphosphate, which trigger Ca^{2+} release and mobilization, resulting in a cascade of intracellular responses mediating T cell activation. Secondly, ionomycin is an ionophoric antibiotic that binds Ca^{2+} and serves as an effective mobile carrier of the cation. The resultant calcium flux leads to several downstream effects, such as up-regulation of CD7 (signal of activation) or the hydrolysis of phosphoinositide and activation of PKC in T cells (Kay, 1991; Chatila *et al.*, 1989).

This study used the mitogenic molecules, PMA and ionomycin, for the experimental activation of Jurkat T cells over three time-points 4, 6, and 24 hours in suspension culture. In agreement with previous activation studies (Diehn *et al.*, 2002; Weiss *et al.*, 1986; Weiss and Imboden, 1987), successful activation of Jurkat T cells occurred following 4-, 6- and 24-hours stimulation. This was measured by detecting the expression of CD69 and the levels of secreted IL-2. Both IL-2 and CD69 are commonly used parameters to measure T cell activation (Bray *et al.*, 2018; Trickett and Kwan, 2003; Kay, 1991). CD69, also known as very early activation antigen (VEA), is expressed on the cell surface and is rapidly upregulated upon activation. The early expression of CD69 after 4 hours activation was noticed in this study and is in agreement with previous reports (Kay, 1991) with expression increasing up to 24 h. Jurkat T cells are considered robust producers of IL-2 following stimulation (Abraham and Weiss, 2004). Data in this study showed a time-dependent increase in T cell activation (CD69 abundance) that corresponded to the increased secretion of IL-2. These data in accordance with those produced by Basak and Banerjee who stimulated Jurkat T cells with PMA and PHA, although less IL-2 was produced in the later study (Basak and Banerjee, 2016).

3.4.2 Transferring Jurkat T cells into different medium

The medium used to culture cells has a profound effect on cellular metabolism, DNA and protein synthesis, and cell proliferation. Some cell types can proliferate in several different types of medium while others are more fastidious and require specific medium for efficient growth. Difficulties occur during co-culture experiments where the choice of medium presents a challenge. Several methods have been used to optimise medium, such as mixed medium, supplemented medium and partitioned culture environments (Vis, Ito and Hofmann, 2020).

Jurkat T cells require basic cell culture medium (RPMI) whilst oral keratinocytes require a specialist medium (Green's) that contains several supplements. Since the ultimate aim of this thesis is to create a T cell-containing 3D oral mucosal model the logical step was to transfer culture of Jurkat T cells from RPMI to Green's medium. Accordingly, the viability and proliferation profile of Jurkat T cells in Green's medium was evaluated to ensure that cells continue to be healthy and perform normally. The gradual transfer of T cells from 100% RPMI into 100% Green was crucial to avoid shocking the cells or exposing them to abrupt changes in culture conditions. Over 12 days in culture, the cells-maintained viability of over 80% in RPMI, as well as 25%, 50%, 75%, and 100% Green's medium. Moreover, the proliferation rates of these cells were unaffected upon transferring medium. Furthermore, changing the media had no effect on the activation pattern of Jurkat T cells as assessed by CD69 cell surface abundance. Although no studies that have adapted Jurkat T cells to a different media were found, reports exist of studies where other immune cells were transferred directly after isolation from blood into a different media than that recommended in the literature. For instance, Hoang *et.al*, 2012, assessed dendritic cell functional properties in a 3D tissue model of human lung mucosa. For this model they used a fibroblast cell line cultured in DMEM, a bronchial cell line cultured in MEM, and isolated blood monocytes in DMEM (these cells are recommended to be cultured in RPMI), then the three cell types were cultured in 3D with in DMEM medium (Hoang *et al.*, 2012). Chometon *et.al*, 2020, in their study assessing monocyte culture methods and how these impact differentiation of monocytes into monocyte-derived dendritic cells (moDCs), found that moDCs cultured in RPMI displayed different scatter characteristics compared to those cultured in DMEM (Chometon *et al.*, 2020). Another study by Kühbacher *et.al*, attempted to assess the protective role of dermal fibroblasts in a skin model, here they cultured fibroblasts in DMEM, immortalized human keratinocytes in Keratinocyte Basal Medium (KBM) supplemented with hydrocortisone, and isolated primary T cells in RPMI. However, upon coculture all cells were grown in KBM supplemented with hydrocortisone (Kühbacher *et al.*, 2017a).

3.4.3 Jurkat T cells in a 3D hydrogel

The growth patterns of cells in 2D are very often different from 3D culture conditions. The proliferation of Jurkat T cells in a collagen hydrogel was examined for a period of 14 days. Results show that different cell densities displayed slightly different characteristics when first introduced to the hydrogel. Cells seeded at $2x10^6$ density displayed a slight drop in cell viability at day 10 while both $0.5x10^6$ and $1x10^6$ maintained viability at this time point. This might suggest that cells were at maximum capacity but higher seeding density such as 2.5 or $3x10^6$ need to be investigated to confirm this (Griffiths, 1971) that lead to an inhibitory interaction when a culture of cells become confluent and hence more scope for proliferation was provided for the $0.5x10^6$ and $1x10^6$. However, although the $0.5x10^6$ and $1x10^6$ cell densities had more space to

thrive, they lost some of their viability/activity over the first day in collagen. Changing the culture conditions from suspension to 3D culture in a collagen scaffold may cause cells to go into a stationary period before they regain their activity. Despite the scarcity of papers reporting culture of immune cells in 3D culture, recent study on T cell mediated protection against fungal infection used a cell density of $1x10^6$ in their collagen models (Kühbacher *et al.*, 2017b). These studies did not incubate cells in the 3D scaffold for long periods following the addition of T cells to established skin models, running their analysis only up to 48 h.

To gain a histologically similar morphology of the T cell sub-epithelial band that characterises an OLP lesion (Canto *et al.*, 2010), Jurkat T cells at a seeding density of $1x10^6$/ml were embedded in a collagen hydrogel for 10 days. Histological analysis showed a scattered T cell distribution through the thickness of the collagen. Similar to 2D culture, Jurkat T cells aggregated and were distributed through the width of the collagen, although were condensed more at the edges. This pattern of cell growth has been reported with thicker scaffolds which limit the proliferation of cells to a few microns from the fluid-scaffold interface as cells rely on diffusion for nutrients and oxygen for their viability (Dunn *et al.*, 2006). Accordingly, embedding T cells into a thinner hydrogel might be preferred for future experiments to reproduce the thin uniform T lymphocytic band seen in OLP.

3.4.4 FNB6 proliferation with or without hydrocortisone

As both a glucocorticoid, hydrocortisone can regulate carbohydrate metabolism, cell development, homeostasis and inflammation *in vivo* (Thompson and Lippman, 1974). Hydrocortisone has been found to be an important cell culture supplement *in vitro* where it has been shown to increase proliferation of adherent and suspension cells. The use of hydrocortisone is concentration-dependent; it can act in a stimulatory manner for some cells but inhibitory to others at the same concentration. Moreover, concentrations of hydrocortisone are inhibitory for the production of granulocyte/macrophage progenitor cells (GM-CFC) (Suda and Dexter, 1981; Gronthos and Simmons, 1995). Thus, hydrocortisone shows a cell-specificity in its actions (Grove *et al.*, 1977; Rosner and Cristofalo, 1979). Hydrocortisone supplemented to keratinocyte growth medium was found to enhance the growth and stratification of the epithelium (Rheinwald and Green, 1975a). Interestingly, corticosteroids have been known for decades as therapeutic immune modulatory agents that have anti-inflammatory and immunosuppressive effects (Hench *et al.*, 1950). *In vitro* and *in vivo* studies have shown that hydrocortisone causes a reduction in the total number of lymphocytes and monocytes and antigen reactivity (Olnes *et al.*, 2016; Gillis, Crabtree and Smith, 1979; Fauci and Dale, 1974). Since it is the aim of this study to combine OME with immune T cells, addition of hydrocortisone in the culture medium may cause a conflict of interest between the optimum epithelium growth and T cell performance.

To prevent this conflict, FNB6 keratinocytes were cultured in hydrocortisone-free conditions and these cells maintained proliferation levels that were similar to cells cultured in the presence of hydrocortisone. Green's medium contains other factors such as EGF, transferrin and T3 that may act synergistically with each other negating the requirement for hydrocortisone (HOSHI *et al.*, 1982).

3.5 Conclusion:

In summary, PMA and ionomycin proved to be efficient activators of Jurkat T cells with both CD69 cell surface abundance and IL-2 secretion increased in a time-dependant manner. Jurkat T cells also displayed plastic growth characteristics in that they were viable and proliferated equally efficiently in RPMI and Green's medium. Jurkat T cells were successfully seeded into a collagen hydrogel with an optimum seeding density of $1x10^6$. FNB6 keratinocytes can be cultured in the absence of hydrocortisone without changing their proliferation rates.

This chapter addressed challenges when coculturing different cells together, in particular, concerning changing media type and compositions. The effect of changing the growth medium upon cells' performance characteristics and viability is an overlooked topic but is particularly important for co-culture experiments. Co-culturing requires a highly specific environment that meets the requirements of all involved cell types and therefore requires optimization in order to study physiological and pathological cell to cell interactions, leading toward the goal of developing more complex, reproducible *in vitro* disease models.

4 Chapter four: Primary T cells isolation, activation, and polarisation

4.1 Introduction

T cells have been shown to play a central role in acquired immune responses and immune regulation. After emigrating from the bone marrow, they enter the thymus, and following positive selection, single positive (CD4+ or CD8+) cells migrate to the periphery as mature T cells (Pennock *et al.*, 2013). Successful maturation and emergence from the thymus results in a resting, "naïve" T cell that migrate through the secondary lymphoid tissues and into the peripheral circulation but are not yet capable of producing any type of immune response (Pennock *et al.*, 2013; Luckheeram *et al.*, 2012). Producing a T cell that can mediate immune response requires activation of the naïve T cell. Upon stimulation by specific interaction with an antigen presenting cell via the T cell receptor and governed by the cytokine milieu, CD4+ helper T (Th) cells differentiate into specialised Th subset, each with distinct receptors, immune modulatory function and cytokine secretory profile. Th cells were traditionally classified into Th1 and Th2 cell subsets. However, the phenotype and role of other Th subsets is becoming more evident including Th17, T- follicular helper (Tfh), induced T-regulatory cells (iTreg), Th9 and Th22 subsets. Recent data support the role of Th1 and Th17 especially in the symptomatic forms of OLP (Luckheeram *et al.*, 2012; El-Howati *et al.*, 2022; Wang *et al.*, 2016) (See Chapter 1).

This chapter reflects what has been learnt from the literature on OLP immune pathogenesis and seeks to recreate the immune elements of this disease *in vitro*. This chapter describes the optimisation of a protocol for the isolation of peripheral blood mononuclear cells (PBMC) from peripheral blood buffy coats and the isolation and enrichment of naïve CD4+ and CD8+ T cells from the PBMC that are then phenotyped using flow cytometry. Next, different methods to activate the naïve T cells *in vitro* to achieve successful activation and expansion were assessed. Finally, Th1, CD8+, and Th17 were differentiated *in vitro* using specific combinations of cytokines and the subsets phenotyped through identification of cell surface markers, intracellular transcriptional factors and their cytokine production profile, using flow cytometry and ELISA.

4.2 Aim and objectives

This chapter aims to isolate, activate and polarise naïve CD4+ and CD8+ T cells from peripheral blood buffy coats and to fully characterise the cells.

Objectives:

- Isolate PBMC from peripheral blood buffy coats using density gradient separation.
- Isolate CD4+ from PBMC using negative selection magnetic isolation kit.
- Activate naïve CD4+ with PMA/ionomycin and CD3/CD28 Dynabeads and measure activation marker using flow cytometry.
- Polarise CD4+ into Th1 cells and confirm their phenotype using flow cytometry, q-PCR, western blot and ELISA.
- Polarise naïve CD4+ into Th17 cells and confirm their phenotype with multicolour flow cytometry and ELISA.
- Activate CD8+ into cytotoxic CD8+ T cells and confirm their phenotype using multicolour flow cytometry.

4.3 Materials and methods

Please refer to chapter 2 for all materials and methods.

4.4 Results

4.4.1 Purity of isolation of naïve CD4+ and CD8+ T cells

4.4.1.1 Gating strategy

PBMC were separated from buffy coats using density gradient centrifugation and primary CD4+ and CD8+ T cells subsequently isolated using negative selection magnetic bead technology. The resulting cell populations was plotted by forward (FSC) and side (SSC) scatter and cell debris excluded, then non-viable cells were excluded from analysis using a live/dead viability stain. Unstained and IgG1 isotype-stained samples were used to adjust gating and exclude background and non-specific staining (**Figure 4.1 A & B**).

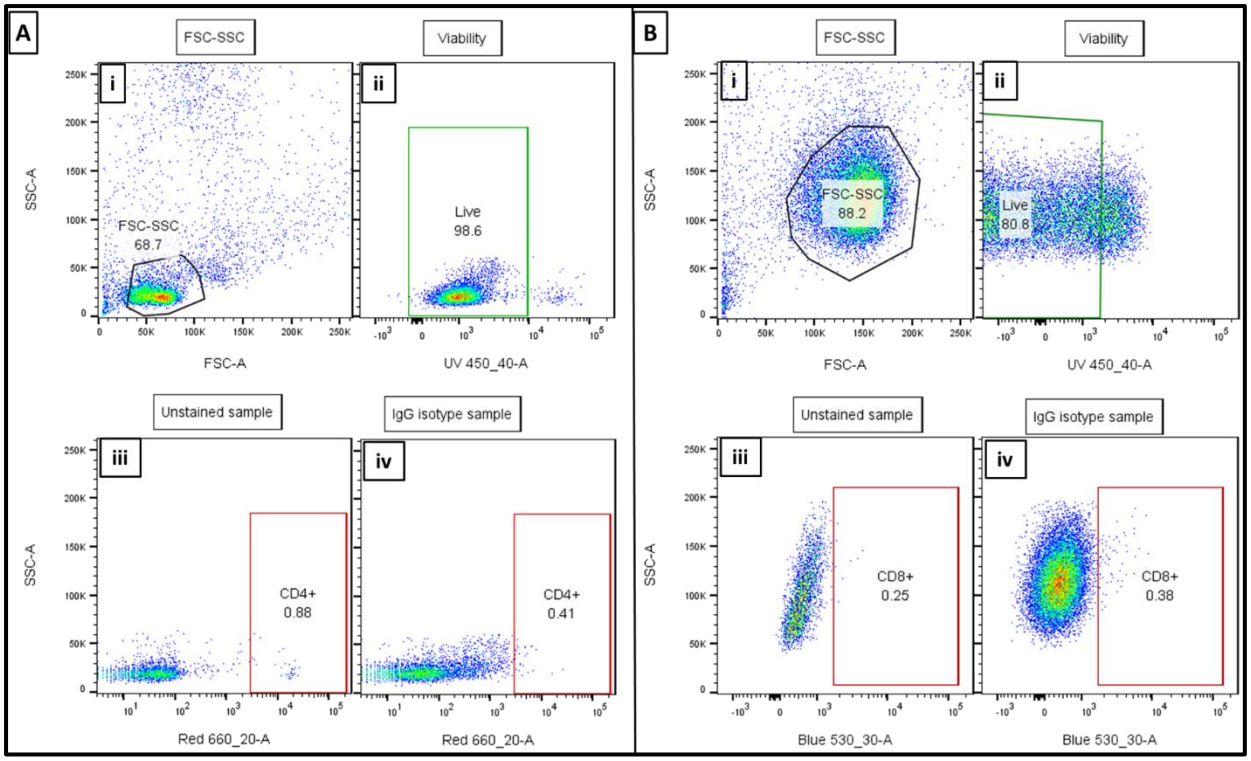

Figure 4.1: Dot plots for the gating strategy to assess the purity and viability of CD4+ and CD8+ T cells. The main population of (A) CD4+ and (B) CD8+ negatively selected T cells were gated on (i) FSC/SSC, then (ii) the viable cell population was gated to exclude any dead cells from the analysis. (iii) Unstained samples were used to adjust the gating on the fluorescent channel for APC (A; iii & iv) or FITC (B; iii & iv) to exclude background staining and (iv) isotype control used to exclude non-specific staining.

4.4.1.2 Purity of CD4+ and CD8+ T cells

The FSC/SSC dot plot for the buffy coat isolated PBMCs revealed different populations of cells including monocytes and granulocytes (**Figure 4.2A**). To enrich the population further, unwanted cells were removed through negative selection using either CD4+ or CD8+ antibody labelling and magnetic sorting, leaving an enriched population of naïve CD4+ or CD8+ T cells, demonstrated by staining with anti-CD4 or CD8. (**Figure 4.2A**). While the CD4+ population in PBMCs was shown to be 40.4 ± 11.5% of the total population, the yield of CD4+ T cells after CD4+ enrichment from PBMC was significantly higher with 91.7 ± 3.5% cell purity (p=0.0003). Similarly, the enrichment of CD8+ T cells significantly increased from 18.4 ± 4% in PBMCs to 92.6 ±3% after CD8+ T cells enrichment from PBMC (p=<0.0001) (**Figure 4.2B**).

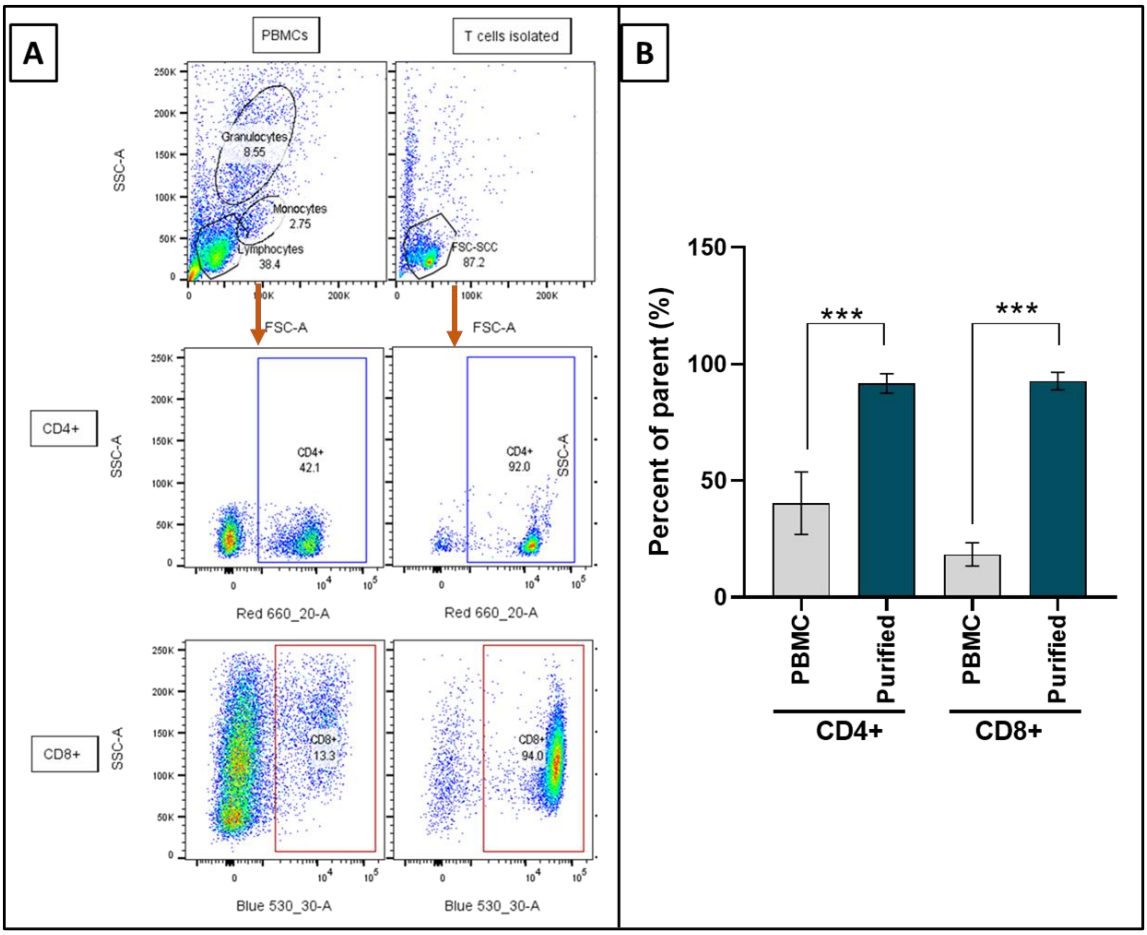

Figure 4.2: Abundance of the cell surface markers CD4 and CD8 before and after naïve T cell isolation from PBMCs. Samples of PBMCs and isolated naïve CD4+ or CD8+ T cells were stained with APC-conjugated anti-CD4 antibody to detect the abundance of CD4+ T cells or stained with FITC-conjugated anti-CD8 antibody to detect the abundance of CD8+ T cells. Positive CD4+ and CD8+ T cells detected by flow cytometry. Data are presented as (A) representative dot plots and as (B) the mean ± SD. A mean difference was considered significant when $p < 0.05$ with ***$p < 0.0001$, using unpaired t- test used to detect the difference between the two groups; n=3.

4.4.1.3 Viability assessment of isolated and purified T cells

To first validate the effectiveness of the fixable blue live/dead dye, samples of viable, dead (induced by DMSO) and a mixed (50:50%; viable and dead cells) population of T cells were stained with fixable blue live/dead dye or propidium iodide, a well-characterised viability dye. The percentages of live cells detected in the viable sample was 83.8% and 80.6% using propidium iodide and fixable blue viability dye, respectively. This decreased in the mixed sample to 37.8% and 26.8% and in the dead samples to 5% and 3.9% for the propidium iodide and the fixable blue dye, respectively. Both dyes had a similar result and hence, gating for the viable population when using flow cytometry was subsequently performed using the fixable blue live/dead stain to exclude non-viable cells from the analysis (**Figure 4.3**).

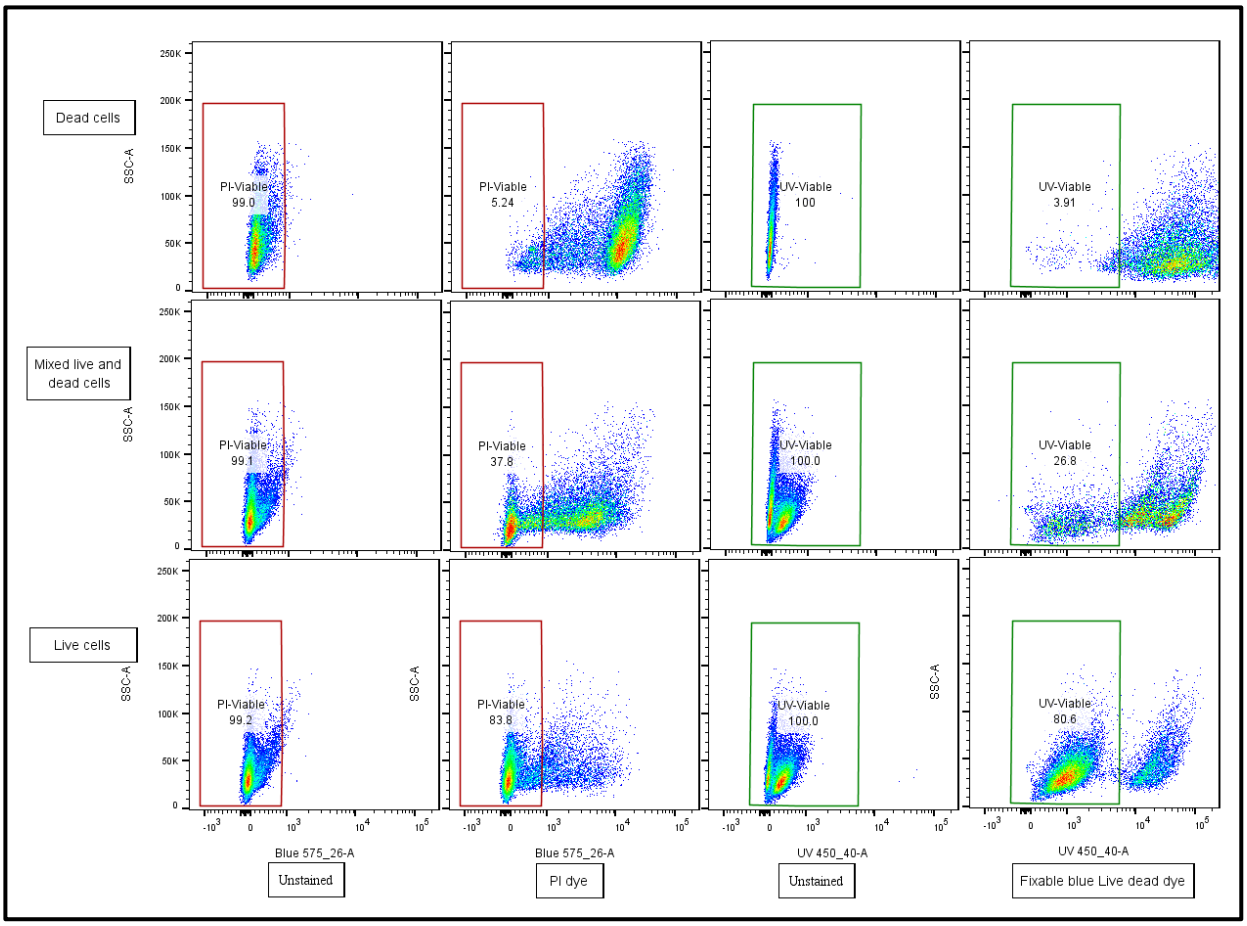

Figure 4.3: Validation of the fixable blue live/dead dye for use with primary T cells. Viable, dead and a mixed population (50:50, live/dead) of T cells were stained with fixable blue dye or propidium iodide (PI). The percentages of viable cells were detected by flow cytometry. Data presented as dot plots; n=1.

Following isolation and enrichment, both CD4+ and CD8+ T cells maintained a high viability with 92.3 ± 7.6% and 87.9 ± 6.3% measured, respectively (**Figure 4.4**).

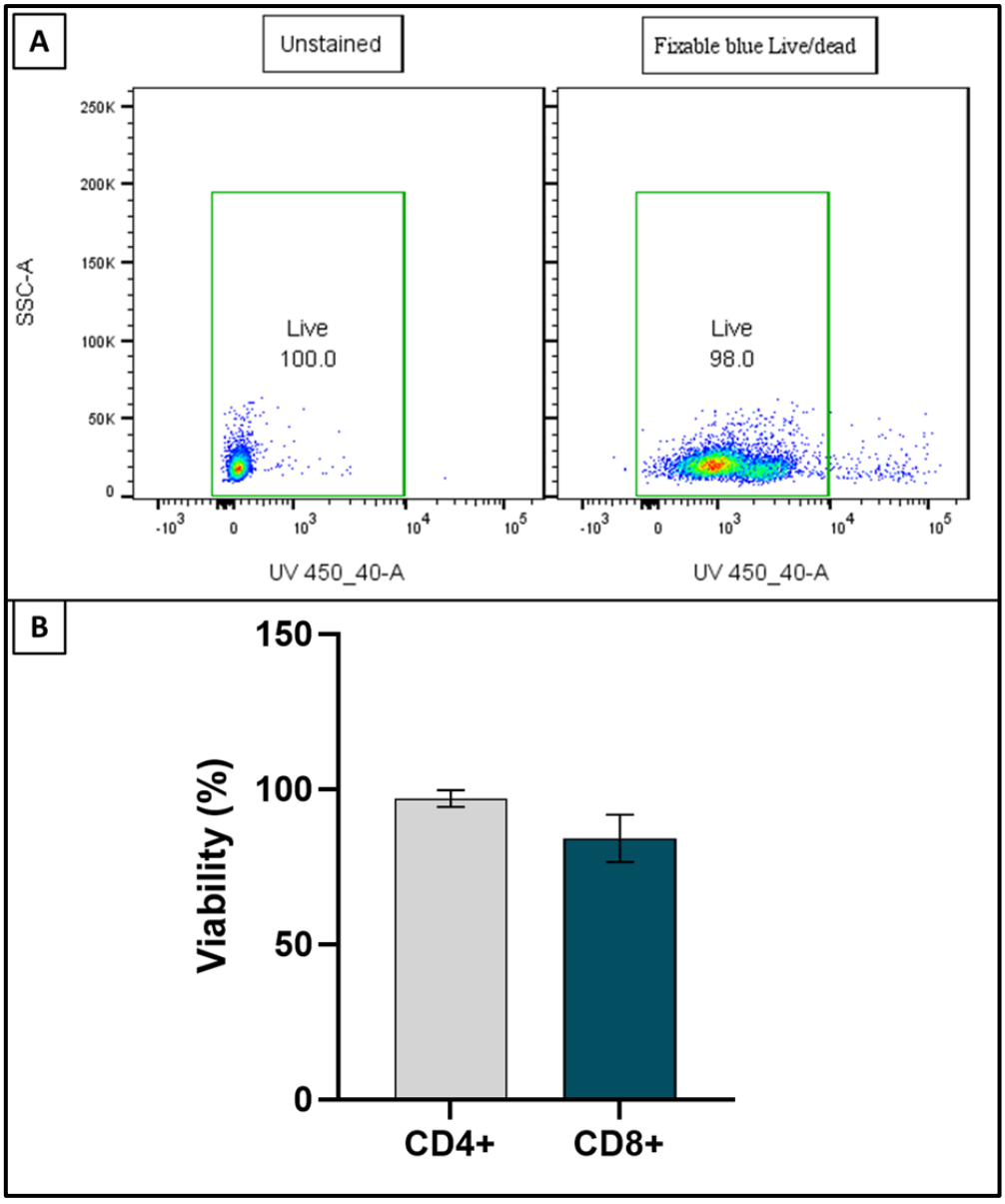

Figure 4.4: The viability of isolated T cells. Isolated CD4+ and CD8+ T cells were stained with live/dead fixable blue stain to detect the viable populations, gated using unstained samples. The viability staining was detected in the UV channel using flow cytometry. Data presented as (A) representative dot plots and (B) the mean ± SD; n=3.

4.4.2 Assessment of activation of CD4+ T cells in different media conditions

Producing a T cell that can mediate immune responses requires activation of the naïve T cell. Therefore, to assess different activation methods CD4+ T cells were activated by incubating the cultures with PMA and ionomycin (final concentration 50 and 500 ng/mL, respectively) or with CD3/CD28 in 1:1 cell to Dynabeads ratio for 24 hours in RPMI or Green's media or left inactivated as a negative control. The cells were examined using light microscopy and the surface protein levels of the T cell activation marker, CD69 determined by staining with a fluorescently conjugated anti-CD69 antibody with

subsequent analysis by flow cytometry. An anti-mouse IgG1 antibody was used as an isotype control to identify any non-specific staining.

When observed using light microscopy, inactivated T cells remain dispersed as small individual cells in culture (**Figure 4.5A**). Observations of changes in the morphological appearance of the cells after culture with CD3/CD28 Dynabeads or PMA/ionomycin for 24 hours revealed the formation of aggregates of cells. T cell activation induced with PMA/ionomycin revealed the formation of large aggregates of cells while those cultured with CD3/CD28 promoted smaller aggregates (**Figure 4.5B&C**).

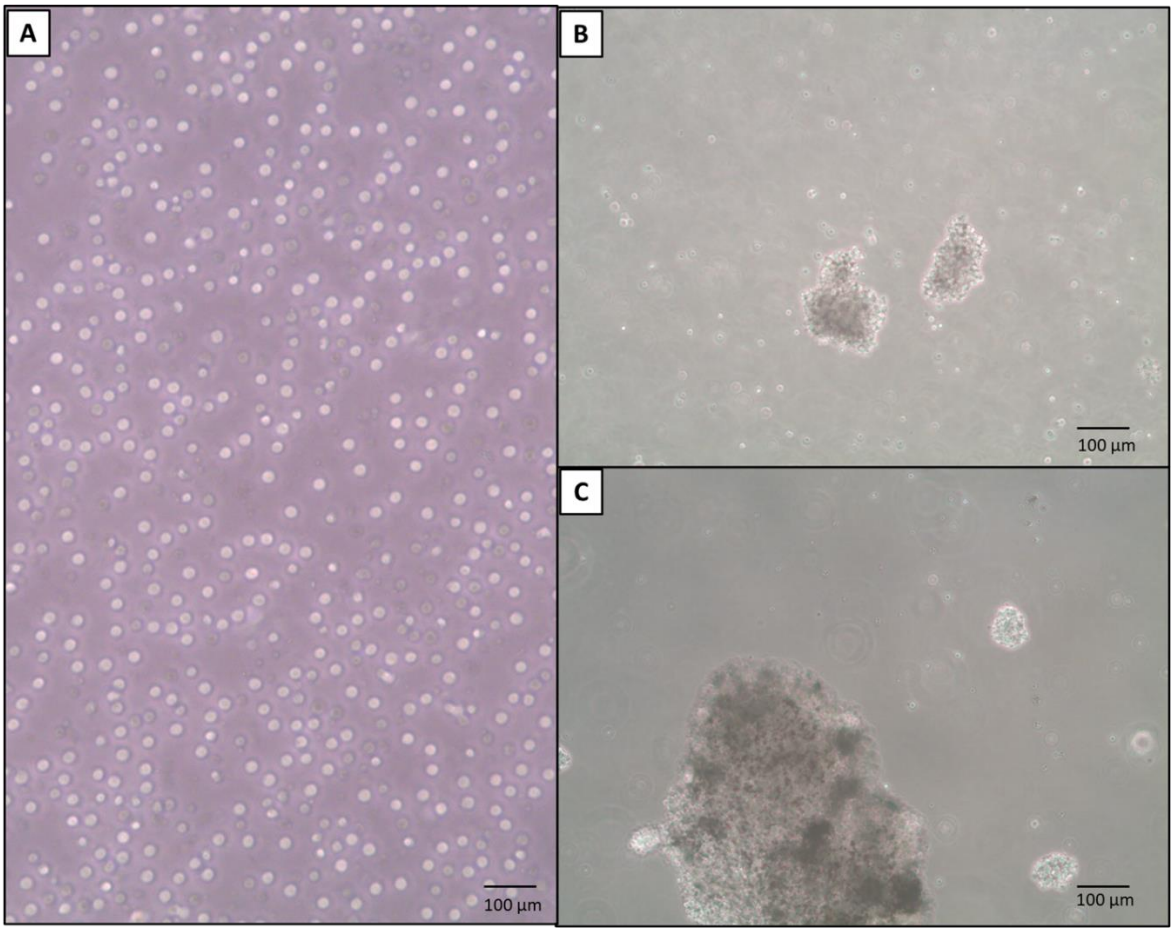

Figure 4.5: Morphology of primary CD4+ T cells activated in suspension culture. Primary T cells were examined in suspension culture after activation for 24 hours under different conditions using light microscopy. (A) Naïve T cells after isolation from buffy coat form small transparent spheres of cells dispersed in cell suspension. (B) Small aggregates of cells were observed when cells were activated with CD3/CD28. (C) T cells activated with PMA & ionomycin form larger aggregates, indicative of proliferating active cells. Scale bar = 100 µm.

Next, to confirm that the T cells were successfully activated using the two methods (PMA/ ionomycin and CD3/CD28 Dynabeads) the cell surface abundance of CD69, indicative of activation, was measured using flow cytometry. The analysis was completed

in both Green's and RPMI-based media to confirm that culture conditions did not affect the activation.

Under Green's medium conditions, the PMA/ionomycin treated samples showed the highest level of activation with 70.9 ± 16.7% positive CD69 cells, followed by 23.8 ± 8.7 positive cells for the CD3/CD28 Dynabeads activation, both activation methods showed a significant difference from the untreated control (1.6 ± 0.9%; $p < 0.0001$and $p = 0.0302$, respectively for PMA/ ionomycin and CD3/CD28 Dynabeads activation) (**Figure 4.6 A&B**).

A similar trend was observed when CD4+ T cells were activated in RPMI medium where PMA/ionomycin caused the highest activation with 62.2 ± 7.7% CD69 positive cells, followed by CD3/CD28 Dynabeads with 25.9 ± 6.5% positivity. Again, both groups showed a significant higher abundance of CD69 when compared to untreated controls (1.6 ± 0.8%; $p<0.0001$ and $p = 0.0172$, respectively).

No significant difference was shown between the activation methods when cultured in RPMI or Green's medium. Accordingly, all further T cells culture was conducted in Green's medium because this medium is used to construct the oral mucosal models into which these T cells will be eventually placed. Even though activation with PMA/ ionomycin superseded that of CD3/CD28 activation with around 3-fold difference, the CD3/CD28-activated T cell procedure was used in all subsequent experiments because this method provides a more specific intracellular signalling pathway targeting and physiologically relevant level of activation.

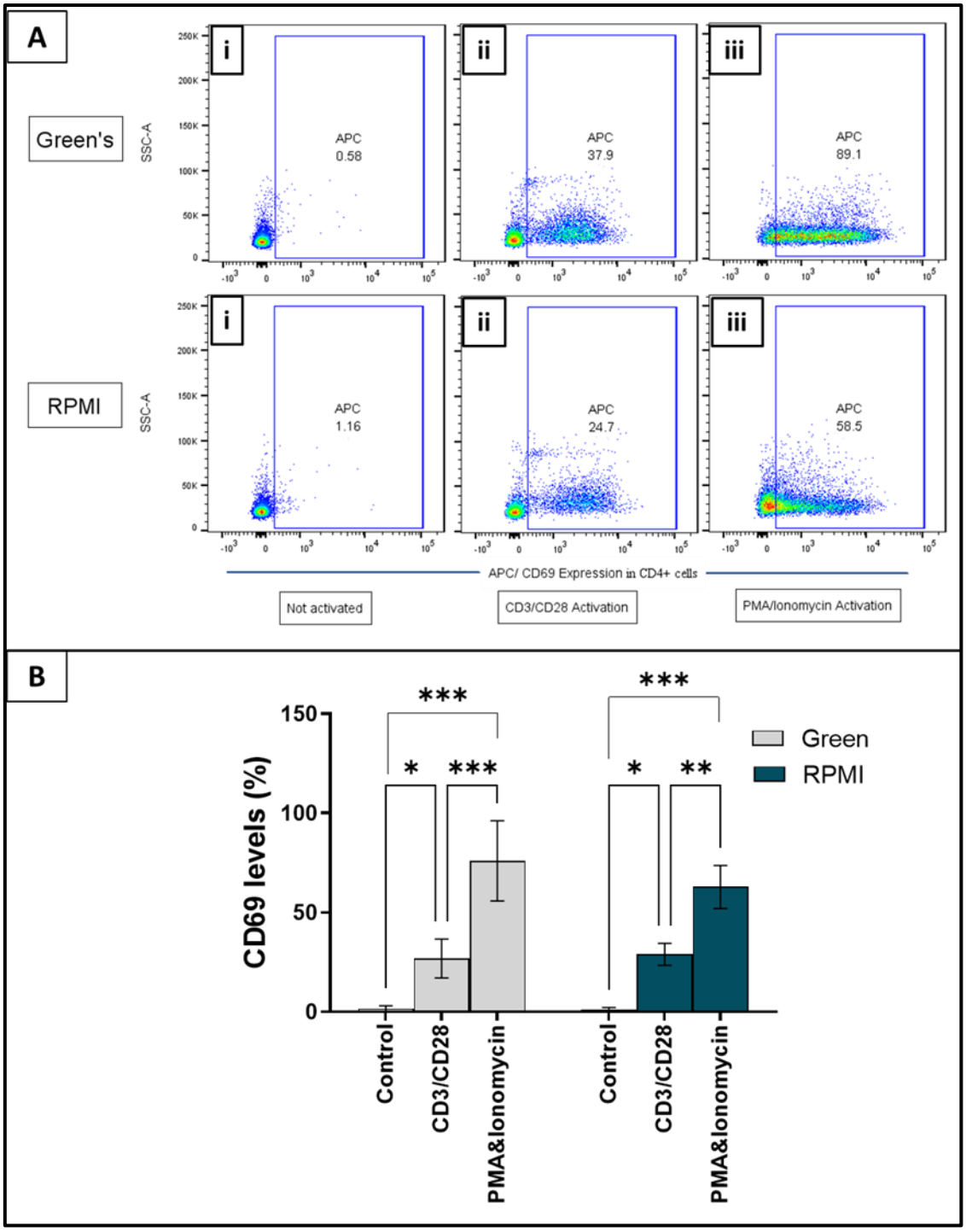

Figure 4.6: Abundance of the cell surface marker CD69 following CD4+ T cell activation. CD4+ T cells were (i) left untreated, (ii) treated with CD3/CD28 Dynabeads beads or (iii) treated with PMA/ionomycin in either Green's or RPMI media for 24 hours before staining with anti-CD69. Viable cells were gated using Live/Dead stain and the percentage of CD69 positive cells detected by flow cytometry. Data are presented as (A) representative dot plots and as (B) the mean ± SD. A mean difference was considered significant when *p < 0.05, **p <0.001, and ***p <0.0001, using two-way ANOVA with Tukey's post-hoc multiple comparison tests to detect difference between groups. ANOVA reported statistically significant effect of activation method ***p <0.0001 but there was no effect of media or of the interaction between the two. n=4.

4.4.3 *In vitro* polarisation of CD4+ T cells into a Th1 subtype

To polarise isolated naïve CD4+ T cells into a Th1 phenotype *in vitro*, CD4+ T cells were treated with either IL-2 alone to create a naïve inactivated sample, in combination with CD3/CD28 Dynabeads to create activated T cells or with IL-2, CD3/CD28 Dynabeads and Th1 differentiation medium (adding 20 ng/ml of human rIL-12 p70, 20 ng/ml of human rIL-18, and 2.5 µg/ml purified anti-human IL-4 antibody) to polarise these cells into the Th1 subset. These cultures will be herewith in be referred to as naïve, activated and Th1, respectively.

Cells were cultured in these 3 conditions for 7 days in Green's medium without the addition of hydrocortisone, which is an immunosuppressant. Cells were examined by light microscopy to monitor cell morphology. After 7 days in culture, naïve cells remain dispersed in cell suspension while activated cells displayed cell aggregation as described previously (**Figure 4.5A&B**). Although the polarised group showed less aggregation than in the activated group, the change in shape and extending secretory processes was more prominent (**Figure 4.7, white arrows**).

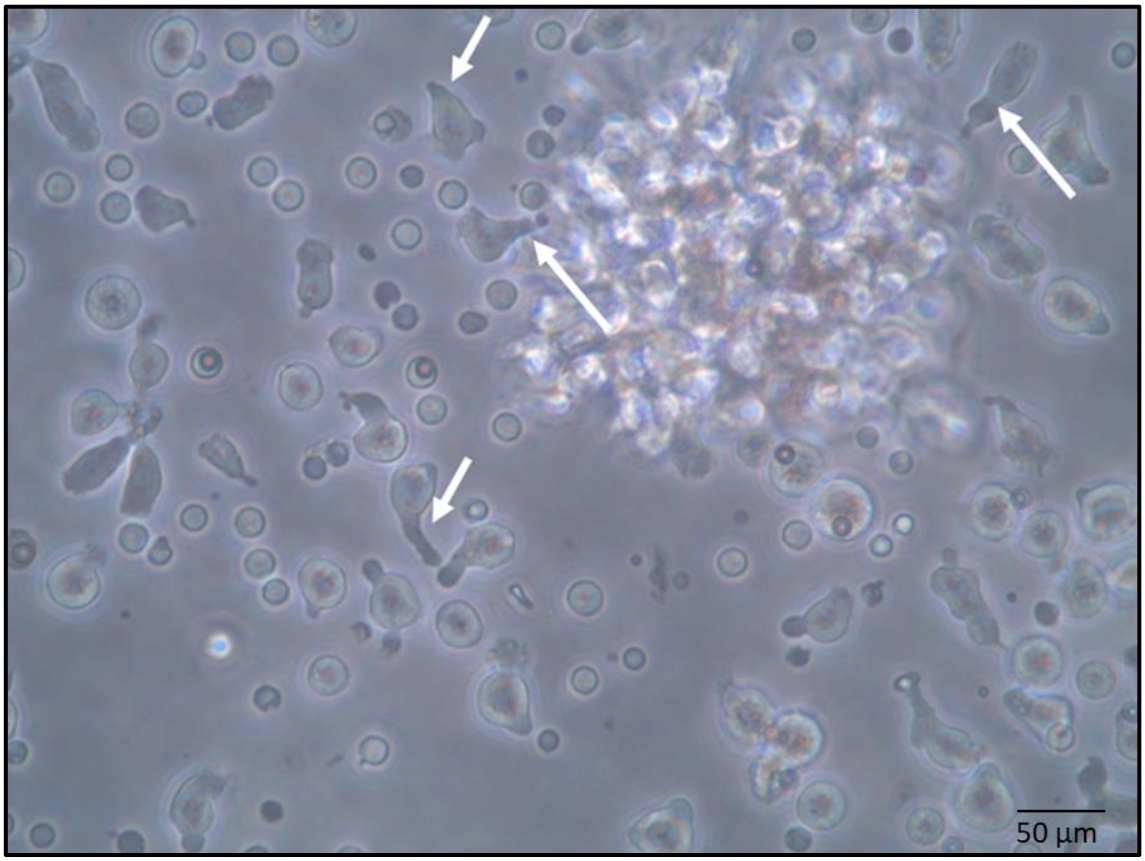

Figure 4.7: Morphology of T cells following differentiation into Th1. Primary T cells were treated with IL-2, CD3/CD28 and Th1 differentiation medium for 7 days and referred Th1 populations. The Th1 population examined under light microscope displayed aggregates of cells around small spherical dark beads and showed evidence of cellular processes (white arrows). Image is representative; n=3. Scale bar = 50 µm.

The proliferation rate of naïve, activated and Th1 cells were compared by direct cell counting on days 0, 3, 5 and 7 and all counts normalised to the cell count on day zero (100%). The activated groups showed the greatest rate of proliferation with five-fold increase by day 7, which was significantly higher compared to all previous time points (all p= p<0.0001), to naïve group at all time points (p<0.0001), and to the Th1 group (p<0.0001) (**Figure 4.8**). Although the differentiated Th1 cells had a lower rate of expansion compared to the active cells, they showed an exponential growth rate after day 3 and reached three-fold increase at day 7 that was significantly higher than the naïve cells at a similar time point (p= 0.0161). Without stimulatory signals, the naïve cells numbers continue to decline gradually and reach a minimum 0.6-fold-decrease at day 7 compared to cells at day 0 (**Figure 4.8**).

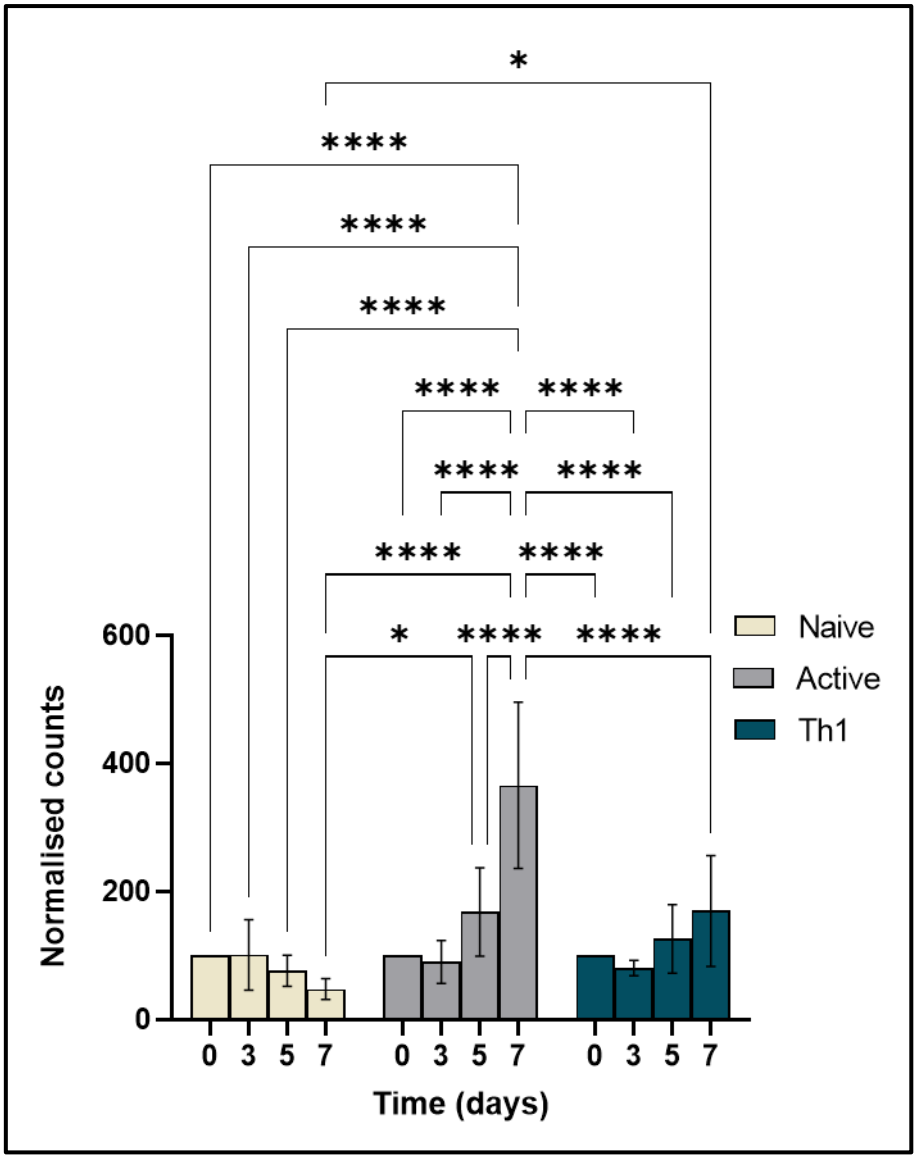

Figure 4.8: Proliferation of T cells in different conditions. Primary T cells were treated with IL-2 alone, IL-2 and CD3/CD28 or with IL-2, CD3/CD28 and Th1 differentiation medium for 7 days and referred to as naïve, activated, and Th1 populations, respectively. Normalised cell counts to day 0 to determine cell proliferation over 7 days in culture. Data presented as the mean ± SD. A mean difference was considered significant when *p < 0.05 and ***p <0.0001, using a two-way ANOVA with Tukey's post-hoc multiple comparison tests to detect difference between groups. Main ANOVA reported ***p <0.0001 for time, activation status, and for interaction. n=3.

For a comprehensive phenotyping of the Th1 subset, the presence of a number of key biomarkers were investigated. First, an antibody panel targeting extracellular surface markers relevant for Th1 including CXCR3, CCR5, CCR6, IL12-Rβ receptor and IFN-γ receptor was conducted. Then, antibody staining targeting intracellular Th1 key cytokine (IFN-γ), and the transcriptional factor (T-bet) was investigated. This analysis involved the establishment of a unique gating strategy that followed a hierarchy by initially gating for total events in the sample, then gating for single cells to exclude cell doublet events, followed by viable cell gating. Finally, the parent population was identified using

the cell surface marker CD4, from which all the above-mentioned surface markers, intracellular cytokines or nuclear transcriptional factors were separately gated. The multicolour experiments excluded non-specific fluorescence produced by spectral overlap between the different fluorophores through compensation and using the FMO samples as described in chapter 2 (**Figure 2.12 and 2.13**). The isolated CD4+ T cells had a purity of at least 84 ± 12% and viability of 80 ± 13.4% (**Figure 4.9**).

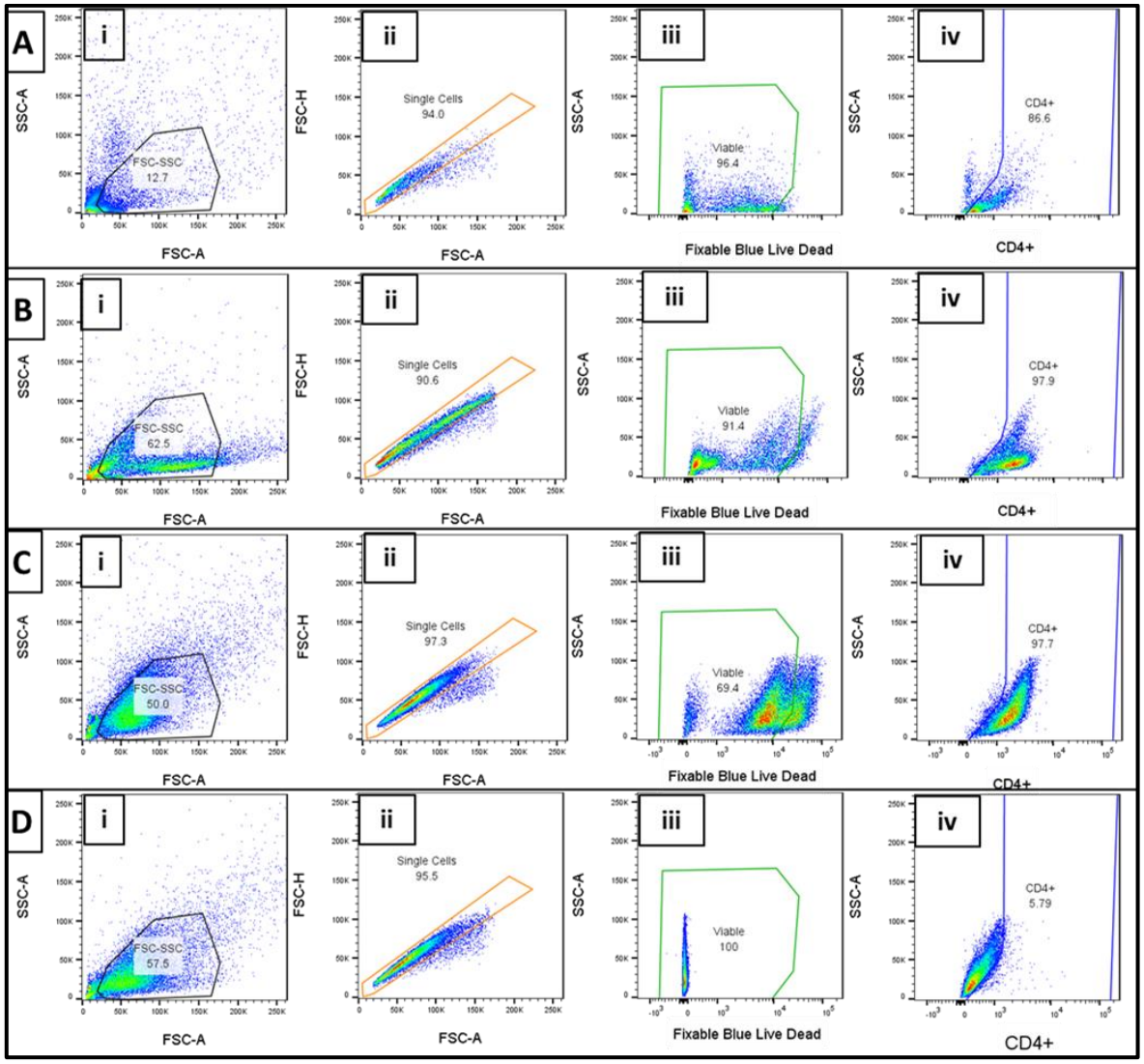

Figure 4.9: The gating strategy to assess the abundance of Th1 extracellular surface markers in the CD4+ population. Primary CD4+ T cells were treated with IL-2 alone, IL-2 and CD3/CD28 or with IL-2, CD3/CD28 and Th1 differentiation medium for 7 days and referred to as (A) naïve, (B) activated and (C) Th1 populations, respectively. The flow cytometry voltages were set using unstained samples, then the gates adjusted using (D) FMO controls. The main T cell population was gated on the (i) FSC/SSC plot, then (ii) gated to single events using the FSC-H/FSC-A plot. (iii) Viable cell populations were gated to exclude dead cells from the analysis, before (iv) the CD4+ stained population was detected by flow cytometry. This strategy allowed analysis of Th1 activation markers on the cell surface of CD4+ T cells in the three treatment groups. Data presented as representative dot plots, n=3.

The Dynabeads in the activated and Th1 samples were removed with a magnet before analysis. However, some of the Dynabeads did not detach and can be observed as a horizontal small separate population when gating for the CD4 antibody in the PE channel. Although this is evident by the absence of this population in the naïve samples that did not contain Dynabeads, it was further confirmed by running a Dynabeads only sample (**Figure 4.10**).

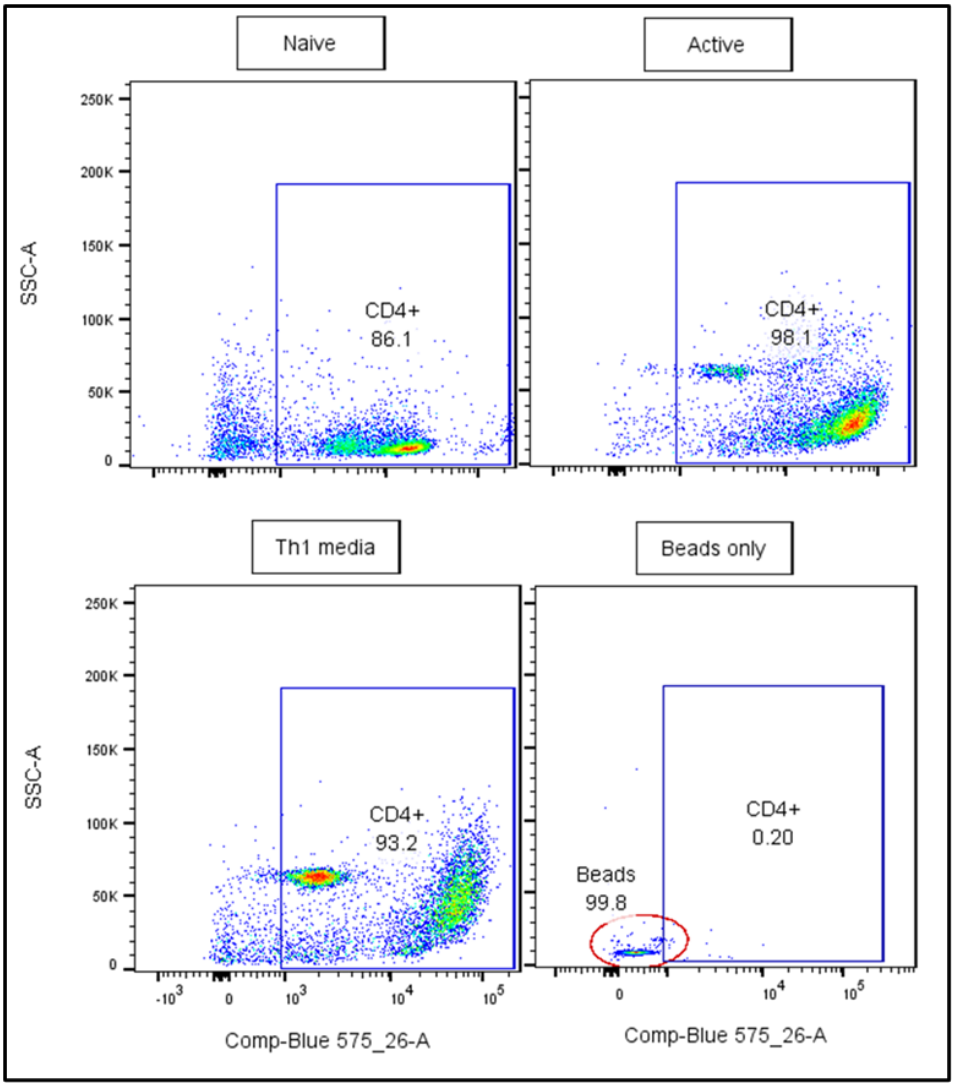

Figure 4.10: Detection of Dynabeads within the CD4+ population. The parent CD4+ stained population was detected by flow cytometry and gated in the naïve, active, Th1 and Dynabeads only sample. Data presented as representative dot plots, n=2.

Following identification of the CD4+ parent population, levels of IL12-Rβ, CXCR3, CCR5, CCR6 and IFN-γ receptor surface markers on the CD4+ T cells was assessed. It can be appreciated from the representative dot plots and analysis that CXCR3 and IL12-Rβ were the most abundant surface markers in the Th1 sample compared to the level of CCR5, CCR6, or IFN-γ receptor (**Figure 4.11A&B**). Activated cells showed the highest abundance of CXCR3 with 78.6 ± 17% positive cells that was significantly higher compared to both the Th1 (42.4 ± 22%) and naïve cells (4.2 ± 3.6%) (p= 0.0291 and p=0.0003, respectively). The Th1 cells also showed a significant increase in CXCR3 compared to naïve cells (p= 0.0185).

Although the same trend was observed for IL-12-Rβ receptor levels with 1.2 ± 0.8%, 15 ± 14%, and 12 ± 7.8% positive for naïve, activated and Th1 cell populations, respectively. Despite this, only the Th1 population had statistically higher levels of IL-12-R β compared to the naïve cells (p=0.0383).

CCR5 levels were low in all groups (naïve 1 ± 0.9%, activated 4.4 ± 5.4% and Th1 3.8 ± 1.9%) and again levels were significantly increased in the Th1 cells compared to the naïve (p=0.0387). Similarly, low levels of CCR6 were detected in the naïve 1.7 ± 1.2%, activated 1.4 ± 0.7% and Th1 3.2 ± 1%. Despite the low levels of CCR6, the level in Th1 cells were significantly higher than the activated group (p=0.0283). Finally, the IFN-γ receptor was not significantly increased in the Th1 group (4.3 ± 3.6%) when compared to both naïve (0.6 ± 0.5%) and active (2.6 ± 2.3%) groups (**Figure 4.11B**). Although the detected surface markers support tendency towards Th1 phenotype in the Th1 group, large significant differences in abundance of markers between groups was not observed.

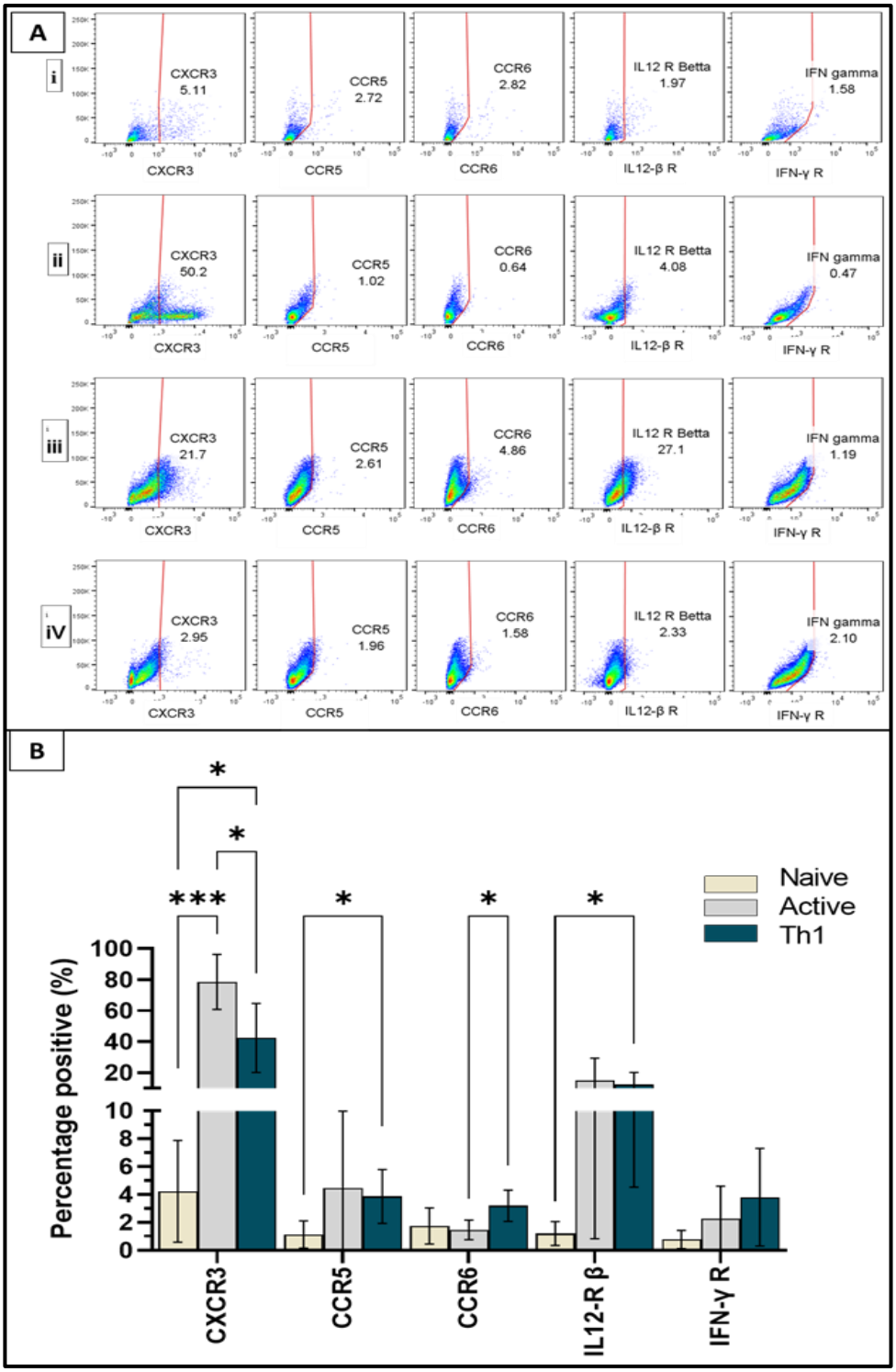

Figure 4.11: The abundance of Th1 surface markers in the CD4+ population. Primary CD4+ T cells were treated with IL-2, IL-2 and CD3/CD28, or IL-2, CD3/CD28 and Th1 differentiation medium for 7 days and referred to as (i) naïve, (ii) activated and (iii) Th1 populations, respectively. Th1 surface markers were gated out from the parent CD4+ population and the normalised median fluorescent intensity (nMFI) of CXCR3, CCR5, CCR6, IL-12Rβ and IFN-γ receptor positive cells detected by flow cytometry. Data are presented as (A) representative dot plots with percentage positive cells indicated in each plot and (B) the mean ± SD of percentage positive. A mean difference was considered significant when *p < 0.05 and ***p <0.0001, using one-way ANOVA with Tukey's post-hoc multiple comparison tests to detect difference between groups. Main ANOVA reported ***p <0.0001. n=3.

To further investigate the development of a Th1 phenotype, conjugated antibodies targeting the Th1 intracellular markers T-bet and IFN-γ were used and investigated for positive staining by flow cytometry. On day 7 of culture and before analysis, T cells were left without re-stimulation or re-stimulated with a cell stimulation cocktail consisting of PMA and ionomycin, to boost levels of intracellular cytokines. To prevent the secretion of any intracellular cytokine produced, a protein transport inhibitor cocktail of Brefeldin A and Monensin was used to inhibit the intracellular protein secretory/transport pathway, ultimately resulting in the accumulation of secreted proteins within the endoplasmic reticulum and Golgi apparatus that can then be detected using intracellular immunostaining.

Although IFN-γ, a key Th1 cytokine, was neither produced in the naïve or the activated T cell samples, there was some detection when samples were treated using the re-stimulation method (**Figure 4.12**). The Th1 population produced the highest levels of intracellular IFN-γ with or without re-stimulation. While Th1 sample produced high levels of IFN-γ without re-stimulation (1.8 ± 0.3 nMFI; percentage: 15 ± 8%) this was further significantly increased when re-stimulated (4 ± 1 nMFI; 45 ± 26%; p= <0.0001) (**Figure 4.12A**). The normalised fluorescence intensity of intracellular IFN-γ in the restimulated Th1 sample was significantly higher when compared to the naïve (0.4 ± 0.07 nMFI; percentage: 4.4 ± 5.6%) and activated (0.8 ± 0.1 n-MFI; percentage 2.3 ± 2,2%) samples (both with p<0.0001) confirming a characteristic of Th1 cells (**Figure 4.12B**).

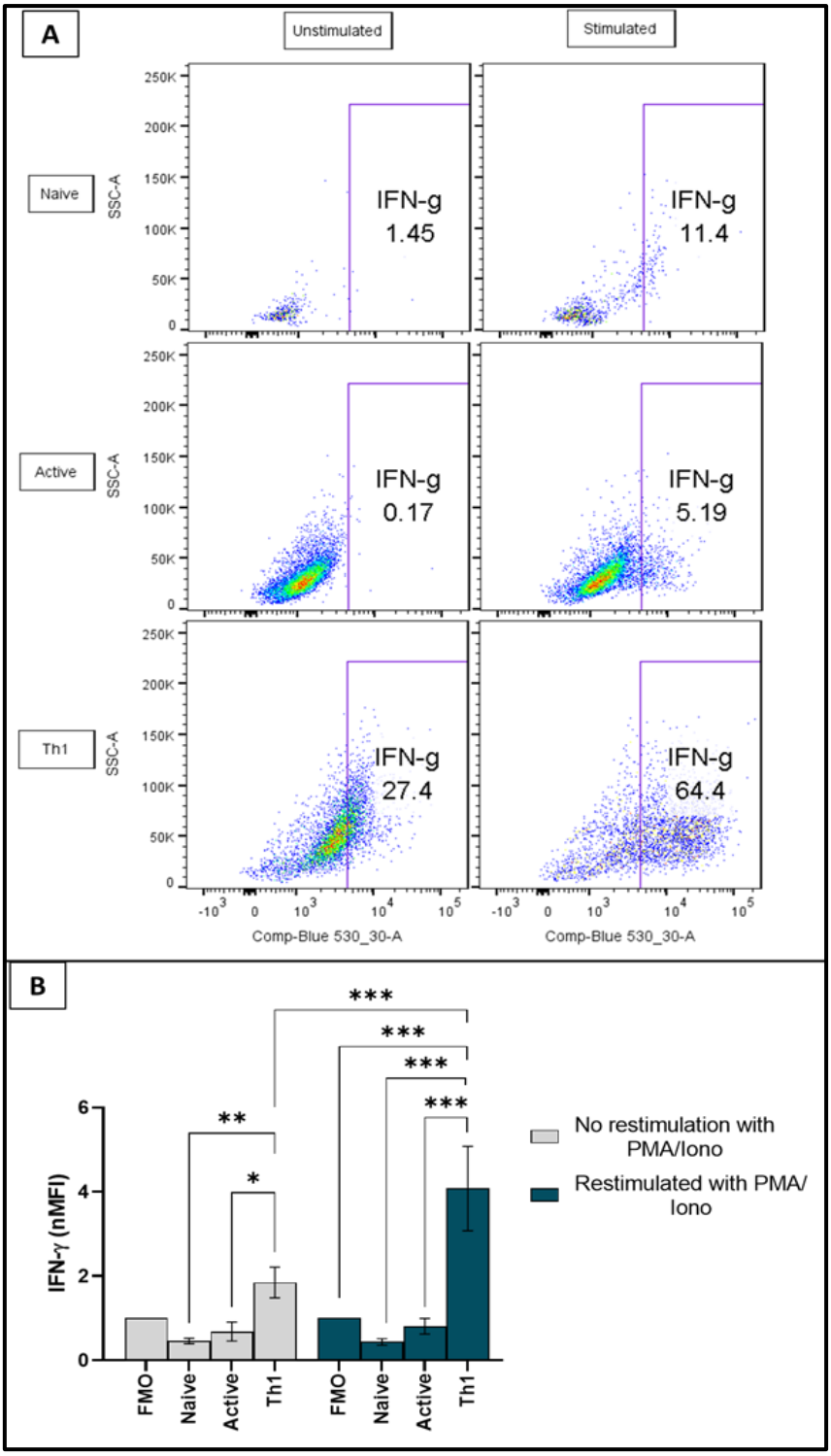

Figure 4.12: Abundance of intracellular IFN-γ following Th1 polarisation. CD4+ T cells were treated with IL-2 alone, IL-2 and CD3/CD28 or IL-2, CD3/CD28 and Th1 differentiation medium for 7 days and referred as naïve, activated and Th1 populations, respectively. Samples were either re-stimulated with PMA, ionomycin and treated with protein inhibitors or left unstimulated but treated with protein inhibitor for 5 hours before analysis. The normalised median fluorescent intensity (nMFI) of intracellular IFN-γ was detected by flow cytometry. Data are presented as (A) representative dot plots and (B) the mean ± SD of percentage positive cells. A mean difference was considered significant when *p < 0.05, **p <0.001 and ***p <0.0001, using a two-way ANOVA with Tukey's post-hoc multiple comparison tests to detect difference between groups. Main

ANOVA reported **p <0.001 effect of restimulation and ***p <0.0001 for activation status and interaction. n=3.

Next, the abundance of intracellular T-bet, a key transcriptional factor for developing Th1 phenotype, was investigated, with or without re-stimulation as previously described. T-bet even without re-stimulation was highly produced by Th1 cells with a nMFI of 32 ± 13 (80.7 ± 16.3%) and was significantly higher than both the naïve cells (2.1 ± 2 nMFI; 15.3 ± 18%; p= 0.0008) and the activated cells (10 ± 1.3 nMFI; 58.6 ± 9.4%; p= 0.0106), providing further evidence of a Th1 phenotype (**Figure 4.13B**).

It can also be appreciated from the representative plots that re-stimulation enhanced the levels of T-bet with an increase in the naïve cells from 4.9 ± 2% to 17 ± 9.8% and 58 ±7.7% to 66.3 ± 6.4% in the activated sample. However, the Th1 sample was not affected by the re-stimulation as it is likely that T-bet levels were at a maximum and could not be elevated with further re-stimulation (80 ± 30%) (**Figure 4.13A**).

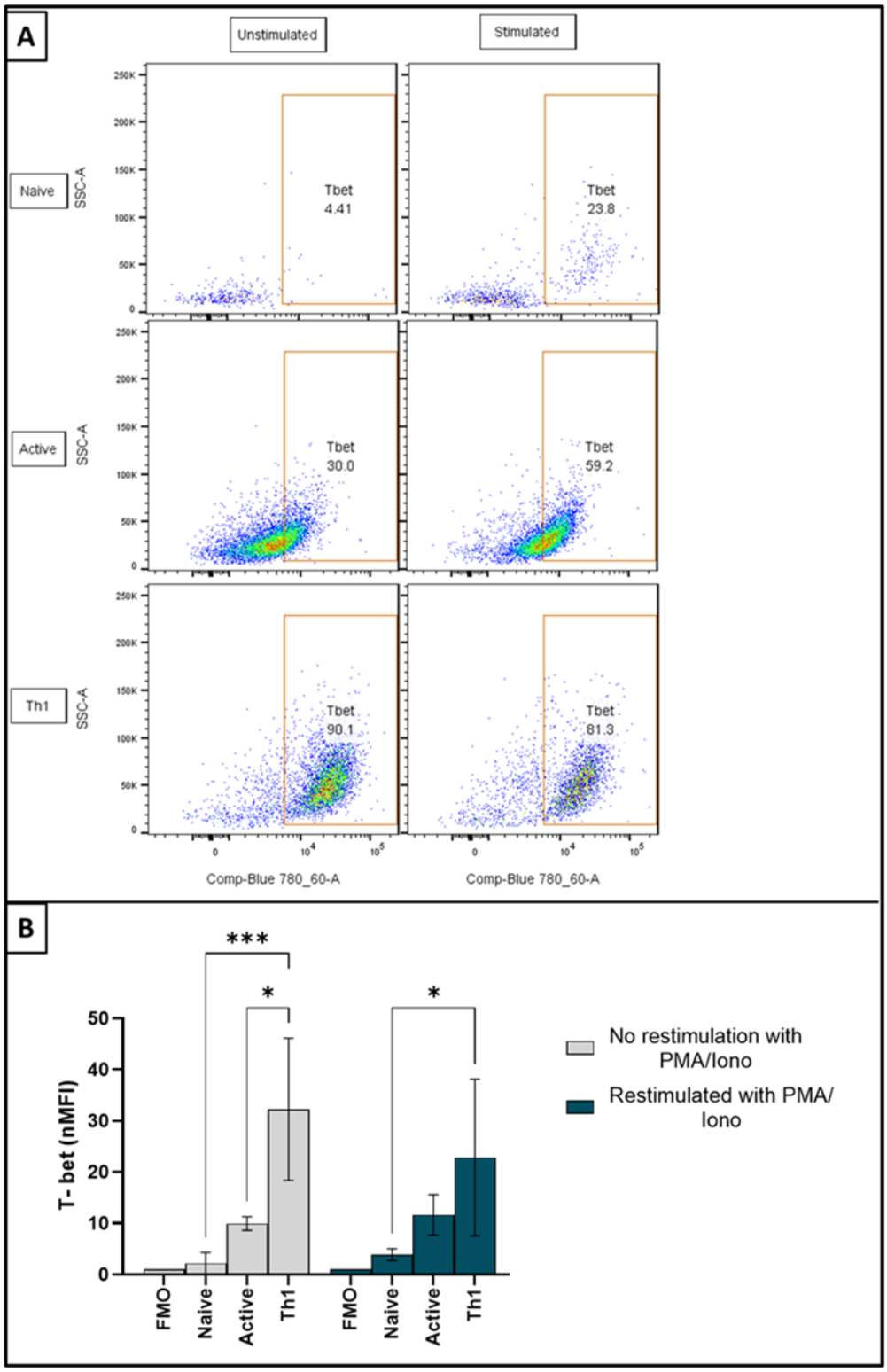

Figure 4.13: Abundance of nuclear T-bet following Th1 polarisation. CD4+ T cells were treated with IL-2, IL-2 and CD3/CD28 or IL-2, CD3/CD28 plus Th1 differentiation medium for 7 days referred to as naïve, activated, and Th1 populations, respectively. The Normalised median fluorescent intensity (nMFI) of nuclear T-bet transcription factor detected by flow cytometry. Data are presented as (A) representative dot plots and as (B) the mean ± SD of percentages. A mean difference was considered significant when *p < 0.05 and ***p <0.0001, using one-way ANOVA with Tukey's post-hoc multiple comparison tests to detect difference between groups. Main ANOVA reported no effect of restimulation or interaction and ***p <0.0001 for activation status. n=3.

In addition, the gene expression of three Th1 transcriptional factors, T-bet, STAT1 and STAT4 were examined (**Figure 4.14A**). The expression of T-bet, a major factor regulating Th1 differentiation, was highest in the Th1 polarised sample and significantly increased when compared to naïve (17-fold, p= 0.0368) and activated samples (15-fold, p= 0.0250). T-bet expression is strongly dependent on signal transducer and activator of transcription 1 (STAT1) (Ji, Sosa and Forsthuber, 2011), which was also increased 5-fold in the Th1 polarised when compared to the naïve sample (**Figure 4.14A**). No significant difference was identified between samples. While the gene expression of STAT4, another important transcription factor involved in the Th1 cell differentiation, was significantly increased in Th1 cells compared to both the naïve (1-fold; 0.0144) and activated T cells (1-fold; 0.0411).

The level of phosphorylated transcription factor STAT1 was also investigated as these transcription factors require phosphorylation to be active. The ratio of total STAT-1 (non-phosphorylated form) to phosphor-STAT1 (the phosphorylated form) was examined by western blot. Levels of phospho-STA1 were increased in Th1 cells compared to activated cells (**Figure 4.14B**). Naïve sample was not enough to conduct WB analysis as cells degenerate if left unstimulated.

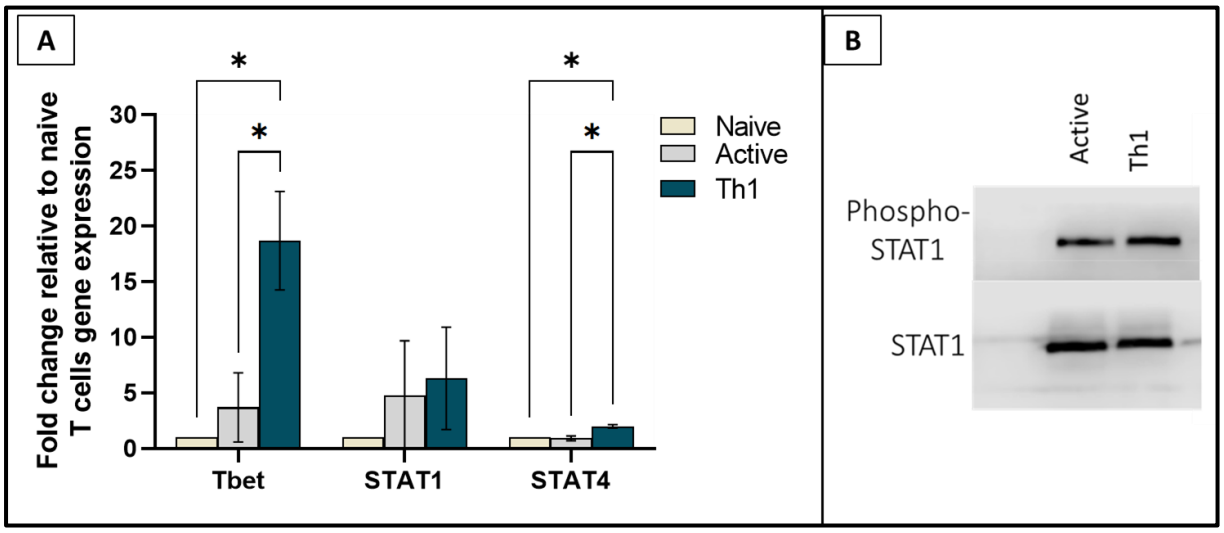

Figure 4.14: Investigation of Th1 transcription factor levels. Primary CD4+ T cells were treated with IL-2 alone, IL-2 and CD3/CD28, or IL-2, CD3/CD28 plus Th1 differentiation medium for 7 days to generate naïve, activated and Th1 populations, respectively. (A) Gene expression for T-bet, STAT1 and STAT4 was analysed by qPCR, calculated relative to the reference control β2-microglobulin. Data presented as the mean ± SD. A mean difference was considered significant when *p < 0.05, using one-way ANOVA with Tukey's post-hoc multiple comparison tests to detect difference between groups. Main ANOVA reported *p <0.01. n=3. (B) The abundance of total and phosphorylated STAT1 in the active and Th1 polarised T cells were analysed by western blot. Blot is representative; n=2.

Following phenotyping of Th1 cells, further investigations into the capacity of these 3 types of T cells to secrete cytokines was investigated by ELISA (**Figure 4.15**). Both IFN-γ and TNF-α, key Th1 cytokines, were secreted by the polarised Th1 cells. Th1 cells secreted 55.4 ± 2.8 ng/ml of IFN-γ cytokine that was significantly more than that produced by activated (2.9 ± 1.1 ng/ml; p= 0.0149) and the naïve cells (0.401 ± 0.02 ng/ml; p= 0.0010). Similarly, TNF-α was produced by the Th1 in higher quantities (12.3 ± 6 ng/ml) than that produced by the activated cells (3.5 ± 1.6 ng/ml) and significantly more than that produced by naïve cells (0.8 ± 0.1 pg/ml; p= 0.0391).

Furthermore, CCL5 levels, a T cell specific chemokine, were significantly increased in the active (0.8 ± 0.1 ng/ml; p= 0.0008) and Th1 (0.631 ± 0.4 ng/ml; p= 0.0092) samples when compared to the naïve (0.1 ± 0.03 ng/ml). IL-10, thought to cause immune suppression by blocking pro-inflammatory cytokines, was produced at higher levels by the activated (0.9 ± 0.3 ng/ml; p= 0.027) and Th1 (1 ± 0.46 ng/ml; p= 0.0105) cells compared to naïve cells (0.2 ± 0.1 ng/ml). Th2 phenotype has a dichotomous relationship to Th1 and to exclude the development of Th2 cells, IL-4 levels, a cytokine that induces Th2 whilst inhibiting Th1 differentiation, was explored. IL-4 was secreted in low levels in the naïve, activated and Th1 samples. As expected, Th1 secretion of IL-4 (0.05 ± 0.01 ng/ml) was considered insignificant compared to the other cytokines investigated (**Figure 4.15**).

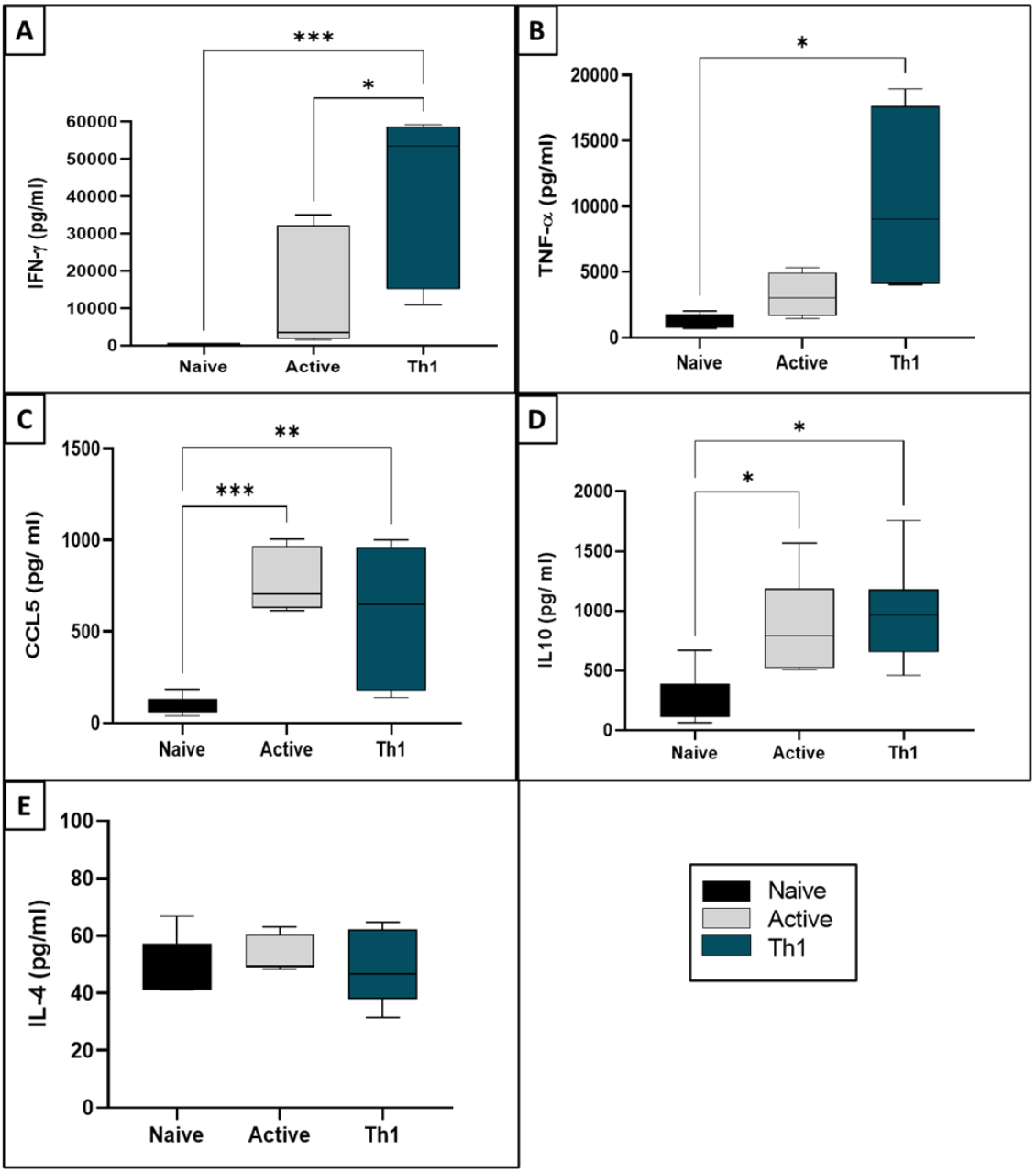

Figure 4.15: Cytokine secretion following Th1 polarisation. Primary CD4+ T cells were treated with IL-2, IL-2 and CD3/CD28 or IL-2, CD3/CD28 and Th1 differentiation medium for 7 days to generate naïve, activated and Th1 populations, respectively. Secretion of cytokines (A) IFN-γ, (B) TNF-α, (C) CCL5, (D) IL-10 and (E) IL-4 were determined by ELISA. Data presented as the mean ± SD. A mean difference was considered significant when *$p < 0.05$, **$p < 0.001$ and ***$p < 0.0001$, using one-way ANOVA with Tukey's post-hoc multiple comparison tests to detect difference between groups; n=3.

4.4.4 *In vitro* polarisation of CD4+ T cells into Th17 subtype to evaluate plasticity

There is increasing evidence that IL-17, a cytokine secreted by Th17 T cells, is a critical pro-inflammatory cytokine in human autoimmune diseases including OLP. To explore the ability to differentiate naïve CD4+ T cells into Th17 and Th17/Th1 phenotypes, isolated naïve CD4+ T cells were treated with IL-2 and cultured in Green's medium (without hydrocortisone), or with Th17 differentiation medium (containing 30 ng/ml human rIL-6, 20 ng/ml human rIL-1β and 2 ng/ml human rTGFβ, along with 2.5 µg/mL each of anti-IL-2, anti-IL-4 and anti-IFN-γ antibody), or with Th17/Th1 differentiation medium (containing 20 ng/ml of human r IL-12 p70, 30 ng/ml human rIL-6, 20 ng/ml human rIL-1β and 2 ng/ml human rTGFβ, along with 2.5 µg/mL each of anti-IL-2 and anti-IL-4) for 7 days. A panel of conjugated antibodies to stain Th17 and Th1 markers including surface CCR6, intracellular IL-17, IFN-γ and nuclear RORC2 and FOXP3 was conducted using flow cytometry. Panel analysis was preceded by a gating strategy to exclude doublets and dead cells from the analysis, then target antibodies were gated from the CD4+ parent population which had a purity of at least 86.2 ± 10% and a viability of 96.3 ± 1% (**Figure 4.16**).

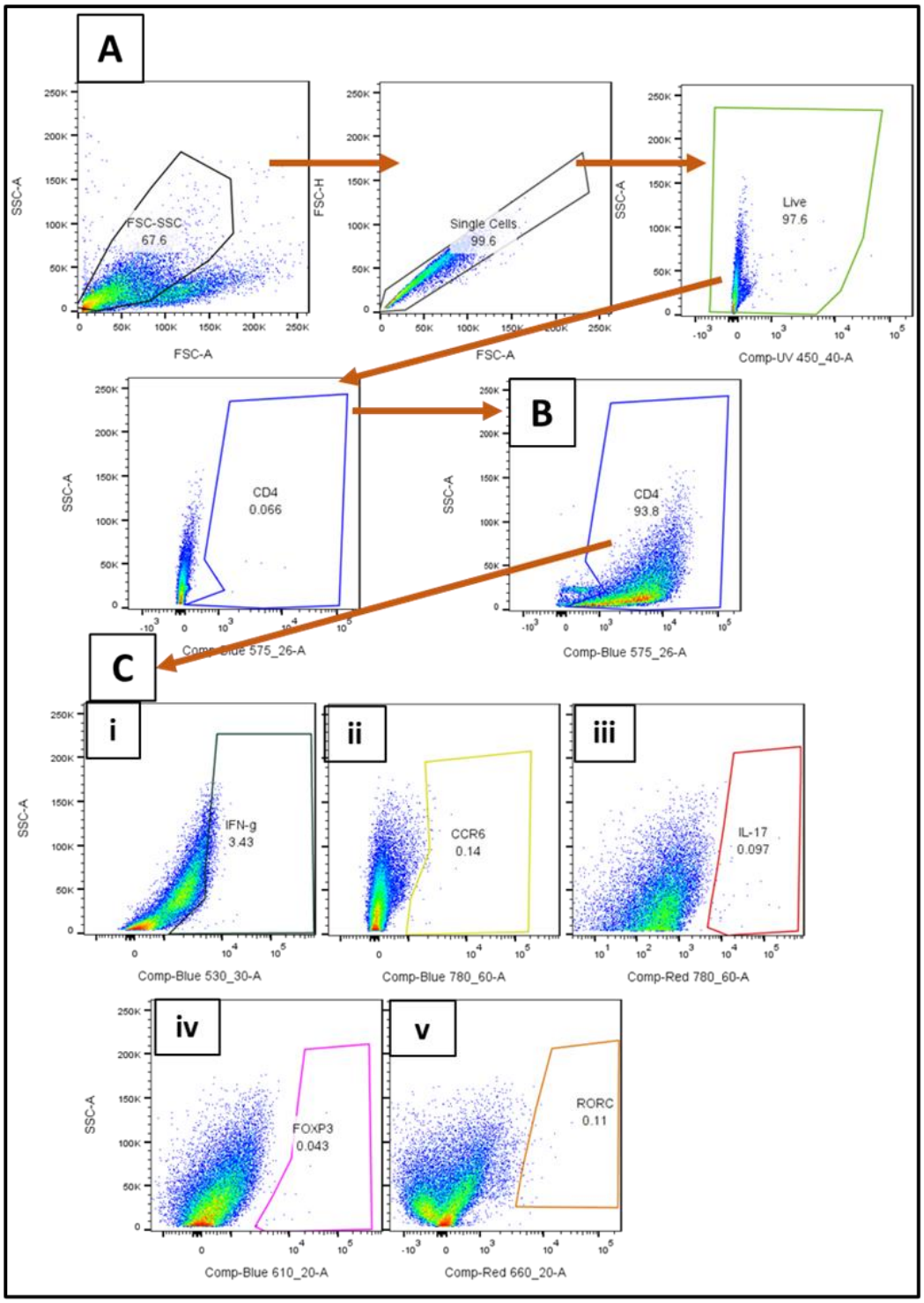

Figure 4.16: Gating strategy to assess the abundance of Th17 markers in the CD4+ population. Primary CD4+ T cells were cultured for 7 days under different conditions to produce naïve, Th17 or Th17/Th1 phenotypes. For flow cytometric analysis, the voltages were set using unstained sample, the main population were gated on (A) the FSC/SSC plot, then gates for single events were included using the FSC-H/FSC-A plot. After the live population was gated to exclude dead cells from the analysis, (B) the CD4+ stained population was detected, then the gates adjusted using the (C) FMO samples for (i) IFN-γ, (ii) CCR6, (iii) IL-17, (iv) FOXP3, and (v) RORC in preparation for marker staining. Data presented as representative dot plots, n=3.

IL-17, a cytokine shown to be exclusively produced by Th17 cells, was markedly produced by cells cultured in the Th17 polarisation medium with over 10-fold increase (mean nMFI = 3.5; percentage = 24%) when compared to control, naïve, (mean nMFI= 1.3; 2.2%). Although, the mixed Th17/ Th1 group showed 4-fold higher percentage of IL-17 than the naïve group, it was less than the Th17 group (average nMFI= 2; 7%) which reflect the difference between a pure Th17 and a mixed phenotype (**Figure 4.17**).

Although IFN-γ, a Th1 key cytokine, was produced more by the Th17 (average nMFI= 2; 6%) compared to the naïve T cells (average nMFI= 0.7; 1.6%), the mixed Th17/Th1 phenotype showed the maximum ability to produce IFN-γ (average nMFI= 2.5; 10%) when compared to the other two groups. The difference between the unstimulated and restimulated samples was unremarkable.

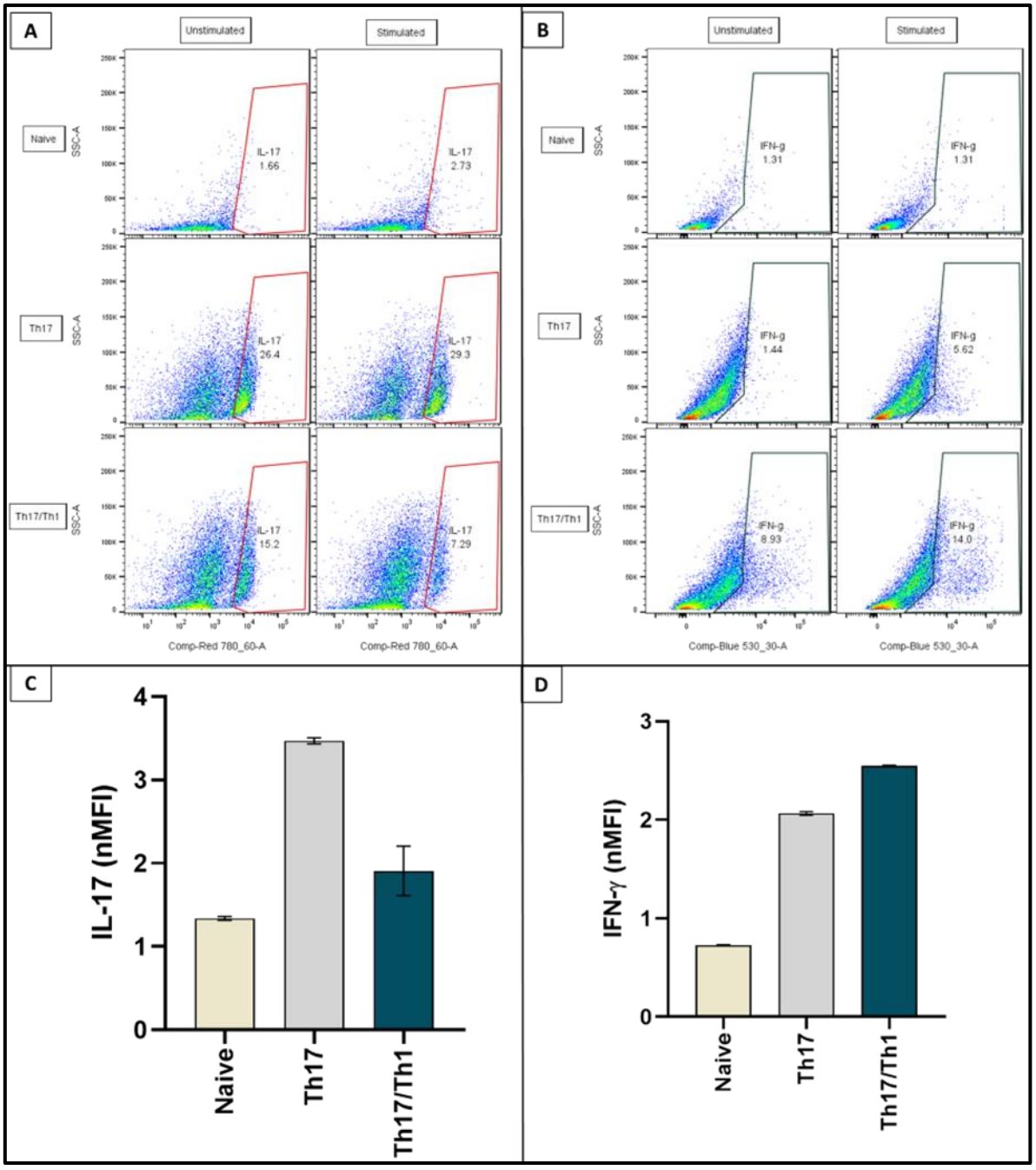

Figure 4.17: Abundance of intracellular cytokines following Th17 and Th17/Th1 polarisation. Primary CD4+ T cells were treated with IL-2, Th17 differentiation medium or Th17/Th1 differentiation medium for 7 days to generate naïve, Th17, and Th17/Th1 populations, respectively. The normalised median fluorescent intensity (nMFI) of intracellular (A & C) IL-17 and (B & D) IFN-γ was detected by flow cytometry. Data are presented as (A & B) representative dot plots and as (C & D) the mean of n-MFI; n=2.

To Further investigate the capacity of these cells to secret IL-17, ELISA was performed (**Figure 4.18**). Production of IL-17 was highest in the polarised Th17 cells (N= 49 pg/ml) followed by the mixed phenotype Th17/ Th1 (N= 46 pg/ml). Naïve T cell production of IL-17 (N= 22.3 pg/ml) was markedly lower than the Th17 and the Th17/Th1 mixed phenotype.

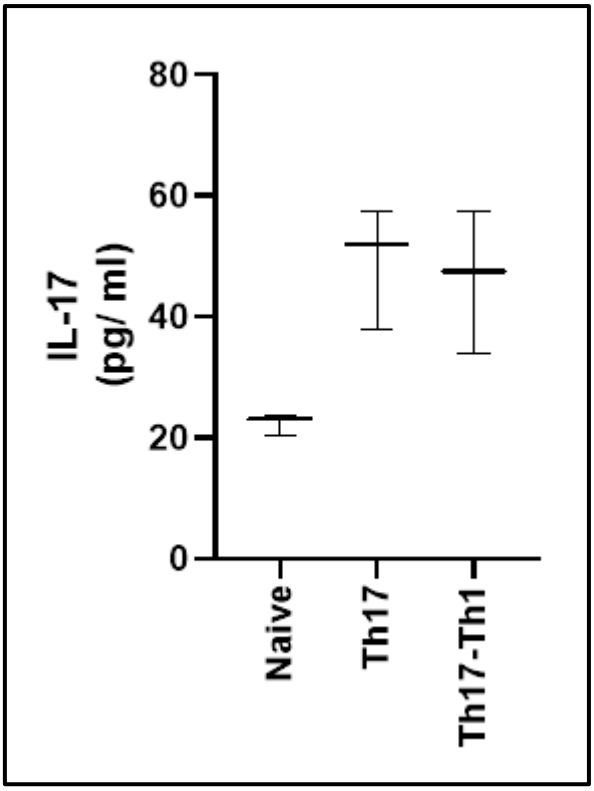

Figure 4.18: IL-17 cytokine secretion following Th17 polarisation. Primary CD4+ T cells were treated with IL-2, Th17 differentiation medium or with Th17/Th1 differentiation medium for 7 days to generate naïve, Th17, and Th17/Th1 populations, respectively. Levels of IL-17 in the conditioned medium was detected by ELISA. Data presented as the mean; n=2.

4.4.5 Developing a multicolour panel to phenotype activated cytotoxic CD8+ T cells

Following CD4+ T cell activation, it is thought that these cells crosstalk with CD8+ T cells and evoke cytotoxic CD8+ T cell responses through production of cytokines (INF-Ɣ, IL2 and TNF-α). To explore the development of cytotoxic CD8+ T cells, naïve CD8+ T cells were isolated from PBMCs and cultured in Green's medium (without hydrocortisone) in the presence of either IL-2, IL-2 with CD3/CD28 Dynabeads or IL-2 and CD3/CD28 Dynabeads in the presence of CD4+ T cells and referred to as naïve, activated or cytotoxic, respectively.

First, the morphology and proliferation rates of CD8+ T cells activated under different conditions were examined **(Figure 4.19).** T cells subtypes, CD4+ and CD8+, could not be distinguished from each other under the light microscope. After 7 days in culture, the naïve CD8+ T cells remain dispersed, and fail to proliferate or form aggregates (**Figure 4.19A**). CD3/CD28 activated cells formed small aggregates (**Figure 4.19B; white arrows**) which are indicative of actively proliferating cells. In contrast, when co-cultured with CD4+ T cells the CD3/CD28 activated CD8+ cells showed increased

activation which can be observed through the enhanced formation of aggregates (**Figure 4.19C**). Moreover, the proliferation rate of naïve, activated, and cytotoxic cells was compared by direct cell counting on days 0, 3, 5 and 7. All counts were normalised to 100% cell count on day zero. All conditions led to a 0.5-fold decrease on day 3 compared to their seeding density at day 0. While the naïve cells did not proliferate within the time period investigated **(Figure 4.20),** the CD3/CD28 activated cells gradually increased by 0.5-fold every two days. However, activation with CD3/CD28 Dynabeads alone was not enough to trigger optimum CD8+ proliferation, as proliferation was not significantly different from the naïve cells. Following a decrease in cell number on day 3, the cytotoxic group (CD3/CD28 + CD4+ cells) showed continuous exponential growth accumulating at a 4-fold increase by day 7, a significant increase when compared to day 3 ($p= 0.010$). By day 7, the cytotoxic group also showed a significant difference when compared to the naïve cells at days 3, 5 and 7 ($p=0.0079$, 0.008 and 0.007, respectively). Overall, both the microscopic images and proliferation data demonstrated increased activation of CD8+ T cells when cultured with CD3/CD28 Dynabeads in the presence of CD4+ T cells.

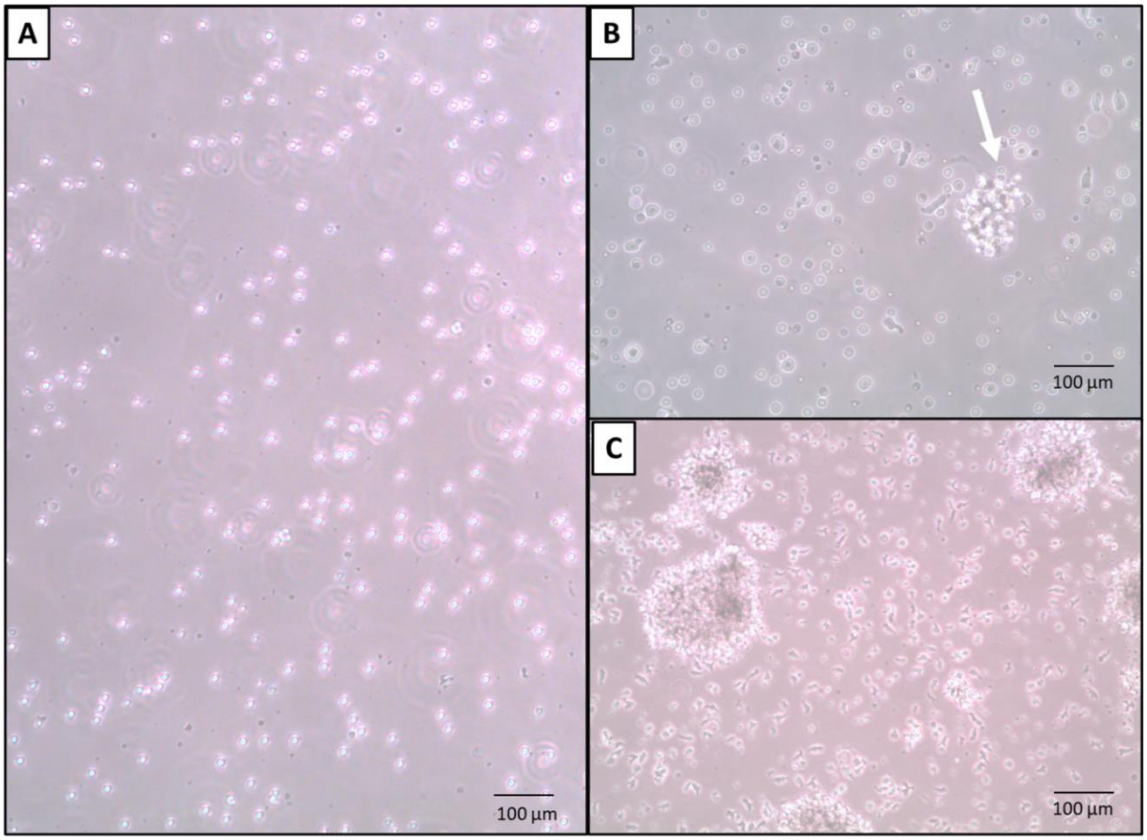

Figure 4.19: Morphology of primary CD8+ T cells under different conditions in suspension culture. Primary CD8+ T cells were treated with IL-2 alone, IL-2 and CD3/CD28, or with CD3/CD28 in the presence of CD4+ T cells for 7 days and referred to as naïve, activated, and cytotoxic CD8+ T cells populations, respectively. Images of suspension culture examined using light microscopy at day 7. (A) Naïve T cells form single cell suspensions (B) CD8+ T cells activated with CD3/CD28 beads form small aggregates (white arrow), (C) more and larger aggregates were observed when cells are activated with CD3/CD28 beads in the presence of CD4+ T cells, indicative of proliferating active cells. Scale bar = 100 µm.

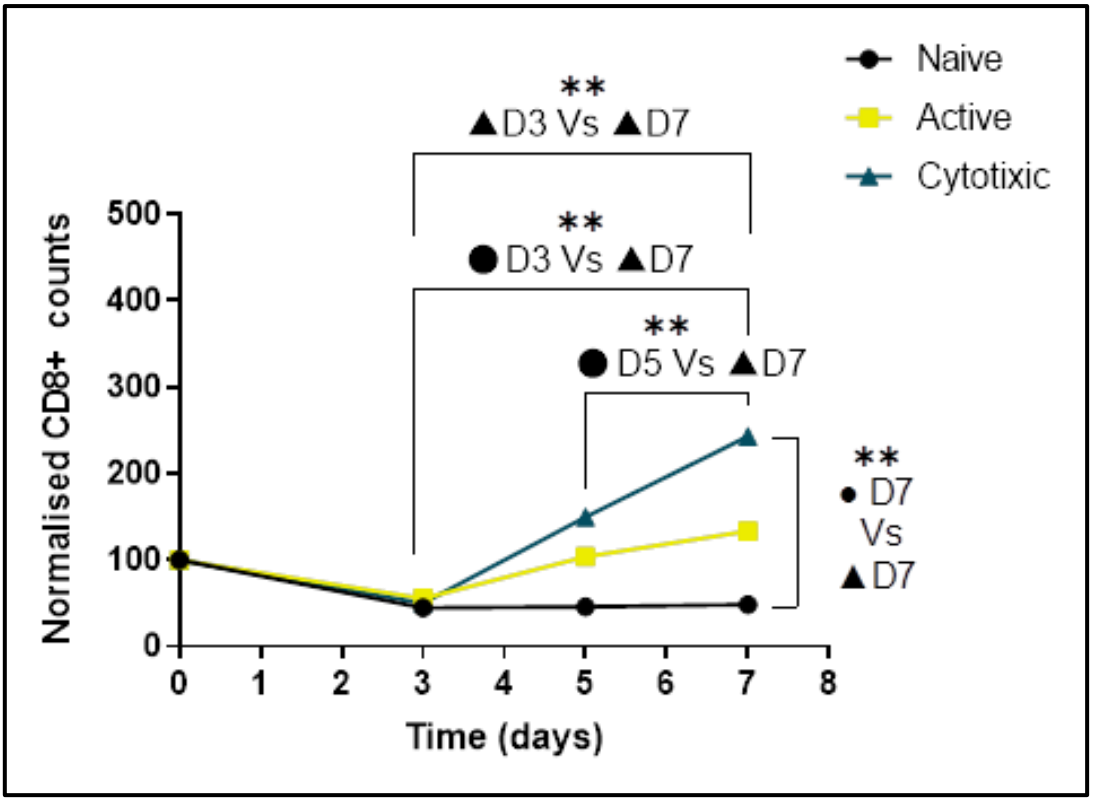

Figure 4.20: Proliferation of CD8+ T cells under different culture conditions. Primary CD8+ T cells were treated with IL-2, IL-2 and CD3/CD28 or CD3/CD28 in the presence of CD4+ T cells for 7 days and referred to as (●) naïve, (■) activated and (▲) cytotoxic CD8+ T cell populations, respectively. Cell counts normalised to cell number on day 0 of culture to determine cell growth over 7 days. Data are expressed as the mean ± SD. A mean difference was considered significant when *p < 0.05 and **p <0.001, using two-way ANOVA with Tukey's post-hoc multiple comparison tests to detect difference between groups. Main ANOVA reported *p <0.01 effect of time and activation status but no effect of interaction. n=3.

Flow cytometric analysis of intracellular granzyme B, a potent cytotoxic factor for cytotoxic CD8+ T cells, achieved through a gating strategy that followed a hierarchy. First gating for total events in the sample was performed followed by gating for single cells to exclude cell doublet events, followed by dead/live staining gate to select only viable cells. Finally, the parent population was identified using the cell surface markers CD4 and CD8 (**Figure 4.21A**). From the CD8+ population, intracellular granzyme B and CD69 surface markers were separately gated after gate adjustments determined by the FMO samples (**Figure 4.21B**) as described in chapter 2. The data shows that the CD8+ purity in the parent population was 80 ± 8% in the naïve and 88.2 ± 10% in the activated samples. The purity of CD8+ T cells in the cytotoxic sample was less as it was a mixed population of CD8+ T cells and CD4+ T cells with levels of 47 ± 3.2% and 29 ±8% seen, respectively (**Figure 4.21C**).

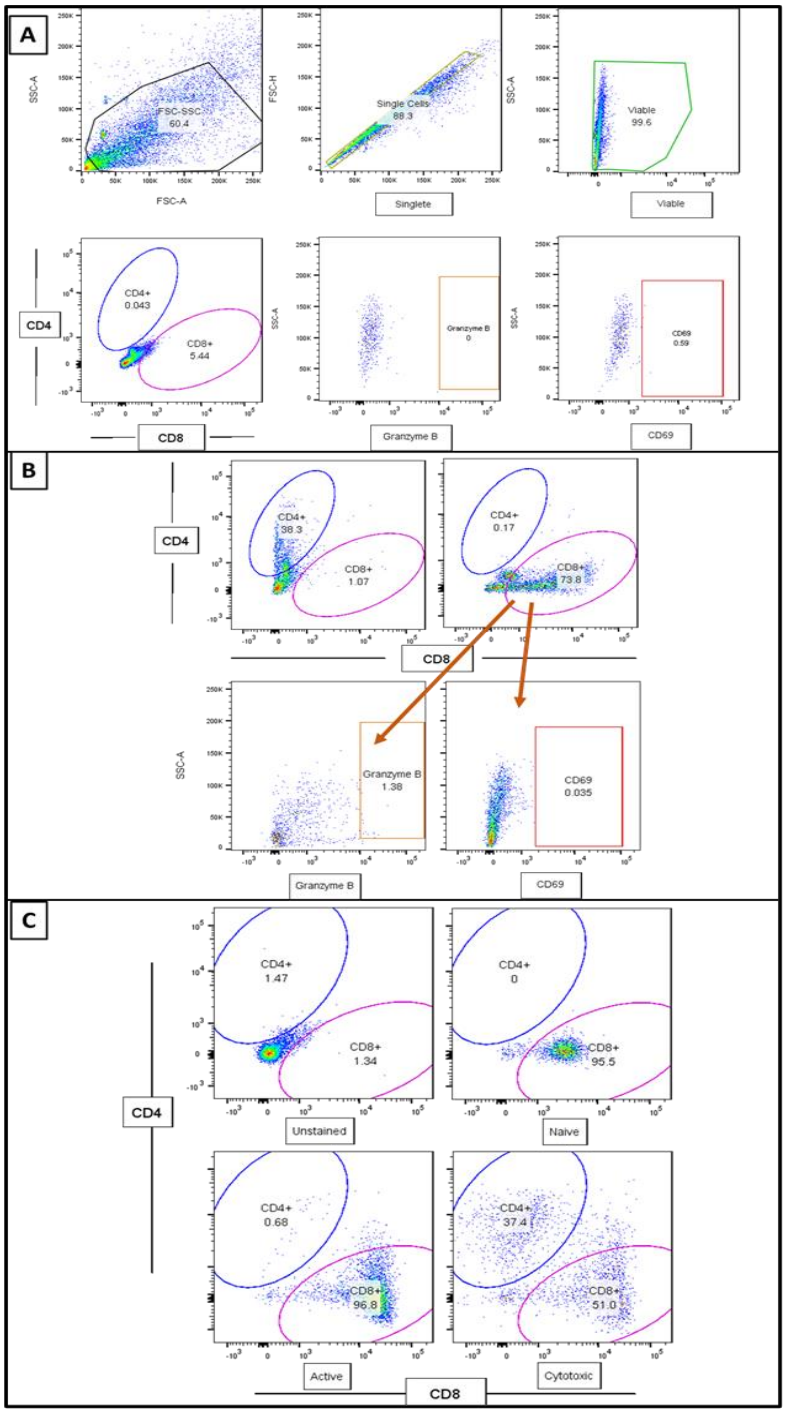

Figure 4.21: Gating strategy devised to assess cytotoxic CD8+ T cell phenotype. Primary CD8+ T cells were treated with IL-2 only, IL-2 and CD3/CD28, or with CD3/CD28 in presence of CD4+ T cells for 7 days to generate naïve, activated and cytotoxic CD8+ T cells populations, respectively. The gating was set using (A) unstained samples, then the gates adjusted using (B) the FMO samples. The main population of T cells was gated on the FSC/SSC plot, then gates single events were included using the FSC-H/FSC-A plot. After the viable population was gated to exclude dead cells from the analysis, (C) the main CD8+ and CD4+ populations were detected by flow cytometry. Data presented as representative dot plots

On day 7 of culture and before analysis, T cells were either left without restimulation or re-stimulated with a stimulation cocktail of PMA and ionomycin in the

presence of secretion inhibitors, Brefeldin A and Monensin. The cytotoxic CD8+ samples showed high levels of granzyme B with nMFI of 86.6 ±17 (65.4 ±24%) that was significantly increased compared to the activated (nMFI= 9 ± 13; 11.3 ±12%; p= <0.0001) and the naïve control (nMFI= 2.3 ± 1.1; 1.1 ±0.5%; p= <0.0001) (**Figure 4.22B**). The difference in granzyme B production can be visually appreciated from the large shift in the cell population on the representative dot blot (**Figure 4.22A).** There was no difference in the abundance of granzyme B in relation to the re-stimulation with PMA/ionomycin. Negligible levels of granzyme B in the naïve and activated samples was seen whether re-stimulated was performed before analysis or not.

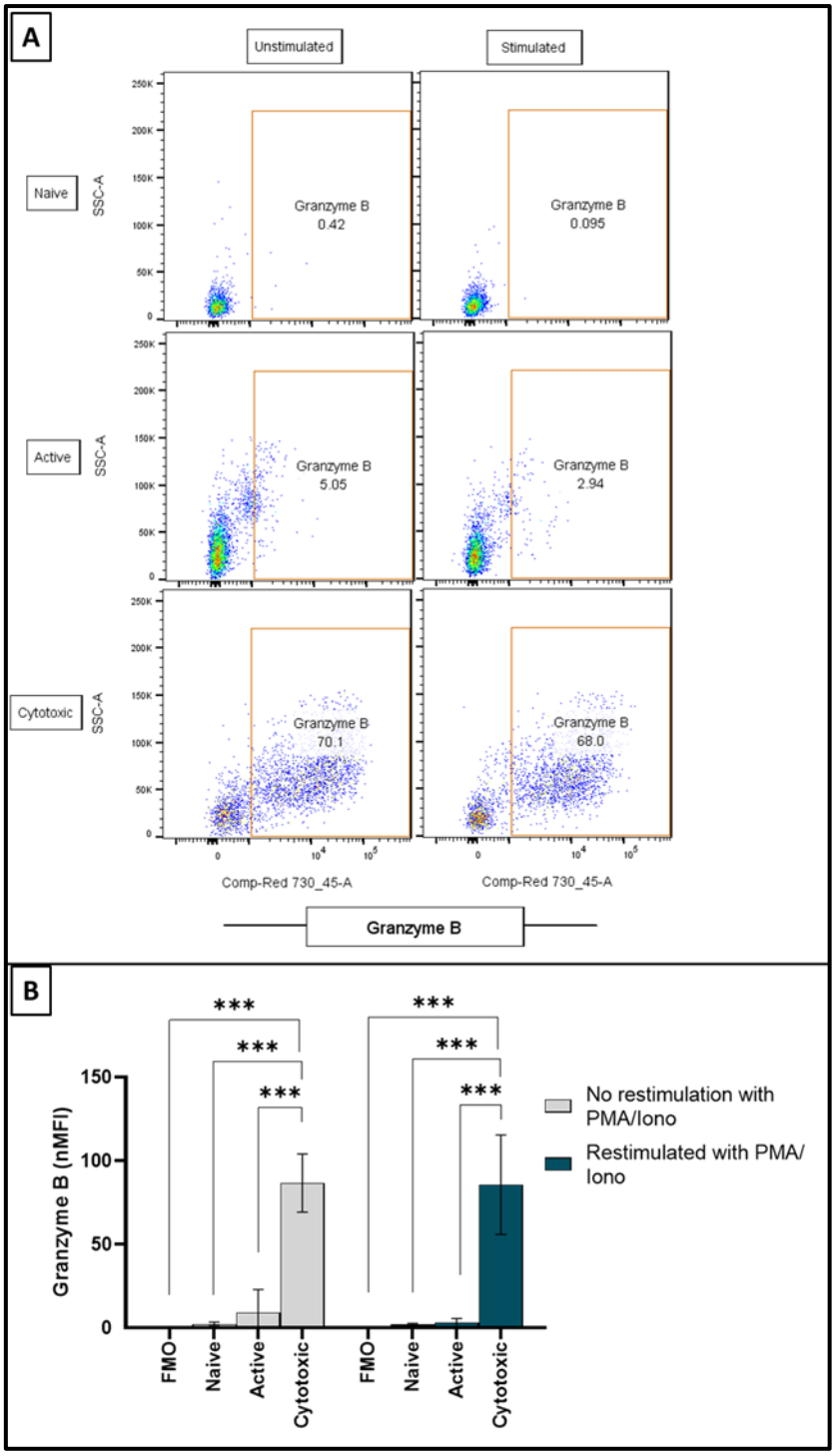

Figure 4.22: Abundance of intracellular granzyme B following CD8+ T cells activation. Primary CD8+ T cells were treated with IL-2 only, IL-2 and CD3/CD28 or with CD3/CD28 in the presence of CD4+ T cells for 7 days to generate naïve, activated and cytotoxic CD8+ T cells populations, respectively. The normalised median fluorescent intensity (nMFI) of intracellular granzyme B was assessed by flow cytometry. Data are presented as (A) representative dot plots and (B) the mean ± SD. A mean difference was considered significant when ***p <0.0001, using two-way ANOVA with Tukey's post-hoc multiple comparison tests to detect difference between groups. Main ANOVA reported ***p <0.001 effect of activation status but no effect for restimulation or interaction. n=3.

4.5 Discussion

The development of a T cell-containing oral mucosal disease model for future therapeutic strategies for OLP depends on the understanding of T cell biology, their mechanism of activation in the disease process and their interactions with other cells.

4.5.1 Purity and viability of isolated T cells *in vitro*

The preparation of PBMCs, which includes lymphocytes (i.e., T cells, B cells and NK cells), monocytes and dendritic cells from whole blood, is a common step prior to the isolation of specific immune cell subsets. Density gradient centrifugation methods have been widely used for decades to separate mononuclear cells from granulocytes and erythrocytes using whole blood or buffy coat (Pertoft *et al.*, 1979; Noble, Cutts and Carroll, 1968). Buffy coats were preferred over whole blood in this study as they represent a concentrate of leukocytes and platelets following blood donation. Therefore, use of buffy coats is considered an efficient way to increase the number of PBMCs for experiments (Repnik, Knezevic and Jeras, 2003). Although, the yield of mononuclear cells was increased following density gradient centrifugation, it still consisted of a mixture of subpopulations of lymphocytes, monocytes and some contaminating granulocytes. For downstream analysis, further purification using robust isolation methods that yield a highly pure T cell population is necessary (Hanamsagar *et al.*, 2020). Multiple methods can be used to perform further cell isolation including immunomagnetic cell separation, fluorescence-activated cell sorting (FACS), immunodensity, sedimentation, adhesion and microfluidic cell separation. Presently, immunomagnetic and FACS are the most widely used separation methods to yield highly pure T cell populations (Gross *et al.*, 2015; Dalili, Samiei and Hoorfar, 2019). Although higher purity of the desired cell population is typically achieved by FACS, there are a variety of benchtop magnetic cell sorters that are less sophisticated, less time consuming, and much less expensive than FACS (Frenea-Robin and Marchalot, 2022). Studies comparing these two methods concluded that although the ability of immunomagnetic cell sorting to isolate increased cell numbers is less time consuming than FACS, both enrichment techniques offer excellent recovery and purity and can be equally used (Tripathi *et al.*, 2020; Sutermaster and Darling, 2019). Hence, CD4+ and CD8+ T cells were isolated using negative selection immunomagnetic separation where all immune cells other than T cells are captured on a magnetised column using antibody-conjugated iron beads, allowing collection of purified T cells. Negative selection is preferable than positive selection as it minimises the chances of antibody-based stimulation during the isolation procedure. The purity of cells in this study

was enriched to reach 92 ± 4% for CD4+ and 93 ± 3% for CD8+ T cells, which is similar to other studies that used immunomagnetic separation (CD4+ cells with >97% purity and CD8+ cells with >96% purity (Gunzer *et al.*, 2001), 85% CD4+ T cells (Bolandi *et al.*, 2020), 93 ± 5% for CD4+ T cells (Schuler *et al.*, 2011), or >95% CD4+ and >90% CD8+ T cells (Lundgren *et al.*, 2003).

High cell viability is often cited as a prerequisite for proceeding with single-cell workflows as significant loss of viability due to poor isolation technique will most likely result in poor quality data. This study reported high viability of 97 ± 2% and 84 ± 6%, for the isolated CD4+ and CD8+ T cells respectively, which is in agreement with previous studies (Schuler *et al.*, 2011; Gunzer *et al.*, 2001). Although many reported the viability of isolated T cells before downstream analysis, the exact values of viability were not reported (Kara *et al.*, 2013; Griffiths *et al.*, 2013; Chattopadhyay *et al.*, 2008).

4.5.2 CD4+ activation

Dendritic cells express both class I and class II major histocompatibility complex (MHC) molecules on their surface that permit the recognition of an antigen epitope by the T Cell Receptor (TCR, CD3) in combination with CD28 on the T cell surface. In response to the appropriate antigen/MHC complex, specific T cells become activated, secrete IL-2, and undergo clonal expansion creating multiple copies of themselves in order to deliver an immune response to cells displaying that specific antigen (Chaplin, 2010).

In vitro, different techniques have been developed to activate T cells either by direct antigen stimulation using dendritic cells or indirectly using mitogenic chemicals or monoclonal antibodies directed against CD3 and CD28. To simulate stimulation, T cells were either activated with iron particles conjugated with antibodies that bind to and activate CD3 and CD28 on the T cell surface to mimic antigen presentation, or with the mitogens PMA and ionomycin. PMA bypasses the need for CD3/CD28 ligation by directly activating the downstream intracellular signalling molecule protein kinase C, whereas the ionophore, ionomycin, increases intracellular calcium levels that is also required to drive artificial T cell activation. Abundance of cell surface CD69 was used to measure T cell activation (as shown in Chapter 3 and by other studies (Olsen and Sollid, 2013). There was more abundance in CD69 when T cells were activated with PMA and ionomycin for 24 hours than with the CD3/CD28 antibody complex. This may be due to the direct and non-receptor specific activation of protein kinase C and calcium signalling pathways. However, and as reported by others (Martkamchan *et al.*, 2016; McLeod *et al.*, 1998; Trickett and Kwan, 2003), efficient T cell activation was also achieved by the CD3/CD28

antibody-conjugated iron beads. Addition of IL-2 along with the CD3/CD28 antibody complex provides important additional stimulatory signals that enhance T cell proliferation. It is reported that autocrine IL-2 production from activated CD4+ T cells induces further T cell activation and proliferation (Martkamchan *et al.*, 2016; Cornish, Sinclair and Cantrell, 2006).

It has been suggested that different activation methods under neutral cytokine conditions may have different effects on T cells (Baran *et al.*, 2001). For example, PMA and ionomycin may influence T cells to polarise into Th1/Th17 clones because they potentiate the levels of IFN-γ and IL-17 when compared CD3/ CD28 stimulation (Olsen and Sollid, 2013). PMA and ionomycin activation might be suited for other purposes such as when maximum cytokine needed, whereas CD3/ CD28 may be preferential for expansion and generation of specific polarision of T cells where stimulation needs to be carefully controlled (Shi *et al.*, 2013; Martkamchan *et al.*, 2016). Despite being less stimulatory than the mitogenic factors, use of CD3/CD28 antibody complex to activate T cells was taken forward for use in the rest of the study because this form of stimulation more closely mimics that of antigen presenting cells that occurs *in vivo*.

4.5.3 Th1 Phenotyping

The direct contact of MHCII-bound antigen on the APCs with the TCR is considered the first step in T cell differentiation toward a T helper (Th) phenotype, where T cells respond in accordance with the type and dose of invading pathogen. However, it is less clear how the immune response is matched to a particular pathogen (Mosmann and Sad, 1996). It has been established that activated naïve CD4+ T cells are differentiated into distinct Th subsets depending on the type of cytokine they experience in the microenvironment. For Th1 polarisation, IL-12 produced by APCs and keratinocytes induces IFN-γ secretion from natural killer cells. Subsequently, IL-12 and IFN-γ stimulate reacting T cells to induce the expression of the transcription factor T-bet, which in turn promotes T cells to differentiate into the Th1 subset (Amsen, Spilianakis and Flavell, 2009). In OLP, the increased production of IL-12 and IL-18 by keratinocytes and Langerhans cells influences CD4+ differentiation towards the Th1 phenotype inducing IL-2, IFN-γ and TNF-α production (Lu *et al.*, 2015; Müller *et al.*, 1994; Aragane *et al.*, 1994), while cytokines such as IL-4, IL-10 and TGF-β negatively regulate Th1 differentiation (Lu *et al.*, 2015).

Unstimulated peripheral blood T cells produce little or no cytokines. Thus, *in vitro* stimulation using exogenous cytokines is required to induce polarisation. Different research groups have used various combinations and cytokine dosages to elicit the Th1 phenotype *in vitro*. IL-12 to drive Th1 differentiation and IL-4 neutralising antibody to block switching into Th2 phenotype are the main components needed for Th1 production (Dubovsky *et al.*, 2011; Suurmond *et al.*, 2014; Sekiya and Yoshimura, 2016). Since IL-12 and IL-18 synergistically enhance IFN-γ by activating STAT4 (Nakahira *et al.*, 2002), IL-18 was included in different Th1 polarisation kits to enhance Th1 differentiation.

Th1 can be distinguished from other T cell subsets based on the cell surface expression of IL-12R β2, IFN-γ R2, IL-18R, CCR5, CCR6 and CXCR3, the expression of the transcriptional regulators, T-bet, STAT1 and STAT4, and their cytokine secretory profile of IFN-γ and TNF-α.

Two flow cytometry marker panels were designed to provide clear distinction of T cell phenotype. The first seven-colour antibody panel targeted distinct profiles of cell surface markers while a second four-coloured panel targeted Th1 selective transcriptional factors and cytokines.

Chemokine receptors are up regulated on T cells after activation where their expression is modulated by specific cytokines. For example, CCR3 and CCR4 are expressed exclusively on Th2 cells, whereas CXCR3 and CCR5 are found on Th0 and Th1 cells (Sallusto *et al.*, 1998; Bonecchi *et al.*, 1998). CXCR3 is rapidly induced on naïve T cells following activation and remains highly expressed on both Th1 and effector CD8+ T cells. Th 1 cells can then bind the CXCR3-specific chemokines CXCL9 (MIG), CXCL10 (IP-10) and CXCL11 (I-TAC) to guide them out of the circulation and into inflammatory sites (Groom and Luster, 2011). In accordance with previous *in vitro* studies, data in this study showed that while CXCR3 was not detected on naive T cells, it was rapidly induced following T cell activation reflecting the differentiation status of Th1 cells (Langenkamp *et al.*, 2003; Groom and Luster, 2011; Bonecchi *et al.*, 1998; Sallusto *et al.*, 1998).

CCR1, CCR3, CCR5, CCR9 and CCR10 are cell surface receptors for CCL5 (also known as RANTES), a potent inflammatory mediator produced by T cells, macrophages, platelets, fibroblasts and keratinocytes and causes chemoattraction of T cells. Increased expression of CCL5 has been identified in oral lichen planus biopsy tissue (Hu *et al.*, 2013; Zhou *et al.*, 2001; Li *et al.*, 1996a; Zhao *et al.*, 2001). Approximately half of the circulating CD4+ were CCR5+ in OLP (Shan *et al.*, 2019; Hu *et al.*, 2013) and CCL5

chemoattracts T cell subsets, including CD8+T cells and Th1 cells into OLP lesions (Li *et al.*, 1996a; Yang *et al.*, 2018). Although CCR5 cell surface abundance was only slightly increased on Th 1 cells in this study, this was statistically significant when compared to naïve T cells. It has been reported that expression of CCR5 on activated T cells is concomitant with a strong Th1 polarization phenotype (Loetscher *et al.*, 1998b; Bonecchi *et al.*, 1998).

CCR6 (also known as CD196), is a chemokine receptor for the ligand CCL20 (MIP-3α). The CCL20/CCR6 axis has also been associated with human immunodeficiency virus (HIV) infection, rheumatoid arthritis, cancer (Osuala and Sloane, 2014; Schutyser, Struyf and Van Damme, 2003) and in OLP (Chen *et al.*, 2011). Although CCR6 is primarily expressed in Th17 cells (Annunziato *et al.*, 2007a), the expression of CXCR3, along with CCR5 and CCR6, was reported to discriminate between different effector T cell populations, especially Th1 (Loetscher *et al.*, 1998b). However, data in this study showed no increase in CCR6 levels compared to unstimulated controls. Interestingly, reports suggest that detection of CCR6 might reflect cells in the early Th1 differentiation stage and expression of CCR6 may not be present in Th1 at established differentiation, which may be the reason for the low cell surface levels found in this study. Also, the coexistence of CXCR3 and CCR6 on CD4+ T cells may indicate a separate population, the Th1/Th17 phenotype that are suggested to have a role in several immune mediated conditions (Duhen and Campbell, 2014; Brand, 2009). In vitro CCR6 levels did not match reports in OLP cases which may reflect difficulty in reproducing a complex in vivo setting. Anyhow, receptors expression and Th1 and Th17 exact roles in disease need further investigations.

IL-12 is synthesized and released from APCs to direct a cell-mediated immune response *in vivo* or added as recombinant IL-12 *in vitro* to direct Th1 differentiation. IL-12 binds to the IL-12 receptor (IL-12R), which consists of beta 1 chain that directly binds IL-12 and a beta 2 chain which triggers the intracellular signalling pathway (Wu *et al.*, 1996) causing activation of the JAK kinases and ultimately phosphorylation of STAT4. Activation of STAT4 results in upregulation of IL-12Rβ and the production of IFN-γ (Kaplan, Wurster and Grusby, 1998; Hanlon, Jang and Salgame, 2002). Hence, it was proposed that IL-12Rβ would be upregulated in Th1 cells. In accordance with previous reports, a significant increase in the percentage of IL-12Rβ was detected in the Th1 population in this study (Smeltz *et al.*, 2002; Rogge *et al.*, 1999). Although a similar increase was present in the active CD4+ sample, this was not consistent among samples, which might reflect random tendency of active CD4+ T cells to polarise to Th1 (Igarashi *et al.*, 1998).

Binding of IFN-γ to its cognate receptor results in the auto- and transphosphorylation of Jak1 and Jak2 tyrosine kinases, which phosphorylate STAT1 that in turn drives the transcription of IFN-γ responsive genes (Hanlon, Jang and Salgame, 2002). Hence, IFN-γ receptor I (IFN-γ R1) is normally expressed in Th1 population (Novick *et al.*, 1987). A significant increase in IFN-γ R1 was not detected in this study. However, levels of IFN-γ, measured as intracellular protein by flow cytometry or as secreted by ELISA, was significantly higher in Th1 cells indicating a Th 1 phenotype. Moreover, increased levels of secreted TNF-α were significantly higher by Th1 population while levels of the Th2 specific cytokine, IL-4 were very low.

Several studies suggest that a higher IFN/IL-4 ratio reflects Th1 dominance. Moreover, increased levels of IFN-γ have been used as a marker of the Th1 phenotype in immune mediated conditions. For instance, erythematous/ulcerated OLP patients had significantly higher levels of IFN-γ in their lesions and saliva than in patients with the reticular type (Tao *et al.*, 2008; Lu *et al.*, 2015; Hu *et al.*, 2015; Wei *et al.*, 2018; Wang *et al.*, 2015; Malekzadeh *et al.*, 2015). Over expression of IFN-γ was widely detected in most studies in OLP (Khan *et al.*, 2003; Yamamoto and Osaki, 1995; Simark-Mattsson *et al.*, 1999; Fayyazi *et al.*, 1999; Tao *et al.*, 2008). Here, IFN-γ is thought to play a major role by inducing CD40 expression on epithelial cells and increased secretion of chemokines such as CCL5 and CXCL10 (Marshall *et al.*, 2017a; Shan *et al.*, 2019; Marshall *et al.*, 2017b). IFN-γ is also involved in the maturation and activation of cytotoxic CD8 T cells and maintenance of the expression of major histocompatibility complex class II and tissue adhesion molecules. Although TNF-α is produced by a wide variety of cell types, including monocytes, macrophages, lymphocytes, endothelial cells, and keratinocytes, its markedly produced by the Th1 population among T helper subsets. TNF-α produced by Th1 synergistically works with IL-1 to induce higher expression of MHC classes I, II and ICAM1 (CD54). High levels of TNF-α have been detected in with OLP (Yamamoto and Osaki, 1995; Simark-Mattsson *et al.*, 1999; Xavier *et al.*, 2007). Interestingly, IL-10 and CCL5 were not markedly produced by Th1 population compared to activated T cells in this study. These factors are reported to have important roles in OLP. IL-10 is reported to broadly inhibit both the proliferation and the cytokine synthesis of Th1 and Th2. It is secreted primarily from monocytes and macrophages and target T cells by inhibiting their pro-inflammatory cytokines release and antigen presentation thereby displaying an inhibitory effect on Th1 cells (Lu *et al.*, 2015).

As part of intracellular signalling mechanism when the cells are stimulated, many transcription factors such as T-bet and STAT proteins must be phosphorylated before

they can bind DNA and transcribe genes (Chen *et al.*, 2011). T-bet transcriptional factor works in coordination with a series of factors to orchestrate Th1 differentiation. As described earlier, IL-12 is considered the main driver for Th1 phenotype as it induces the expression of STAT4 transcription factor which promotes expression of multiple Th1-related genes, including IFN-γ. Auto/paracrine IFN-γ action induces STAT1 phosphorylation, which in turn elevates T-bet expression (Ji, Sosa and Forsthuber, 2011). T-bet collaborates with STAT4 in promoting transcription of multiple Th1 genes including the IL12R, IFN-γ, whilst simultaneously antagonising the Th2 transcriptional factor, GATA3 (Zhu *et al.*, 2012; Luckheeram *et al.*, 2012; Amsen, Spilianakis and Flavell, 2009). Data here align with the literature for Th1 cells as both T-bet and STAT4 levels were markedly increased in the Th1 population. Moreover, phosphorylated STAT1 was increased in the Th1 cells compared to activated only T cells.

Although, data in this thesis showed that the Th1 polarised cells continue to expand in culture, their proliferation was reduced when compared to the only activated sample. It has been reported that during Th1 cell differentiation, IL-2 transcription is also attenuated upon induction of T-bet (Oh and Hwang, 2014). This IL-2 inhibition may affect cell populationexpansion.

4.5.4 Th17 phenotyping

Th17 cells are a Th subset that selectively produce IL-17. Under the actions of IL-12, Th17 can transform into a mixed phenotype called Th17/ Th1 or under longer induction they can acquire Th1 features while losing their Th17 phenotype resulting in a Th1 phenotype termed as 'non-classic' Th1 (Annunziato *et al.*, 2007a; Peck and Mellins, 2010). The presence of Th17, Th17/ Th1, and non-classic Th1 cells, although not fully understood, but have been detected increasingly in different inflammatory and autoimmune diseases including OLP (Kamali *et al.*, 2019; Xie *et al.*, 2012). These disorders have been in the past associated to classic Th1 responses but more recently to Th17 cells, because of the ability of the latter to polarize toward the Th1 phenotype. Owing to the plastic phenotype of Th17, the opportunity to discriminate between their related subsets by using a panel of markers offers the possibility to better understand their respective pathogenic roles in chronic inflammatory disorders including OLP.

Most current culturing methods used to generate effector Th17 cell subsets *in vitro* through the activation and addition of exogenous cytokines such as IL-1B, TGF-β, IL-6 or IL-23, and blocking antibodies such as anti-IL-4, anti-IFN-γ, and anti-IL-2 antibodies for the generation of Th17 (Nakae *et al.*, 2007; Sekiya and Yoshimura, 2016; Read *et al.*,

2019). In this study, Th17 was generated from naïve CD4+ T cells isolated from healthy donors following general CD4+ subsets phenotyping protocols (Read *et al.*, 2019).

IL-1β and IL-6, a proinflammatory cytokines, were found to work with TGFβ, an immunoregulatory cytokine, to enhance Th17 programming *in vitro* through upregulating IL-23R and activating of STAT3 transcriptional factor, which is necessary to induce RORγt (Zhou *et al.*, 2007; Chung *et al.*, 2009). low concentrations of TGFβ were reported to promote the Th17 cell differentiation, while high concentrations of TGFβ repress RORγt activity through induction of Foxp3 preferring the T-reg phenotype development (Zhou *et al.*, 2008; Veldhoen *et al.*, 2006; Bettelli *et al.*, 2006). Moreover, the role of IL-23 was shown to be important in the maintenance of Th17 phenotype rather than establishing the Th17 phenotype (McGeachy *et al.*, 2009).

To optimise Th17 polarising conditions, Hakemi *et al*, suggested that variable conditions such as the combinations of IL-1β either with IL-6 or IL-23 or the combination of TGF-β and IL-23 with IL-6 and IL-1β is effective to induce human Th17 cells differentiation (Ganjalikhani Hakemi *et al.*, 2011). It was also confirmed that IL-12 or IFN-γ can negatively regulate Th17 cell differentiation *in vitro* resulting in the developing of a mixed Th17/ Th1 phenotype.

Annunziato *et.al*, classified T cell clones producing IL-17 alone, IFN- γ alone, or IL-4 alone, as Th17, Th1, and Th2, respectively, while those producing both IL-4 and IFN-γ, but not IL-17, as Th0, and those producing both IL-17 and IFN-γ or both IL-17 and IL-4 as Th17/Th1 or Th17/Th2, respectively (Annunziato *et al.*, 2007a). Similarly, the resulted phenotypes in this study were classified according to the production of IL-17 alone or IL-17 with IFN-γ as Th17, or Th17/Th1 phenotypes, respectively. The Th17/ Th2 phenotype was not investigated here because Th1 and Th17 may have more similarities as they have a close developmental relationship. Nakae *et al*, investigated the phenotypic differences between Th1 and Th17 and found that IL-18 receptor α, CXCR3, CCR6, and T cell Ig domain, mucin-like domain-3 (TIM-3) were present on both Th1 &Th17 which suggested the expression pattern of cell surface molecules by Th17 cells is closer to that of Th1 cells than that of Th2 cells. (Cosmi *et al.*, 2008; Cosmi *et al.*, 2014; Nakae *et al.*, 2007). Although there was slight difference between the restimulated and un-restimulated samples regarding cytokine production, other studies have confirmed that re-stimulating Th17 cells by adding PMA and ionomycin was an important and necessary step for the *in vitro* measurement of Th17 cells through measuring intracellular IL-17 levels (Knebel *et al.*, 2022).

While adding IL-2 to the *in vitro* T cell culture is essential for the growth and proliferation of Th1, Th2, and CD8+ T cells, it was shown to be actively inhibiting for Th17 differentiation. It was reported that Treg may promote Th17 development through repressing IL-2 production (Laurence *et al.*, 2007; Stockinger, 2007; Luo *et al.*, 2018). Hence, blocking the endogenous IL-2 by adding neutralizing antibodies IL-2 was important factor to enhance Th17 development at the expense of cell proliferation rate. This has presented a challenge to the yield of cells which were limited to run analysis of other factors such as RORC, FOXP3, and CCR6.

4.5.5 Cytotoxic CD8+ T cell phenotyping

Naive CD8+ T cells are maintained in a quiescent state until they encounter an antigen where they get activated, proliferate and differentiate, resulting in the acquisition of key functional properties, including the capacity to produce cytokines (Butz and Bevan, 1998). CD8+ cytotoxic T cells perform a cytolytic cytotoxic effect mediated through different mechanisms including the delivery of cytolytic proteins such as Granzyme and Perforin that are stored in cytoplasmic granules. These granules release their content during cytotoxic targeted cell lysis and cause cellular damage. Perforin targets the cell membrane to create pores that result in the destruction of the normal cellular gradient, ultimately causing osmotic lysis and cell death (Kägi *et al.*, 1994). Granzyme B can pass through perforin-mediated pores causing DNA fragmentation and apoptosis (Russell, 1983). Granzyme B has been considered the major killing mechanism for cytotoxic T cells because it can activate a number of apoptotic pathways (Lord *et al.*, 2003). A study assessed the immune phenotyping of activated CD8 *in vitro* using a polychromatic flow cytometry panel for the functional markers IFN-γ, MIP1β, perforin, and granzyme and found that the most upregulated marker was Granzyme B (Patel *et al.*, 2018). Therefore, the panel developed in this study, analysed CD8+ T cells in a context specific to CD8 cytotoxic by measuring levels of intracellular Granzyme B.

Although development of CD8+ T cell effector responses during a number of viral infections appears to be independent of helper cells, CD4+ T cells, in general, contribute to immunity not only by secretion of antimicrobial cytokines such as IFN-γ but also by providing help for maintaining optimal CD8+ T cell cytotoxic responses (Serbina, Lazarevic and Flynn, 2001; Frasca, Piazza and Piccolella, 1998). Similar to naïve CD4+ T cells stimulation, CD8+ T cells require a primary signal provided by the TCR stimulation by mature APCs expressing cognate antigen and a secondary signals from co-stimulatory molecules to enhance activation and functionality (Cronin and Penninger, 2007).

However, inflammatory cytokines were reported to act as third signals to endorse optimal differentiation of cytotoxic CD8 T cells (Curtsinger and Mescher, 2010). IL-12 and IFN-γ were reported to encourage the accumulation of activated CD8 T cells by extending their cellular division and by sustaining IL-2 signalling (Starbeck-Miller, Xue and Harty, 2014). In agreement, this study reported a significant difference in the CD8+ T cell expansion capacity and their ability to secret Granzyme B when they were cultured in presence or absence of Th cells, mainly Th1, that in turn were able to secret IFN-γ. Hence, the presence of Th1 was essential for optimum activation of CD8+ T cells. It was important to isolate and establish a confirmed cytotoxic phenotype of CD8+ T cells as these are consistently reported to be the principal cell type responsible for keratinocyte death in OLP (Sugerman *et al.*, 2002; Zhou *et al.*, 2002).

4.6 Conclusion

Improved methods have enabled the immunological downstream analysis of lymphocytes through isolation techniques and *in vitro* culturing methods. For instance, T cell populations that were initially expanded *in vitro* through coculturing with antigen or APCs can now be done using monoclonal antibodies such as CD3/ CD28. This simple culture system provides a more physiologically relevant mechanism and is the basis for T cells *in vitro* culturing conditions described in this study. Although the specific cytokine signalling pathways and lineage-specific transcription factors that define individual T helper cell subset has been well established in literature, this chapter provided detailed summary of current culturing methods to establish Th1, Th17 and cytotoxic CD8+ T cells *in vitro* in context of the knowledge of T cell mediated immune disease, mainly OLP. This will serve as a valuable set of tools when combined with 3D culture methods to help explore mechanisms that govern immune mediated diseases including the role of different Th subsets and the debated role of Th17 cells. In the following chapter, the T cell component of OLP that was accomplished here will be incorporated into a 3D oral mucosal model following tissue engineering methods to construct a complex model of T cell inflammatory disease that will hopefully contribute to the better understanding of OLP and identify new fields of research for treatment options.

5 Chapter five: Development of a full thickness tissue engineered T cell mediated inflammatory disease model

5.1 Introduction

The only available models to study OLP are murine models which were developed for investigating lichenoid tissue reaction or GvHD. In these *in vivo* models disease develops by the adoptive transfer of CD8+ T cells or auto aggressive CD4+ cells reactive to self MHCI (Christofidou-Solomidou et al., 1997) or through the transfer of donor T cells (Chakraverty et al., 2006). Their use is limited due to interspecies differences in immune system function and ethical considerations with a drive to replace, reduce or refine experimental animal model systems (3R's principle) where possible. With recent advances in 3D cell culture, there is now an increasing interest in the use of tissue engineered models to determine the pharmacokinetics, pharmacodynamics and toxicity of drug candidates (Selvaratnam *et al.*, 2001; Moharamzadeh *et al.*, 2009; Duval *et al.*, 2017). Several such models exist, comprising co-culture of different cell types in culture inserts, as described previously (Chapter 1), including a reproducible and well-characterised tissue engineered oral mucosa model (Dongari-Bagtzoglou and Kashleva, 2006a). These oral mucosal equivalents (OME) provide the basis for further development to study different disease mechanisms and potential therapeutic interventions. With defined, reproducible models, recent research has focused on the inclusion of an immune counterpart. However, advanced T cell inflammatory tissue engineered oral mucosal models containing appropriately primed T cells has not yet been achieved. Establishment of such a model will hold great potential for delineating the disease mechanisms in, for example, OLP and for the development of novel drug delivery systems.

This chapter describes the strategy followed to incorporate primed immune cells into full thickness OME to produce a T cell inflammatory immune disease model. Initially, it explores the viability, morphology, and proliferation of immune cells within a collagen hydrogel with or without NOF. Then, in a systematic manner, the incorporation into a tissue-engineered oral mucosa equivalent, composed of FNB6 and NOF.

The coordinated secretion of chemokines by non-immune and immune cells is essential for mediating the adhesion and migration of T cells from bloodstream to the local tissue at a steady state. T cell accumulation in the subepithelium is key characteristic of OLP. To ensure that the OME produced the chemokines known to be involved in this process, chemokine profile analysis from culture supernatant of stimulated OME was

performed. Then, to confirm that T cells will respond to the resultant chemokine gradient, a chemotaxis assay was performed to assess their migration capacity. Thereafter, primed Th1 and cytotoxic CD8 cells were combined to produce a standardised, reproducible OME where an immune response could be provoked through direct stimulation with INF-γ and TNF-α, as a substitute for antigen activated dendritic cells to simulate an inflammatory microenvironment in OLP. It was hypothesised that primed immune cells would interact with the epithelium and thereby create a serial of inflammatory signals that attracts T cells to the epithelium, causing epithelial apoptosis and basement membrane destruction. The disease progression was evaluated over time and compared to OME without T cells as well as additional validation against biopsies of normal oral mucosa and from OLP patients.

5.2 Aims and objectives

The aim of the work presented in this chapter was to develop a full thickness tissue-engineered model of OLP, validated again patient biopsies:

Objectives:

- Create tissue engineered normal OME composed of FNB6 and NOF and assess histology with H&E.
- Incorporate Th1 into collagen hydrogels and assess their metabolic rate overtime using a PrestoBlue™ assay and determination of cell viability by flow cytometry and morphology by H&E and IHC..
- Assess the morphology of Th1 and NOF incorporated into collagen hydrogels over 14 days.
- Stimulate OME and evaluate cytokines release using a cytokine array and ELISA.
- Assess T cell chemoattraction towards a chemokine gradient using a live imaging chemotaxis assay.
- Incorporate CD8+ T cells and Th1 within OME using a layering strategy and assess the histology of the full thickness tissue engineered T cell OME inflammatory model and their chemokine secretion overtime using ELISA.
- Validate the full thickness tissue engineered OME inflammatory model against healthy and OLP patient biopsies using immunohistochemistry.

5.3 Materials and methods

Please refer to chapter 2 for all materials and methods.

5.4 Results

5.4.1 The development of an oral mucosal equivalent

OME were generated by seeding FNB6 keratinocytes on top of a hydrogel embedded with NOF for 2-5 days then raised to an air-to-liquid interface (ALI) for 12 days before tissue fixation. Histological analysis was carried out on the fixed OME by staining with haematoxylin and eosin (H&E). The OME reflected a morphology similar to the native buccal normal oral mucosa three distinct components; a stratified squamous epithelium overlying a fibroblast-populated connective tissue with a basement membrane separating the two layers. The FNB6 keratinocytes successfully differentiated into a stratified epithelial layer with evidence of a basal cell layer (stratum basale), followed by a spinous or prickle cells layer (stratum spinosum) with cells polygonal in shape and greater in size, before the cells became flattened forming a superficial layer, and finally a keratin layer. The oral buccal mucosa histology, displayed a nucleated, para-keratinised layer. The NOF seeded into the collagen hydrogel in the OME were evenly distributed within the connective tissue (**Figure 5.1**).

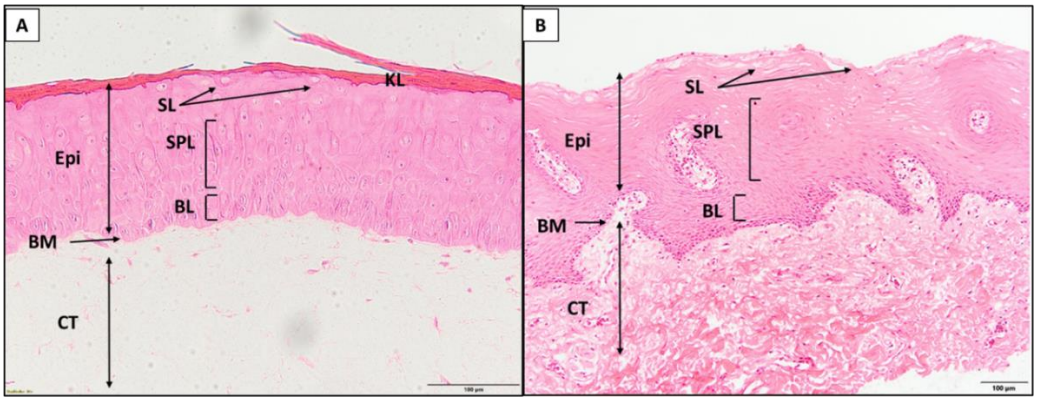

Figure 5.1: Histological analysis of normal oral mucosa equivalent and normal oral mucosa. (A) Normal OME cultured for 12 days at an air-to-liquid interface and (B) normal oral mucosa were analysed by histology after staining with haematoxylin and eosin. Representative images show a stratified epithelium (Epi), basement membrane (BM) and connective tissue (CT) components. The epithelium constitutes a basal layer (BL), spinous/prickle layer (SPL), superficial layer (SL) and keratin layer (KL). Images are representative of n=3 independent OME. Scale bar = 100 µm.

5.4.2 Incorporation of T cells in collagen hydrogels with or without NOF

Before generating a full model of T cell mucosal disease, the viability of T cells that were isolated, activated and polarised in suspension culture were assessed for their ability to be cultured in 3D by seeding them within a collagen hydrogel. Th1 ($1X10^6$ cells) were seeded within a collagen hydrogel for 1, 7 and 14 days before either fixation with formalin or extracted with collagenase to assess their viability with flow cytometry. The

histological appearance of T cells embedded within a hydrogel was examined following H&E staining. Small, rounded cells with large dense nuclei that occupy most of the cell, characteristic of T cells was evident and evenly distributed throughout the collagen hydrogel (**Figure 5.2A**). T cells subtypes were not distinguished from each other when examined under the light microscope. To confirm the cell phenotype, IHC was performed with anti- CD4 and CD8, revealing positive staining for CD4+ (**Figure 5.2B**) and CD8+ T cells (**Figure 5.2C**).

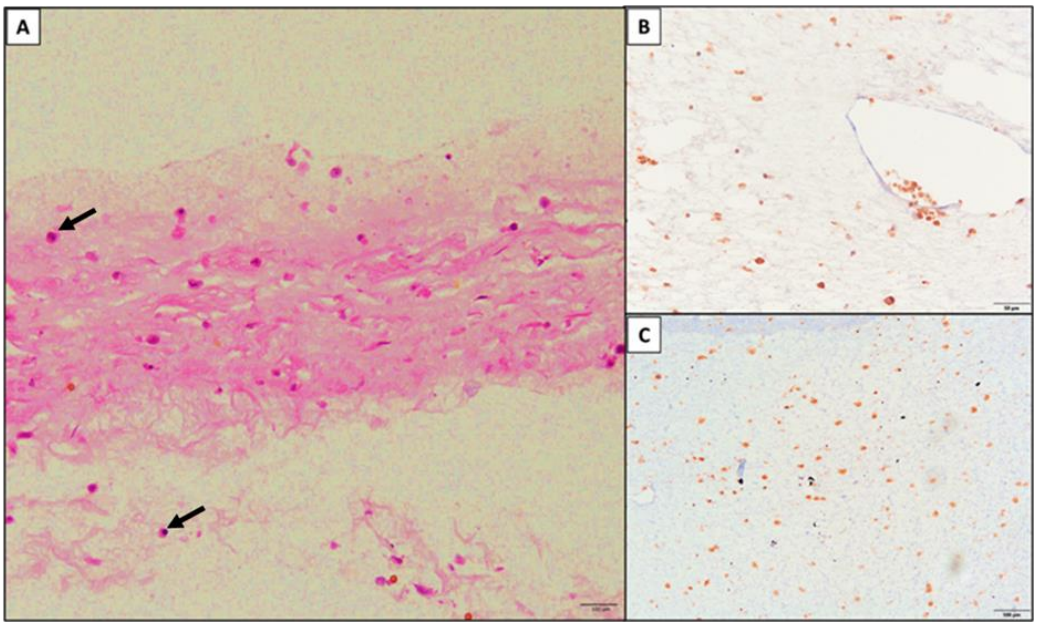

Figure 5.2: Histological examination of T cells embedded within a collagen hydrogel. T cells ($1x10^6$) were incorporated into collagen hydrogels and cultured for 14 days before fixation and histological analysis by staining with (A) H&E which revealed small round T cells with large dark nuclei (black arrows) and by (B) IHC to identify CD4+ and (C) CD8+. T cells which were distributed evenly within the collagen hydrogels. Data are expressed as representative images; n=3. Scale bar A&C = 100 µm, B= 50 µm.

To explore the ability to extract and analyse cells following culture in the hydrogels, cell-free hydrogels (as a negative control) and hydrogels containing CD4+ T cells ($1x10^6$) were treated with collagenase and the extracted cells analysed using flow cytometry (**Figure 5.3**). Cell-free hydrogels had an extremely variable number of impurities and background fluorescence, most likely due to un-digested auto-fluorescent collagen fibres, ranging from 0 to 68% with a mean of 25 ± 23% events. The T cell-containing hydrogels reported higher total events and less variation of 54.4 ± 15.7%, due to the presence of T cells besides the collagen impurities (**Figure 5.4**). However, there was no significant difference between the cell-free or T cells containing hydrogels ($p=0.15$). Although a number of methods were tested to reduce the number of impurities from the hydrogels including the type of collagenase, treatment time and the addition of a filtering step, it was

determined that they could not be consistently reduced and hence, it was difficult to identify a pure population of CD4+ for further analysis using this simple method.

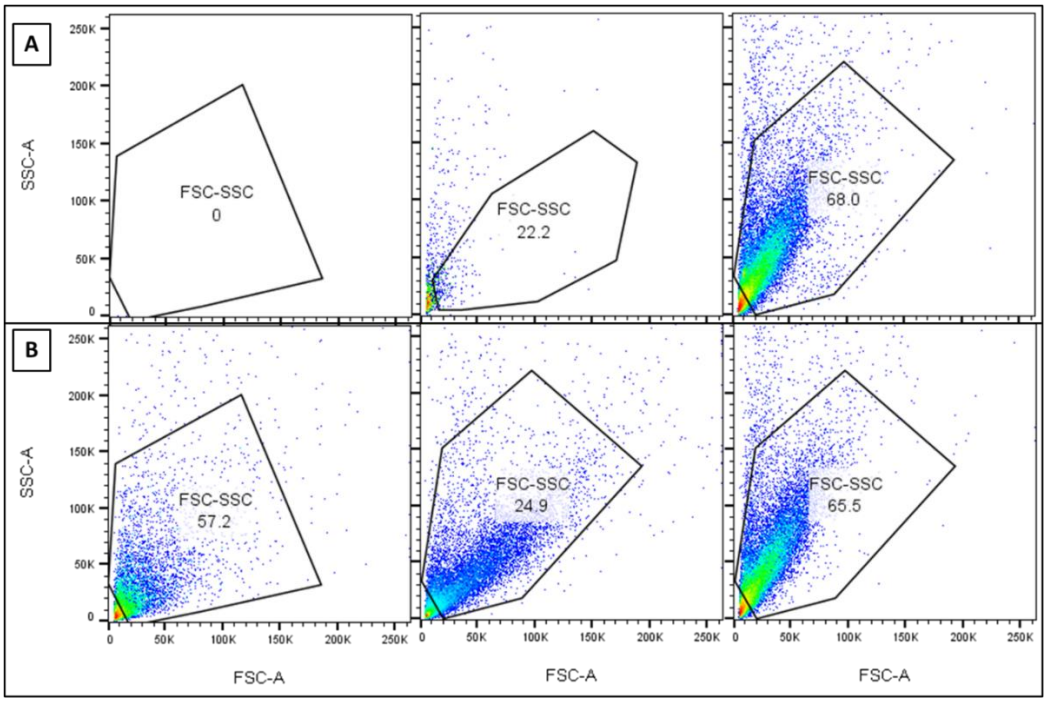

Figure 5.3: Flow cytometry analysis of cells following extraction from collagen hydrogels. Collagen hydrogels were constructed (A) without cells (B) or with T cell ($1x10^6$) incorporation before treatment with collagenase I for 1 hour at 37°C and analysis by flow cytometry. Data are expressed as three independent dot plots to show the intra-experimental variation in the collagen impurities.

Based on these observations, it was decided to also stain the samples with violet-conjugated anti-CD4+ surface marker to gate out the impurities introduced from the collagen hydrogel and enable further analysis on the extracted cells using excitation wavelengths that will not detect the natural auto-fluorescence of collagen fibres. A distinct population of CD4+ cells were identified in the T cell containing hydrogel totalling 43 ± 24% of the total events. Furthermore, collagen impurities were successfully reduced to 2 ± 1.7% in the CD4+ gate which was significantly less than the number of events detected in the T cells hydrogel ($p=0.03$). These results confirm that T cells incorporated into hydrogel can be extracted as a pure population and used for further analysis. (**Figure 5.4C**).

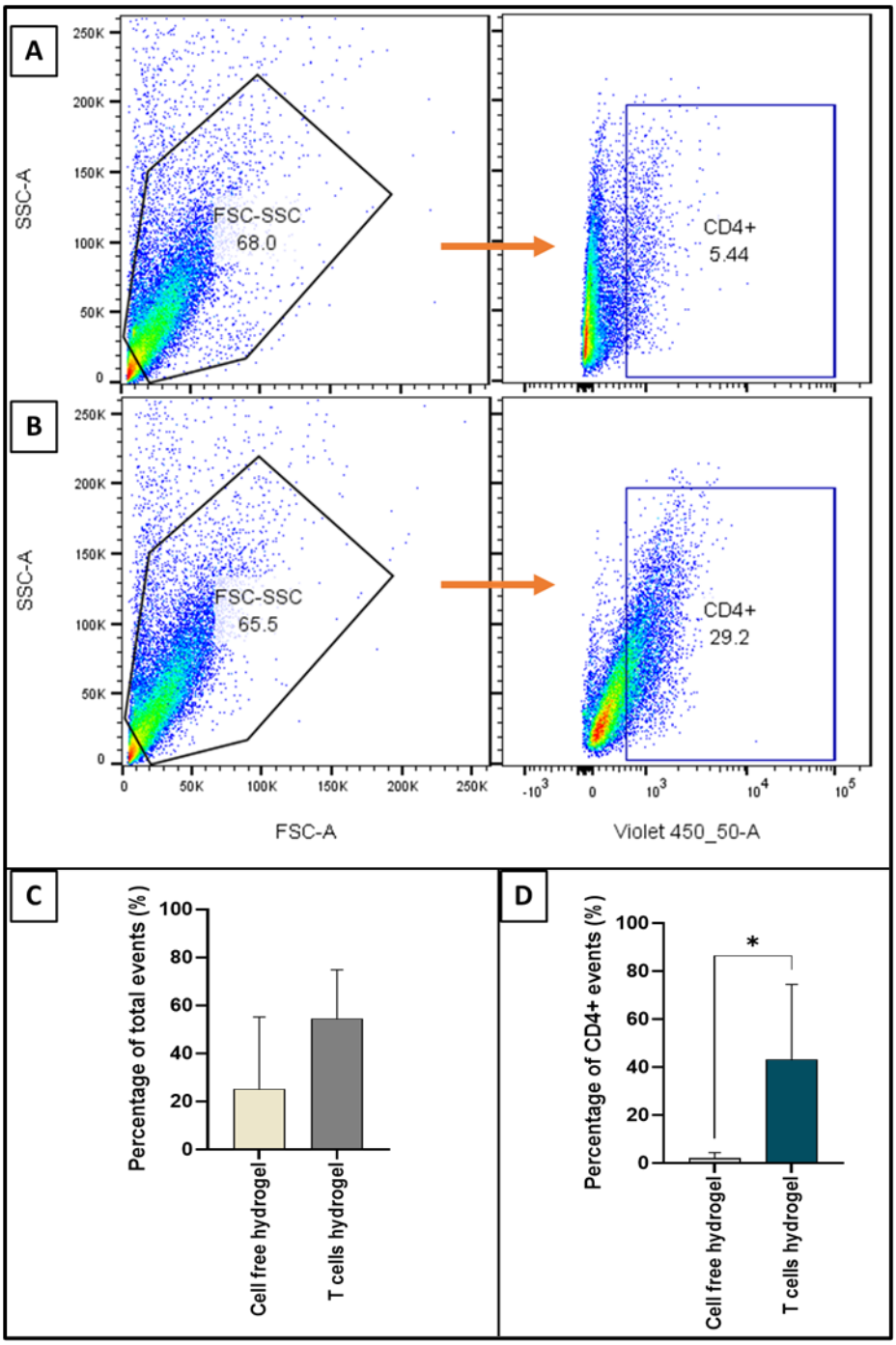

Figure 5.4: Flow cytometry analysis of cells following extraction from collagen hydrogels and detection of CD4+ population. (A) Cell-free hydrogel and (B) T cell hydrogel constructed with 1x10^6 T cells were treated with collagenase I for 1 hour at 37°C before staining with anti-CD4 surface marker and analysed by flow cytometry. Data are expressed as representative dot plots of the total events and the CD4+ stained population (right panel) and the mean ± SD of (C) the total events and (D) CD4+ population. A mean difference was considered significant when *p < 0.05 using unpaired T tests to detect difference between two groups, n=4.

Next, the viability of T cells in the collagen hydrogels at different time points was evaluated. T cells were isolated, activated, incorporated in the hydrogels and then extracted on day 1, 7 and 14 of culture before being stained with fixable blue viability dye and analysed by flow cytometry (**Figure 5.5**).

The viability of T cells following isolation from buffy coat and subsequently cultured in suspension were determined previously as 92.3 ± 7.6% viability (Chapter 4; section 4.4.1.2). Following 24 hours of 3D culture, the viability of the extracted T cells reduced to 57.4 ± 12.3%, but the percentage of viable cells gradually increased to 64.5 ± 5.9% and 89.5 ± 4.8% on days 7 and 14 of 3D culture, respectively. T cell viability was significantly higher when T cell-containing hydrogels were cultured for 14 days compared to cells extracted on day 1 ($p= 0.008$) and day 7 ($p= 0.0247$) (Figure 5.5B). From these data, it could be postulated that the reduced viability of T cells initially observed was the result of shock following changing the environment from 2D to 3D. However, T cells started to adapt by day 7 where increased viability was observed, likely due to proliferating cells.

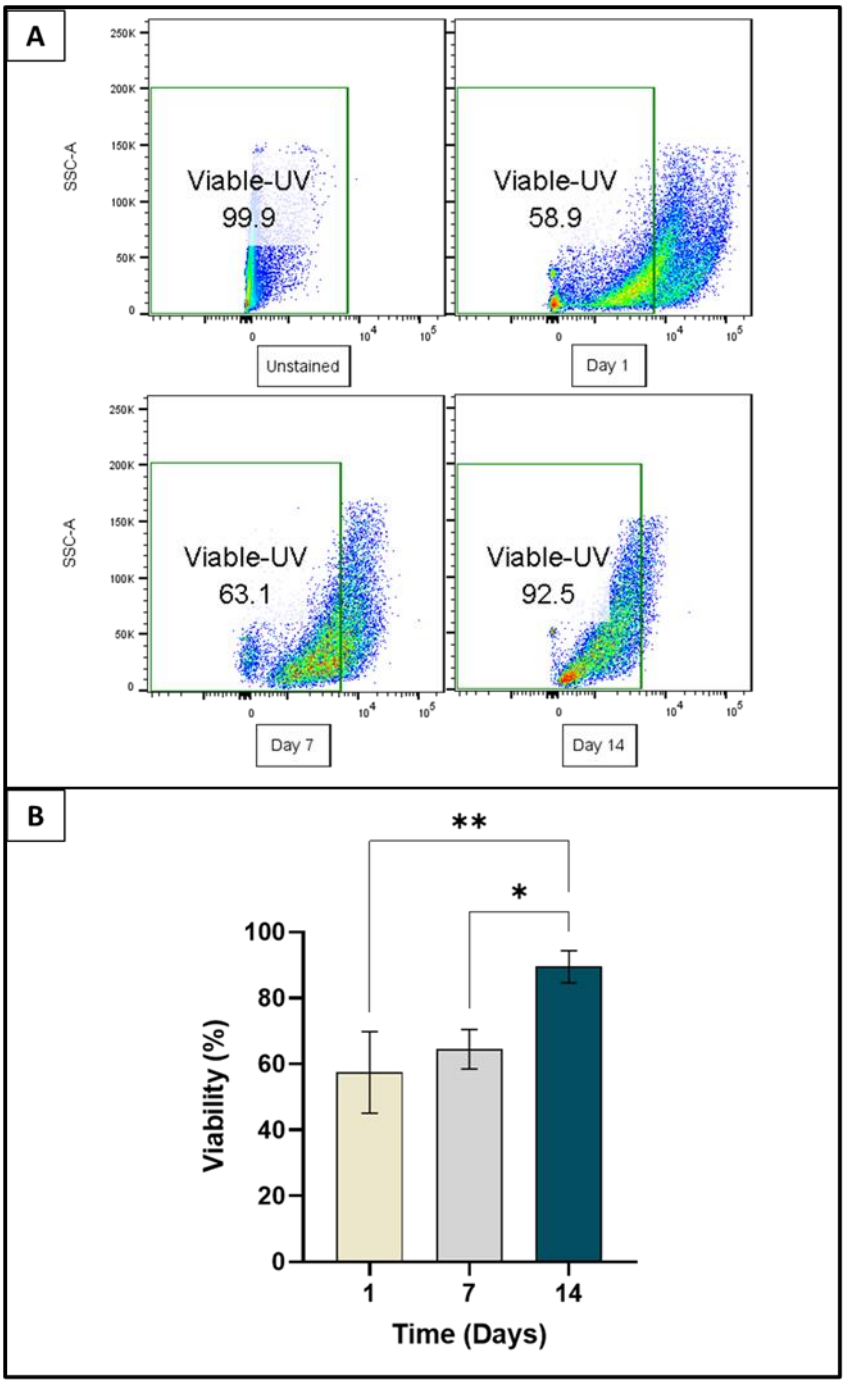

Figure 5.5: Viability of CD4 + T cells following extraction from hydrogel. T cells were incorporated into a collagen hydrogel then extracted with collagenase I on days 1, 7 and 14, stained with fixable blue viability dye and analysed using flow cytometry. Viability was seen to reduce on day 1 then increased gradually over time to reach a maximum at day 14. Data are expressed as (A) representative dot plots and (B) the mean ± SD. A mean difference was considered significant when *p < 0.05 and **p <0.001 using one-way ANOVA with Tukey's post-hoc multiple comparison tests to detect difference between groups; n=3.

Finally, to assess metabolic activity of T cells within a hydrogel without the need to extract them from the 3D culture, a PrestoBlue® assay was used that can also indirectly infer the viability of cells in a population by measuring their metabolic activity. To further explore if there was a difference in the viability of T cells related to the time of polarisation,

three different conditions were assessed. These comprised; naïve T cells, activated T cells that were previously polarised to Th1 in 2D for 5 days or activated T cells that were polarised to Th1 in 3D following incorporation into a hydrogel. The three conditions were termed naïve, Th1-2D, or Th1-3D, respectively with viability assessed on days 1, 3, 5, 7 and 10 of culture (**Figure 5.6**).

Naïve, Th1 and Th1-polarised had a similar metabolic activity from day 1 to day 5. There was a general trend for the Th1-3D and Th1-2D metabolism to increase gradually after day 5 to reach a maximum at day 10. At day 10, both the Th1-3D and Th1-2D showed a similar significant increase when compared to the metabolism for naïve cells (**Figure 5.6**) The increased metabolic activity for Th1-3D and Th1-2D at day 10 was also significant when compared to day 7 (Th1-3D; $p= 0.0053$, and Th1-2D; $p= 0.0040$), and all previous time points ($p<0.0001$) (**Figure 5.6**). In spite of a slight increase for naïve cells at day 5, there was no significant increase in their metabolic rate as they continued to show low metabolic activity by day 10. These data support the results observed in the previous assays, that T cells incorporated into collagen hydrogels recover after day 5 and continue to proliferate. Accordingly, it was postulated that optimal conditions for the T cell would be to culture the cells for 5-7 days in 3D before incorporation into a full thickness disease model. These data also suggest that T cells, whether polarised in 2D for 5 days or polarised following incorporation in hydrogel, have comparable metabolic activity, and hence, this allows for flexibility in the experimental set up (**Figure 5.6**).

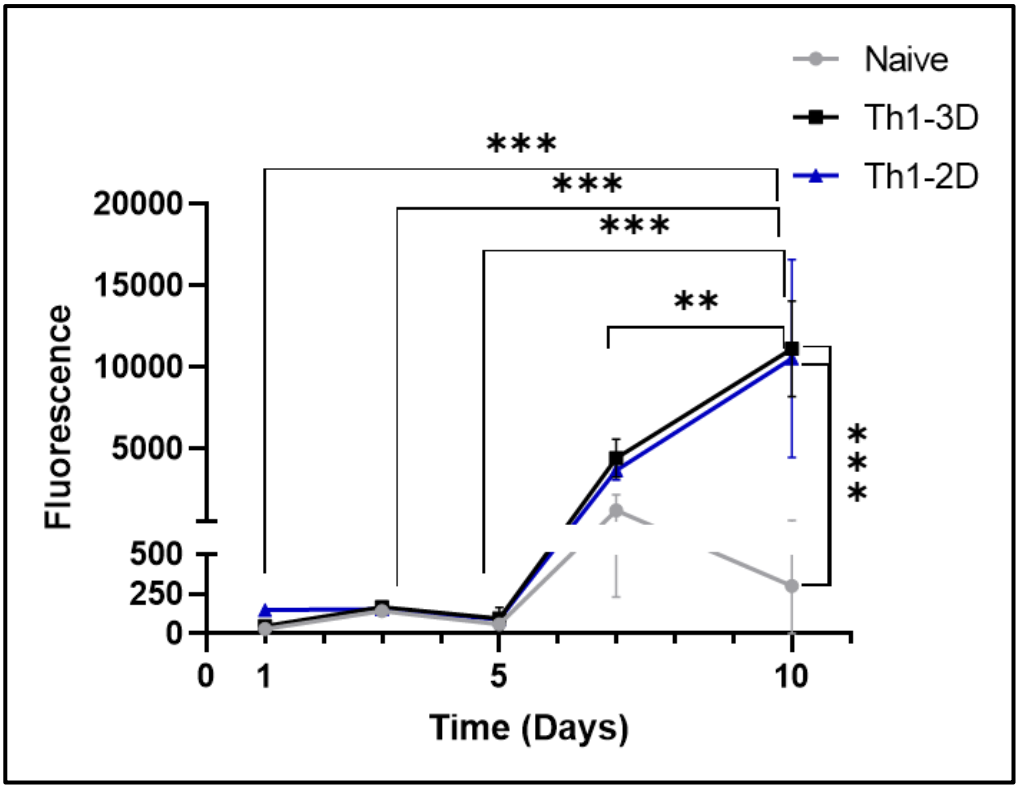

Figure 5.6: T cell metabolic activity in collagen hydrogels overtime. The metabolic rate of naïve, Th1 and Th1-polarised cells seeded in collagen hydrogels were assessed overtime using a PrestoBlue® assay and fluorescence measured. Metabolic activity was low but increased gradually at days 7 and 10. Data are expressed as mean ± SD. A mean difference was considered significant when *p < 0.05, **p <0.001, and ***p<0.0001 using two-way ANOVA with Tukey's post-hoc multiple comparison tests to detect difference between and among groups. Main ANOVA reported ***p <0.0001 effect of time, activation status, and interaction. n=3.

Following a step-by-step strategy towards building a complex disease model, next a co-culture of NOF and T cells within the collagen hydrogels was examined, prior to inclusion in a more complex model system. H&E staining revealed a dense collagen matrix that was stained strongly by eosin, with evenly dispersed cells identified by haematoxylin staining throughout the examined area. The Dynabeads, used to activate the T cells, appeared as small smooth rounded brown spheres within the hydrogel ((**Figure 5.7B;** blue arrow). Nearby, small, rounded nucleated cells representative of T cells were present (**Figure 5.7B;** yellow arrow). Finally, fibroblasts were also evident and distinct from T cells with a spindle shaped cell morphology, larger in size with larger nuclei (**Figure 5.7B black arrow**).

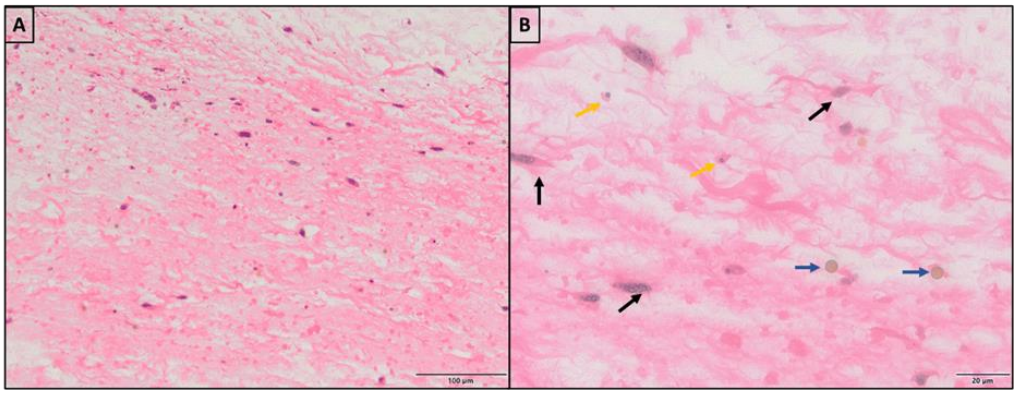

Figure 5.7: Histological analysis of co-culture of NOF and T cells in collagen hydrogels. NOF and T cells were incorporated into hydrogels and fixed at day 10 of culture and histologically analysed following H&E staining. NOF (black arrow), T cells (yellow arrow), and Dynabeads (blue arrow) were detected and distributed evenly within the hydrogel. Data are presented as representative images. Scale bar (A) = 100 µm and (B) = 20µm.

5.4.3 Assessment of the cytokine secretion profile of stimulated OME

Oral keratinocytes together with fibroblasts in OLP can modulate the immune response through activation and production of chemokines and cytokines that drive chemotaxis and the recruitment of inflammatory cells to the local area. To investigate if OME activation *in vitro* can mimic the cytokine milieu reported in the OLP microenvironment, OME were constructed as reported (section 5.4.1) then either left unstimulated or stimulated with IFN-γ and TNF-α, cytokines that are released by activated DC upon antigen detection during the pathogenesis of OLP, Th1 conditioned media (CM) as this will contain cytokines produced by polarised Th1 cells mimicking the chronic OLP microenvironment, or Th1 differentiation media (DM) containing IL-12, IL-18, and anti-IL-4 as control at day 10 of ALI for 48 hours.

Histological assessment of the stimulated OME models reflected an intact epithelium with hyperproliferation of keratinocytes along with a subsequent increase in epithelial thickness (IFN-γ and TNF-α; 368.3 ± 66 µm, DM; 193 ± 75 µm, CM; 232.3 ± 73.8 µm) (**Figure 5.8B-D**) when compared to the unstimulated control model (118.3 ± 21.4 µm) (**Figure 5.8A**). However, only the epithelium stimulated with IFN-γ and TNF-α showed a significant increase in epithelial thickness ($p= 0.017$). No epithelial apoptosis or basement membrane disruption was observed.

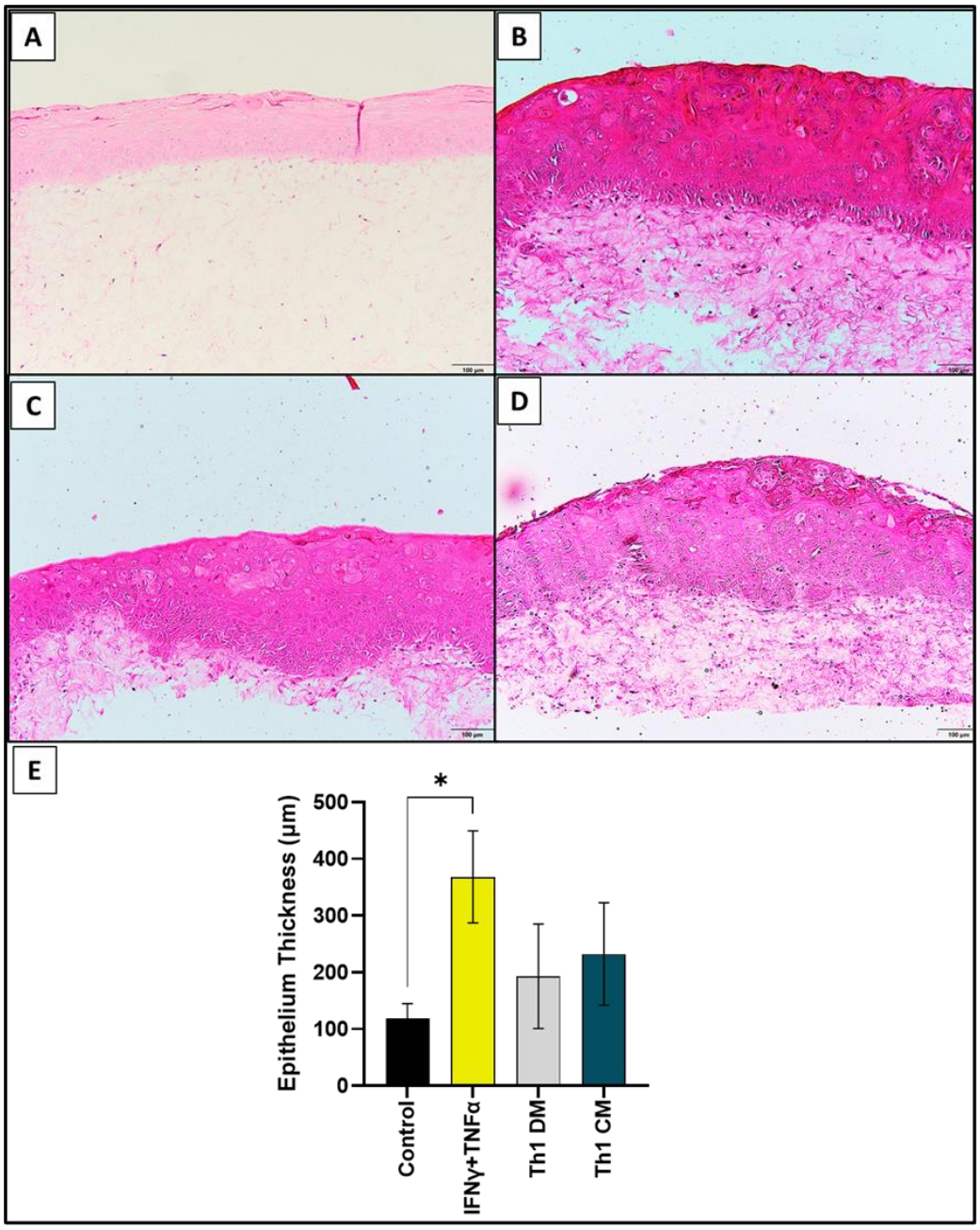

Figure 5.8: Histological analysis of normal OME following stimulation. OME were cultured for 10 days at ALI before being (A) left unstimulated, (B) stimulated with IFN-γ and TNF-α, (C) Th1 differentiation media (DM) or (D) Th1 conditioned media (CM) for 48 hours, then fixed and analysed following H&E staining. Stimulated OME showed epithelial hyperproliferation compared to unstimulated OME. Data are presented as representative images and (E) the mean ± SD. A mean difference was considered significant when *p < 0.05, using one-way ANOVA with Tukey's post-hoc multiple comparison tests to detect difference between groups; n=3. Scale bar = 100 µm.

Next, to investigate the cytokine secretion profile of stimulated OME in to the receptor media, a cytokine array that detects 80 inflammatory cytokines and chemokines was performed. Densitometry data were determined from the array using the array analyser plug-in associated with the ImageJ software. To normalise data, the background was subtracted, and the control (unstimulated media) used as a reference array to which

the other arrays were normalised. The global intensity of the spot can be visually examined and compared between samples. Generally, more positive spots and higher intensity were detected from the media collected from models stimulated with IFN-γ and TNF-α or Th1 conditioned media (**Figure 5.9B&D**) when compared to control and models stimulated with Th1 differentiation media (**Figure 5.9A&C**). The cytokine array map can be used to reference each cytokine location (**Table 5.9E**)

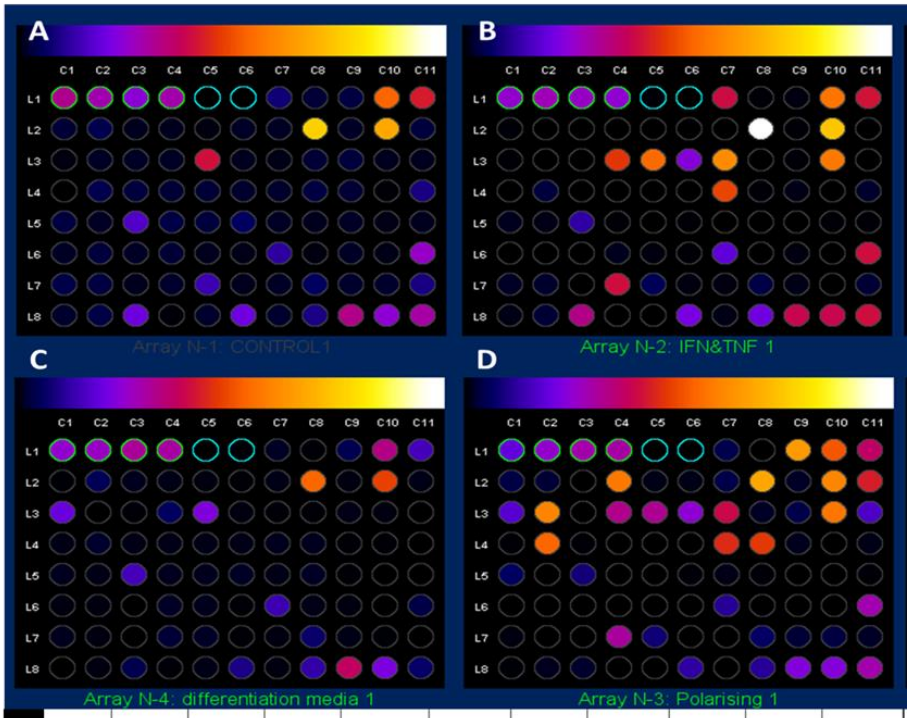

E	A	B	C	D	E	F	G	H	I	J	K
1	POS	POS	POS	POS	NEG	NEG	ENA-78 (CXCL5)	G-CSF	GM-CSF	GRO a/b/g	GRO alpha (CXCL1)
2	I-309 (CCL1)	IL-1 alpha (IL-1 F1)	IL-1 beta (IL-1 F2)	IL-2	IL-3	IL-4	IL-5	IL-6	IL-7	IL-8 (CXCL8)	IL-10
3	IL-12 p40/p70	IL-13	IL-15	IFN-gamma	MCP-1 (CCL2)	MCP-2 (CCL8)	MCP-3 (CCL7)	M-CSF	MDC (CCL22)	MIG (CXCL9)	MIP-1 beta (CCL4)
4	MIP-1 delta	RANTES (CCL5)	SCF	SDF-1 alpha	TARC (CCL17)	TGF beta 1	TNF alpha	TNF beta (TNFSF1B)	EGF	IGF-1	Angiogenin
5	OSM	TPO	VEGF-A	PDGF-BB	Leptin	BDNF	BLC (CXCL13)	Ck beta 8-1 (CCL23)	Eotaxin-1 (CCL11)	Eotaxin-2 (CCL24)	Eotaxin-3 (CCL26)
6	FGF-4	FGF-6	FGF-7 (KGF)	FGF-9	FLT-3 Ligand	Fractalkine (CX3CL1)	GCP-2 (CXCL6)	GDNF	HGF	IGFBP-1	IGFBP-2
7	IGFBP-3	IGFBP-4	IL-16	IP-10 (CXCL10)	LIF	LIGHT (TNFSF14)	MCP-4 (CCL13)	MIF	MIP-3 alpha	NAP-2 (CXCL7)	NT-3
8	NT-4	OPN (SPP1)	OPG (TNFRSF11	PARC	PLGF	TGF beta 2	TGF beta 3	TIMP-1	TIMP-2	POS	POS

Figure 5.9: Assessment of the cytokine secretion profile of stimulated OME. OME cultured for 10 days at an ALI were (A) left unstimulated, stimulated with either (B) IFN-γ and TNF-α, (C) Th1 differentiation media or (D) Th1 conditioned media for 48 hours. The secretion of 80 inflammatory cytokines was semi-quantified using a cytokine array. Data presented as representative global modelled image of the arrays normalised to the unstimulated control array; n=2.

The inflammatory cytokines, CXCL8 (IL-8) and IL-6 were detected in all four conditions tested. Although a high intensity reflected high concentrations in the IFN-γ and TNF-α stimulated OME, an overall fold increase was not observed compared to the control. Other inflammatory markers were highly secreted, in particular, GM-CSF revealed a 15-fold increase in Th1 conditioned medium and 2.5-fold in the IFN-γ and TNF-α stimulated models compared to the unstimulated OME medium. IL-1α was increased by 1.5-fold in the Th1 conditioned group only (**Figure 5.10**).

Secretion of T cell-related chemokines CXCL9 (MIG), CXCL10 (IP10) and CCL5 (RANTES) increased in the IFN-γ and TNF-α sample by 2.7-fold, 5.7-fold, and 8.9-fold, respectively, and in the Th1 conditioned medium to 2.8-fold, 4.9-fold and 13.4-fold, respectively. This is particularly important in evidencing the role of stimulated mucosa in the inflammatory process and in recruiting T cells. Monocyte chemoattractant proteins, MCP-2 (CCL7) and MCP-3 (CCL8) recorded an 8-fold and 26.3-fold increase, respectively, in the IFN-γ and TNF-α stimulated medium and 5-fold, 11.3-fold increase, respectively, in the Th1 conditioned medium. CCL1 (I-309), a monocyte chemoattractant that is released from activated T-cells showed a 3.9-fold increase in the Th1 conditioned medium compared to unstimulated OME medium. Macrophage inflammatory proteins, MIP-1β (CCL4), MIP-1δ (CCL15), and MIP-3α (CCL20), showed 8.4, 16.8, and 1.6-fold increase, respectively, in Th1 conditioned media but only the MIP-1δ that was increased, 5.5-fold, in the media related to the IFN-γ and TNF-α stimulation (**Figure 5.10**).

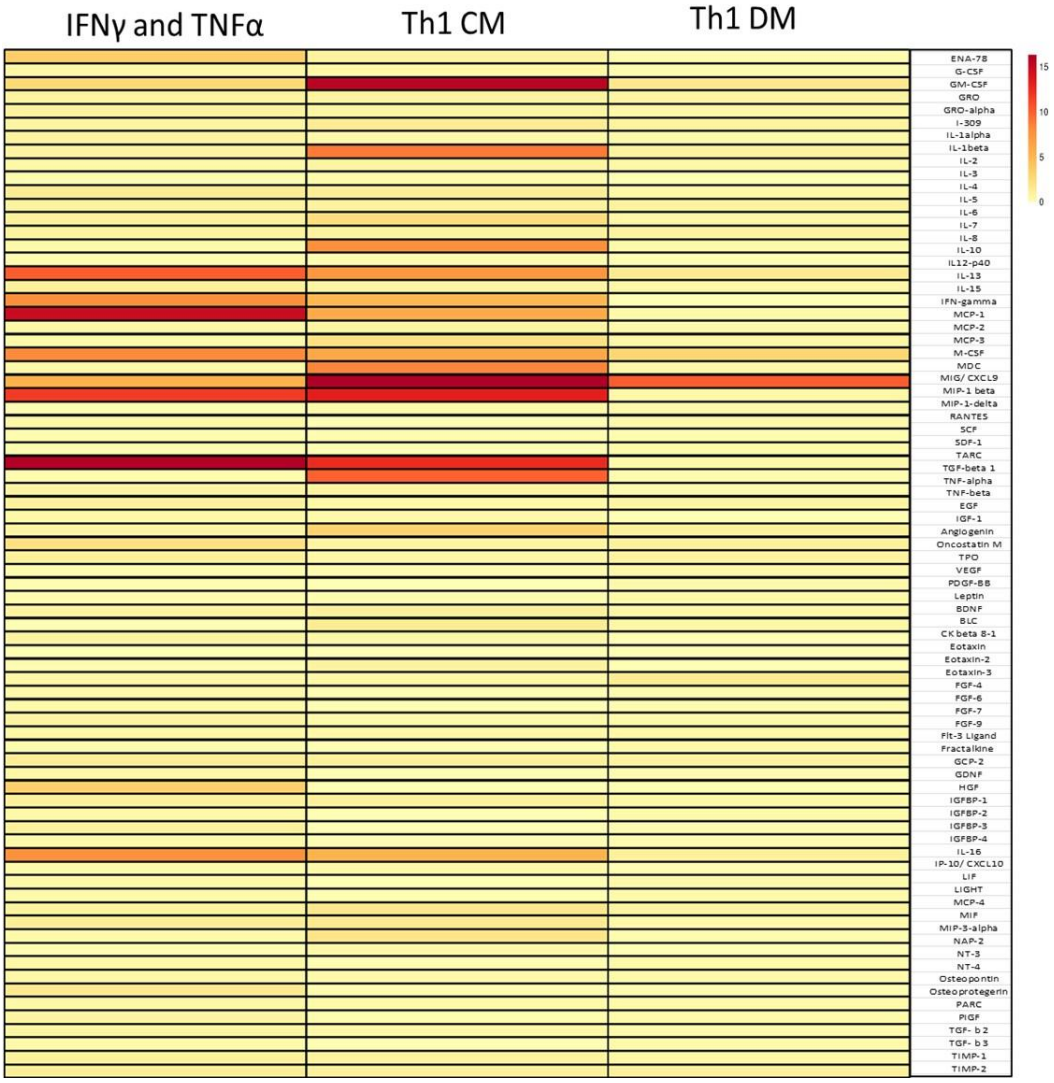

Figure 5.10: Assessment of cytokine secretion profile of stimulated OME. OME cultured for 10 days at ALI were left unstimulated, stimulated with IFN-γ and TNF-α, Th1 differentiation media (Th1 DM) or Th1 conditioned media (Th1 CM) for 48 hours. The secretion of 80 inflammatory cytokines were semi-quantified using a cytokine array. Data presented as a heat map; n=2.

As the cytokine array analysis is only semi-quantitative, ELISA was additionally performed to quantify the levels of secreted molecules of interest CXCL9, CXCL10 and CCL5. A similar pattern of increased secretion was observed for all three chemokines in both the IFN-γ and TNF-α stimulated medium and the Th1 conditioned medium when compared to the control and Th1 differentiation media. CXCL9 was highly secreted in the IFN-γ and TNF-α (2.7 ± 0.2 ng/ml) and in the Th1-CM (2.6 ± 0.5 ng/ml), both were significantly increased compared to the control (0.1 ± 0.09 ng/ml; $p<0.0001$) and Th1-DM (0.2 ± 0.2 ng/ml; $p<0.0001$) samples (**Figure 5.11A**). Similarly, CXCL10 reported the same pattern with high levels detected in the IFN-γ & TNF-α (1.7 ± 0.5 ng/ml) and Th1-CM (1.7 ± 0.4 ng/ml) samples and were significantly different from the control (0.06 ± 0.05

ng/ml; p = 0.0001) and Th1-DM (0.2 ± 0.2 ng/ml; p= 0.0003 for IFN-γ & TNF-α or p =0.0002 for Th1-CM) (**Figure 5.11B**).

Although no significant difference in CCL5 levels were found between samples, there was an increase in the levels after stimulation with IFN-γ and TNF-α (0.3 ± 0.2 ng/ml) and Th1-CM (0.3 ± 0.1 ng/ml) when compared to the control (0.05 ± 0.02 ng/ml) and Th1-DM (0.07 ± 0.02 ng/ml) (**Figure 5.11C**), but no significant difference was reached due to the variation observed between experimental repeats.

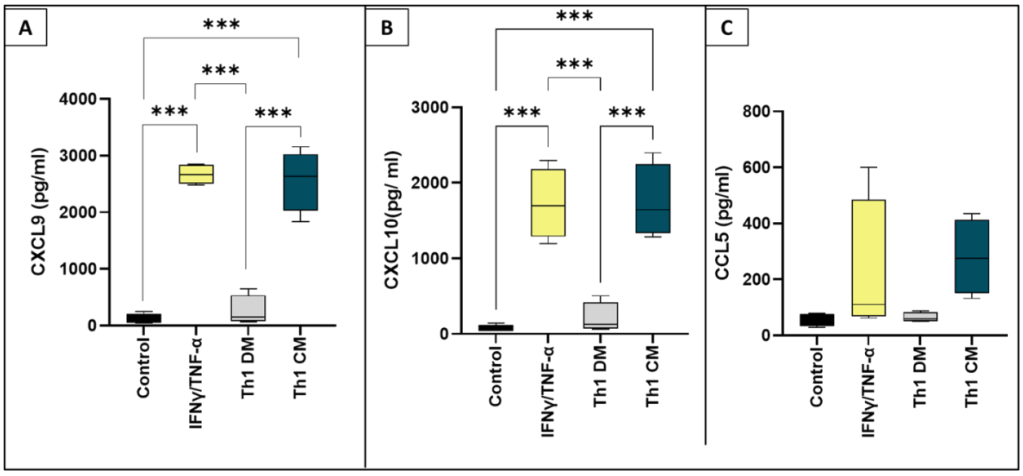

Figure 5.11: Quantification of chemokine secretion by stimulated OME. OME cultured for 10 days at an ALI were left unstimulated (negative control), stimulated with IFN-γ and TNF-α, Th1 differentiation media (DM) or Th1 conditioned media (CM) for 48 hours. Secretion of T cell chemokines (A) CXCL9, (B) CXCL10 and (C) CCL5 were quantified by ELISA. Data presented as the mean ± SD of three independent experiments. A mean difference was considered significant with ***p <0.0001 using one-way ANOVA tests with Tukey's post-hoc multiple comparison tests to detect difference between groups; n=3.

These data confirms that stimulation with IFN-γ and TNF-α caused a hyper-proliferation response and did not cause apoptosis of the epithelium. Moreover, OME are able to secret inflammatory cytokines and T cells related chemokines. It may suggest that T cells introduced to the bottom of the OME may migrate towards the chemokine gradient produced by the stimulated epithelium. To explore this theory further, a T-cells chemotaxis assay was performed.

5.4.4 T cell chemotaxis

To detect if T cells could migrate towards a chemoattractant gradient created by the stimulated OME, a chemotaxis assay was performed using µ-slide chambers and cells tracked over time using live cell time-lapse imaging and computational tracking of their movement.

After tracking, the path of cells was visualised in a trajectory plot. Cell coordinates at x and y plot were extrapolated to (x, y) = 0 at time 0 hour allowing the general path of cell migration to be displayed. Representative plots of three independent experiments revealed that while CD4+ T cells in the negative control conditions (serum free media) on both sides of the well, migrated in different directions (**Figure 5.12A**), CD4+ T-cells moved in a uni-directional fashion up along a chemotaxis gradient created by the chemokine CCL5 (**Figure 5.12B**) or the gradient generated by conditioned media from OME stimulated with INF-γ and TNF-α (**Figure 5.12C**).

In order to statistically analyse the chemotaxis data, a centre of mass displacement (CoM) was plotted. This provides information on the average of all the cell endpoints, where x and y values indicate the direction in which a group of cells travelled. The CoM displacement for the non-stimulated cells was found to be 6.05 ± 2.1 µm, while chemotaxis gradient achieved by conditioned medium from stimulated OME increased the CoM displacement to 13.7 ± 3.3 µm, a concentration gradient of 200 ng/ml of CCL5 (acting as a positive control) caused the highest shift in cells towards the chemotaxis gradient that was significantly higher than the negative control (22.6 ± 7.9 µm; p= 0.017) (**Figure 5.12D and 5.13A**).

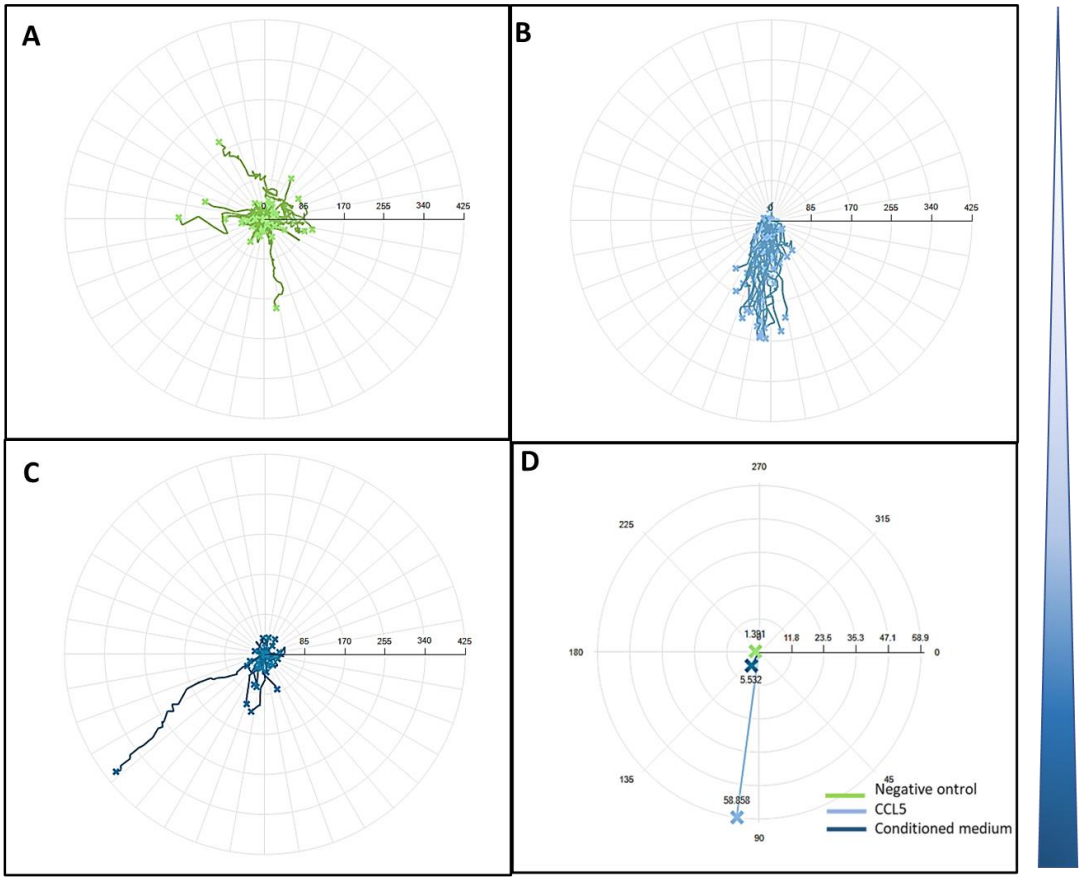

Figure 5.12: T cell chemotaxis analysis. T cell migration was tracked over 24 hours using µ-slide chambers. Cells were either exposed to (A) serum-free medium (negative control), (B) a CCL5 gradient or (C) a conditioned medium gradient generated from stimulated OME. (D) The general path of migration was calculated using the Centre of Mass (CoM) displacement. Data presented as representative trajectory plots; n=3.

Further quantitative analysis of the trajectory plots was performed to determine four migration parameters: accumulated distance, Euclidean distance, velocity and the directness of migrating cells. Accumulated distance is the total distance covered by a cell whether it migrated in circles or a straight line whereas the Euclidean distance is a measure of a straight line between the cell start and end points. Hence, if a cell ends where it starts, regardless of total distance travelled, its Euclidean distance will be zero. Our data reveal that while the total distance travelled by T cells towards the conditioned medium (41.3 ± 33.9 mm) was greater than two-fold compared to cells in the CCL5 group (15.2 ± 5.2 mm), and approximately four-fold the distance travelled by cells in the negative control group (10.3 ± 3.2 mm), despite these differences no statistically significant differences were found (**Figure 5.13B**). Similarly, the Euclidean distance travelled by cells towards the conditioned medium (10.9 ± 8.7 mm) was twice that of cells which migrated towards CCL5 (5.2 ± 1 mm) and six times greater than the negative control (1.7 ± 0.9 mm), again these differences did not reach a statistical significance (**Figure 5.13C**).

The directness is a measure of the straightness of the cell track trajectory. It is calculated by comparing the Euclidean distance and the accumulated distance. A directness of 1.0 equals a straight-line migration. The T cells in the CCL5 and conditioned medium groups reflected comparable directional movement (0.4 ± 0.05 µm and 0.4 ± 0.07 µm, respectively) towards a chemotaxis gradient that was significantly more directional (p= 0.0191 and 0.0219, respectively) when compared to the negative control group (0.2 ± 0 µm) (**Figure 5.13D)**. Moreover, the velocity of migrating cells, an indicator of the chemotactic effect, was comparable in both CCL5 and conditioned media (0.1 ± 0.02 µm/min and 0.1 ± 0.017 µm/min, respectively). Both of these groups had a significantly higher velocity (p= 0.0138 and 0.0172, respectively) when compared to the negative control group (0.04 ±0.02 µm/min) (**Figure 5.13E**).

These data confirm that T cells migrate towards a concentration gradient of conditioned medium from stimulated OME. Subsequently, this led to the hypothesis that OME containing T cells stimulated with IFN-γ and TNF-α, Th1 and cytotoxic T-cells will be attracted towards the epithelium.

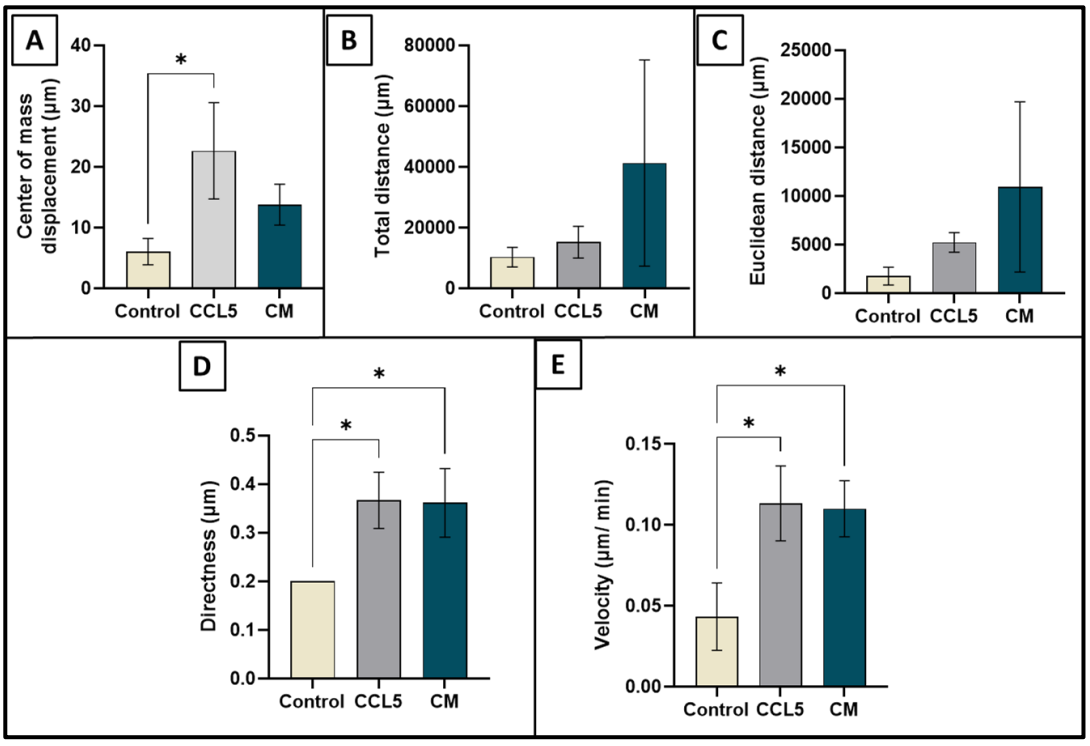

Figure 5.13: Parameters exploring the chemotaxis. T cell migration was tracked over 24 hours using µ-slide chambers. Cells were either exposed to serum free medium gradient (negative control), a CCL5 gradient or a conditioned medium (CM) gradient generated from stimulated OME. (A) The Centre of Mass displacement, (B) total distance travelled, (C) Euclidean distance travelled, (D) the directness, (E) and the velocity of migrated cells was calculated using the FastTrack automated AI software. Data presented as the mean ± SD of three independent experiments. A mean difference was considered significant when *p <0.05 using one-way ANOVA tests with Tukey's post-hoc multiple comparison tests to detect difference between groups; n=3.

5.4.5 Developing and characterising a full thickness tissue engineered T cell inflammatory disease model

A number of different methods were investigated to establish the best way to incorporate T cells into OME. The first method, termed the 'all-in-one method' involved adding previously primed T cells at the point when the OME was established. Here, Th1 and CD8+ T cells were incorporated with the NOF into the collagen hydrogel before seeding FNB6 on top. A OME without T cells cultured for 7 days in Green's medium without hydrocortisone but supplemented with Th1 differentiation cytokines, macroscopically looked consistent with previous reports showing minimal hydrogel contraction and a white shiny surface indicative of an epithelial layer (**Figure 5.14A**). This was confirmed with H&E staining which revealed a stratified squamous epithelium on top of fibroblast populated connective tissue replicating normal oral mucosa (**Figure 5.14B**). Whereas an OME model created with the addition of Th1 and cytotoxic T cells within the collagen hydrogel showed extreme contraction by day 7 of culture at an ALI along with marked discoloration (**Figure 5.14C**). H&E staining revealed a complete disintegration of the epithelium and connective tissue layer (**Figure 5.14D**). These data show that adding T cells before allowing the OME layer to establish caused early tissue destruction and necrosis that made further analysis unachievable.

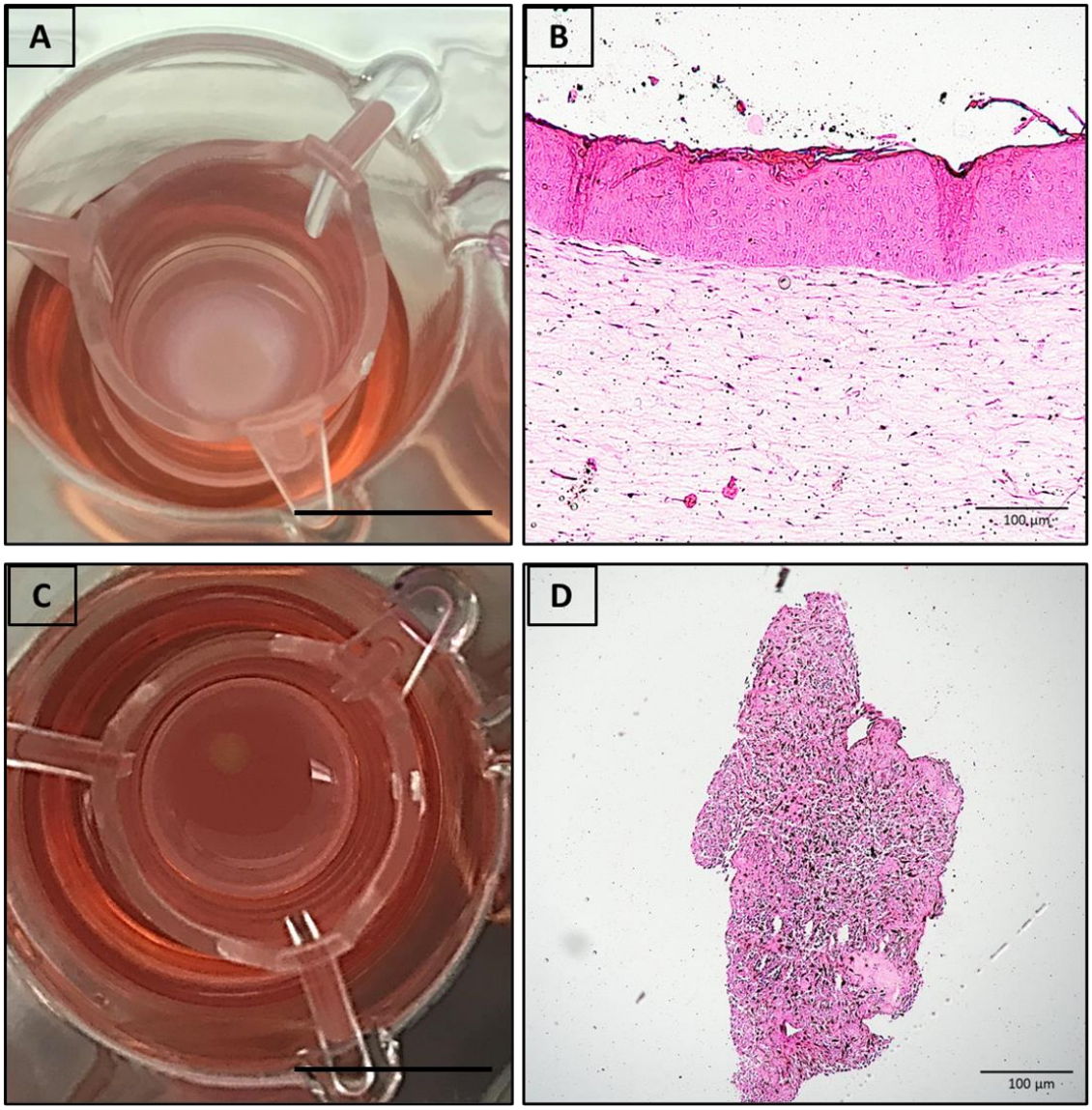

Figure 5.14: Assessment of the 'all-in-one' technique to create tissue engineered full thickness T cell disease models. (A) An image of a normal OME model in culture after 10 days at an ALI before stimulation with IFN-γ and TNF-α. (B) Histological analysis with H&E staining revealed a stratified squamous epithelium on top of fibroblast-populated connective tissue. (C) NOF, CD4+ and CD8+ T cells were incorporated together into a collagen hydrogel at day 0 and FNB6 were seeded on top then raised to ALI two days later and cultured for 10 days before stimulation with IFN-γ and TNF-α. (C) A image of the model in culture and (D) H&E staining revealed disintegration and contraction of 'all-in-one' models compared to (A&B) normal OME. Images are representatives; n=3. Scale bar B & D =100 µm, A & C= 10 mm.

As this approach was not conducive to enable incorporation of T cells into the tissue engineered full thickness OME, a new method was tested and termed the 'layering technique'. This method consisted of creating a developed OME that was cultured in complete Green's medium until day 7 of culture at ALI and, separately, a T cell containing hydrogel that was cultured in Th1 differentiation medium for 7 days to enable them to adapt to 3D environment as previously shown (**Figure 5.5 and 5.6**). After this time, the OME was transferred on to the top of the T cell-containing hydrogel and the two layers

adhered together using 100 µl of collagen. The layers were cultured for 2-3 days in Green's medium without hydrocortisone and with Th1 differentiation cytokines before further challenging with IFN-γ and TNF-α which was performed only on day 10. The layered models were analysed on days 10, 12, 16, 20 and 25.

Overall analysis of the disease model from day 10 and day 12 reaching to days 16, 20 and 25 revealed that tissue destruction gradually progressing untill reached complete tissue destruction and collapse on day 25 (**Figure 5.15 A**). This was not observed with normal OME which has started to show signs of destruction only at day 25 of ALI (**Figure 5.15 B**). No restimulation with IFN-γ and TNF-α was needed to produce this continous damage. The main features of OLP disease consisted of basal cell apoptosis, basement membrane damage, and T cell recruitment towards the epithelium were established at days 10 and 12 while the integrity of the model tissue was maintained to allow for further analysis. Although the slow and gradual progression of the destruction over days 16, 20, and 25 indicate the reproduction of an inflammatory cycle and feed back loops, the model tissue was friable and difficult to handle. These data suggest that days 10 and 12 are the best time points to represent the disease and applicable for further analysis.

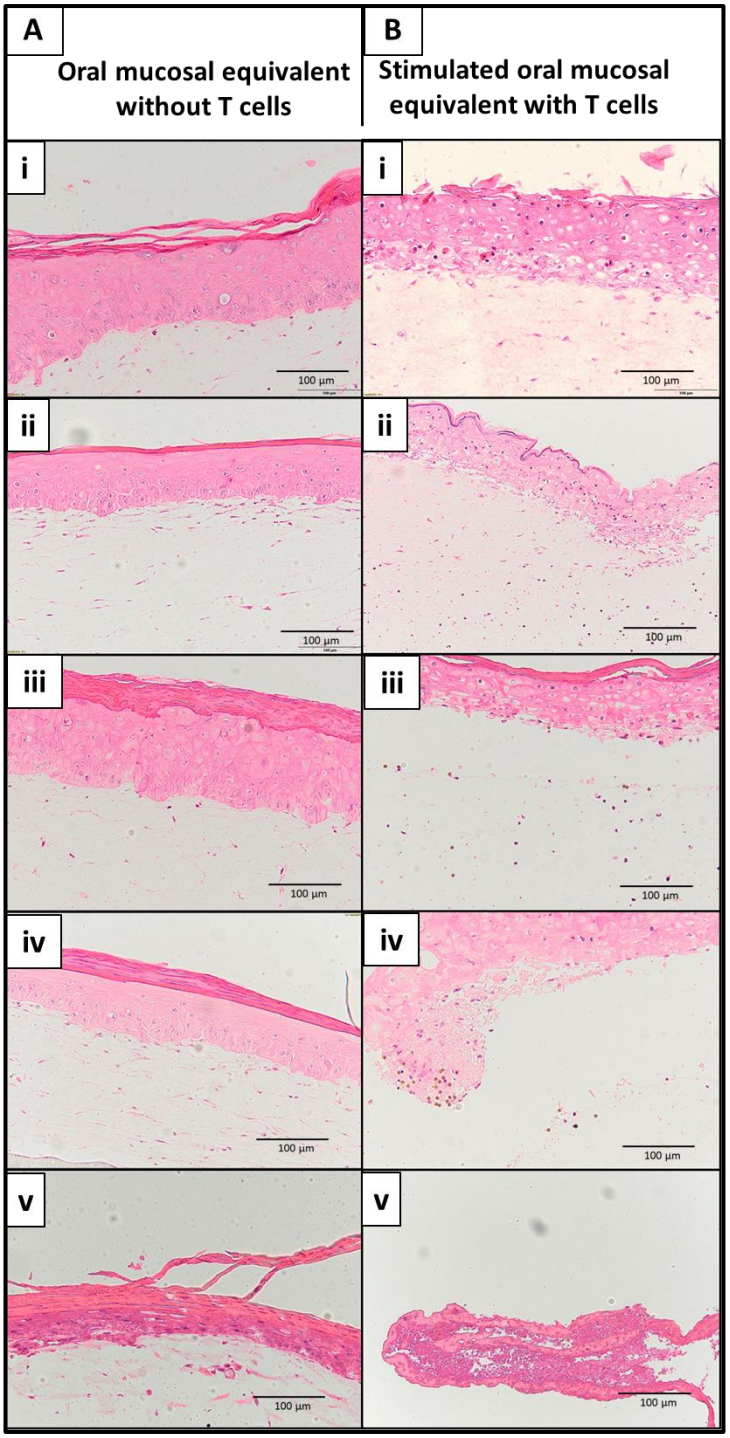

Figure 5.15: Progressive tissue destruction in a T cell inflammatory disease model. OME at day-7 of ALI was transferred on top of a T cell containing hydrogel then stimulated at day-10 of ALI with IFN-γ and TNF-α. Histological analysis with H&E revealed (A) normal OME with normal tissue architecture at (i) day 10 and (ii) day 12, but with an increased para-keratinised layer at (iii) day 16, (iv) day 20, and initial degeneration started at (v) day 25, while (B) the T cell disease model showed signs of basement membrane degeneration and basal cell apoptosis at (i) day-10. The tissue degeneration progressed slowly from (ii) day-12 to (iii) day-16, (iv) day-20, reaching complete tissue collapse (v) at day 25. Images are representative; n=3. Scale bar = 100 µm.

H&E staining at day-10 revealed a full thickness layered oral mucosa consisting of an epithelium, an underlying connective tissue layer and a lower layer containing T

cells (**Figure 5.16A**). Cellular degeneration of basal cells was observed reflecting basal cells apoptosis. Moreover, the basement membrane was no longer identifiable and appeared degenerated (**Figure 5.16B**). This indicates that soluble factors produced by T cells were able to induce inflammatory changes even before stimulation with IFN-γ and TNF-α. Higher magnification of the lower T cell-containing layer revealed the presence of T cells, evident as small, rounded nucleated cells, accompanied by small smooth spherical brown beads that were used to activate the T cells (**Figure 5.16C**).

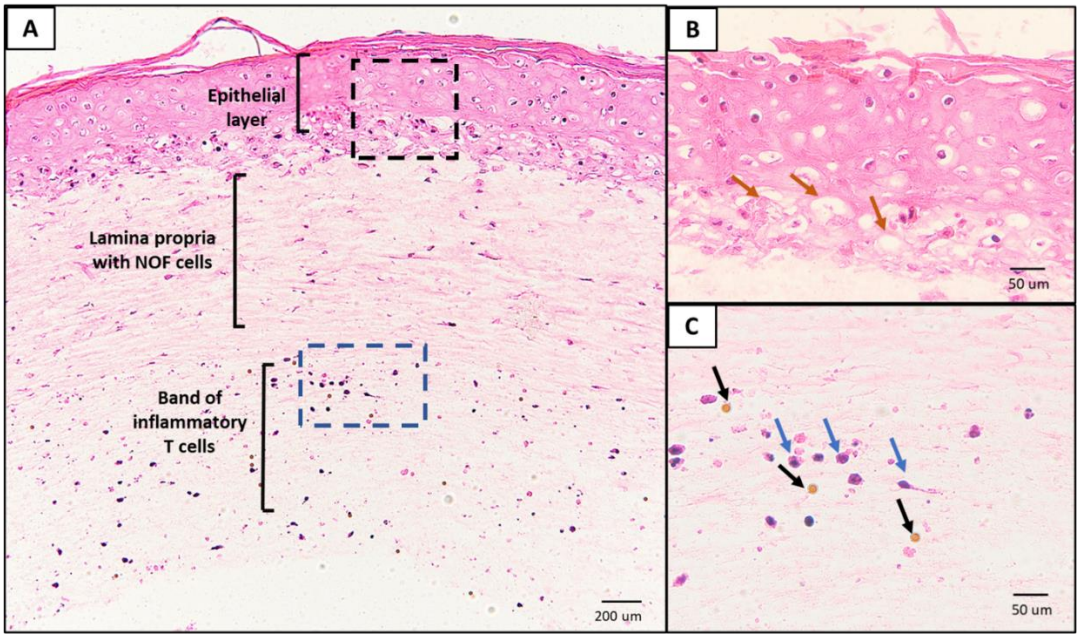

Figure 5.16: Histological characterisation of a full thickness tissue engineered model of T cell mediated inflammatory disease model. OME at day-7 of culture at an ALI was transferred on top of a T cell containing collagen hydrogel and stimulated on day 10 with IFN-γ and TNF-α. Histological analysis with H&E revealed (A) OME composed of stratified squamous epithelium and underlying connective tissue on top of a dense band of inflammatory T cells in the subepithelial compartment. (B) Magnified image of area depicted in A (black hatched box) showing basal cells apoptosis (orange arrows) and basement membrane destruction while (blue hatched area) (D) showing T cells (blue arrows) and CD3/CD28 conjugated beads (black arrow). Images are representative; n=3. Scale bar in A= 200 µm, B & C= 50 µm.

Histological assessment at day-12, 48 hours following stimulation with IFN-γ and TNF-α, revealed further destruction of the epithelium and basement membrane and areas of epithelial separation (**Figure 5.17A**). T cell recruitment towards the epithelium, particularly near the advanced areas of destruction were evident (**Figure 5.17A&B**). This was confirmed through IHC staining for CD4, a cell surface marker that confirmed the presence of CD4+ T cells near and within the epithelium (**Figure 5.17C**).

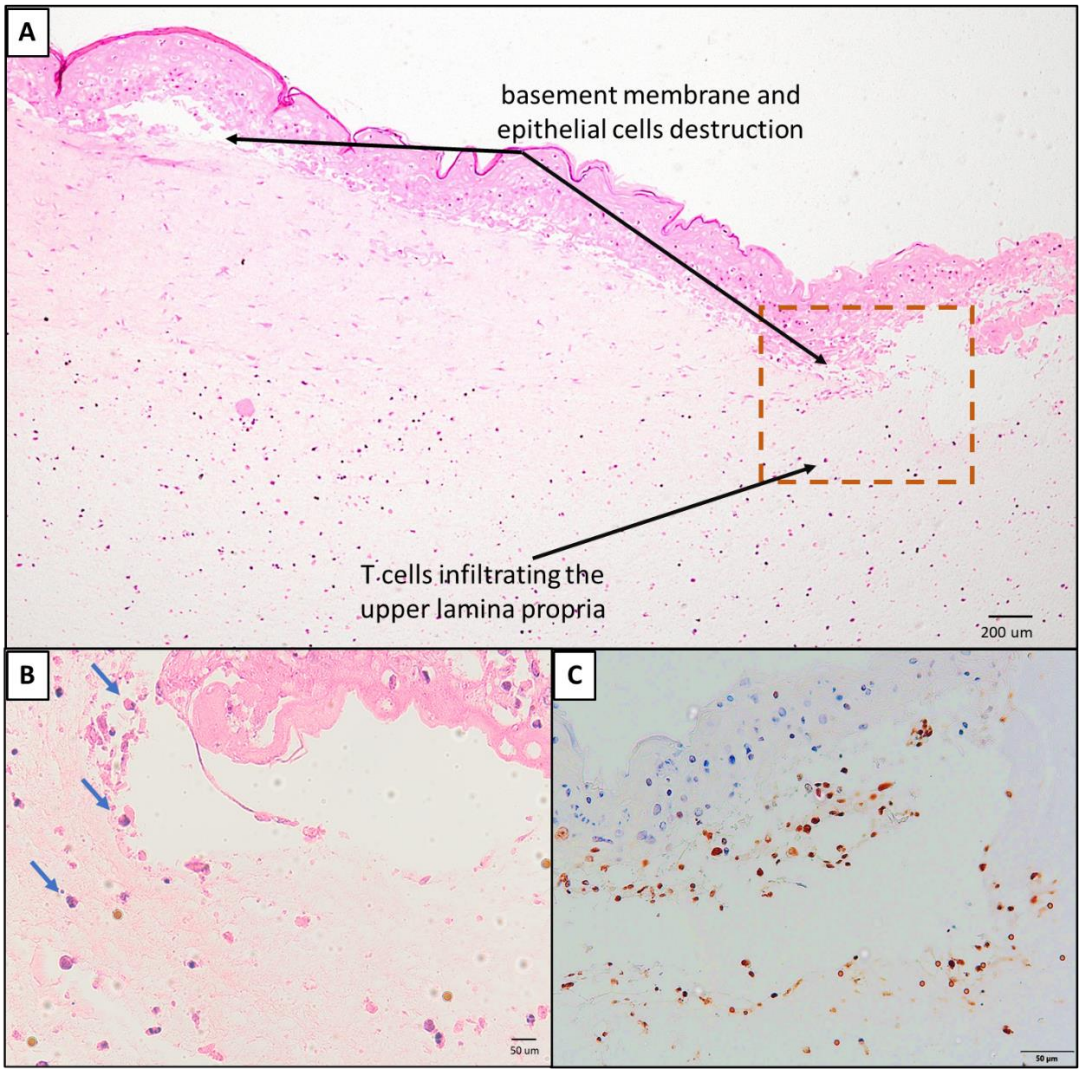

Figure 5.17: Histological characterisation of a full thickness tissue engineered model of T cell mediated inflammatory disease model. OME at day-7 of culture at ALI transferred on top of a T cell containing hydrogel and stimulated on day-10 with IFN-γ and TNF-α. Histological analysis with H&E on day-12 revealed (A) epithelial destruction and evidence of T cells infiltrating towards the epithelium. (B) Magnified image of destructed area depicted in A (orange hatched area) showed the presence of T cells (blue arrows) near to the epithelium and destructed basement membrane. (C) IHC positive staining (brown) for CD4+T cells within the epithelium. Images are representative; n=3. Scale bar in A= 100 µm, B&C = 50 µm.

5.4.6 Validating the full thickness tissue engineered T cell inflammatory disease model

5.4.6.1 General histological characterisation

To validate the structure of the models, histological sections of normal OME were compared to native oral mucosa and the T cell inflammatory disease model compared to tissue taken from patients with OLP. H&E staining revealed that native oral mucosa and normal OME were similarly structured, composed of an intact stratified epithelial layer on top of a fibroblast populated connective tissue (**Figure 5.18 A&B**). While the OLP and T-

cell disease model consisted of the same layers, epithelium and connective tissue, they shared characteristics of inflammatory disease represented by T cells infiltrating the sub-epithelium and basal cell damage (**Figure 5.18 C& D**). The patient tissue sample relates to a reticular OLP (**Figure 5.18C**). The T cells disease model presented here reflects an active stage of inflammation with damage to the local tissue (**Figure 5.18D**).

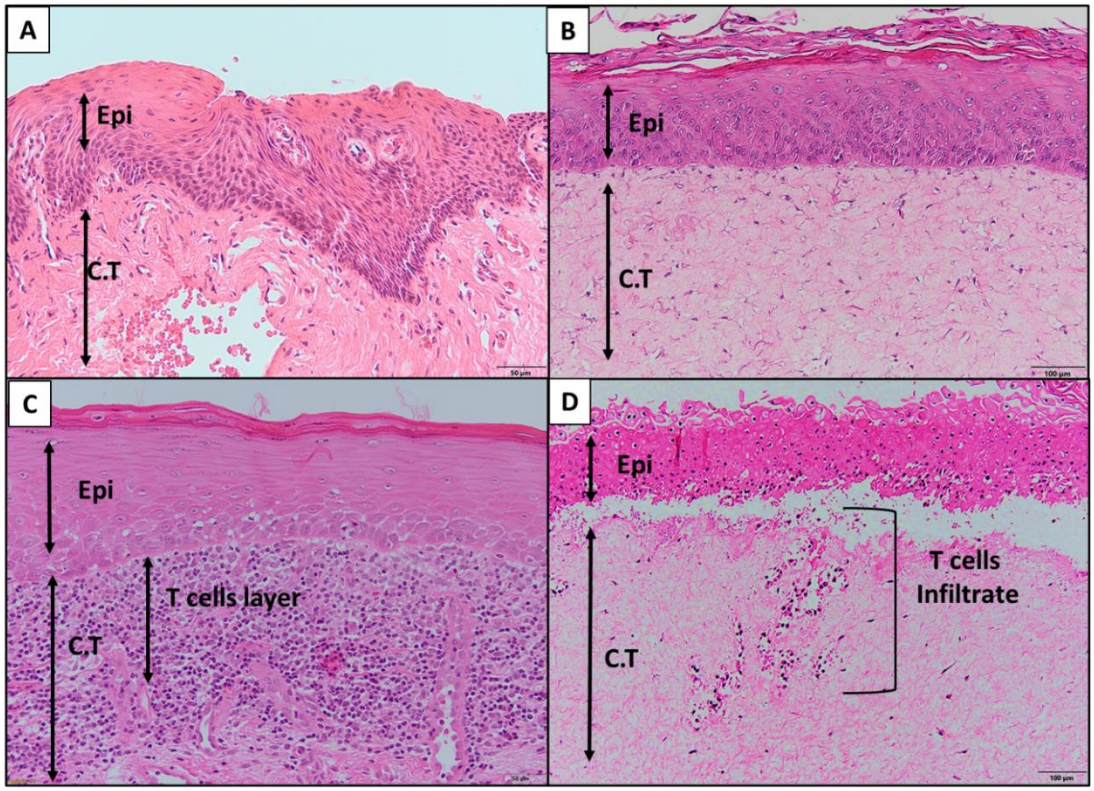

Figure 5.18: Histological validation of the structure of T cell inflammatory disease model in comparison to native oral mucosa, normal OME and OLP biopsy. H&E staining revealed both (A) native oral mucosa and (B) normal OME consisted of epithelium on top of connective tissue, while (C) OLP biopsy and (D) T cell inflammatory disease model both showed characteristics of subepithelial T cell infiltration and basal cell apoptosis. Images are representative; n=3. Scale bar A&C = 50 µm, B&D = 100µm.

5.4.6.2 Fibroblast characterisation in normal and disease model compared to normal and OLP native tissues.

Vimentin staining was used to show the presence of NOF within the models compared to patient samples. The expression of vimentin in the native oral mucosa (**Figure 5.19A**), normal OME (**Figure 5.19B**), OLP (**Figure 5.19C**), and T cell disease model (**Figure 5.19D**), was comparable and localised to the fibroblasts within the connective tissue layer. There was slightly higher density staining in the native tissues when compared to tissue engineered models but both model and native tissues reflected similar distribution with higher intensity staining towards the epithelium (**Figure 5.19**).

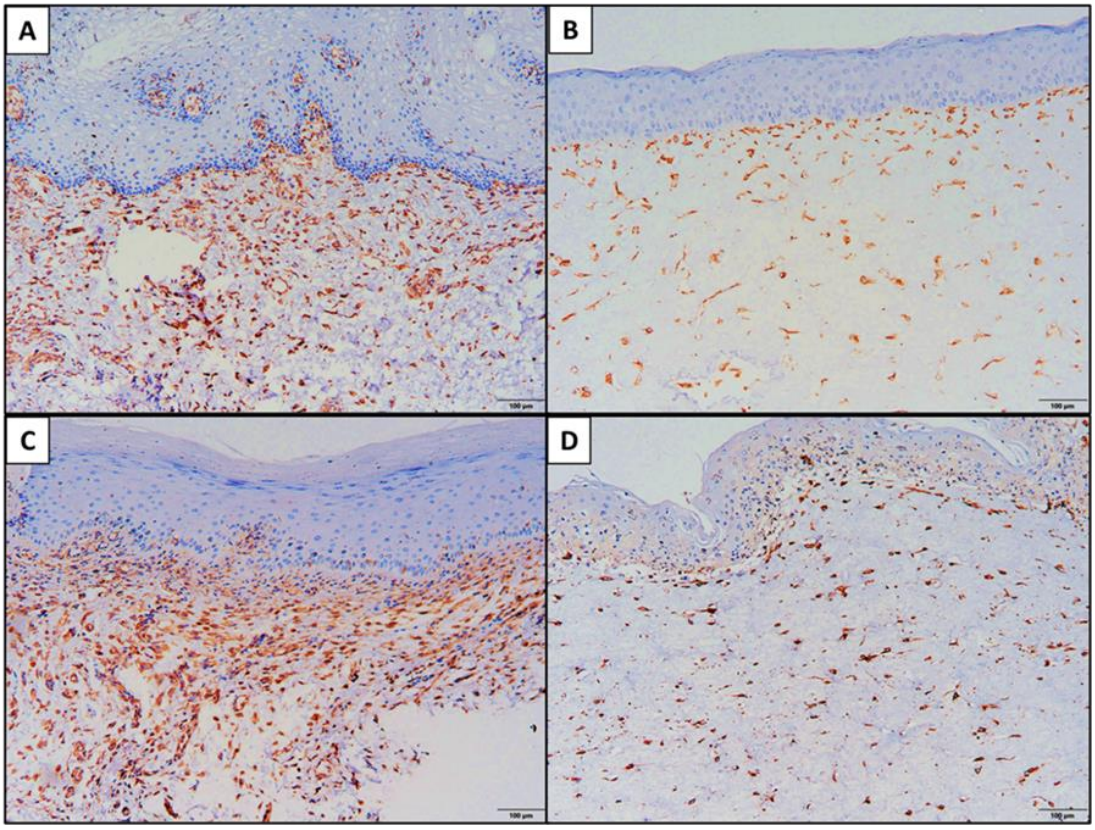

Figure 5.19: Immunohistochemical analysis of vimentin in a full thickness tissue engineered model of normal oral mucosa and a T cell inflammatory disease model compared to native tissue. Tissue engineered model of normal oral mucosa and T cell inflammatory disease were created and stimulated on day-10 with IFN-γ and TNF-α. IHC staining with an anti-vimentin antibody, counterstained with haematoxylin (blue) revealed vimentin (brown) staining comparable in (A) native oral mucosa, (B) normal OME, (C) OLP patient biopsy and (D) T cell inflammatory disease model. Images are representative; n=3. Scale bar = 100 µm.

5.4.6.3 Immune T cell characterisation

The inflammatory T cell disease model stained positively for T cell markers CD4 and CD8 on day-10 and day-12 but only at day-12 were T cells evident near and in the epithelium. The disease model at day-12 of ALI and following 48 hours of stimulation stained positively for CD4 surface marker (**Figure 5.20A**) and CD8 surface marker (**Figure 5.20B**) near and within areas of destruction which is comparable to OLP biopsies samples (**Figure 5.20C& D**). These data indicate that T cells migrated towards the epithelium following stimulation which also confirmed a characteristic feature for OLP, the presence of T cell within the targeted epithelium.

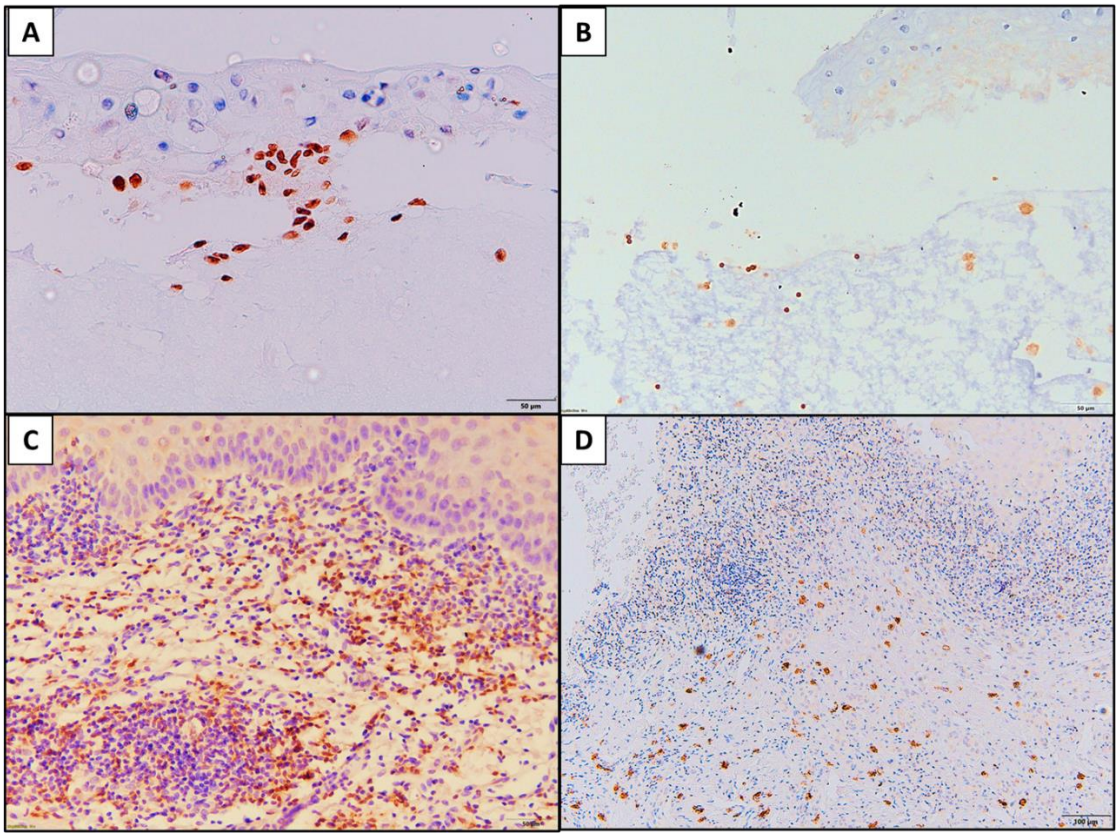

Figure 5.20: Immunohistochemical analysis of CD4 and CD8 in a full thickness tissue engineered model of T cell inflammatory disease model compared to OLP patient tissue. OME at day-7 of culture at ALI transferred on top of a T-cell containing hydrogel and stimulated on day-10 with IFN-γ and TNF-α. IHC staining with anti-CD4 and CD8 revealed positive (brown) staining for (A) CD4+ and (B) CD8+ T cells in the epithelium that was comparable to (C) CD4+ and (D) CD8+ staining in OLP biopsies. Images are representative; n=3. Scale bar in A, B & C = 50 µm, D= 100 µm.

5.4.6.4 Detecting the integrity of basement membrane through Periodic acid-Schiff and laminin staining

Periodic acid-Schiff (PAS) staining was used to detect the basement membrane through the staining of glycoproteins in the basement membrane. Although positive staining delineating the base of the epithelium was detected in the native oral mucosa (**Figure 5.21A**) and the normal OME (**Figure 5.21B**), the staining was less evident or had occasional discontinuity in the OLP patient samples (**Figure 5.21C**). In the T-cell disease model, staining revealed a basement membrane that was fragmented with discontinuation in the areas of disruption (**Figure 5.21D**), reflecting the loss of basement membrane integrity in the disease state.

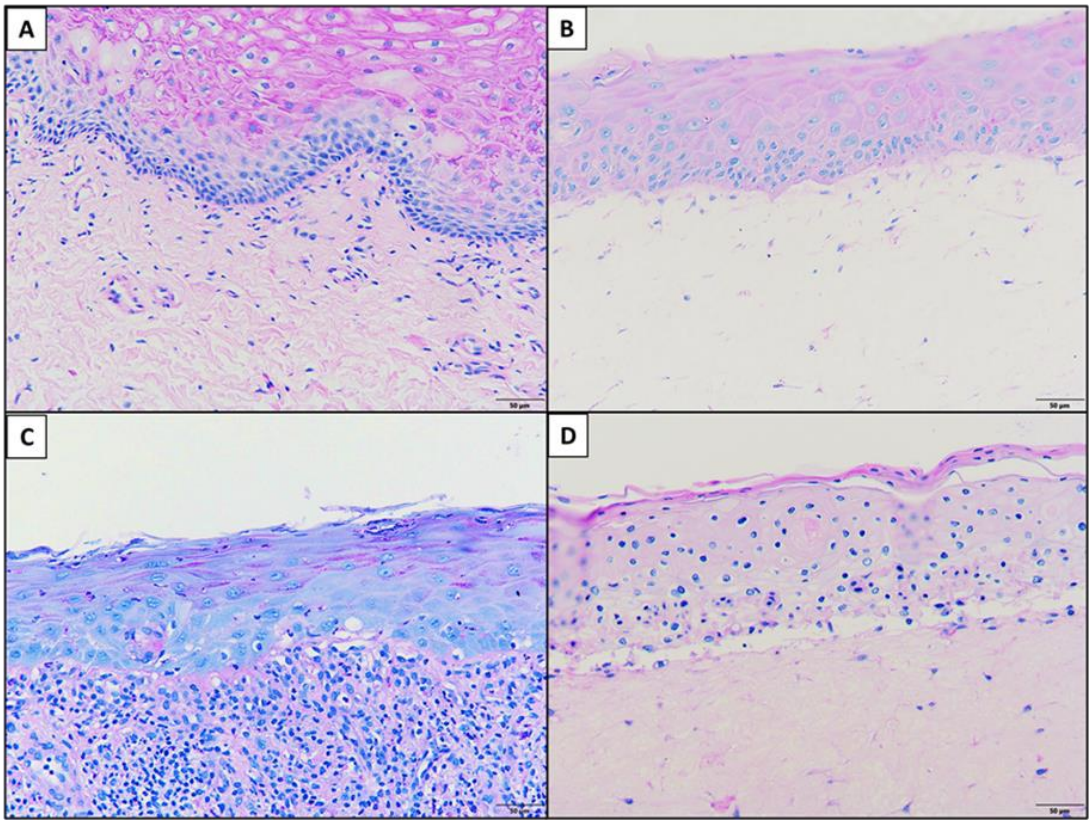

Figure 5.21: Periodic acid-Schiff (PAS) staining of the basement membrane in a full thickness tissue engineered model of normal oral mucosa and T cell inflammatory disease model compared to native tissue. Tissue engineered model of normal oral mucosa and T cell inflammatory disease were created and stimulated on day-10 with IFN-γ and TNF-α. PAS staining positive (light purple) counterstained with haematoxylin (blue) revealed purple continuous line at the base of the epithelium in (A) native oral mucosa, and (B) normal OME, while revealed less evident and defragmented line in (C) OLP patient biopsy, and (D) T cell inflammatory disease model. Images are representative; n=3. Scale bar = 50 μm.

To further assess the integrity of the basement membrane, the T cell inflammatory disease model was stained for laminin. Laminin is a glycoprotein that significantly contributes to the structure of the basement membrane and is involved in the biological processes that maintain the epithelium integrity. Laminin staining revealed a continuous positive band at the basement membrane zone and the intercellular spaces of the basal cells layer in normal OME (**Figure 5.22A**). This brown band was more diffuse in the T cell disease model with staining revealing thin irregular scattered filaments (**Figure 5.22B**). The OLP sample showed positive staining delineating areas of epithelial separation (**Figure 5.22C**) confirming the destruction of the basement membrane.

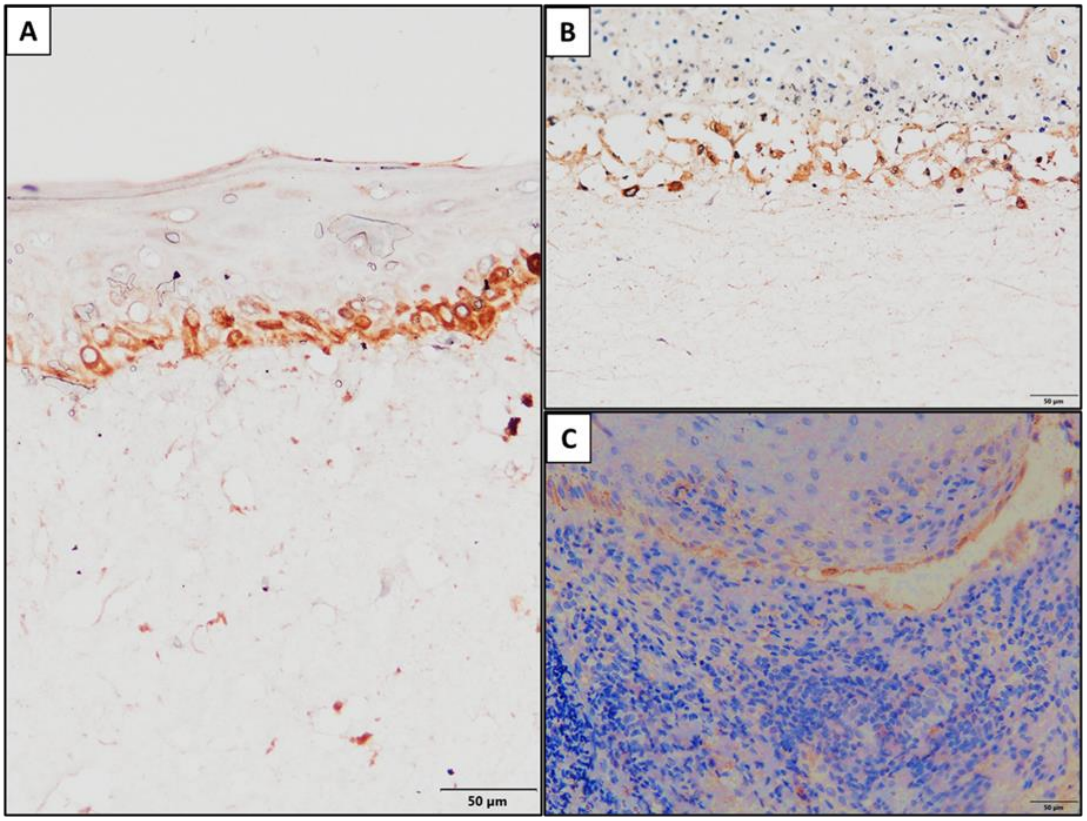

Figure 5.22: Immunohistochemical analysis of laminin in a full thickness tissue engineered model of normal oral mucosa and a T cell inflammatory disease model compared to native tissue. Tissue engineered model of normal oral mucosa and T cell inflammatory disease were created and stimulated on day 10 with IFN-γ and TNF-α. IHC staining with anti-laminin antibody, counterstained with haematoxylin (blue) revealed laminin (brown) staining continuous band in (A) normal OME, while defragmented thin staining in the (B) T cell disease model and (C) OLP patient biopsy evidencing basement membrane destruction. Images are representative; n=3 Scale bar = 50 µm.

5.4.6.5 Detecting the integrity of basal cells and basement membrane attachment through integrin α6β4 staining

To assess integrity of the basal epithelium, integrin α6β4 IHC staining was performed. Integrin α6β4 is mainly expressed in the basal surface of epithelial cells adjacent to the basement membrane and supports the formation of hemidesmosomes. These adhesions are important for epithelial integrity. Staining of normal OME revealed a continuous positive integrin staining at the basal epithelial layer (**Figure 5.23A**), while the T cell disease model revealed diffuse staining in the basal epithelium and areas of epithelial separation (**Figure 5.23A**). This staining profile evidences the loss of basal layer integrity in the T cell disease model.

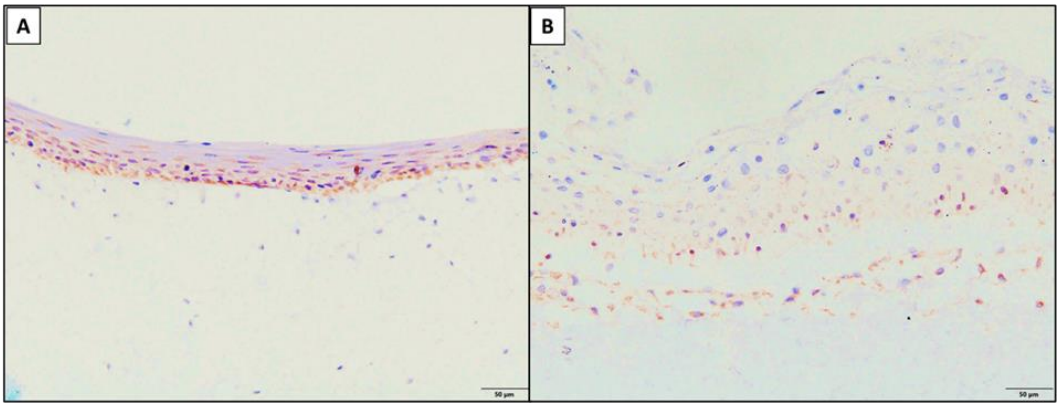

Figure 5.23: Immunohistochemical analysis for the presence of integrin α6β4 in a full thickness tissue engineered model of normal oral mucosa and a T cell inflammatory disease model. Tissue-engineered model of normal oral mucosa and T cell inflammatory disease were created and stimulated on day-10 with IFN-γ and TNF-α. IHC staining with anti-integrin α6β4 antibody, counterstained with haematoxylin (blue) revealed integrin (brown) staining continuous band in (A) OME, while defragmented faint staining in the (B) T cell disease model evidencing basement membrane destruction. Images are representative; n=2. Scale bar = 50 µm.

5.4.6.6 Detecting apoptosis through cleaved caspase-3 staining

Cleaved caspase-3 is a lysosomal enzyme involved in the apoptotic pathway. To investigate apoptosis in the T cell disease model, IHC staining for cleaved caspase-3 was performed. No cleaved caspase-3 was detected in normal oral mucosa (**Figure 5.24A**) or normal OME (**Figure 5.24B**). However, cleaved caspase-3 was detected in the basal and the suprabasal areas of the epithelium in the T cell disease model (**Figure 5.24C**), while it was more confined to the basal layer in the OLP biopsy (**Figure 5.24D**). Moreover, positive cleaved caspase-3 staining was detected within the subepithelial T cells inflammatory infiltrate in both the disease model and OLP cases. This confirms there is apoptosis in the basal epithelial layer in the OLP and T cell disease model, a feature not seen in normal tissue or OME and, in part, explains the tissue destruction observed.

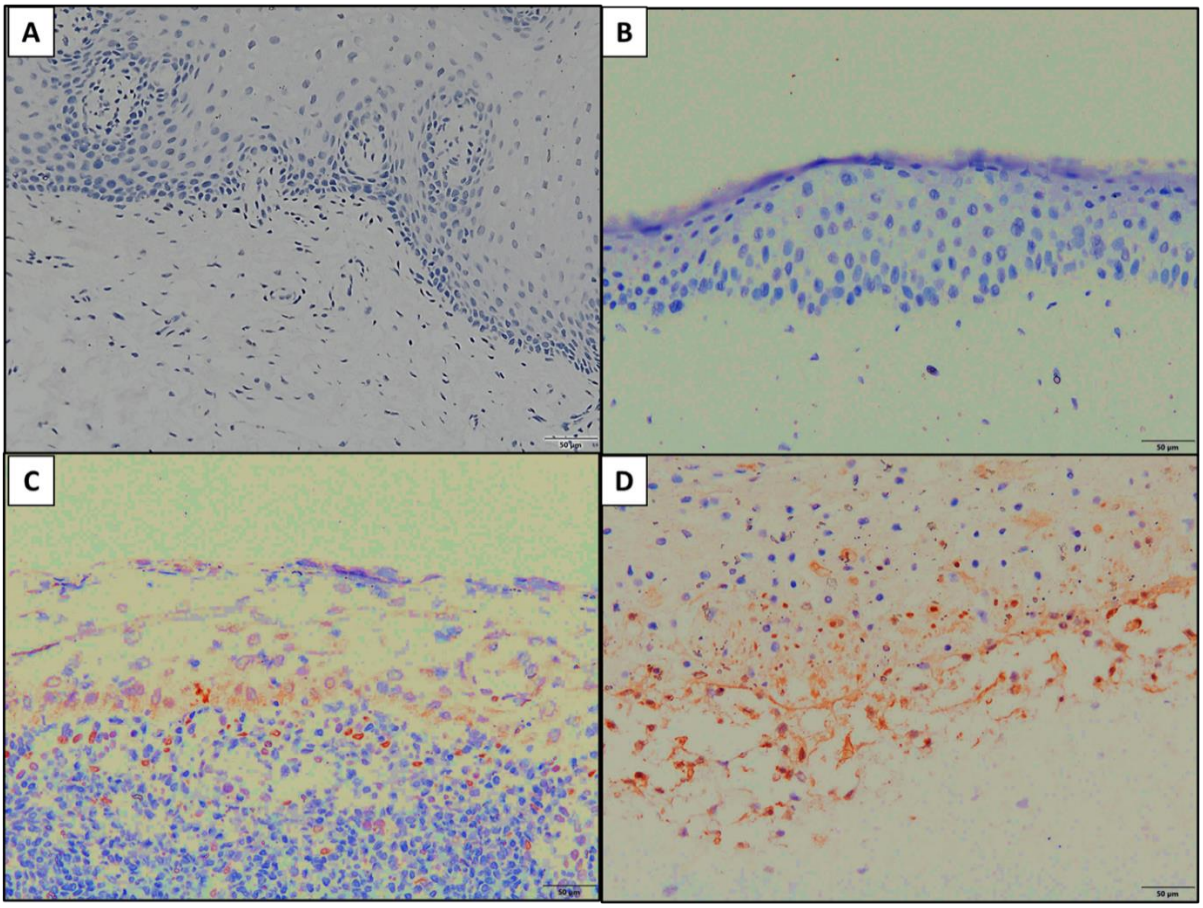

Figure 5.24: Immunohistochemical analysis of cleaved caspase-3 in a full thickness tissue engineered model of normal oral mucosa and a T cell inflammatory disease model compared to native tissue. Tissue engineered model of normal oral mucosa and T cell inflammatory disease were created and stimulated on day-10 with IFN-γ and TNF-α. IHC staining with anti-cleaved caspase-3 antibody, counterstained with haematoxylin (blue) revealed cleaved caspase-3 (brown) staining not detected in (A) native oral mucosa, or (B) normal OME, while detected in the basal layer of (C) OLP patient biopsy and (D) T cell inflammatory disease model. Images are representative; n=3. Scale bar = 50 µm.

5.4.6.7 T cell inflammatory chemokines secretion by the T cell disease model

To confirm the secretion of key inflammatory drivers reponsible for the destruction observed, conditioned media was collected from the models on days 10 to 25 and levels of three chemokines, CXCL9, CXCL10 and CCL5, quantified by ELISA. There was a significant increase in the levels of all three chemokines secreted by the disease model when compared to normal OME models at each time point investigated.

On day 10, which represents three days of mucosa and T cells coculture but without IFN-γ and TNF-α stimulation, the T cell disease model secreted 2.9 ± 0.6 ng/ml of CXCL9 that was 30-fold higher than that secreted by normal OME (0.1 ± 0.03 ng/ml; $p<0.0001$). The disease model maintained the same levels of CXCL9 secretion overtime, after stimulation, with between 2.7-2.9 ng/ml continuing to be detected until the final time-

point on day 25 and was significantly higher than OME ($p<0.0001$) at all time-points (**Figure 5.25A**). Similarly, CXCL10 secretion in the T cell disease model was higher when compared to OME secretion at all time-points investigated ($p= <0.0001$). The CXCL10 levels detected were found to be consistently between 0.8-1.2 ng/ml and 0.05-0.9 ng/ml for the T cell disease model and normal OME, respectively (**Figure 5.25B**).

Similar to CXCL9 and CXCL10, levels of CCL5 secreted by the disease model remained significantly higher than the OME ($p<0.0001$) at all time points examined. While OME models secreted on average 0.06 ± 0.04 ng/ml at day 10, the disease model secreted significantly higher levels (0.5 ± 0.1 ng/ml; $p= <0.0001$). Of interest, the levels of CCL5 secreted by the disease model were found to increase significantly on days 20 (1 ± 0.03 ng/ml) and 25 (0.9 ± 0.08 ng/ml) compared to earlier time points (0.5 ± 0.1, 0.5 ± 0.1, 0.6 ± 0.06 ng/ml on day 10, 12 and 16, respectively). No difference in CCL5 secretion overtime was detected within the normal OME (**Figure 5.25C**).

These data imply the development of a feedback loop that drives chemokine levels and maintain their cycle of production. Particularly, there is strong indication for the development of the CXCR3/CXCL9, CXCL10 axis and the CCR5/CCL5 axis which encourages the progression of the inflammatory condition at a stable rate creating chronicity of the disease.

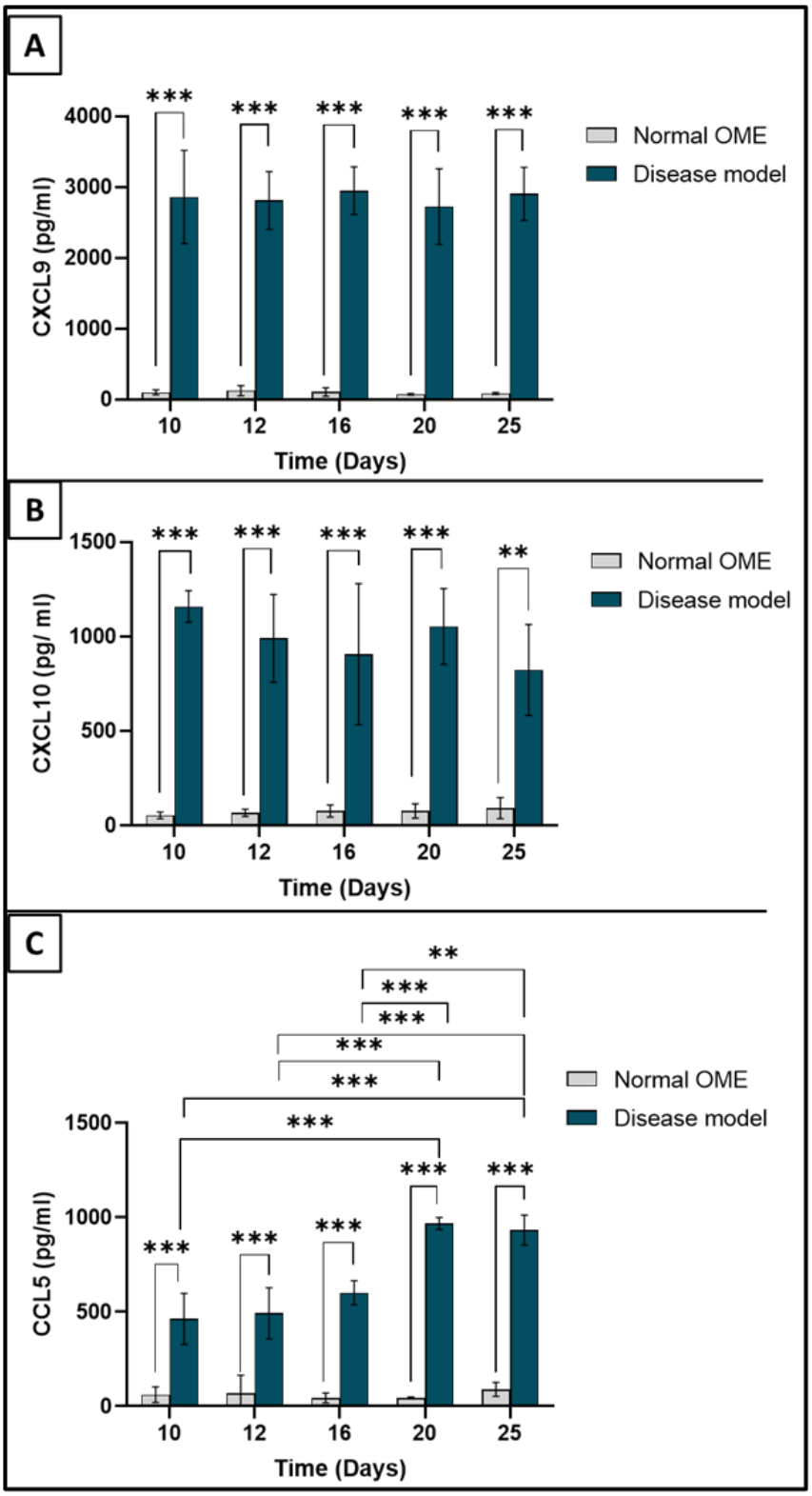

Figure 5.25: Chemokines secretion by full T cell disease model. Full thickness tissue engineered models of T cell inflammatory disease were generated using the 'layering' technique and stimulated after 72 hours (day-10 of culture) with IFN-γ and TNF-α. Secretion of T cell chemokines (A) CXCL9, (B) CXCL10, and (C) CCL5 were quantified by ELISA on day 10, 12, 16, 20 and 25. Data presented as the mean ± SD. A mean difference was considered significant when **p <0.001 and ***p <0.0001 using one-way ANOVA tests to detect difference between groups. Main ANOVA for CXCL9 and CXCL10 reported **p <0.001 effect of model type but no effect of time or interaction while CCL5 reported ***p <0.0001 effect of time, model type, and interaction. n=3.

5.5 Discussion

5.5.1 Oral mucosal equivalents

In an attempt to culture human epithelial cells in 3D, human TR146 keratinocytes, which are a non-keratinised epithelial cell line derived from a metastasis of oral buccal squamous cell carcinoma, were used. The potential usefulness of such an immortal cell line in modelling the human buccal epithelium in 3D for drug permeation and transport was shown by Jacobsen *et al* (Jacobsen *et al.*, 1995). However, it is commonly acknowledged that cancer cell lines do not precisely represent normal epithelial cells (Dongari-Bagtzoglou and Kashleva, 2006b). Primary keratinocytes are short-lived cells and after a limited number of cells divisions, these cells enter senescence, which significantly alters their phenotype. Experiments using these cells also suffer from donor-to-donor variability (Hayflick and Moorhead, 1961). Despite these limitations, primary cells used to make 3D models hold close resemblance to native tissue in terms of tissue structure and the inter-donor variability may be considered a better representation of the biological variation that exists in the general population. However, obtaining enough cells from multiple donors, to accurately study donor variability may not be feasible due to technical complexity, access to tissue or ethical concerns. Hence, FNB6, an immortalised cell line by ectopic expression of human telomerase reverse transcriptase (hTERT) in buccal keratinocytes, came into popular use to overcome the limitation of using primary keratinocytes and cancer cell lines (McGregor *et al.*, 2002). These cells maintain many of the key characteristic features of the primary keratinocytes from which they were derived but can be cultured *in vitro* over prolonged periods and over many population doublings. The use of these cells provides increased reproducibility of experiments and removes the need for continual access to primary tissue. Eventually, even immortalised cells, if passaged for extended periods of time, may undergo genetic and phenotypic change which may considerably affect their phenotype (Kaur and Dufour, 2012).

Use of FNB6 along with NOF and the cell culture protocol used in this research has been previously shown to generate a reproducible intact 3D oral mucosa composed of stratified squamous epithelium and fibroblast-populated connective tissue which is similar in histological structure to *in vivo* tissue (Jennings *et al.*, 2016). This agrees to A Dongari-Bagtzoglou *et. al*, who similarly reported a reproducible characterised tissue engineered *in vitro* oral mucosa using the TERT-2 immortalized human oral floor of the mouth-derived keratinocyte cell line (OKF6) cultured on a fibroblast embedded collagen scaffold. These full thickness OME based on immortalised keratinocytes, are a closer match to normal tissue in terms of structure and marker expression than those based on

TR146 cells with the latter models displaying dyskeratotic changes (Dongari-Bagtzoglou and Kashleva, 2006a; Yadev *et al.*, 2011). Furthermore, hTERT-immortalised keratinocytes resemble primary oral keratinocytes in studies of cytotoxicity or inducible cytokine and beta-defensin expression, and thus are a valuable and reproducible model of normal oral epithelial cells (Dickson *et al.*, 2000; Dongari-Bagtzoglou and Kashleva, 2006a; Feucht, DeSanti and Weinberg, 2003; Yadev *et al.*, 2011). Similar to data presented by Jennings et al (2016), data in this chapter shows that OME based on immortalised FNB6 cells were able to mimic the native oral mucosa structure and therefore provide a readily available alternative to NOK (Jennings *et al.*, 2016). Although this model system provides an invaluable base to study a variety of oral tissue diseases, the lack of an immune counterpart is a limitation in their use.

There are no studies to date that have comprehensively assessed T cell viability in a 3D environment. Changing the cell culture environment from a media suspension to 3D may shock the cells and affect their viability or proliferation. Hence, careful assessment of the T cells viability in 3D was performed here by either extracting T cells from the collagen hydrogel and performing direct viability staining with flow cytometry or through metabolic rate assessment within the collagen hydrogel. The latter will exclude any effect of the extraction procedure on the viability of cells. Ascertaining the viability and behaviour of T cells within the 3D hydrogel validated successful incorporation of immune cells within the model and aided the reproducibility. Moreover, because T cell viability initially reduced before recovering by- day 7 of 3D culture, it was decided to combine the T cell hydrogel with OME on day 7 of 3D culture. This was to ensure that an optimum immune response was produced.

5.5.2 Stimulation of normal OME

Besides priming the immune components *in vitro* to simulate the different T cell phenotypes reported in OLP, it was essential to explore the cytokine secretion profile of normal OME upon stimulation with pro-inflammatory factors to confirm their immune responsive role. *In vivo*, normal oral keratinocytes have roles beyond acting as a physical protective barrier, by interacting with several cells such as DCs, macrophages, and endothelial cells to orchestrate an immune response. It has been shown DC/epithelial cross talk affects the function of cells in unstimulated as well in inflammatory conditions (Paplinska-Goryca *et al.*, 2020). Similar to macrophages and DCs, keratinocytes can protect the host through innate immune responses as they are able to detect a broad range of pathogen-associated molecular patterns (PAMPs), such as LPS through their

expression of several pattern recognition receptors (PRRs), including a variety of toll-like receptors (TLRs) along with secretion of antimicrobial peptides that display broad spectrum activity against bacteria, yeasts, and viruses (Chung and Dale, 2004). Upon activation, keratinocytes were reported to modulate the immune response through activation of downstream signalling cascades and production of chemokines and cytokines (Coates, Blanchard and MacLeod, 2018; Miller and Modlin, 2007). The secreted chemokines can aid in chemotaxis and recruitment of inflammatory cells to the local area via up-regulation of adhesion molecule expression that facilitates trans-endothelial cell migration (Yamamoto, Nakane and Osaki, 2000). In agreement, it is also established that, through their secretion of pro-inflammatory cytokines and chemokines, oral keratinocytes have a crucial role in the initial stages as well as in sustaining the chronic phase of OLP. Therefore, the immune role of keratinocytes and NOF within the OME was explored in this study.

Previous studies have suggested that the type of chemokines secreted by keratinocytes exert a degree of selectivity on the type of leukocytes recruited to the diseased site and hence on the nature of the disease itself. IFN-γ and TNF-α were reported to synergise together in inducing optimum oral keratinocyte activation leading to the production of chemokines (Barker *et al.*, 1990; Shalaby *et al.*, 1985). The local cytokine network in OLP depends largely on the actions of DC-derived IFN-γ and TNF-α. IFN-γ in particular appears to be critical in priming the epithelium to participate in immuno-inflammatory events, by inducing keratinocytes to express ICAM-1 and MHC class II molecules, and the release of chemokines and cytokines that enhance leukocyte-endothelial and leukocyte-keratinocyte interactions (Li *et al.*, 1996b). *In vivo*, IFN-γ and the potent pyrogenic cytokine, TNF-α, in particular is initially provided by activated DC and LC within the epithelium as they encounter OLP-mediating antigens, whereas IFN-γ is usually provided by the T cells (mainly Th1) recruited to the area during the course of the infection (Santoro *et al.*, 2005). Macrophages also secrete TNF-α in the first stages of an immune response (Arango Duque and Descoteaux, 2014; Murray *et al.*, 2005). A number of other factors are capable of mediating keratinocyte cytokine production, including cytokines themselves (Ansel *et al.*, 1990). Accordingly, this study induced the oral keratinocyte, in 3D, with a combination of the recombinant IFN-γ and TNF-α as a substitute for activated DC to simulate an inflammatory microenvironment similar to that seen in OLP.

OME stimulated with IFN-γ and TNF-α or with Th1 conditioned media in this study showed an upregulation of important pro-inflammatory cytokines such as GM-CSF,

CCL1, CCL8 (MCP-2), CCL7 (MCP-3), and IL-13. However, some cytokines reported in OLP were either not increased or increased but with no difference to the unstimulated control. For instance, IL-1β, a pro-inflammatory cytokine produced mainly by activated macrophages was not increased upon stimulation while IL-1α was increased when OME were cultured only with Th1 conditioned media. In comparison, culture supernatants of OLP-keratinocytes contained higher concentrations of IL-1β, GM-CSF, and TNF-α compared to those of normal keratinocytes (Yamamoto, Nakane and Osaki, 2000). Moreover, IL-1β was reported to work in concert with TNF-α and IFN-γ to enhance cell surface expression of intercellular adhesion molecule in OLP (Yamamoto *et al.*, 1994). However, it is reported that upon first stimulus, IL-1β is produced as an inactive precursor called pro-IL-1β that must be processed by the actions of another PAMP stimulus to form mature IL-1β. Hence, the low detection of IL-1β in this study is likely due to the absence of IL-1β-producing macrophages, and to the lack of subsequent pathogen stimulus (Lopez-Castejon and Brough, 2011; Thornberry *et al.*, 1992).

Both IL-6 and CXCL8 levels were high in all four conditions, including unstimulated controls. Hence, upon IFN-γ and TN-Fα stimulation or Th1 conditioned media stimulation, IL-6 and CXCL8 levels were not different from normal unstimulated OME. On the contrary, IL-6 was detected in OLP and a recent meta-analysis study of IL-6 in serum and saliva of OLP reported that six studies showed significantly high saliva IL-6 levels in OLP patients compared with healthy controls and seven studies showed significantly high serum IL-6 levels in OLP patients compared with healthy controls (Mozaffari, Sharifi and Sadeghi, 2018; Wu *et al.*, 2013; Khan *et al.*, 2003; Wei *et al.*, 2018; Xavier *et al.*, 2007). However, these studies were conducted using body fluids that reflect a systemic state of inflammatory cytokines which may be altered in the OLP local tissue. In accordance, a study by Yamamoto *et al.*, reported IL-6 production in both a co-culture of normal keratinocytes and PBMC as well as by OLP-derived keratinocytes (Yamamoto *et al.*, 1994).

CXCL8, primarily a neutrophil chemoattractant produced by various immune cells, such as monocytes, T cells, neutrophils and NK cells, and non-immune cells, was reported to be secreted by oral keratinocytes in response to IFN-γ and TNF-α stimulation. This chemokine has a role in lymphocyte recruitment through their synergy with other chemokines (Barker *et al.*, 1990; Li *et al.*, 1996a). High levels of CXCL8 have been observed in OLP samples (Mozaffari *et al.*, 2018). In this study the levels of CXCL8 were high in all four conditions, and not different from levels produced by unstimulated OME. This could be explained by the following: first and similar to IL-6, most studies that have

investigated CXCL8 in OLP have used serum and saliva for detection of this interleukin and reported higher levels of IL-8 in OLP compared to healthy controls (Mozaffari *et al.*, 2018; Lu *et al.*, 2015). Second, stimulation of OME with only IFN-γ and TNF-α did not produce the substantial damage as seen in OLP, where high levels of CXCL8 were reported to increase in severe forms of OLP, hence, it was used as an indicator for OLP progression and as a biomarker for malignant change in OLP (Sun *et al.*, 2005; Amr *et al.*, 2018). Moreover, and as IL-1β was not detected here, it was reported that induction by IL-1β is the main stimulator of CXCL8 release, which leads to excessive infiltration of T cells locally in OLP (Amr *et al.*, 2018).

Interestingly, T cell-specific chemokines such as CXCL9, CXCL10 and CCL5 were produced at high levels in stimulated OME. The expression of T cell-specific chemo-attractants following OME stimulation was of prime importance and interest in this study to recreate a criterion specific for immune T cell disease. CXCR3, an interferon-inducible chemokine receptor that is present on the cell surface of various cell types including activated T cells (mainly Th1), binds and responds to three interferon-inducible chemokines: CXCL9, CXCL10 and CXCL11 (Loetscher *et al.*, 1998a; Groom and Luster, 2011). Both CXCL9 and CXCL10 production was upregulated following stimulation with IFN-γ and TNF-α as detected with cytokine array and confirmed with ELISA. CXCL11 was not included in the cytokine array membrane and so was not investigated. This is in accordance with previous studies that have showed their upregulation in response to IFN-γ and then synergistically enhanced by TNF-α (Ohmori *et al.*, 1993; Ohmori, Schreiber and Hamilton, 1997). Besides their role in T cell chemoattraction, these chemokines have been reported to also influence T cell polarisation through skewing the Th1/Th2 balance in favour Th1 (Wildbaum, Netzer and Karin, 2002; Kim *et al.*, 2001). It was a key to ascertain the CXCL9, CXCL10, CXCL11/ CXCR3 ligand axis in an OLP disease model as its role in OLP has been established previously through detecting the expression of the CXCL9, CXCL10, and CXCL11 genes by lesional OLP keratinocytes and in the submucosa and the CXCR3 detection on lesional T cells (Iijima *et al.*, 2003; Ichimura *et al.*, 2006). It has also been reported that different T cell based inflammatory diseases present different expression patterns of the CXCR3 inducing chemokines which correlates to distinct location of CXCR3 expressing T cells. For instance, a band-like pattern of CXCL9, CXCL10, and CXCL11 m-RNA was detected in lichen planus which may explain the subepithelial band like distribution of attracted T cells and infer a characteristic feature for the disease (Flier *et al.*, 2001).

CCL5, another T cell chemoattractant that has been identified in OLP (Hu *et al.*, 2013; Zhao *et al.*, 2001; Li *et al.*, 1996a; Ichimura *et al.*, 2006; Iijima *et al.*, 2003), was upregulated in this study upon OME induction which support the development of an OLP similar microenvironment in the disease model in this research. Immunostaining showed that CCL5 was expressed by keratinocytes in 21 of 24 frozen OLP biopsy samples and seven of seven cases of OLR but not by healthy tissue (Little *et al.*, 2003a). The importance of the CCL5-CCR5 axis in OLP has been highlighted, not as a potent chemoattractant only, but as a stimulant for T cell longevity and supportive for a positive feedback loop to establish chronicity of OLP (Shan *et al.*, 2019). Although the CCL5 levels secreted by stimulated OME were high but they were not significant when compared with the other conditions. This could be related to the absence of mast cells and T cells, other sources for CCL5 *in vivo*, in the OME which also explains higher CCL5 levels when OME treated with Th1 conditioned media. This could also suggest that keratinocytes and NOF were the main source of CXCL9 and CXCL10 in the stimulated OME. These data show that upon stimulation with the DC-expressed cytokines IFN-γ and TNF-α, and to a lesser extent Th1 conditioned medium, potent T cell chemokines are secreted that will facilitate T cell migration toward the epithelium of the OME.

Other chemoattractants such as CCL2 (MCP) has been shown to chemoattract memory T lymphocytes (Taub *et al.*, 1995). The levels of CCL2 here were not increased while reported previously to be produced highly by oral keratinocytes grown as monolayers upon stimulation with IFN-γ and TNFα (Li, Farthing and Thornhill, 2000). However, both CCL8 (MCP-2) and CCL7 (MCP-3), monocyte chemoattractants of comparable potency and homology to CCL2 (Van Damme *et al.*, 1992), were highly detected in this study. Ozturk et al, suggested that MCP-1 and its receptor CCR2 play an important role in the pathogenesis of OLP by recruiting macrophages to the local lesion. They reported a positive association between the MCP-1 gene and the presence of OLP in patients (Ozturk *et al.*, 2021). Although the levels of CCL7 and CCL8 were high, their role in OLP has not been investigated and further studies exploring their role in OLP are necessary. Macrophage inflammatory protein, CCL4 (MIP-1β), a chemokine secreted by macrophages and T cells, showed higher expression upon Th1 conditioned media than with IFN-γ and TNF-α stimulation in this study. MIP-1α (CCL3) and CCL4 were correlated with OLP (Zhu *et al.*, 2022) and with type 1 immune response (Yoshie, Imai and Nomiyama, 2001; Iijima *et al.*, 2003). CCL15 binds to CCR1 and 3 and has a chemoattractant effect on monocytes and eosinophils, but less effect on lymphocytes (Pardigol *et al.*, 1998). CCL15 has been increased both in the Th1 conditioned medium

and IFN-γ and TNF-α medium but there are no studies performed to investigate its role in OLP.

In summary, both IFN-γ/ TNF-α stimulation or Th1 conditioned media reflect two elements of the OLP disease that will be combined later within one model system. While the IFN-γ/ TNF-α response mimics an early DC-like response, the Th1 CM represented a late/chronic response mimicking the response of the OME to Th1 generated cytokines once these cells have arrived at the OLP lesion site. Understanding the cytokine secretion profile for both separately is important to anticipate subsequent events when T cells are added to the model. The cytokine and chemokine profile observed in stimulated OME was supportive to what has been previously reported in the OLP microenvironment. Therefore, the data presented here suggests that FNB6 and NOF, when cultured in a 3D model have the ability to release T cell-related chemokines establishing a concentration gradient within the OME that will facilitate the migration of T cells towards the epithelium when these cells are added to the OME, resulting in the accumulation of T cells to produce a sub-epithelial band-like distribution of T cells that is characteristic of OLP.

5.5.3 T cells chemotaxis

Having established that a T cell chemoattractant profile was created upon OME stimulation, the next question faced by this study was will T cells migrate towards the chemoattractant gradient created by stimulated OME? T cells continuously scan their local environment in an exploratory or search behaviour that is characterized by changing velocity and direction that allows for cell-cell interactions while migrating to and from, and even within lymphoid organs and tissues (Dupré *et al.*, 2015). To assess T cell chemotaxis, different methods have been used to investigate cell migration including the widely used Boyden chamber method, where cells are added to the top of a microporous membrane above a chemotactic agent and so cells are exposed to a steep concentration gradient. In this assay, cells that migrate through the membrane to the chemoattractant are counted. Although this chemotaxis assays is used widespread, the information obtained is limited to the number of cells migrated (Chen, 2005). In the agar spot method, a chemokine is contained in an agarose drop which is applied to the surface of a glass-bottom petri dish (several spots can be added to the surface each containing a different chemokine), and then a cell suspension added to the dish. The chemokine slowly diffuses outwards from the agarose spot creating a transient chemotactic gradient within the spot to which cells are attracted (Ahmed *et al.*, 2017). This method can provide simultaneous comparison of cell migration towards different chemokines, direct counting of cell number

under the drop, distance travelled by cells, and their velocity can be recorded with video images. However, problems with this assay include unstable and poorly defined gradients and variability in the drop production. In the current study, the µ-Slide Chemotaxis assay was used as it allows for the development of stable concentration gradients and to measure chemotaxis of cells in a 3D construct using live-imaging time-lapse microscopy enabling several parameters to be quantitatively measured (Zengel *et al.*, 2011)

Although T cell movement can be modified by environmental cues and internal signals, it is established that chemokine gradients direct trafficking of lymphocytes within tissues (Miller *et al.*, 2003). Both recombinant CCL5 and conditioned media from TNFα and IFNγ-stimulated OME caused T cells to migrate towards the chemokine gradient in a directed manner and increased their overall distance travelled. While the velocity reported here was less than other reports (Dupré *et al.*, 2015), the velocity of cells exposed to the chemokine gradient was markedly higher than the ones in the control media. The conditioned media from stimulated OME caused significant T cells attraction, although this was not as much as that caused by recombinant CCL5, which could be due to differences in overall levels of chemoattractant used and the presence of other factors that may inhibit migration in the conditioned medium. Similarly, Yamamoto et al (2000) found that conditioned medium from OLP-keratinocytes induced increased trans-endothelial migratory capacity of mononuclear cells (Yamamoto, Nakane and Osaki, 2000). Although beyond the scope of this study, it would be interesting to identify which chemokines are the most important in directing T cell migration toward the stimulated OME conditioned medium by using a combination of either chemokine-specific neutralising antibodies or antibodies aimed at blocking chemokine receptors on the T cells. Nevertheless, these data support the strategy to construct a full T cell disease model where instead of adding T cells in subepithelial location prematurely, it can be achievable to add a layer of T cells later beneath the OME and rely on a chemokine gradient produced by stimulated OME to attract T cells towards the epithelium in an OLP-like mechanism.

5.5.4 Full T cell inflammatory model

The complete tissue destruction observed with the all-in-one technique confirmed the importance of identifying specific time points to combine different elements in the layered full disease model. It was essential to have well established normal oral mucosa model created before the addition of activated and polarised Th1 and cytotoxic T cells. When T cells were arbitrarily added with oral fibroblasts and keratinocytes at the same

time, day zero, they attacked the tissue before establishing the epithelium or the connective tissue causing a premature destruction. Fabricating a T cell disease model using the layered technique with IFN-γ and TNF-α stimulation once at day 10, the tissue damage in the T cell-containing OME was shown to progress gradually over time when models were fixed at days 12, 16, 20, and 25 of ALI. In the 'all-in-one' models, no specific disease features could be tracked. In contrast, disease models fabricated using the layered technique showed gradual progression of events and increasing degrees of damage until the model reached complete destruction at day 25 of ALI. The presence of T cells caused apoptosis in the basal layer of the epithelium even before stimulation with IFN-γ and TNF-α. In contrast, previous stimulation of OME in the absence of T cells produced a hyperproliferative epithelium and no destruction was noticed which evidence the importance of the presence of Th1 and cytotoxic CD8 T cells in creating the disease model.

CD4 and CD8 T cells were added in separate hydrogel then adhered beneath the OME to allow for T cells to migrate towards epithelium following chemoattractant gradient as in OLP. Although signs of basal cells apoptosis were evident on day 10, T cells were mainly at the lower part of the OME connective tissue. similarly, T cell were also reported within the lower epidermis in lichen planus in earlier stages of the disease (Ragaz and Ackerman, 1981). As disease progresses in the models, more T cells were evident in the sub-epithelium and even within the epithelium. However, unlike the uniform dense subepithelial band of lymphocytes reported in OLP patients' tissues (Anitua, Piñas and Alkhraisat, 2019), T cells in the disease model formed sporadic T cell infiltrates beneath and within the epithelium. This did not impact the reproduction of the OLP features evidenced histologically by basal cells apoptosis and vacuolar alteration, T cells infiltration toward epithelium, and basement membrane destruction.

The basement membrane (BM) is a sheet of extracellular matrix molecules that forms the boundary between the epithelium and the connective tissue. It facilitates epithelial-mesenchymal interactions that are necessary for the development and survival of the oral epithelium (Manjunatha and Kumar, 2005). H&E is routinely used to stain tissue sections but this method makes it difficult to identify BM. Therefore, more specific stains are used to examine the BM. PAS binds to proteoglycan-rich regions and as such staining with these reagents highlights the intact BM as a fine magenta line that can be judged according to its continuity and contrast (Jones, 1951; Pujar *et al.*, 2015). PAS staining of OME was similar to healthy human oral mucosa, whereas both the T cell-containing model and OLP biopsy sections showed a discontinuous layer with detached basal cells.

A similar PAS staining pattern, was reported by Juneja et al, who described both cases of focal thickening or discontinuity of the BM but also a thin continuous linear band of BM with occasional faults and with numerous strands extending into the connective tissue (Juneja *et al.*, 2006).

Laminin is a major component of the BM that can be used as a marker for presence of intact or degraded BM. Loss of laminin staining has been used as an indicator for oral squamous cell cancer invasion into the underlying connective tissue (Shruthy *et al.*, 2013). Basal keratinocytes secrete collagen IV and laminin V into the oral epithelial basement membrane zone, which in return allows attachment of basal cells to the BM, maintaining their viability (Moharamzadeh *et al.*, 2007). In OLP, BM destruction is driven mainly by MMPs which are secreted by mast cells but could be produced by T cells. MMPs, mainly 2 and 9, cause lysis of collagen IV and V and damage the BM and basal cells by allowing greater access for CD8 T cells to attack basal cells or indirectly through depriving basal cells from survival signals received from BM attachment (Roopashree *et al.*, 2010; Zhou *et al.*, 2001). Although MMP9 was not added in this study, BM destruction was evident and hence, confirming MMP9 secretion in future follow up studies would be interesting. Laminin-positive staining of intact BM in healthy oral mucosa has been described as a continuous brown line. Likewise, OME displayed a continuous line as well as laminin-positive staining within the basal cells. In contrast, laminin staining in OLP has been described as absent, discontinuous, intensified, or a thickened band with finger-like projections into the connective tissue (Haapalainen *et al.*, 1995). Laminin staining was evident in both OLP biopsy and T cell-containing OME but it was discontinuous and patchy, indicating degradation. A study by Hirota *et al*, to determine the degree of BM destruction by immunohistochemical examination of laminin, reported that ulcerative/erosive OLP showed more destructive BM than asymptomatic cases and that laminin and collagen IV were best markers to reflect the BM integrity (Hirota, Yoneda and Osaki, 1989).

Integrin α6β4 is one of the components of the hemidesmosomal protein complex that connects basal keratinocytes to laminin in the basal membrane where positive staining of the normal oral mucosa was reported to be as a continuous band in the region of the BM (Ramirez-Amador *et al.*, 1996), which was in agreement to the staining observed for the OME. In OLP, α6β4 staining has been reported to have interruptions along the BM and circumferential membranous staining of basal and suprabasal keratinocytes (Schreurs *et al.*, 2020; Ramirez-Amador *et al.*, 1996), which was similar to observations in the T cell-containing OME. The disturbed expression of integrin α6β4 and

laminin in OLP indicates deficient attachment of the basal cell layer, which can contribute to detachment and cell death of basal keratinocytes seen in the OLP and T-cell disease model.

Apoptosis refers to programmed cell death that occurs through different intracellular pathways. Several assays have been used to characterise apoptosis in tissues such as terminal deoxynucleotidyl transferase dutp nickel end labelling (TUNEL) and insitu nickel translation assay labelling (ISNT) which detect DNA fragmentation but are subject to misinterpretation because this can be detected also in necrotic cells (Cohen, 1997). Other methods used to detect apoptosis but are not applicable to paraffin-embedded sections (Barrett *et al.*, 2001). Caspases, enzymes that are activated in the apoptosis pathway, are a pivotal cascade that is unique to apoptotic cells and is not active in healthy cells. Caspase-3 is probably the most clearly associated with cell death. It is present as caspase-3 which is activated by the cleavage of its interdomain linker and then subsequent cleavage of its N-terminal pro-domain, therefore the active form of the enzyme is often termed cleaved caspase-3. Detection of this cleaved form is used as a unique and sensitive indicator of cell apoptosis (Gown and Willingham, 2002), where it has been used as a marker to detect apoptosis in OLP (Woo et al., 1998). In agreement to the findings in this study, previous research has reported keratinocyte apoptosis and cleaved caspase-3 expression were mainly co-localized to the basal and parabasal epithelial layers. Laminin and BM defect were reported in similar location which suggest that apoptosis could be driven by either direct effect of T cells or driven by loss of attachment and survival signals from the BM (Tobón-Arroyave et al., 2004; Neppelberg, Johannessen and Jonsson, 2001; Mattila and Syrjänen, 2010). Interestingly, The apoptosis in the subepithelial infiltrate that was detected in this study, was also reported before with OLP cases (Neppelberg, Johannessen and Jonsson, 2001; Maraeea, El-Rebey and Zaky, 2016).

The secretion of CXCL9/CXCL10 was significantly high at day 10, a time point before stimulation and after three days of coculture with T cells, when compared to unstimulated normal OME and continue to maintain high levels till day 25 where the full models undergo a complete destruction. This proves that the inflammatory cycle continued at a steady pace reflecting a state of chronicity. CCL5 levels when models were stimulated earlier without T cell contact were not significant, however, their levels were significantly increased in the full disease model and continue to increase as disease progresses at days 20 and 25 suggesting that T cells are required for continued production of CCL5 making these models similar to *in vivo* situation. Also, this provides

evidence that these disease models can be used to study therapies targeted at blocking T cell recruitment. Blockade of CXCR3-CXCL9/CXCL10/CXCL11 or the CCR5-CCL5 axis has been suggested as a potential therapeutic treatment for OLP. T cells isolated from OLP patients showed supressed proliferation and migration while increase in apoptosis when treated by maraviroc, a blockade of CCR5. Moreover, improvement in the signs and symptoms of inflammation were noted in a murine model of colitis when treated by maraviroc or antibodies directed against CXCL10. (Wildbaum, Netzer and Karin, 2002; Shan *et al.*, 2019; Mencarelli *et al.*, 2016; Singh *et al.*, 2007). Establishing such critical pathways in a T cell inflammatory disease model will provide a relevant and more specific alternative to murine models to be utilised by research into innovative treatment strategies. Although the chemokines level was not greatly affected by the IFN-γ and TNF-α stimulation, the T cell attraction towards epithelium was only evident after stimulation. This also confirm that the stimulation created a chemokine gradient towards the epithelium.

5.6 Conclusion

This complex OLP/T cell-mediated disease model displayed basal cell apoptosis, T cell infiltration and BM destruction, which are key characteristics of OLP. Although the disease model was stimulated once at day-10, the tissue damage progressed gradually over-time, suggesting establishment of cyclic inflammatory events. Localisation of T cells close to and in the epithelium suggests the establishment of chemotactic gradients probably by the CXCR3/CXCL10 and CCR5-CCL5 axes in the disease model. T cell co-localisation with basement membrane destruction and keratinocyte apoptosis is highly representative of that observed in OLP patient tissue. In conclusion, this chapter has reported the establishment of an *in vitro* T cell mediated inflammatory disease model that has potentials to provide a more physiologically relevant replacement for animal testing. Also, it will aid studies aimed at examining the efficacy and safety of novel treatments.

6 Chapter six: General discussion, conclusion and future work

6.1 General discussion

Immune mechanisms in health and disease are a sophisticated and well organised series of events involving feedback loops and cellular cross talks. Designing an *in vitro* immune disease model requires deep understanding, careful planning and integration of key events involving multiple cell types. By producing a thorough review of the literature on the immune mechanisms of OLP (El-Howati *et al.*, 2022), this thesis first sought to identify the key areas of OLP pathogenesis that would be required to be reproduced *in vitro* to form the basis of an inflammatory model indicative of what is seen *in vivo*. The OLP inflammatory model generated was developed in stages. The first stage aimed to isolate and characterise, in culture, the main immune components involved in OLP. Secondly, to incorporate those immune components within an OME model at defined time points. Finally, inducing the combined full model with stimuli to direct the immune response towards an OLP-like inflammatory response.

Basic cell culture conditions and cellular behaviour needed to be defined and optimised before combining them into a complex 3D construct. This vigorous characterisation aimed to facilitate analysis of the complex immune model when fully combined and aid its reproducibility. In Chapter three methodologies on cell culture, proliferation, activation and the ability of immune cells to survive in a 3D environment were explored, developed and mastered for later use on primary T cells. For example, knowledge that the viability of T cells, when initially cultured in 3D collagen hydrogels dropped, only to recover after day 7 of culture, saved time in later experiments when the T cell-containing model was being established. The glucocorticoid, hydrocortisone, is often added to supplement keratinocyte growth medium as it enhances the growth of keratinocytes (Rheinwald and Green, 1975b), however, it is also well known for its anti-inflammatory and immuno-suppressive effects (Hench *et al.*, 1950; Olnes *et al.*, 2016). Hence, both T cells and keratinocytes were adapted to be cultured in Green's medium without hydrocortisone. Attention to culture medium has not been accounted for in previous studies where T cells were abruptly transferred into the skin equivalent medium that contained hydrocortisone, which presumably would dampen any immune response observed in these models (Kühbacher *et al.*, 2017a; Shin *et al.*, 2020; Van Den Bogaard *et al.*, 2014).

The results of chapter four demonstrated that Th1, Th17 phenotypes, and cytotoxic CD8+ T cells were successfully developed and characterised *in vitro*. Moreover, their ability to secret inflammatory cytokines important for the OLP pathogenesis such as IFN-γ, IL-17, and Granzyme B, was established. Said et al, added Jurkat T cells to OME medium to replicate OLP but their model did not fully replicate the Th1 phenotype that dominates in OLP, or the other T cell subsets such as CD8+ T cells present in these lesions (Said *et al.*, 2021). Th1 and Th17 subsets and their cytokines are also strongly associated with psoriasis pathology. Therefore, studies that reported the reproduction of psoriatic skin model equivalents have incorporated Th1 and Th17 polarised T cells within their models and demonstrated that they can skew the inflammatory response towards a psoriasis like response (Van Den Bogaard *et al.*, 2014; Lorthois *et al.*, 2019; Shin *et al.*, 2020). None of the above studies incorporated CD8+ T cells along with the Th1 or Th17 phenotypes. A study investigating the crosstalk between tongue carcinoma cells, extracellular vesicles, and immune cells in 3D models incorporated only natural killers and CD8+ T cells (Al-Samadi *et al.*, 2017). For an optimum immune response, coculture of CD8+ and CD4+ T cells is necessary to establish the cross talk between these cells. The activation of CD4+ T cells after encountering an antigen stimulates the production of IL-2 and IFN-Y. These cytokines stimulate CD8+ cells to release TNF-α which is perceived as a confirmation signal from the CD4+ cells for the CD8+ cells to proceed with keratinocyte basal cells lysis. Hence, the lack of this cross talk may undermine further analysis and interpretation of the immune response replicated in 3D *in vitro* models.

Chapter five then demonstrates the strategy followed to combine primed CD4+ and CD8+ T cells with a 3D OME to establish a full thickness inflammatory disease model of OLP. First, a characterised and reproducible OME formed using FNB6 and NOF was constructed as reported previously (Colley *et al.*, 2013; Jennings *et al.*, 2016). In accordance, OME based on immortalised FNB6 cells were able to mimic the native oral mucosa structure and replicate tissue responses to inflammatory mediators.

OLP is initially provoked through the exposure of the epithelium to an unknown antigen that activates DC/LC to secrete pro-inflammatory cytokines such as TNF-α and migrate to the local lymph nodes to activate antigen-specific T cells (Odell, 2017). Antigen-specific activation of T cells was not possible in the *in vitro* model as the exact antigen causing OLP is unknown, therefore, artificial stimulation using CD3/CD28 beads is the option when the antigens are unknown and replace the need for DCs (Shi *et al.*, 2013). Also, to substitute the role of DCs and macrophages in stimulating the oral mucosa through their cytokines secretion, the OME were stimulated with IFN-γ and TNF-α. T cell

migration from the circulation, through the endothelium and into lesional tissue in OLP is directed by chemokine gradients produced by IFN-γ and TNF-α-activated immune and non-immune lesional cells and increased expression of CD54 on the surface of oral keratinocytes that facilitate leukocyte migration through the epithelium (Little *et al.*, 2003b). Upon stimulation, keratinocyte and fibroblasts were reported to be able to modulate the immune response through activation of downstream signalling cascades and production of chemokines and cytokines (Coates, Blanchard and MacLeod, 2018; Miller and Modlin, 2007; Kühbacher *et al.*, 2017b; Kühbacher *et al.*, 2017a). In agreement, the results of a cytokine array performed in this study on conditioned medium from the IFN-γ and TNF-α stimulated OME show increased expression of key T cell-specific chemokines such as CCL5, CXCL9 and CXCL10. Moreover, this conditioned medium caused directional migration of T cells in a chemotaxis assay, suggesting that these and potentially other chemokines can attract T cells to the epithelium in a 3D model.

Finally, a full thickness tissue engineered T cell inflammatory disease model of OLP was constructed following a protocol based on the results reported in this study. Critical points key to the production of a successful and reproducible disease model of OLP are: development of a fully differentiated normal OME; cell culture in Green's medium without hydrocortisone, especially critical for Th1 and cytotoxic CD8 T cells to allow optimum viability before coculture; use of high numbers of T cells to simulate the dense T cell population in OLP; stimulation of the model with IFN-γ and TNF-α two days following addition of the T cell-containing hydrogel. Embedding immune T cells into the 3D construct is important criteria as it demonstrates physiological relevance to *in vivo* conditions and prevents cell loss into the medium.

The key pathogenic features of T cell inflammatory disease and more specifically OLP were reproduced in our model. First, coculture the OME with the T cell-containing hydrogel resulted in the destruction of the basement membrane evidenced by faint PAS stain and interrupted expression of laminin and integrin α6β4 which were also reported in OLP (Juneja *et al.*, 2006; Schreurs *et al.*, 2020; Hirota, Yoneda and Osaki, 1989). Also, basal cell apoptosis, a characteristic feature of OLP, was observed with positive cleaved caspase-3 staining (Mattila and Syrjänen, 2010). Similar to OLP, T cells migration into the subepithelial area and intra-epithelial infiltration was evident with H&E and IHC staining for anti-CD4 and anti-CD8 surface markers. Although basal cell apoptosis was noticed at day-10 before the stimulation, T cell migration was mainly detected following stimulation of the OME. This supports the findings of Bogaard et al, who although did not add T cells into their 3D constructs, added the cells as a suspension beneath skin equivalents, and

reported that no direct contact between the keratinocytes and T cells was needed as soluble factors produced by these cells were enough to establish a psoriasis phenotype (Van Den Bogaard *et al.*, 2014). However, they also reported a lack of psoriatic epidermal morphology in their model. This agrees also with Discoid and systemic lupus erythematosus where inflammation is peri-vascular but epithelial response is similar to OLP.

Although the models were stimulated at a single time point, the inflammatory cycle continued and progressed until day 25 of ALI where the disease model was observed to be completely damaged with complete loss of structural integrity. CCL5, CXCL9 and CXCL10 levels were shown to have sustained elevation until day 25 of ALI which suggest the development of a positive feedback loop of inflammatory events that are likely to perpetuate disease and directly relate to the chronicity that is frequently observed in the more severe forms of OLP. The role of both these axes in the chronicity of OLP has previously been reported (Iijima *et al.*, 2003; Ichimura *et al.*, 2006). However, the regulatory components responsible for controlling the disease or protecion in the body such as Treg cells or the balance to Th1 produced by Th2. This may also explain the degree of severity exist in this model.

An exact *in vitro* replica of OLP may prove to be difficult due to the anonymity of the causative antigen and the variable presentation of the disease, which is considered a characteristic feature for OLP. Hence, a fundamental question for this research may arise; which OLP subtype should the *in vitro* model in this research replicate? An easy answer is that it depends on the purpose of reproducing the model. For example, to investigate the pathogenesis of the disease, different types, reticular and erosive subtypes mainly, may be aimed for. Then again, for drug therapeutic development and testing, the symptomatic atrophic/ erosive form of OLP that usually require treatment should be reproduced and used for testing.

The imbalance in the immune mechanism may be responsible for the different clinical subtypes of OLP. It has been suggested that an imbalance between the dominance of Th1, Th17, Treg and Th2 may underlie the degree of cytotoxic activity in the disease which subsequently explains the presence of different clinical variants of OLP. For instance, the role of Th17, Th17/Th1, or Th1, has been connected to the symptomatic subtype of OLP which drive potent inflammatory cytokines and cause more damage to the epithelium and this was attributed to cause the erosive OLP, whereas if the immune imbalance has favoured Th2 and T regulatory T subtypes, which are in

dichotomous relationship with Th1 and Th17, respectively, quiescence of potent inflammatory events will follow and inhibition of the disease activity that may subsequently lead to quiescence of the disease or reticular/ asymptomatic OLP. The amount of damage shown in this model in the epithelium and basement membrane is more severe than active forms of OLP in the clinic which could be attributed to imbalance that favoured aggressive Th1 and CD8 responses. There is also the potential unwanted allogenic response produced by the different cell donors or the rat tail collagen.

This study represents a significant step forward in modelling T cell inflammatory oral mucosal diseases. Yet, it can still be redefined further. Other OLP related immune cells such as mast cells and DCs could be incorporated to improve the immunological relevance. Also, the use of patient-derived keratinocytes and T cells or tissue resident T cells would be a valuable application of this model through limiting the bias induced by allogenic cells.

6.2 General conclusion

Herein, it is shown that T cell inflammatory oral mucosal equivalent is a novel model to reflect some of the key characteristics associated with OLP. This model represents a new and innovative replacement that bridges the gap between 2D cultures and animal models. Conditions associated with this model system, mainly the immune element, were highly defined, and contributed to the quality and reproducibility of this model. This novel preclinical disease model has great potential to probe for molecular mechanisms of disease and as a platform to test for novel therapeutics and modes of treatment.

6.3 Future work

This T cell inflammatory disease model of the oral mucosa could provide a new approach to enhance the fundamental understanding of complex disease processes and to enable more rapid, accurate, cost-effective and clinically relevant testing of drugs. Several approaches to replicate different immune mediated diseases of the oral mucosa can be built on the foundation established here.

6.3.1 The T cell inflammatory disease model could be adapted further to create a highly complex specific disease model

The more complete the immune model are, the less chances that key biological elements are missing, which increases the likelihood that these models are more representative of the *in vivo* situation. It is paramount to add more disease relevant cells, especially immune cells, thereby increasing the biological relevance of the models in order to enable their application into drug development. However, it is also important to understand that with added complexity comes more challenges regarding reproducibility, quality, cost, analysis and interpretation. Therefore, it is necessary to create or use models that are as simple as possible, yet as complex as necessary (Alepee *et al.*, 2014).

There is scarcity in studies that have investigated immune oral mucosal equivalents development despite the increasing need to develop novel therapeutic strategies for oral mucosal diseases. Most of the immune oral models developed are still a simple approach containing only one type of immune cells. These include incorporation of PBMCs in a gingival model (Tschachojan *et al.*, 2014), MDM in an oral buccal mucosa model (Ollington, Colley and Murdoch, 2021), polymorphonuclear leukocytes incorporated into reconstructed human oral epithelium to assess defence against fungal infection (Schaller *et al.*, 2004) and CD8 to assess the effects on tongue carcinoma (Al-Samadi *et al.*, 2017). There are no reports of a full oral mucosal model that incorporates T cells under defined conditions to replicate an immune disease. Although dendritic cells were substituted by addition of their related cytokines, their presence in the model may highlight early events in the pathogenesis that can be targeted. Models utilising dendritic cell line have been previously developed. These include models incorporating LCs generated from the MUTZ-3 cell line (MUTZ-LC) which were reported to provide a suitable test system to evaluate early events during skin sensitisation in comparison to primary monocytes (Bock *et al.*, 2018). MUTZ-LC were reported to display a similar phenotypic plasticity as their primary counterparts when incorporated into a skin equivalent model (Kosten *et al.*, 2015).

Mast cells are reported to work in concert with T cells in the pathogenesis of OLP through secretion of TNF-α and CCL5, which act with the chemokines secreted by keratinocytes to perpetuate the disease progression and cause chronicity of OLP (Zhao *et al.*, 2002; Shan *et al.*, 2019). Although mast cells are difficult to isolate from primary tissue, cell lines are available and so their use could add to the model created in this study.

To overcome the issues of the limited lifespan and inter-individual variability associated with using primary cells, cell lines could be used. The T cell line, Jurkat, was used to assess skin defences against fungal infection (Kühbacher *et al.*, 2017b). Moreover, a gingival model containing the monocyte cell lines, U937, showed high inflammatory response to LPS while reduced inflammation following treatment application (Morin and Grenier, 2017). Nevertheless, there are concerns regarding using immune cell lines due to their changed phenotype and reduced efficacy, which may deem them not representative of the *in vivo* environment. For instance, the THP-1 monocyte cell line, showed reduced responses to activation and inflammatory stimuli when compared to human monocyte-derived macrophages (MDMs) and although they responded to polarisation protocols, their responses, to some extent, vary from the primary macrophages (Tedesco *et al.*, 2018).

Building a highly specific autologous model is another approach as to how this model could be taken forward. This will remove any bias that might been produced by unwanted allogenic immune reactions between cells of different donors or cell lines and replicate the specificity of the disease. The immune system differs from person to person based on both genetic and epigenetic factors, and as a consequence requires large sample sizes to be able to draw conclusions. Although a major advantage of such model is the specificity to the disease, it suffers from variability which may affect reproducibility. Additionally, obtaining epithelial, fibroblast and immune cells from the same donor might not be feasible.

Therefore, patient-specific induced pluripotent stem cells (iPSCs) could serve as valuable source of cells that could be employed in unlimited disease models without ethical concerns or the immune barrier. These cells have capacity for self-renewal and to differentiate into any somatic cell type (Takahashi *et al.*, 2007). Models based on iPSCs could help to understand disease pathophysiology, drug toxicity testing, and might even enable personalised therapies in future tailored to patients' conditions and genetic make-up. iPSCs have been used widely to produce intestinal, lung, hepatic and myocardial tissues (Liu *et al.*, 2018). iPSCs have been used to produce skin models (van den Broek *et al.*, 2017) and were reported to can be differentiated into several types of immune cells including T cells (Lei *et al.*, 2009).

Moreover, it was suggested that isolating and immortalising primary patients' cells could be a valid option to create an autologous model system. For instance, an *in vitro* 2D culture system for OLP based on primary keratinocytes isolated from 48 patients were

optimised and shown to mimic the local inflammatory environment of OLP (Cao *et al.*, 2017). Also, keratinocytes from dermal lichen planus were immortalised by transfection with the E6 and E7 genes from human papillomavirus 16 (HPV16) to create a lichen planus keratinocyte cell line and lesional skin T cells from lichen planus and normal skin were isolated and cloned. When cultured together in a simple 2D co-culture, lesional T cell line was reported to be more cytotoxic to autologous keratinocytes than normal skin keratinocytes (Sugerman, Satterwhite and Bigby, 2000). In future, developing a 3D model composed of autologous immortalised lesional T cells, oral fibroblasts and oral keratinocytes or from differentiated iPSC from an OLP patient may be relevant in immunopharmacology studies and drug screening programs. Henceforth, such 3D culture system could be adapted for other cell types including cells obtained from different oral mucosal diseases such as pemphigus and recurrent aphthous stomatitis.

6.3.2 T cell disease model could be used as preclinical drug testing

Although different forms of drugs and protocols have been used to treat OLP, there is no consensus on one formula being more effective than another. Research into the efficacy of topical treatments is hampered by the lack of adherence to the oral mucosa (Lavanya *et al.*, 2011). A new drug dosage form involving mucoadhesive polymer-based patches pre-loaded with corticosteroid has just completed phase IIb clinical trials (Brennan *et al.*, 2022). These patches adhere for long periods to the oral mucosa and offer drug delivery directly to the lesion over a number of hours. Patch-delivered clobetasol-17-propionate has been shown to traverse the epithelium and inhibit T cell cytokine production in an elementary model of OLP using tissue engineered oral mucosa and activated T cells added in medium (Colley *et al.*, 2018; Said *et al.*, 2021). Although barrier properties of the tissue would need to be established and compared to normal oral tissue, *in vitro* oral mucosal model offers an alternative approach for studies of local and systemic trans-mucosal drug delivery as well as a means for the testing of factors that may be important in the pathogenesis of oral diseases (Selvaratnam *et al.*, 2001; Moharamzadeh *et al.*, 2009; Edmans *et al.*, 2020). The T cell inflammatory disease model developed here provides a platform close to the *in vivo* OLP situation which is imperative to recapitulate complex pharmacokinetics and pharmacodynamics necessary for drug testing. Further investigations into drug delivery testing using *in vitro* complex immune models are indispensable for drug development.

Bibliography

Abraham, R. T. and Weiss, A. (2004) 'Jurkat T cells and development of the T-cell receptor signalling paradigm', *Nature Reviews Immunology,* 4(4), pp. 301.

Abusleme, L. and Moutsopoulos, N. M. (2017) 'IL-17: overview and role in oral immunity and microbiome', *Oral diseases,* 23(7), pp. 854-865.

Adan, A., Kiraz, Y. and Baran, Y. (2016) 'Cell proliferation and cytotoxicity assays', *Current pharmaceutical biotechnology,* 17(14), pp. 1213-1221.

Ahmed, M., Basheer, H. A., Ayuso, J. M., Ahmet, D., Mazzini, M., Patel, R., Shnyder, S. D., Vinader, V. and Afarinkia, K. (2017) 'Agarose spot as a comparative method for in situ analysis of simultaneous chemotactic responses to multiple chemokines', *Scientific reports,* 7(1), pp. 1-11.

Aksoy, B. A., Aksoy, P., Wyatt, M., Paulos, C. and Hammerbacher, J. (2018) 'Human primary T cells: A practical guide', *PeerJ Preprints,* 6, pp. e26993v1.

Al-Hashimi, I., Schifter, M., Lockhart, P. B., Wray, D., Brennan, M., Migliorati, C. A., Axéll, T., Bruce, A. J., Carpenter, W. and Eisenberg, E. (2007) 'Oral lichen planus and oral lichenoid lesions: diagnostic and therapeutic considerations', *Oral Surgery, Oral Medicine, Oral Pathology, Oral Radiology, and Endodontology,* 103, pp. S25. e1-S25. e12.

Al-Samadi, A., Awad, S. A., Tuomainen, K., Zhao, Y., Salem, A., Parikka, M. and Salo, T. (2017) 'Crosstalk between tongue carcinoma cells, extracellular vesicles, and immune cells in in vitro and in vivo models', *Oncotarget,* 8(36), pp. 60123.

Alaizari, N., Al-Maweri, S., Al-Shamiri, H., Tarakji, B. and Shugaa-Addin, B. (2016) 'Hepatitis C virus infections in oral lichen planus: A systematic review and meta-analysis', *Australian Dental Journal,* 61(3), pp. 282-287.

Alepee, N., Bahinski, A., Daneshian, M., De Wever, B., Fritsche, E., Goldberg, A., Hansmann, J., Hartung, T., Haycock, J. and Hogberg, H. T. (2014) 't4 workshop report: State-of-the-art of 3D cultures (organs-on-a-chip) in safety testing and pathophysiology', *Altex,* 31(4), pp. 441.

Amin, N. R., Yussif, N. and Ahmed, E. (2020) 'The effect of smoking on clinical presentation and expression of TLR-2 and CD34 in Oral lichen Planus patients: clinical and immunohistochemical study', *BMC oral health,* 20(1), pp. 1-7.

Amr, E. M., Hussine, A. A., Mostafa, R. W. and Shaker, O. G. (2018) 'Evaluation of the role of YKL-40 and interleukin-8 (IL-8) as biomarkers for malignant transformation in oral lichen planus', *Egyptian Dental Journal,* 64(2-April (Oral Medicine, X-Ray, Oral Biology & Oral Pathology)), pp. 1353-1364.

Amsen, D., Spilianakis, C. G. and Flavell, R. A. (2009) 'How are TH1 and TH2 effector cells made?', *Current opinion in immunology,* 21(2), pp. 153-160.

Anitua, E., Piñas, L. and Alkhraisat, M. H. (2019) 'Histopathological features of oral lichen planus and its response to corticosteroid therapy: A retrospective study', *Medicine,* 98(51).

Annunziato, F., Cosmi, L., Liotta, F., Maggi, E. and Romagnani, S. (2012) 'Defining the human T helper 17 cell phenotype', *Trends in immunology,* 33(10), pp. 505-512.

Annunziato, F., Cosmi, L., Santarlasci, V., Maggi, L., Liotta, F., Mazzinghi, B., Parente, E., Filì, L., Ferri, S. and Frosali, F. (2007a) 'Phenotypic and functional features of human Th17 cells', *Journal of Experimental Medicine,* 204(8), pp. 1849-1861.

Annunziato, F., Cosmi, L., Santarlasci, V., Maggi, L., Liotta, F., Mazzinghi, B., Parente, E., Filì, L., Ferri, S. and Frosali, F. (2007b) 'Phenotypic and functional features of human Th17 cells', *The Journal of experimental medicine,* 204(8), pp. 1849-1861.

Ansel, J., Perry, P., Brown, J., Damm, D., Phan, T., Hart, C., Luger, T. and Hefeneider, S. (1990) 'Cytokine modulation of keratinocyte cytokines', *Journal of Investigative Dermatology,* 94(6), pp. s101-s107.

Aragane, Y., Riemann, H., Bhardwaj, R. S., Schwarz, A., Sawada, Y., Yamada, H., Luger, T. A., Kubin, M., Trinchieri, G. and Schwarz, T. (1994) 'IL-12 is expressed and released by human keratinocytes and epidermoid carcinoma cell lines', *The Journal of Immunology,* 153(12), pp. 5366-5372.

Arango Duque, G. and Descoteaux, A. (2014) 'Macrophage cytokines: involvement in immunity and infectious diseases', *Frontiers in immunology,* 5, pp. 491.

Asarch, A., Gottlieb, A. B., Lee, J., Masterpol, K. S., Scheinman, P. L., Stadecker, M. J., Massarotti, E. M. and Bush, M. L. (2009) 'Lichen planus–like eruptions: An emerging side effect of tumor necrosis factor-α antagonists', *Journal of the American Academy of Dermatology,* 61(1), pp. 104-111.

Ashraf, S., Al-Maweri, S. A., Alaizari, N., Umair, A., Ariffin, Z., Alhajj, M. N., Kassim, S. and Awan, K. H. (2020) 'The association between Epstein-Barr virus and oral lichen planus: A systematic review and meta-analysis', *Journal of Oral Pathology & Medicine,* 49(10), pp. 969-976.

Azukizawa, H., Kosaka, H., Sano, S., Heath, W. R., Takahashi, I., Gao, X. H., Sumikawa, Y., Okabe, M., Yoshikawa, K. and Itami, S. (2003) 'Induction of T-cell-mediated skin disease specific for antigen transgenically expressed in keratinocytes', *European journal of immunology,* 33(7), pp. 1879-1888.

Baek, K. and Choi, Y. (2018) 'The microbiology of oral lichen planus: Is microbial infection the cause of oral lichen planus?', *Molecular oral microbiology,* 33(1), pp. 22-28.

Baek, K., Lee, J., Lee, A., Lee, J., Yoon, H.-J., Park, H. K., Chun, J. and Choi, Y. (2020) 'Characterization of intratissue bacterial communities and isolation of Escherichia coli from oral lichen planus lesions', *Scientific reports,* 10(1), pp. 1-11.

Bao, K., Papadimitropoulos, A., Akgül, B., Belibasakis, G. N. and Bostanci, N. (2015) 'Establishment of an oral infection model resembling the periodontal pocket in a perfusion bioreactor system', *Virulence,* 6(3), pp. 265-273.

Baran, J., Kowalczyk, D., Oz˙ óg, M. and Zembala, M. (2001) 'Three-color flow cytometry detection of intracellular cytokines in peripheral blood mononuclear cells: comparative analysis of phorbol myristate acetate-ionomycin and phytohemagglutinin stimulation', *Clinical Diagnostic Laboratory Immunology,* 8(2), pp. 303-313.

Barker, J., Sarma, V., Mitra, R. S., Dixit, V. and Nickoloff, B. J. (1990) 'Marked synergism between tumor necrosis factor-alpha and interferon-gamma in regulation of keratinocyte-derived adhesion molecules and chemotactic factors', *The Journal of clinical investigation,* 85(2), pp. 605-608.

Barrett, A., Cruchley, A. and Williams, D. (1996) 'Oral mucosal Langerhans' cells', *Critical Reviews in Oral Biology & Medicine,* 7(1), pp. 36-58.

Barrett, K. L., Willingham, J. M., Garvin, A. J. and Willingham, M. C. (2001) 'Advances in cytochemical methods for detection of apoptosis', *Journal of Histochemistry & Cytochemistry,* 49(7), pp. 821-832.

Bechetoille, N., Dezutter-Dambuyant, C., Damour, O., André, V., Orly, I. and Perrier, E. (2007) 'Effects of solar ultraviolet radiation on engineered human skin equivalent containing both Langerhans cells and dermal dendritic cells', *Tissue engineering,* 13(11), pp. 2667-2679.

Bechetoille, N., Vachon, H., Gaydon, A., Boher, A., Fontaine, T., Schaeffer, E., Decossas, M., André-Frei, V. and Mueller, C. G. (2011) 'A new organotypic model containing dermal-type macrophages', *Experimental dermatology,* 20(12), pp. 1035-1037.

Bell, E., Ivarsson, B. and Merrill, C. (1979) 'Production of a tissue-like structure by contraction of collagen lattices by human fibroblasts of different proliferative potential in vitro', *Proceedings of the National Academy of Sciences,* 76(3), pp. 1274-1278.

Benowitz, N. L. and Burbank, A. D. (2016) 'Cardiovascular toxicity of nicotine: implications for electronic cigarette use', *Trends in cardiovascular medicine,* 26(6), pp. 515-523.

Berthiaume, F., Maguire, T. J. and Yarmush, M. L. (2011) 'Tissue engineering and regenerative medicine: history, progress, and challenges', *Annual review of chemical and biomolecular engineering,* 2, pp. 403-430.

Bettelli, E., Carrier, Y., Gao, W., Korn, T., Strom, T. B., Oukka, M., Weiner, H. L. and Kuchroo, V. K. (2006) 'Reciprocal developmental pathways for the generation of pathogenic effector TH17 and regulatory T cells', *Nature,* 441(7090), pp. 235-238.

Beyersdorf, N., Gaupp, S., Balbach, K., Schmidt, J., Toyka, K. V., Lin, C.-H., Hanke, T., Hünig, T., Kerkau, T. and Gold, R. (2005) 'Selective targeting of regulatory T cells with CD28 superagonists allows effective therapy of experimental autoimmune encephalomyelitis', *The Journal of experimental medicine,* 202(3), pp. 445-455.

Black, A. F., Berthod, F., L'Heureux, N., Germain, L. and Auger, F. A. (1998) 'In vitro reconstruction of a human capillary-like network in a tissue-engineered skin equivalent', *The FASEB journal,* 12(13), pp. 1331-1340.

Bock, S., Said, A., Müller, G., Schäfer-Korting, M., Zoschke, C. and Weindl, G. (2018) 'Characterization of reconstructed human skin containing Langerhans cells to monitor molecular events in skin sensitization', *Toxicology in Vitro,* 46, pp. 77-85.

Boelsma, E., Gibbs, S., Faller, C. and Ponec, M. (2000) 'Characterization and comparison of reconstructed skin models: morphological and immunohistochemical evaluation'.

Bolandi, Z., Mokhberian, N., Eftekhary, M., Sharifi, K., Soudi, S., Ghanbarian, H. and Hashemi, S. M. (2020) 'Adipose derived mesenchymal stem cell exosomes loaded with miR-10a promote the differentiation of Th17 and Treg from naive CD4+ T cell', *Life Sciences,* 259, pp. 118218.

Bonecchi, R., Bianchi, G., Bordignon, P. P., D'Ambrosio, D., Lang, R., Borsatti, A., Sozzani, S., Allavena, P., Gray, P. A. and Mantovani, A. (1998) 'Differential expression of chemokine receptors and chemotactic responsiveness of type 1 T helper cells (Th1s) and Th2s', *The Journal of experimental medicine,* 187(1), pp. 129-134.

Boniface, K., Bernard, F.-X., Garcia, M., Gurney, A. L., Lecron, J.-C. and Morel, F. (2005) 'IL-22 inhibits epidermal differentiation and induces proinflammatory gene expression and migration of human keratinocytes', *The Journal of Immunology,* 174(6), pp. 3695-3702.

Bornstein, M. M., Hakimi, B. and Persson, G. R. (2008) 'Microbiological findings in subjects with asymptomatic oral lichen planus: A cross-sectional comparative study', *Journal of periodontology,* 79(12), pp. 2347-2355.

Brand, S. (2009) 'Crohn's disease: Th1, Th17 or both? The change of a paradigm: new immunological and genetic insights implicate Th17 cells in the pathogenesis of Crohn's disease', *Gut,* 58(8), pp. 1152-1167.

Bray, C., Wright, D., Haupt, S., Thomas, S., Stauss, H. J. and Zamoyska, R. (2018) 'Crispr/Cas mediated deletion of PTPN22 in Jurkat T cells enhances TCR signaling and production of IL-2', *Frontiers in Immunology,* 9, pp. 2595.

Brennan, M. T., Madsen, L. S., Saunders, D. P., Napenas, J. J., McCreary, C., Ni Riordain, R., Pedersen, A. M. L., Fedele, S., Cook, R. J. and Abdelsayed, R. (2022) 'Efficacy and safety of a novel mucoadhesive clobetasol patch for treatment of erosive oral lichen planus: A phase 2 randomized clinical trial', *Journal of Oral Pathology & Medicine,* 51(1), pp. 86-97.

Butz, E. A. and Bevan, M. J. (1998) 'Massive expansion of antigen-specific CD8+ T cells during an acute virus infection', *Immunity,* 8(2), pp. 167-175.

Canto, A. M., Muller, H., Freitas, R. R. and Santos, P. S. (2010) 'Oral lichen planus (OLP): clinical and complementary diagnosis', *An Bras Dermatol,* 85(5), pp. 669-75.

Cao, T., Zhang, H., Zhou, L., Wang, Y., Du, G., Yao, H., Luo, Q., Chen, F. and Wang, W. (2017) 'In vitro cell culture system optimization of keratinocytes from oral lichen planus (OLP) patients', *Oral Diseases,* 23(2), pp. 225-232.

Carrozzo, M., Porter, S., Mercadante, V. and Fedele, S. (2019) 'Oral lichen planus: A disease or a spectrum of tissue reactions? Types, causes, diagnostic algorhythms, prognosis, management strategies', *Periodontology 2000,* 80(1), pp. 105-125.

Castells-Sala, C., Alemany-Ribes, M., Fernández-Muiños, T., Recha-Sancho, L., López-Chicón, P., Aloy-Reverté, C., Caballero-Camino, J., Márquez-Gil, A. and Semino, C. E. (2013) 'Current applications of tissue engineering in biomedicine', *Journal of Biochips & Tissue Chips,* (S2), pp. 1.

Chakraverty, R., Côté, D., Buchli, J., Cotter, P., Hsu, R., Zhao, G., Sachs, T., Pitsillides, C. M., Bronson, R. and Means, T. (2006) 'An inflammatory checkpoint regulates recruitment of graft-versus-host reactive T cells to peripheral tissues', *The Journal of experimental medicine,* 203(8), pp. 2021-2031.

Chaplin, D. D. (2010) 'Overview of the immune response', *Journal of allergy and clinical immunology,* 125(2), pp. S3-S23.

Chatila, T., Silverman, L., Miller, R. and Geha, R. (1989) 'Mechanisms of T cell activation by the calcium ionophore ionomycin', *The Journal of Immunology,* 143(4), pp. 1283-1289.

Chattopadhyay, P. K., Melenhorst, J. J., Ladell, K., Gostick, E., Scheinberg, P., Barrett, A. J., Wooldridge, L., Roederer, M., Sewell, A. K. and Price, D. A. (2008) 'Techniques to improve the direct ex vivo detection of low frequency antigen-specific CD8+ T cells with peptide-major histocompatibility complex class I tetramers', *Cytometry Part A,* 73(11), pp. 1001-1009.

Chen, A., Lee, S.-M., Gao, B., Shannon, S., Zhu, Z. and Fang, D. (2011) 'c-Abl-mediated tyrosine phosphorylation of the T-bet DNA-binding domain regulates CD4+ T-cell differentiation and allergic lung inflammation', *Molecular and cellular biology,* 31(16), pp. 3445-3456.

Chen, H.-C. (2005) 'Boyden chamber assay', *Cell migration*: Springer, pp. 15-22.

Chen, J., Feng, J., Chen, X., Xu, H., Zhou, Z., Shen, X., Bao, Z., Liu, W. and Shen, Z. (2013) 'Immunoexpression of interleukin-22 and interleukin-23 in oral and cutaneous lichen planus lesions: a preliminary study', *Mediators of Inflammation,* 2013.

Choi, Y. S., Kim, Y., Yoon, H.-J., Baek, K. J., Alam, J., Park, H. K. and Choi, Y. (2016) 'The presence of bacteria within tissue provides insights into the pathogenesis of oral lichen planus', *Scientific reports,* 6(1), pp. 1-13.

Chometon, T. Q., Siqueira, M. d. S., Sant´ anna, J. C., Almeida, M. R., Gandini, M., Martins de Almeida Nogueira, A. C. and Antas, P. R. Z. (2020) 'A protocol for rapid monocyte isolation and generation of singular human monocyte-derived dendritic cells', *PloS one,* 15(4), pp. e0231132.

Christofidou-Solomidou, M., Albelda, S. M., Bennett, F. C. and Murphy, G. F. (1997) 'Experimental production and modulation of human cytotoxic dermatitis in human-murine chimeras', *The American journal of pathology,* 150(2), pp. 631.

Chung, S., Kim, S. H., Seo, Y., Kim, S. K. and Lee, J. Y. (2017) 'Quantitative analysis of cell proliferation by a dye dilution assay: application to cell lines and cocultures', *Cytometry Part A,* 91(7), pp. 704-712.

Chung, W. O. and Dale, B. A. (2004) 'Innate immune response of oral and foreskin keratinocytes: utilization of different signaling pathways by various bacterial species', *Infection and immunity,* 72(1), pp. 352-358.

Chung, Y., Chang, S. H., Martinez, G. J., Yang, X. O., Nurieva, R., Kang, H. S., Ma, L., Watowich, S. S., Jetten, A. M. and Tian, Q. (2009) 'Critical regulation of early Th17 cell differentiation by interleukin-1 signaling', *Immunity,* 30(4), pp. 576-587.

Coates, M., Blanchard, S. and MacLeod, A. S. (2018) 'Innate antimicrobial immunity in the skin: A protective barrier against bacteria, viruses, and fungi', *PLoS pathogens,* 14(12), pp. e1007353.

Cohen, G. M. (1997) 'Caspases: the executioners of apoptosis', *Biochemical Journal,* 326(1), pp. 1-16.

Colley, H., Hearnden, V., Jones, A., Weinreb, P., Violette, S., Macneil, S., Thornhill, M. and Murdoch, C. (2011) 'Development of tissue-engineered models of oral dysplasia and early invasive oral squamous cell carcinoma', *British journal of cancer,* 105(10), pp. 1582.

Colley, H. E., Eves, P. C., Pinnock, A., Thornhill, M. H. and Murdoch, C. (2013) 'Tissue-engineered oral mucosa to study radiotherapy-induced oral mucositis', *International journal of radiation biology,* 89(11), pp. 907-914.

Colley, H. E., Said, Z., Santocildes-Romero, M. E., Baker, S. R., D'Apice, K., Hansen, J., Madsen, L. S., Thornhill, M. H., Hatton, P. V. and Murdoch, C. (2018) 'Novel Bilayer Mucoadhesive Patches for Delivery of Clobetasol-17-Propionate to the Oral Mucosa to Treat Oral Lichen Planus; an in Vitro and in Vivo Evaluation', *Oral Surgery, Oral Medicine, Oral Pathology and Oral Radiology,* 126(4), pp. e204.

Collins, L. and Dawes, C. (1987) 'The surface area of the adult human mouth and thickness of the salivary film covering the teeth and oral mucosa', *Journal of dental research,* 66(8), pp. 1300-1302.

Cornish, G. H., Sinclair, L. V. and Cantrell, D. A. (2006) 'Differential regulation of T-cell growth by IL-2 and IL-15', *Blood,* 108(2), pp. 600-608.

Cosmi, L., De Palma, R., Santarlasci, V., Maggi, L., Capone, M., Frosali, F., Rodolico, G., Querci, V., Abbate, G. and Angeli, R. (2008) 'Human interleukin 17–producing cells originate from a CD161+ CD4+ T cell precursor', *The Journal of experimental medicine,* 205(8), pp. 1903-1916.

Cosmi, L., Liotta, F., Maggi, E., Romagnani, S. and Annunziato, F. (2014) 'Th17 and non-classic Th1 cells in chronic inflammatory disorders: two sides of the same coin', *International archives of allergy and immunology,* 164(3), pp. 171-177.

Cossarizza, A., Chang, H. D., Radbruch, A., Akdis, M., Andrä, I., Annunziato, F., Bacher, P., Barnaba, V., Battistini, L. and Bauer, W. M. (2017) 'Guidelines for the use of flow cytometry and cell sorting in immunological studies', *European journal of immunology,* 47(10), pp. 1584-1797.

Costea, D. E., Johannessen, A. C. and Vintermyr, O. K. (2005) 'Fibroblast control on epithelial differentiation is gradually lost during in vitro tumor progression', *Differentiation,* 73(4), pp. 134-141.

Cox, M. A., Kahan, S. M. and Zajac, A. J. (2013) 'Anti-viral CD8 T cells and the cytokines that they love', *Virology,* 435(1), pp. 157-169.

Crane, I. J. and Forrester, J. V. (2005) 'Th1 and Th2 lymphocytes in autoimmune disease', *Critical Reviews™ in Immunology,* 25(2).

Cronin, S. J. and Penninger, J. M. (2007) 'From T-cell activation signals to signaling control of anti-cancer immunity', *Immunological reviews,* 220(1), pp. 151-168.

Curtsinger, J. M. and Mescher, M. F. (2010) 'Inflammatory cytokines as a third signal for T cell activation', *Current opinion in immunology,* 22(3), pp. 333-340.

Dalili, A., Samiei, E. and Hoorfar, M. (2019) 'A review of sorting, separation and isolation of cells and microbeads for biomedical applications: Microfluidic approaches', *Analyst,* 144(1), pp. 87-113.

De Brugerolle, A. (2007) 'SkinEthic laboratories, a company devoted to develop and produce in vitro alternative methods to the animal use', *ALTEX-Alternatives to animal experimentation,* 24(3), pp. 167-171.

De Wever, B., Petersohn, D. and Mewes, K. R. (2013) 'Overview of human three-dimensional (3D) skin models used for dermal toxicity assessment (Part 1)', *Household and Personal Care Today,* 8(1), pp. 18-22.

DeAngelis, L. M., Cirillo, N. and McCullough, M. J. (2019) 'The immunopathogenesis of oral lichen planus—Is there a role for mucosal associated invariant T cells?', *Journal of Oral Pathology & Medicine,* 48(7), pp. 552-559.

Decani, S., Federighi, V., Baruzzi, E., Sardella, A. and Lodi, G. (2014) 'Iatrogenic Cushing's syndrome and topical steroid therapy: case series and review of the literature', *Journal of Dermatological Treatment,* 25(6), pp. 495-500.

Dekker, N. P., Lozada-Nur, F., Lagenaur, L. A., MacPhail, L. A., Bloom, C. Y. and Regezi, J. A. (1997) 'Apoptosis-associated markers in oral lichen planus', *Journal of oral pathology & medicine,* 26(4), pp. 170-175.

Del Rio, M., Larcher, F., Serrano, F., Meana, A., Muñoz, M., Garcia, M., Muñoz, E., Martin, C., Bernad, A. and Jorcano, J. L. (2002) 'A preclinical model for the analysis of genetically modified human skin in vivo', *Human gene therapy,* 13(8), pp. 959-968.

Dickson, M. A., Hahn, W. C., Ino, Y., Ronfard, V., Wu, J. Y., Weinberg, R. A., Louis, D. N., Li, F. P. and Rheinwald, J. G. (2000) 'Human keratinocytes that express hTERT and also bypass a p16INK4a-enforced mechanism that limits life span become immortal yet retain normal growth and differentiation characteristics', *Molecular and cellular biology,* 20(4), pp. 1436-1447.

Diehn, M., Alizadeh, A. A., Rando, O. J., Liu, C. L., Stankunas, K., Botstein, D., Crabtree, G. R. and Brown, P. O. (2002) 'Genomic expression programs and the integration of the CD28 costimulatory signal in T cell activation', *Proceedings of the National Academy of Sciences,* 99(18), pp. 11796-11801.

Dongari-Bagtzoglou, A. and Kashleva, H. (2006a) 'Development of a highly reproducible three-dimensional organotypic model of the oral mucosa', *Nature protocols,* 1(4), pp. 2012.

Dongari-Bagtzoglou, A. and Kashleva, H. (2006b) 'Development of a novel three-dimensional in vitro model of oral Candida infection', *Microbial pathogenesis,* 40(6), pp. 271-278.

Dubovsky, J. A., Powers, J. J., Gao, Y., Mariusso, L. F., Sotomayor, E. M. and Pinilla-Ibarz, J. A. (2011) 'Epigenetic repolarization of T lymphocytes from chronic lymphocytic leukemia patients using 5-aza-2′-deoxycytidine', *Leukemia research,* 35(9), pp. 1193-1199.

Duhen, T. and Campbell, D. J. (2014) 'IL-1β promotes the differentiation of polyfunctional human CCR6+ CXCR3+ Th1/17 cells that are specific for pathogenic and commensal microbes', *The Journal of Immunology,* 193(1), pp. 120-129.

Dunn, J. C., Chan, W.-Y., Cristini, V., Kim, J., Lowengrub, J., Singh, S. and Wu, B. M. (2006) 'Analysis of cell growth in three-dimensional scaffolds', *Tissue engineering,* 12(4), pp. 705-716.

Dupré, L., Houmadi, R., Tang, C. and Rey-Barroso, J. (2015) 'T lymphocyte migration: an action movie starring the actin and associated actors', *Frontiers in immunology,* 6, pp. 586.

Duval, K., Grover, H., Han, L.-H., Mou, Y., Pegoraro, A. F., Fredberg, J. and Chen, Z. (2017) 'Modeling physiological events in 2D vs. 3D cell culture', *Physiology,* 32(4), pp. 266-277.

Ebrahimi, M., Lundqvist, L., Wahlin, Y. B. and Nylander, E. (2012) 'Mucosal lichen planus, a systemic disease requiring multidisciplinary care: a cross-sectional clinical review from a multidisciplinary perspective', *J Low Genit Tract Dis,* 16(4), pp. 377-80.

Edmans, J. G., Clitherow, K. H., Murdoch, C., Hatton, P. V., Spain, S. G. and Colley, H. E. (2020) 'Mucoadhesive electrospun fibre-based technologies for oral medicine', *Pharmaceutics,* 12(6), pp. 504.

Edwards, P. C. and Kelsch, R. (2002) 'Oral lichen planus: clinical presentation and management', *Journal of Canadian dental association,* 68(8), pp. 494-9.

Ehrmann, R. L. and Gey, G. O. (1956) 'The growth of cells on a transparent gel of reconstituted rat-tail collagen', *Journal of the National Cancer Institute,* 16(6), pp. 1375-1403.

Elsdale, T. and Bard, J. (1972) 'Collagen substrata for studies on cell behavior', *The Journal of cell biology,* 54(3), pp. 626-637.

El-Howati, A., Thornhill, M. H., Colley, H. E. and Murdoch, C. (2022) 'Immune mechanisms in oral lichen planus', *Oral Diseases,* 00, pp. 1-16.

Engelhart, K., El Hindi, T., Biesalski, H.-K. and Pfitzner, I. (2005) 'In vitro reproduction of clinical hallmarks of eczematous dermatitis in organotypic skin models', *Archives of dermatological research,* 297(1), pp. 1-9.

Ertugrul, A. S., Arslan, U., Dursun, R. and Hakki, S. S. (2013) 'Periodontopathogen profile of healthy and oral lichen planus patients with gingivitis or periodontitis', *International journal of oral science,* 5(2), pp. 92-97.

Fang, J., Wang, C., Shen, C., Shan, J., Wang, X., Liu, L. and Fan, Y. (2019) 'The expression of CXCL10/CXCR3 and effect of the axis on the function of T lymphocyte involved in oral lichen planus', *Inflammation,* 42(3), pp. 799-810.

Farhi, D. and Dupin, N. (2010) 'Pathophysiology, etiologic factors, and clinical management of oral lichen planus, part I: facts and controversies', *Clin Dermatol,* 28(1), pp. 100-8.

Farthing, P. and Cruchley, A. (1989) 'Expression of MHC class II antigens (HLA DR, DP and DQ) by keratinocytes in oral lichen planus', *Journal of Oral Pathology & Medicine,* 18(5), pp. 305-309.

Fauci, A. S. and Dale, D. C. (1974) 'The effect of in vivo hydrocortisone on subpopulations of human lymphocytes', *The Journal of Clinical Investigation,* 53(1), pp. 240-246.

Fayyazi, A., Schweyer, S., Soruri, A., Duong, L., Radzun, H., Peters, J., Parwaresch, R. and Berger, H. (1999) 'T lymphocytes and altered keratinocytes express interferon-γ and interleukin 6 in lichen planus', *Archives of Dermatological Research,* 291(9), pp. 485-490.

Ferrisse, T. M., de Oliveira, A. B., Palaçon, M. P., Silva, E. V., Massucato, E. M. S., de Almeida, L. Y., Léon, J. E. and Bufalino, A. (2021) 'The role of CD68+ and CD163+ macrophages in immunopathogenesis of oral lichen planus and oral lichenoid lesions', *Immunobiology,* 226(3), pp. 152072.

Feucht, E., DeSanti, C. and Weinberg, A. (2003) 'Selective induction of human beta-defensin mRNAs by Actinobacillus actinomycetemcomitans in primary and immortalized oral epithelial cells', *Oral microbiology and immunology,* 18(6), pp. 359-363.

Field, A. and Longman, L. (2003) *Tyldesley's oral medicine.* 5th edition edn.: Oxford University Press Oxford.

Filby, A., Begum, J., Jalal, M. and Day, W. (2015) 'Appraising the suitability of succinimidyl and lipophilic fluorescent dyes to track proliferation in non-quiescent cells by dye dilution', *Methods,* 82, pp. 29-37.

Filby, A., Perucha, E., Summers, H., Rees, P., Chana, P., Heck, S., Lord, G. M. and Davies, D. (2011) 'An imaging flow cytometric method for measuring cell division history and molecular symmetry during mitosis', *Cytometry Part A,* 79(7), pp. 496-506.

Finotto, S., Mekori, Y. A. and Metcalfe, D. D. (1997) 'Glucocorticoids decrease tissue mast cell number by reducing the production of the c-kit ligand, stem cell factor, by resident cells: in vitro and in vivo evidence in murine systems', *The Journal of clinical investigation,* 99(7), pp. 1721-1728.

Firestein, G., Roeder, W., Laxer, J., Townsend, K., Weaver, C., Hom, J., Linton, J., Torbett, B. and Glasebrook, A. (1989) 'A new murine CD4+ T cell subset with an unrestricted cytokine profile', *The Journal of Immunology,* 143(2), pp. 518-525.

Flier, J., Boorsma, D. M., van Beek, P. J., Nieboer, C., Stoof, T. J., Willemze, R. and Tensen, C. P. (2001) 'Differential expression of CXCR3 targeting chemokines CXCL10, CXCL9, and CXCL11 in different types of skin inflammation', *The Journal of Pathology: A Journal of the Pathological Society of Great Britain and Ireland,* 194(4), pp. 398-405.

Frasca, L., Piazza, C. and Piccolella, E. (1998) 'CD4+ T cells orchestrate both amplification and deletion of CD8+ T cells', *Critical Reviews™ in Immunology,* 18(6).

Frenea-Robin, M. and Marchalot, J. (2022) 'Basic Principles and Recent Advances in Magnetic Cell Separation', *Magnetochemistry,* 8(1), pp. 11.

Freshney, R. I. (2015) *Culture of animal cells: a manual of basic technique and specialized applications.* John Wiley & Sons.

Gaballah, K., Costea, D., Hills, A., Gollin, S., Harrison, P. and Partridge, M. (2008) 'Tissue engineering of oral dysplasia', *The Journal of Pathology: A Journal of the Pathological Society of Great Britain and Ireland,* 215(3), pp. 280-289.

Gaggioli, C., Hooper, S., Hidalgo-Carcedo, C., Grosse, R., Marshall, J. F., Harrington, K. and Sahai, E. (2007) 'Fibroblast-led collective invasion of carcinoma cells with differing roles for RhoGTPases in leading and following cells', *Nature cell biology,* 9(12), pp. 1392.

Ganjalikhani Hakemi, M., Ghaedi, K., Andalib, A., Hosseini, M. and Rezaei, A. (2011) 'Optimization of human Th17 cell differentiation in vitro: evaluating different polarizing factors', *In Vitro Cellular & Developmental Biology-Animal,* 47(8), pp. 581-592.

Geissmann, F., Manz, M. G., Jung, S., Sieweke, M. H., Merad, M. and Ley, K. (2010) 'Development of monocytes, macrophages, and dendritic cells', *Science,* 327(5966), pp. 656-661.

Gillis, S., Crabtree, G. R. and Smith, K. A. (1979) 'Glucocorticoid-induced inhibition of T cell growth factor production: I. The effect on mitogen-induced lymphocyte proliferation', *The Journal of Immunology,* 123(4), pp. 1624-1631.

Gobet, R., Raghunath, M., Altermatt, S., Meuli-Simmen, C., Benathan, M., Dietl, A. and Meuli, M. (1997) 'Efficacy of cultured epithelial autografts in pediatric burns and reconstructive surgery', *Surgery,* 121(6), pp. 654-661.

Gonzalez-Moles, M. A., Morales, P., Rodriguez-Archilla, A., Isabel, I. R.-A. and Gonzalez-Moles, S. (2002) 'Treatment of severe chronic oral erosive lesions with clobetasol propionate in aqueous solution', *Oral Surgery, Oral Medicine, Oral Pathology, Oral Radiology, and Endodontology,* 93(3), pp. 264-270.

González-Moles, M. Á., Warnakulasuriya, S., González-Ruiz, I., González-Ruiz, L., Ayén, Á., Lenouvel, D., Ruiz-Ávila, I. and Ramos-García, P. (2020) 'Worldwide prevalence of oral lichen planus: A systematic review and meta-analysis', *Oral Diseases,* 27(4), pp. 813-828.

Gouirand, V., Habrylo, I. and Rosenblum, M. D. (2021) 'Regulatory T cells and inflammatory mediators in autoimmune disease', *Journal of Investigative Dermatology,* 142(3), pp. 774-780.

Gown, A. M. and Willingham, M. C. (2002) 'Improved detection of apoptotic cells in archival paraffin sections: immunohistochemistry using antibodies to cleaved caspase 3', *Journal of Histochemistry & Cytochemistry,* 50(4), pp. 449-454.

Grell, M., Zimmermann, G., Gottfried, E., Chen, C. M., Grünwald, U., Huang, D. C., Lee, Y. H. W., Dürkop, H., Engelmann, H. and Scheurich, P. (1999) 'Induction of cell death by tumour necrosis factor (TNF) receptor 2, CD40 and CD30: a role for TNF-R1 activation by endogenous membrane-anchored TNF', *The EMBO journal,* 18(11), pp. 3034-3043.

Griffiths, J. (1971) 'The effect of medium changes on the growth and metabolism of the human diploid cell, W1-38', *Journal of cell science,* 8(1), pp. 43-52.

Griffiths, S. J., Riddell, N. E., Masters, J., Libri, V., Henson, S. M., Wertheimer, A., Wallace, D., Sims, S., Rivino, L. and Larbi, A. (2013) 'Age-associated increase of low-avidity cytomegalovirus-specific CD8+ T cells that re-express CD45RA', *The Journal of Immunology,* 190(11), pp. 5363-5372.

Gronthos, S. and Simmons, P. J. (1995) 'The growth factor requirements of STRO-1-positive human bone marrow stromal precursors under serum-deprived conditions in vitro', *Blood,* 15;85, pp. 929-40.

Groom, J. R. and Luster, A. D. (2011) 'CXCR3 in T cell function', *Experimental cell research,* 317(5), pp. 620-631.

Gross, A., Schoendube, J., Zimmermann, S., Steeb, M., Zengerle, R. and Koltay, P. (2015) 'Technologies for single-cell isolation', *International journal of molecular sciences,* 16(8), pp. 16897-16919.

Grossmann, J. (2002) 'Molecular mechanisms of “detachment-induced apoptosis—Anoikis”', *Apoptosis,* 7(3), pp. 247-260.

Grove, G., Houghton, B., Cochran, J., Kress, E. and Cristofalo, V. (1977) 'Hydrocortisone effects on cell proliferation: specificity of response among various cell types', *Cell biology international reports,* 1(2), pp. 147-155.

Gunzer, M., Weishaupt, C., Planelles, L. and Grabbe, S. (2001) 'Two-step negative enrichment of CD4+ and CD8+ T cells from murine spleen via nylon wool adherence and an optimized antibody cocktail', *Journal of immunological methods,* 258(1-2), pp. 55-63.

Gupta, S. and Jawanda, M. K. (2015) 'Oral lichen planus: an update on etiology, pathogenesis, clinical presentation, diagnosis and management', *Indian journal of dermatology,* 60(3), pp. 222.

Haapalainen, T., Oksala, O., Kallioinen, M., Oikarinen, A., Larjava, H. and Salo, T. (1995) 'Destruction of the epithelial anchoring system in lichen planus', *Journal of investigative dermatology,* 105(1), pp. 100-103.

Hanamsagar, R., Reizis, T., Chamberlain, M., Marcus, R., Nestle, F. O., de Rinaldis, E. and Savova, V. (2020) 'An optimized workflow for single-cell transcriptomics and repertoire profiling of purified lymphocytes from clinical samples', *Scientific reports,* 10(1), pp. 1-15.

Hancock, W. W., Sayegh, M. H., Zheng, X.-G., Peach, R., Linsley, P. S. and Turka, L. A. (1996) 'Costimulatory function and expression of CD40 ligand, CD80, and CD86 in vascularized murine cardiac allograft rejection', *Proceedings of the National Academy of Sciences,* 93(24), pp. 13967-13972.

Hanlon, A. M., Jang, S. and Salgame, P. (2002) 'Signaling from cytokine receptors that affect Th1 responses', *Front Biosci,* 7, pp. d1247-d1254.

Harkness, R. (1961) 'Biological functions of collagen', *Biological Reviews,* 36(4), pp. 399-455.

Hashimoto, K. (1972) 'Fine structure of Merkel cell in human oral mucosa', *Journal of Investigative Dermatology,* 58(6), pp. 381-387.

Hayflick, L. and Moorhead, P. S. (1961) 'The serial cultivation of human diploid cell strains', *Experimental cell research,* 25(3), pp. 585-621.

Hedley, S. J., Layton, C., Heaton, M., Chakrabarty, K. H., Dawson, R. A., Gawkrodger, D. J. and Neil, S. M. (2002) 'Fibroblasts play a regulatory role in the control of pigmentation in reconstructed human skin from skin types I and II', *Pigment cell research,* 15(1), pp. 49-56.

Hegarty, A., Hodgson, T., Lewsey, J. and Porter, S. (2002) 'Fluticasone propionate spray and betamethasone sodium phosphate mouthrinse: a randomized crossover study for the treatment of symptomatic oral lichen planus', *Journal of the American Academy of Dermatology,* 47(2), pp. 271-279.

Hench, P. S., Kendall, E. C., Slocumb, C. H. and Polley, H. F. (1950) 'Effects of cortisone acetate and pituitary ACTH on rheumatoid arthritis, rheumatic fever and certain other conditions: a study in clinical physiology', *Archives of internal medicine,* 85(4), pp. 545-666.

Hiremath, S. K., Kale, A. D. and Charantimath, S. (2011) 'Oral lichenoid lesions: clinico-pathological mimicry and its diagnostic implications', *Indian J Dent Res,* 22(6), pp. 827-34.

Hirota, J., Yoneda, K. and Osaki, T. (1989) 'Destruction of basement membrane and cell infiltrates in oral lichen planus', *Pathology-Research and Practice,* 185(2), pp. 218-224.

Hoang, A. T. N., Chen, P., Juarez, J., Sachamitr, P., Billing, B., Bosnjak, L., Dahlén, B., Coles, M. and Svensson, M. (2012) 'Dendritic cell functional properties in a three-dimensional tissue model of human lung mucosa', *American Journal of Physiology-Lung Cellular and Molecular Physiology,* 302(2), pp. L226-L237.

Hofmann, M. A., Kiecker, F. and Zuberbier, T. (2016) 'A systematic review of the role of interleukin-17 and the interleukin-20 family in inflammatory allergic skin diseases', *Current Opinion in Allergy and Clinical Immunology,* 16(5), pp. 451-457.

Hoogstraate, A. J. and Bodde, H. E. (1993) 'Methods for assessing the buccal mucosa as a route of drug delivery', *Advanced drug delivery reviews,* 12(1-2), pp. 99-125.

Hoque, M. E., Nuge, T., Yeow, T. K., Nordin, N. and Prasad, R. (2015) 'Gelatin based scaffolds for tissue engineering-a review', *Polymers Research Journal,* 9(1), pp. 15.

HOSHI, H., KAN, M., MINAMOTO, Y. and YAMANE, I. (1982) 'Hydrocortisone potentiates cell proliferation and promotes cell spreading on tissue culture substrata of human diploid fibroblasts in a serum-free hormone-supplemented medium', *Biomedical Research,* 3(5), pp. 546-552.

Hu, J.-Y., Zhang, J., Cui, J.-L., Liang, X.-Y., Lu, R., Du, G.-F., Xu, X.-Y. and Zhou, G. (2013) 'Increasing CCL5/CCR5 on CD4+ T cells in peripheral blood of oral lichen planus', *Cytokine,* 62(1), pp. 141-145.

Hu, J.-Y., Zhang, J., Ma, J.-Z., Liang, X.-Y., Chen, G.-Y., Lu, R., Du, G.-F. and Zhou, G. (2015) 'MicroRNA-155-IFN-γ Feedback Loop in CD4+ T Cells of Erosive type Oral Lichen Planus', *Scientific reports,* 5, pp. 16935.

Ichimura, M., Hiratsuka, K., Ogura, N., Utsunomiya, T., Sakamaki, H., Kondoh, T., Abiko, Y., Otake, S. and Yamamoto, M. (2006) 'Expression profile of chemokines and chemokine receptors in epithelial cell layers of oral lichen planus', *Journal of oral pathology & medicine,* 35(3), pp. 167-174.

Igarashi, O., Yamane, H., Imajoh-Ohmi, S. and Nariuchi, H. (1998) 'IL-12 receptor (IL-12R) expression and accumulation of IL-12Rβ1 and IL-12Rβ2 mRNAs in CD4+ T cells by costimulation with B7-2 molecules', *The Journal of Immunology,* 160(4), pp. 1638-1646.

Iijima, W., Ohtani, H., Nakayama, T., Sugawara, Y., Sato, E., Nagura, H., Yoshie, O. and Sasano, T. (2003) 'Infiltrating CD8+ T cells in oral lichen planus predominantly express CCR5 and CXCR3 and carry respective chemokine ligands RANTES/CCL5 and IP-10/CXCL10 in their cytolytic granules: a potential self-recruiting mechanism', *The American journal of pathology,* 163(1), pp. 261-268.

Isaac, C., Rego, F. M., Ladeir, P. R. S. d., Altram, S. C., Oliveira, R. C. d., Aldunate, J. L., Paggiaro, A. O. and Ferreira, M. C. (2012) 'Construction of a skin substitute composed of porcine collagen matrix populated with human dermal fibroblasts and keratinocytes: histological evaluation', *Revista Brasileira de Cirurgia Plástica,* 27(4), pp. 503-508.

Izumi, K., Takacs, G., Terashi, H. and Feinberg, S. E. (1999) 'Ex vivo development of a composite human oral mucosal equivalent', *Journal of oral and maxillofacial surgery,* 57(5), pp. 571-577.

Jacobsen, J., van Deurs, B., Pedersen, M. and Rassing, M. R. (1995) 'TR146 cells grown on filters as a model for human buccal epithelium: I. Morphology, growth, barrier properties, and permeability', *International journal of pharmaceutics,* 125(2), pp. 165-184.

Janeway, C., Travers, P. and Walport, M. (2001) 'Chapter 7, The Development and Survival of Lymphocytes', *Immunobiology: The Immune System in Health and Disease, Garland Science, USA*, pp. 600.

Janeway Jr, C. A., Travers, P., Walport, M. and Shlomchik, M. J. (2001a) 'T cell-mediated cytotoxicity', *Immunobiology: The Immune System in Health and Disease. 5th edition*: Garland Science.

Janeway Jr, C. A., Travers, P., Walport, M. and Shlomchik, M. J. (2001b) 'The components of the immune system', *Immunobiology: The Immune System in Health and Disease. 5th edition*: Garland Science.

Janeway Jr, C. A., Travers, P., Walport, M. and Shlomchik, M. J. (2001c) 'The rearrangement of antigen-receptor gene segments controls lymphocyte development', *Immunobiology: The Immune System in Health and Disease. 5th edition*: Garland Science.

Jennings, L. R., Colley, H. E., Ong, J., Panagakos, F., Masters, J. G., Trivedi, H. M., Murdoch, C. and Whawell, S. (2016) 'Development and characterization of in vitro human oral mucosal equivalents derived from immortalized oral keratinocytes', *Tissue Engineering Part C: Methods,* 22(12), pp. 1108-1117.

Ji, N., Sosa, R. A. and Forsthuber, T. G. (2011) 'More than just a T-box: the role of T-bet as a possible biomarker and therapeutic target in autoimmune diseases', *Immunotherapy,* 3(3), pp. 435-441.

Jones, D. B. (1951) 'Inflammation and repair of the glomerulus', *The American journal of pathology,* 27(6), pp. 991.

Jontell, M., Hansson, H. A. and Nygren, H. (1986) 'Mast cells in oral lichen planus', *Journal of Oral Pathology & Medicine,* 15(5), pp. 273-275.

Joshi, N. S., Cui, W., Chandele, A., Lee, H. K., Urso, D. R., Hagman, J., Gapin, L. and Kaech, S. M. (2007) 'Inflammation directs memory precursor and short-lived effector CD8+ T cell fates via the graded expression of T-bet transcription factor', *Immunity,* 27(2), pp. 281-295.

Juneja, M., Mahajan, S., Rao, N. N., George, T. and Boaz, K. (2006) 'Histochemical analysis of pathological alterations in oral lichen planus and oral lichenoid lesions', *Journal of oral science,* 48(4), pp. 185-193.

Jung, S., Panchalingam, K. M., Rosenberg, L. and Behie, L. A. (2012) 'Ex vivo expansion of human mesenchymal stem cells in defined serum-free media', *Stem cells international,* 2012(123030).

JUNGELL, P., KONTTINEN, Y. T., NORTAMO, P. and MALMSTRÖM, M. (1989) 'Immunoelectron microscopic study of distribution of T cell subsets in oral lichen planus', *European Journal of Oral Sciences,* 97(4), pp. 361-367.

Kaech, S. M. and Wherry, E. J. (2007) 'Heterogeneity and cell-fate decisions in effector and memory CD8+ T cell differentiation during viral infection', *Immunity,* 27(3), pp. 393-405.

Kamali, A. N., Noorbakhsh, S. M., Hamedifar, H., Jadidi-Niaragh, F., Yazdani, R., Bautista, J. M. and Azizi, G. (2019) 'A role for Th1-like Th17 cells in the pathogenesis of inflammatory and autoimmune disorders', *Molecular immunology,* 105, pp. 107-115.

Kambayashi, T., Allenspach, E. J., Chang, J. T., Zou, T., Shoag, J. E., Reiner, S. L., Caton, A. J. and Koretzky, G. A. (2009) 'Inducible MHC class II expression by mast cells supports effector and regulatory T cell activation', *The Journal of Immunology,* 182(8), pp. 4686-4695.

Kaplan, M. H., Wurster, A. L. and Grusby, M. J. (1998) 'A signal transducer and activator of transcription (Stat) 4-independent pathway for the development of T helper type 1 cells', *The Journal of experimental medicine,* 188(6), pp. 1191-1196.

Kara, E. E., Comerford, I., Bastow, C. R., Fenix, K. A., Litchfield, W., Handel, T. M. and McColl, S. R. (2013) 'Distinct chemokine receptor axes regulate Th9 cell trafficking to allergic and autoimmune inflammatory sites', *The Journal of Immunology,* 191(3), pp. 1110-1117.

Kaur, G. and Dufour, J. M. (2012) 'Cell lines: Valuable tools or useless artifacts', *Spermatogenesis,* 1(1), pp. 1-5.

Kay, J. E. (1991) 'Mechanisms of T lymphocyte activation', *Immunology letters,* 29(1-2), pp. 51-54.

Khan, A., Farah, C. S., Savage, N. W., Walsh, L. J., Harbrow, D. J. and Sugerman, P. B. (2003) 'Th1 cytokines in oral lichen planus', *Journal of oral pathology & medicine,* 32(2), pp. 77-83.

Kim, C. H., Rott, L., Kunkel, E. J., Genovese, M. C., Andrew, D. P., Wu, L. and Butcher, E. C. (2001) 'Rules of chemokine receptor association with T cell polarization in vivo', *The Journal of clinical investigation,* 108(9), pp. 1331-1339.

Knebel, A., Kaempe, A., Carlson, R., Rohn, K. and Tipold, A. (2022) 'Measurement of canine Th17 cells by flow cytometry', *Veterinary immunology and immunopathology,* 243, pp. 110366.

Komi, D. E. A., Khomtchouk, K. and Santa Maria, P. L. (2020) 'A review of the contribution of mast cells in wound healing: involved molecular and cellular mechanisms', *Clinical reviews in allergy & immunology,* 58(3), pp. 298-312.

Koning, J. J., Rodrigues Neves, C. T., Schimek, K., Thon, M., Spiekstra, S. W., Waaijman, T., de Gruijl, T. D. and Gibbs, S. (2022) 'A Multi-Organ-on-Chip Approach to Investigate How Oral Exposure to Metals Can Cause Systemic Toxicity Leading to Langerhans Cell Activation in Skin', *Frontiers in toxicology*, pp. 70.

Konya, C., Goronzy, J. J. and Weyand, C. M. (2009) 'Treating autoimmune disease by targeting CD8+ T suppressor cells', *Expert opinion on biological therapy,* 9(8), pp. 951-965.

Kosten, I. J., Spiekstra, S. W., de Gruijl, T. D. and Gibbs, S. (2015) 'MUTZ-3 derived Langerhans cells in human skin equivalents show differential migration and phenotypic plasticity after allergen or irritant exposure', *Toxicology and applied pharmacology,* 287(1), pp. 35-42.

Kriegebaum, U., Mildenberger, M., Mueller-Richter, U. D., Klammert, U., Kuebler, A. C. and Reuther, T. (2012) 'Tissue engineering of human oral mucosa on different scaffolds: in vitro experiments as a basis for clinical applications', *Oral surgery, oral medicine, oral pathology and oral radiology,* 114(5), pp. S190-S198.

Krugluger, W., Rohrbacher, W., Laciak, K., Moser, K., Moser, C. and Hugeneck, J. (2005) 'Reorganization of hair follicles in human skin organ culture induced by cultured human follicle-derived cells', *Experimental dermatology,* 14(8), pp. 580-585.

Krummel, M. F. and Allison, J. P. (1995) 'CD28 and CTLA-4 have opposing effects on the response of T cells to stimulation', *The Journal of experimental medicine,* 182(2), pp. 459-465.

Krystel-Whittemore, M., Dileepan, K. N. and Wood, J. G. (2016) 'Mast cell: a multi-functional master cell', *Frontiers in immunology*, pp. 620.

Kulasekara, K. K., Lukandu, O. M., Neppelberg, E., Vintermyr, O. K., Johannessen, A. C. and Costea, D. E. (2009) 'Cancer progression is associated with increased expression of basement membrane proteins in three-dimensional in vitro models of human oral cancer', *archives of oral biology,* 54(10), pp. 924-931.

Kurago, Z. B. (2016) 'Etiology and pathogenesis of oral lichen planus: an overview', *Oral surgery, oral medicine, oral pathology and oral radiology,* 122(1), pp. 72-80.

Kägi, D., Ledermann, B., Bürki, K., Seiler, P., Odermatt, B., Olsen, K. J., Podack, E. R., Zinkernagel, R. M. and Hengartner, H. (1994) 'Cytotoxicity mediated by T cells and natural killer cells is greatly impaired in perforin-deficient mice', *Nature,* 369(6475), pp. 31-37.

Kühbacher, A., Henkel, H., Stevens, P., Grumaz, C., Finkelmeier, D., Burger-Kentischer, A., Sohn, K. and Rupp, S. (2017a) 'Central Role for Dermal Fibroblasts in Skin Model Protection against Candida albicans', *The Journal of infectious diseases,* 215(11), pp. 1742-1752.

Kühbacher, A., Sohn, K., Burger-Kentischer, A. and Rupp, S. (2017b) 'Immune cell-supplemented human skin model for studying fungal infections', *Human Fungal Pathogen Identification*: Springer, pp. 439-449.

Langenkamp, A., Nagata, K., Murphy, K., Wu, L., Lanzavecchia, A. and Sallusto, F. (2003) 'Kinetics and expression patterns of chemokine receptors in human CD4+ T lymphocytes primed by myeloid or plasmacytoid dendritic cells', *European journal of immunology,* 33(2), pp. 474-482.

Lauer, G. (1994) 'Autografting of feeder-cellfree cultured gingival epithelium', *J Cranio Maxillo Facial Surg,* 22, pp. 23-32.

Lauer, G. and Schimming, R. (2001) 'Tissue-engineered mucosa graft for reconstruction of the intraoral lining after freeing of the tongue: a clinical and immunohistologic study', *Journal of oral and maxillofacial surgery,* 59(2), pp. 169-175.

Laurence, A., Tato, C. M., Davidson, T. S., Kanno, Y., Chen, Z., Yao, Z., Blank, R. B., Meylan, F., Siegel, R. and Hennighausen, L. (2007) 'Interleukin-2 signaling via STAT5 constrains T helper 17 cell generation', *Immunity,* 26(3), pp. 371-381.

Lavanya, A., Khan, W., Singh, P., Augustine, D., Rao, R. S., Sowmya, S., Haragannavar, V. C. and Nambiar, K. S. (2020) 'PECAM-1 overexpression signifies aggressive biologic behavior of oral lichen planus–A pilot study', *Indian Journal of Dental Research,* 31(2), pp. 277.

Lavanya, N., Jayanthi, P., Rao, U. K. and Ranganathan, K. (2011) 'Oral lichen planus: An update on pathogenesis and treatment', *J Oral Maxillofac Pathol,* 15(2), pp. 127-32.

LeBien, T. W. and Tedder, T. F. (2008) 'B lymphocytes: how they develop and function', *Blood, The Journal of the American Society of Hematology,* 112(5), pp. 1570-1580.

Lee, K. M., Choi, K. H. and Ouellette, M. M. (2004) 'Use of exogenous hTERT to immortalize primary human cells', *Cytotechnology,* 45(1), pp. 33-38.

Lei, F., Haque, R., Weiler, L., Vrana, K. E. and Song, J. (2009) 'T lineage differentiation from induced pluripotent stem cells', *Cellular immunology,* 260(1), pp. 1-5.

Lei, L., Zhan, L., Tan, W., Chen, S., Li, Y. and Reynolds, M. (2014) 'Foxp3 gene expression in oral lichen planus: a clinicopathological study', *Molecular medicine reports,* 9(3), pp. 928-934.

Levin, C. and Maibach, H. I. (2002) 'Topical corticosteroid-induced adrenocortical insufficiency', *American journal of clinical dermatology,* 3(3), pp. 141-147.

Li, J., Farthing, P. M. and Thornhill, M. H. (2000) 'Oral and skin keratinocytes are stimulated to secrete monocyte chemoattractant protein-1 by tumour necrosis factor-α and interferon-γ', *Journal of oral pathology & medicine,* 29(9), pp. 438-444.

Li, J., Ireland, G. W., Farthing, P. M. and Thornhill, M. H. (1996a) 'Epidermal and oral keratinocytes are induced to produce RANTES and IL-8 by cytokine stimulation', *Journal of investigative dermatology,* 106(4), pp. 661-666.

Li, J., Mahiouz, D., Farthing, P., Haskard, D. and Thornhili, M. (1996b) 'Heterogeneity of ICAM-1 expression, and cytokine regulation of ICAM-1 expression, in skin and oral keratinocytes', *Journal of oral pathology & medicine,* 25(3), pp. 112-118.

Li, T.-J. and Cui, J. (2013) 'COX-2, MMP-7 expression in oral lichen planus and oral squamous cell carcinoma', *Asian Pacific journal of tropical medicine,* 6(8), pp. 640-643.

Lim, J. F., Berger, H. and Su, I.-h. (2016) 'Isolation and activation of murine lymphocytes', *JoVE (Journal of Visualized Experiments),* (116), pp. e54596.

Limat, A., Hunziker, T., Boillat, C., Bayreuther, K. and Noser, F. (1989) 'Post-mitotic human dermal fibroblasts efficiently support the growth of human follicular keratinocytes', *Journal of Investigative Dermatology,* 92(5), pp. 758-762.

Lindstein, T., June, C. H., Ledbetter, J. A., Stella, G. and Thompson, C. B. (1989) 'Regulation of lymphokine messenger RNA stability by a surface-mediated T cell activation pathway', *Science,* 244(4902), pp. 339-343.

Little, M., Griffiths, C., Watson, R., Pemberton, M. and Thornhill, M. (2003a) 'Oral mucosal keratinocytes express RANTES and ICAM-1, but not interleukin-8, in oral lichen planus and oral lichenoid reactions induced by amalgam fillings', *Clinical and Experimental Dermatology: Clinicopathological cases,* 28(1), pp. 64-69.

Little, M., Griffiths, C., Watson, R., Pemberton, M. and Thornhill, M. H. (2003b) 'Oral mucosal keratinocytes express RANTES and ICAM-1, but not interleukin-8, in oral lichen planus and oral lichenoid reactions induced by amalgam fillings', *Clinical and Experimental Dermatology: Clinicopathological cases,* 28(1), pp. 64-69.

Livak, K. J. and Schmittgen, T. D. (2001) 'Analysis of relative gene expression data using real-time quantitative PCR and the 2− ΔΔCT method', *methods,* 25(4), pp. 402-408.

Lodi, G., Pellicano, R. and Carrozzo, M. (2010) 'Hepatitis C virus infection and lichen planus: a systematic review with meta-analysis', *Oral Dis,* 16(7), pp. 601-12.

Lodi, G., Scully, C., Carrozzo, M., Griffiths, M., Sugerman, P. B. and Thongprasom, K. (2005) 'Current controversies in oral lichen planus: report of an international consensus meeting. Part 2. Clinical management and malignant transformation', *Oral Surgery, Oral Medicine, Oral Pathology, Oral Radiology, and Endodontology,* 100(2), pp. 164-178.

Loetscher, M., Loetscher, P., Brass, N., Meese, E. and Moser, B. (1998a) 'Lymphocyte-specific chemokine receptor CXCR3: regulation, chemokine binding and gene localization', *European journal of immunology,* 28(11), pp. 3696-3705.

Loetscher, P., Uguccioni, M., Bordoli, L., Baggiolini, M., Moser, B., Chizzolini, C. and Dayer, J.-M. (1998b) 'CCR5 is characteristic of Th1 lymphocytes', *Nature,* 391(6665), pp. 344-345.

Lopez-Castejon, G. and Brough, D. (2011) 'Understanding the mechanism of IL-1β secretion', *Cytokine & growth factor reviews,* 22(4), pp. 189-195.

Lord, S. J., Rajotte, R. V., Korbutt, G. S. and Bleackley, R. C. (2003) 'Granzyme B: a natural born killer', *Immunological reviews,* 193(1), pp. 31-38.

Lorthois, I., Simard, M., Morin, S. and Pouliot, R. (2019) 'Infiltration of T cells into a three-dimensional psoriatic skin model mimics pathological key features', *International journal of molecular sciences,* 20(7), pp. 1670.

Lu, R., Zhang, J., Sun, W., Du, G. and Zhou, G. (2015) 'Inflammation-related cytokines in oral lichen planus: an overview', *Journal of Oral Pathology & Medicine,* 44(1), pp. 1-14.

Lu, R., Zhou, G., Du, G., Xu, X., Yang, J. and Hu, J. (2011) 'Expression of T-bet and GATA-3 in peripheral blood mononuclear cells of patients with oral lichen planus', *Archives of oral biology,* 56(5), pp. 499-505.

Luckheeram, R. V., Zhou, R., Verma, A. D. and Xia, B. (2012) 'CD4+ T cells: differentiation and functions', *Clinical and developmental immunology,* 2012.

Lundgren, A., Suri-Payer, E., Enarsson, K., Svennerholm, A.-M. and Lundin, B. S. (2003) 'Helicobacter pylori-specific CD4+ CD25high regulatory T cells suppress memory T-cell responses to H. pylori in infected individuals', *Infection and immunity,* 71(4), pp. 1755-1762.

Luo, J., Ming, B., Zhang, C., Deng, X., Li, P., Wei, Z., Xia, Y., Jiang, K., Ye, H. and Ma, W. (2018) 'IL-2 inhibition of Th17 generation rather than induction of treg cells is impaired in primary Sjögren's syndrome patients', *Frontiers in immunology,* 9, pp. 1755.

Ma, J., Zhang, J., Zhang, Y., Lv, T. and Liu, J. (2016) 'The magnitude of the association between human papillomavirus and oral lichen planus: A meta-analysis', *PloS one,* 11(8).

Maas-Szabowski, N., Shimotoyodome, A. and Fusenig, N. E. (1999) 'Keratinocyte growth regulation in fibroblast cocultures via a double paracrine mechanism', *Journal of cell science,* 112(12), pp. 1843-1853.

Maas-Szabowski, N., Stark, H.-J. and Fusenig, N. E. (2000) 'Keratinocyte growth regulation in defined organotypic cultures through IL-1-induced keratinocyte growth factor expression in resting fibroblasts', *Journal of investigative dermatology,* 114(6), pp. 1075-1084.

Maas-Szabowski, N., Stark, H.-J. and Fusenig, N. E. (2002) 'Cell interaction and epithelial differentiation', *Culture of epithelial cells*, pp. 31-63.

MacLennan, I. C., Toellner, K. M., Cunningham, A. F., Serre, K., Sze, D. M. Y., Zúñiga, E., Cook, M. C. and Vinuesa, C. G. (2003) 'Extrafollicular antibody responses', *Immunological reviews,* 194(1), pp. 8-18.

Madden, M. R., Finkelstein, J. L., Staiano-Coico, L., Goodwin, C. W., Shires, G. T., Nolan, E. E. and Hefton, J. M. (1986) 'Grafting of cultured allogeneic epidermis on second-and third-degree burn wounds on 26 patients', *The Journal of trauma,* 26(11), pp. 955-962.

Maecker, H. and Trotter, J. (2009) 'Selecting reagents for multicolor flow cytometry', *Application Note. BD Biosciences: San Jose, CA*.

Maggi, L., Santarlasci, V., Capone, M., Rossi, M. C., Querci, V., Mazzoni, A., Cimaz, R., De Palma, R., Liotta, F. and Maggi, E. (2012) 'Distinctive features of classic and nonclassic (T h17 derived) human T h1 cells', *European journal of immunology,* 42(12), pp. 3180-3188.

Malekzadeh, H., Robati, M., Yousefimanesh, H., Boroujerdnia, M. G. and Nadripour, R. (2015) 'Salivary interferon gamma and interleukin-4 levels in patients suffering from oral lichen planus', *Cell Journal (Yakhteh),* 17(3), pp. 554.

Manjunatha, B. and Kumar, G. (2005) 'Epithelial mesenchymal interactions in odontogenesis', *J Oral Maxillofac Pathol,* 9, pp. 51-7.

Maraeea, A. H., El-Rebey, H. S. and Zaky, E. A. (2016) 'Caspase-3 expression in lichen planus', *Menoufia Medical Journal,* 29(2), pp. 396.

Markeson, D., Pleat, J. M., Sharpe, J. R., Harris, A. L., Seifalian, A. M. and Watt, S. M. (2015) 'Scarring, stem cells, scaffolds and skin repair', *Journal of tissue engineering and regenerative medicine,* 9(6), pp. 649-668.

Marshall, A., Celentano, A., Cirillo, N., McCullough, M. and Porter, S. (2017a) 'Tissue-specific regulation of CXCL9/10/11 chemokines in keratinocytes: Implications for oral inflammatory disease', *PLoS One,* 12(3).

Marshall, A., Celentano, A., Cirillo, N., Mirams, M., McCullough, M. and Porter, S. (2017b) 'Immune receptors CD40 and CD86 in oral keratinocytes and implications for oral lichen planus', *Journal of oral science,* 59(3), pp. 373-382.

Marshall, J. S., Warrington, R., Watson, W. and Kim, H. L. (2018) 'An introduction to immunology and immunopathology', *Allergy, Asthma & Clinical Immunology,* 14(2), pp. 1-10.

Martkamchan, S., Onlamoon, N., Wang, S., Pattanapanyasat, K. and Ammaranond, P. (2016) 'The effects of anti-CD3/CD28 coated beads and IL-2 on expanded T cell for immunotherapy', *Advances in Clinical and Experimental Medicine,* 25(5), pp. 821-828.

Masuda, I. (1996) 'An in vitro oral mucosal model reconstructed from human normal gingival cells', *Kokubyo Gakkai zasshi. The Journal of the Stomatological Society, Japan,* 63(2), pp. 334-353.

Matthews, J., Scully, C. and Potts, A. (1984) 'Oral lichen planus: an immunoperoxidase study using monoclonal antibodies to lymphocyte subsets', *British Journal of Dermatology,* 111(5), pp. 587-595.

Mattila, R. and Syrjänen, S. (2010) 'Caspase cascade pathways in apoptosis of oral lichen planus', *Oral Surg Oral Med Oral Pathol Oral Radiol Endod,* 110(5), pp. 618-23.

Mattsson, C. S., Jontell, M., Bergenholtz, G., Heyden, M. and Dahlgren, U. (1998) 'Distribution of interferon-y mRNA-positive cells in oral lichen planus lesions', *Journal of oral pathology & medicine,* 27(10), pp. 483-488.

Mazzoni, A., Maggi, L., Liotta, F., Cosmi, L. and Annunziato, F. (2019) 'Biological and clinical significance of T helper 17 cell plasticity', *Immunology,* 158(4), pp. 287-295.

McGeachy, M. J., Chen, Y., Tato, C. M., Laurence, A., Joyce-Shaikh, B., Blumenschein, W. M., McClanahan, T. K., O'shea, J. J. and Cua, D. J. (2009) 'The interleukin 23 receptor is essential for the terminal differentiation of interleukin 17–producing effector T helper cells in vivo', *Nature immunology,* 10(3), pp. 314-324.

McGregor, F., Muntoni, A., Fleming, J., Brown, J., Felix, D. H., MacDonald, D. G., Parkinson, E. K. and Harrison, P. R. (2002) 'Molecular changes associated with oral dysplasia progression and acquisition of immortality: potential for its reversal by 5-azacytidine', *Cancer research,* 62(16), pp. 4757-4766.

McLeod, J. D., Walker, L. S., Patel, Y. I., Boulougouris, G. and Sansom, D. M. (1998) 'Activation of human T cells with superantigen (staphylococcal enterotoxin B) and CD28 confers resistance to apoptosis via CD95', *The Journal of Immunology,* 160(5), pp. 2072-2079.

Meager, A. (1999) 'Cytokine regulation of cellular adhesion molecule expression in inflammation', *Cytokine & growth factor reviews,* 10(1), pp. 27-39.

Mehling, A., Loser, K., Varga, G., Metze, D., Luger, T. A., Schwarz, T., Grabbe, S. and Beissert, S. (2001) 'Overexpression of CD40 ligand in murine epidermis results in chronic skin inflammation and systemic autoimmunity', *Journal of Experimental Medicine,* 194(5), pp. 615-628.

Mencarelli, A., Cipriani, S., Francisci, D., Santucci, L., Baldelli, F., Distrutti, E. and Fiorucci, S. (2016) 'Highly specific blockade of CCR5 inhibits leukocyte trafficking and reduces mucosal inflammation in murine colitis', *Scientific reports,* 6(1), pp. 1-12.

Merad, M., Manz, M. G., Karsunky, H., Wagers, A., Peters, W., Charo, I., Weissman, I. L., Cyster, J. G. and Engleman, E. G. (2002) 'Langerhans cells renew in the skin throughout life under steady-state conditions', *Nature immunology,* 3(12), pp. 1135-1141.

Miller, L. S. and Modlin, R. L. (2007) 'Human keratinocyte Toll-like receptors promote distinct immune responses', *Journal of Investigative Dermatology,* 127(2).

Miller, M. J., Wei, S. H., Cahalan, M. D. and Parker, I. (2003) 'Autonomous T cell trafficking examined in vivo with intravital two-photon microscopy', *Proceedings of the National Academy of Sciences,* 100(5), pp. 2604-2609.

Miyazaki, D., Nakamura, T., Toda, M., Cheung-Chau, K.-W., Richardson, R. M. and Ono, S. J. (2005) 'Macrophage inflammatory protein–1α as a costimulatory signal for mast cell–mediated immediate hypersensitivity reactions', *The Journal of clinical investigation,* 115(2), pp. 434-442.

Moharamzadeh, K., Brook, I., Van Noort, R., Scutt, A. and Thornhill, M. (2007) 'Tissue-engineered oral mucosa: a review of the scientific literature', *Journal of dental research,* 86(2), pp. 115-124.

Moharamzadeh, K., Franklin, K. L., Brook, I. M. and van Noort, R. (2009) 'Biologic assessment of antiseptic mouthwashes using a three-dimensional human oral mucosal model', *Journal of periodontology,* 80(5), pp. 769-775.

Monteiro, B. V. d. B., Pereira, J. d. S., Nonaka, C. F., Godoy, G. P., da Silveira, É. J. and Miguel, M. C. d. C. (2015) 'Immunoexpression of Th17-related cytokines in oral lichen planus', *Applied Immunohistochemistry & Molecular Morphology,* 23(6), pp. 409-415.

Morin, M.-P. and Grenier, D. (2017) 'Regulation of matrix metalloproteinase secretion by green tea catechins in a three-dimensional co-culture model of macrophages and gingival fibroblasts', *Archives of Oral Biology,* 75, pp. 89-99.

Moriyama, T., Asahina, I., Ishii, M., Oda, M., Ishii, Y. and Enomoto, S. (2001) 'Development of composite cultured oral mucosa utilizing collagen sponge matrix and contracted collagen gel: a preliminary study for clinical applications', *Tissue engineering,* 7(4), pp. 415-427.

Mosmann, T. R. and Sad, S. (1996) 'The expanding universe of T-cell subsets: Th1, Th2 and more', *Immunology today,* 17(3), pp. 138-146.

Mozaffari, H. R., Sharifi, R., Mirbahari, S., Montazerian, S., Sadeghi, M. and Rostami, S. (2018) 'A systematic review and meta-analysis study of salivary and serum interleukin-8 levels in oral lichen planus', *Advances in Dermatology and Allergology/Postępy Dermatologii i Alergologii,* 35(6), pp. 599.

Mozaffari, H. R., Sharifi, R. and Sadeghi, M. (2018) 'Interleukin-6 levels in the serum and saliva of patients with oral lichen planus compared with healthy controls: a meta-analysis study', *Central-European journal of immunology,* 43(1), pp. 103.

Murray, R. Z., Kay, J. G., Sangermani, D. G. and Stow, J. L. (2005) 'A role for the phagosome in cytokine secretion', *Science,* 310(5753), pp. 1492-1495.

Müller, G., Saloga, J., Germann, T., Bellinghausen, I., Mohamadzadeh, M., Knop, J. and Enk, A. H. (1994) 'Identification and induction of human keratinocyte-derived IL-12', *The Journal of clinical investigation,* 94(5), pp. 1799-1805.

Müller, S. (2017) 'Oral lichenoid lesions: distinguishing the benign from the deadly', *Modern Pathology,* 30(1), pp. S54-S67.

Nakae, S., Iwakura, Y., Suto, H. and Galli, S. J. (2007) 'Phenotypic differences between Th1 and Th17 cells and negative regulation of Th1 cell differentiation by IL-17', *Journal of leukocyte biology,* 81(5), pp. 1258-1268.

Nakahira, M., Ahn, H.-J., Park, W.-R., Gao, P., Tomura, M., Park, C.-S., Hamaoka, T., Ohta, T., Kurimoto, M. and Fujiwara, H. (2002) 'Synergy of IL-12 and IL-18 for IFN-γ gene expression: IL-12-induced STAT4 contributes to IFN-γ promoter activation by up-regulating the binding activity of IL-18-induced activator protein 1', *The Journal of Immunology,* 168(3), pp. 1146-1153.

Nanci, A. (2013) *Ten Cate's Oral Histology: Development, Structure, and Function, 8th edn St.* 8th edn.: Louis: Elsevier.

Nauseef, W. M. and Borregaard, N. (2014) 'Neutrophils at work', *Nature immunology,* 15(7), pp. 602-611.

Negi, D., Urs, A. B., Kumar, P., Mahajan, B., Singh, H., Polipalli, S. K. and Kapoor, S. (2019) 'Assessment of Interleukin-18 gene polymorphism and serum levels in oral lichen planus in an Indian population', *Journal of Oral Pathology & Medicine,* 48(3), pp. 244-250.

Neppelberg, E., Johannessen, A. C. and Jonsson, R. (2001) 'Apoptosis in oral lichen planus', *European journal of oral sciences,* 109(5), pp. 361-364.

Neppelberg, E., Loro, L., Øijordsbakken, G. and Johannessen, A. (2007) 'Altered CD40 and E-cadherin expression–putative role in oral lichen planus', *Journal of oral pathology & medicine,* 36(3), pp. 153-160.

Netzlaff, F., Lehr, C.-M., Wertz, P. and Schaefer, U. (2005) 'The human epidermis models EpiSkin®, SkinEthic® and EpiDerm®: an evaluation of morphology and their suitability for testing phototoxicity, irritancy, corrosivity, and substance transport', *European Journal of Pharmaceutics and Biopharmaceutics,* 60(2), pp. 167-178.

Neville, B. W., Damm, D. D., Allen, C. M. and Bouquot, J. E. (2002) 'Oral and Maxillofacial Pathology. 2 [sup] nd ed', *Philadelphia, PA: Saunders*, pp. 337-69.

Nicholson, L. B. (2016) 'The immune system', *Essays in biochemistry,* 60(3), pp. 275-301.

Nico, M. M., Fernandes, J. D. and Lourenco, S. V. (2011) 'Oral lichen planus', *An Bras Dermatol,* 86(4), pp. 633-41; quiz 642-3.

Noble, P., Cutts, J. H. and Carroll, K. (1968) 'Ficoll flotation for the separation of blood leukocyte types', *Blood,* 31(1), pp. 66-73.

Novick, D., Orchansky, P., Revel, M. and Rubinstein, M. (1987) 'The human interferon-gamma receptor. Purification, characterization, and preparation of antibodies', *Journal of Biological Chemistry,* 262(18), pp. 8483-8487.

Nutt, S. L., Hodgkin, P. D., Tarlinton, D. M. and Corcoran, L. M. (2015) 'The generation of antibody-secreting plasma cells', *Nature Reviews Immunology,* 15(3), pp. 160-171.

Odell, E. W. (2017) *Cawson's essentials of oral pathology and oral medicine.* 9th edn.: Elsevier Health Sciences.

Oh, S. and Hwang, E. S. (2014) 'The role of protein modifications of T-bet in cytokine production and differentiation of T helper cells', *Journal of immunology research,* 2014.

Ohmori, Y., Schreiber, R. D. and Hamilton, T. A. (1997) 'Synergy between interferon-γ and tumor necrosis factor-α in transcriptional activation is mediated by cooperation between signal transducer and activator of transcription 1 and nuclear factor κB', *Journal of Biological Chemistry,* 272(23), pp. 14899-14907.

Ohmori, Y., Wyner, L., Narumi, S., Armstrong, D., Stoler, M. and Hamilton, T. A. (1993) 'Tumor necrosis factor-alpha induces cell type and tissue-specific expression of chemoattractant cytokines in vivo', *The American journal of pathology,* 142(3), pp. 861.

Okayama, Y. and Kawakami, T. (2006) 'Development, migration, and survival of mast cells', *Immunologic research,* 34(2), pp. 97-115.

Ollington, B., Colley, H. E. and Murdoch, C. (2021) 'Immunoresponsive tissue-engineered Oral mucosal equivalents containing macrophages', *Tissue Engineering Part C: Methods,* 27(8), pp. 462-471.

Olnes, M. J., Kotliarov, Y., Biancotto, A., Cheung, F., Chen, J., Shi, R., Zhou, H., Wang, E., Tsang, J. S. and Nussenblatt, R. (2016) 'Effects of systemically administered hydrocortisone on the human immunome', *Scientific reports,* 6(1), pp. 1-15.

Olsen, I. and Sollid, L. M. (2013) 'Pitfalls in determining the cytokine profile of human T cells', *Journal of immunological methods,* 390(1-2), pp. 106-112.

Orlando, B., Bragazzi, N. and Nicolini, C. (2013) 'Bioinformatics and systems biology analysis of genes network involved in OLP (Oral Lichen Planus) pathogenesis', *Archives of oral biology,* 58(6), pp. 664-673.

Osuala, K. O. and Sloane, B. F. (2014) 'Many roles of CCL20: emphasis on breast cancer', *Postdoc journal: a journal of postdoctoral research and postdoctoral affairs,* 2(3), pp. 7.

Ouwehand, K., Spiekstra, S. W., Waaijman, T., Breetveld, M., Scheper, R. J., de Gruijl, T. D. and Gibbs, S. (2012) 'CCL5 and CCL20 mediate immigration of Langerhans cells into the epidermis of full thickness human skin equivalents', *European Journal of Cell Biology,* 91(10), pp. 765-773.

Ozturk, O., Cakmakoglu, B., Ozturk, G. N. and Unur, M. (2021) 'An association of the MCP-1 and CCR2 gene polymorphisms with oral lichen planus', *Oral Surgery, Oral Medicine, Oral Pathology and Oral Radiology,* 132(6), pp. 708-714.

Paguirigan, A. and Beebe, D. (2006) 'Gelatin based microfluidic devices for cell culture', *Lab on a Chip,* 6(3), pp. 407-413.

PALACIOS, R. t. and Sugawara, I. (1982) 'Hydrocortisone Abrogates Proliferation of T Cells in Autologous Mixed Lymphocyte Reaction by Rendering the Interleukin-2 Producer T Cells Unresponsive to Interleukin-1 and Unable to Synthesize the T-Cell Growth Factor', *Scandinavian journal of immunology,* 15(1), pp. 25-31.

Pan, C., Kumar, C., Bohl, S., Klingmueller, U. and Mann, M. (2009) 'Comparative proteomic phenotyping of cell lines and primary cells to assess preservation of cell type-specific functions', *Molecular & Cellular Proteomics,* 8(3), pp. 443-450.

Paplinska-Goryca, M., Misiukiewicz-Stepien, P., Nejman-Gryz, P., Proboszcz, M., Mlacki, M., Gorska, K. and Krenke, R. (2020) 'Epithelial-macrophage-dendritic cell interactions impact alarmins expression in asthma and COPD', *Clinical Immunology,* 215, pp. 108421.

Pardigol, A., Forssmann, U., Zucht, H.-D., Loetscher, P., Schulz-Knappe, P., Baggiolini, M., Forssmann, W.-G. and Mägert, H.-J. (1998) 'HCC-2, a human chemokine: gene structure, expression pattern, and biological activity', *Proceedings of the National Academy of Sciences,* 95(11), pp. 6308-6313.

Park, H.-K., Hurwitz, S. and Woo, S.-B. (2012) 'Oral lichen planus: REU scoring system correlates with pain', *Oral surgery, oral medicine, oral pathology and oral radiology,* 114(1), pp. 75-82.

Parker, D. C. (1993) 'T cell-dependent B cell activation', *Annual review of immunology,* 11(1), pp. 331-360.

Patel, T., Cunningham, A., Holland, M., Daley, J., Lazo, S., Hodi, F. S. and Severgnini, M. (2018) 'Development of an 8-color antibody panel for functional phenotyping of human CD8+ cytotoxic T cells from peripheral blood mononuclear cells', *Cytotechnology,* 70(1), pp. 1-11.

Payeras, M. R., Cherubini, K., Figueiredo, M. A. and Salum, F. G. (2013) 'Oral lichen planus: focus on etiopathogenesis', *Arch Oral Biol,* 58(9), pp. 1057-69.

Peck, A. and Mellins, E. D. (2010) 'Plasticity of T-cell phenotype and function: the T helper type 17 example', *Immunology,* 129(2), pp. 147-153.

Pekiner, F. N., Demirel, G. Y., Borahan, M. O. and Özbayrak, S. (2012) 'Cytokine profiles in serum of patients with oral lichen planus', *Cytokine,* 60(3), pp. 701-706.

Pennock, N. D., White, J. T., Cross, E. W., Cheney, E. E., Tamburini, B. A. and Kedl, R. M. (2013) 'T cell responses: naive to memory and everything in between', *Advances in physiology education,* 37(4), pp. 273-283.

Pereira, J. S., Monteiro, B. V., Nonaka, C. F., Silveira, É. J. and Miguel, M. C. (2012) 'FoxP3+ T regulatory cells in oral lichen planus and its correlation with the distinct clinical appearance of the lesions', *International journal of experimental pathology,* 93(4), pp. 287-294.

Pereira, T. F., Levin, G., DeOcesano-Pereira, C., Caodaglio, A. S., Fujita, A., Tonso, A. and Sogayar, M. C. (2020) 'Fluorescence-based method is more accurate than counting-based methods for plotting growth curves of adherent cells', *BMC research notes,* 13(1), pp. 1-7.

Pertoft, H., Laurent, T., Seljelid, R., Kågedal, L. and Hirtenstein, M. (1979) 'The use of density gradients of Percoll® for the separation of biological particles', *Separation of cells and subcellular elements*: Elsevier, pp. 67-72.

Petti, S., Rabiei, M., De Luca, M. and Scully, C. (2011) 'The magnitude of the association between hepatitis C virus infection and oral lichen planus: meta-analysis and case control study', *Odontology,* 99(2), pp. 168-178.

Piccinni, M. P., Lombardelli, L., Logiodice, F., Tesi, D., Kullolli, O., Biagiotti, R., Giudizi, M., Romagnani, S., Maggi, E. and Ficarra, G. (2014) 'Potential pathogenetic role of Th17, Th0, and Th2 cells in erosive and reticular oral lichen planus', *Oral diseases,* 20(2), pp. 212-218.

Pirilä, E., Väyrynen, O., Sundquist, E., Päkkilä, K., Nyberg, P., Nurmenniemi, S., Pääkkönen, V., Pesonen, P., Dayan, D. and Vered, M. (2015) 'Macrophages modulate migration and invasion of human tongue squamous cell carcinoma', *PLoS One,* 10(3), pp. e0120895.

Ponec, M. (1991) 'Reconstruction of human epidermis on de-epidermized dermis: expression of differentiation-specific protein markers and lipid composition', *Toxicology in vitro,* 5(5-6), pp. 597-606.

Ponec, M., Boelsma, E., Gibbs, S. and Mommaas, M. (2002) 'Characterization of reconstructed skin models', *Skin Pharmacology and Physiology,* 15(Suppl. 1), pp. 4-17.

Prussin, C. and Metcalfe, D. D. (2003) '4. IgE, mast cells, basophils, and eosinophils', *Journal of Allergy and Clinical Immunology,* 111(2), pp. S486-S494.

Pujar, A., Pereira, T., Tamgadge, A., Bhalerao, S. and Tamgadge, S. (2015) 'Comparing the efficacy of hematoxylin and eosin, periodic acid schiff and fluorescent periodic acid schiff-acriflavine techniques for demonstration of basement membrane in oral lichen planus: a histochemical study', *Indian Journal of Dermatology,* 60(5), pp. 450.

Rad, M., Hashemipoor, M. A., Mojtahedi, A., Zarei, M. R., Chamani, G., Kakoei, S. and Izadi, N. (2009) 'Correlation between clinical and histopathologic diagnoses of oral lichen planus based on modified WHO diagnostic criteria', *Oral Surg Oral Med Oral Pathol Oral Radiol Endod,* 107(6), pp. 796-800.

Ragaz, A. and Ackerman, A. B. (1981) 'Evolution, maturation, and regression of lesions of lichen planus. New observations and correlations of clinical and histologic findings', *The American Journal of Dermatopathology,* 3(1), pp. 5-25.

Ramirez-Amador, V., Dekker, N., Lozada-Nur, F., Mirowski, G., MacPhail, L. and Regezi, J. (1996) 'Altered interface adhesion molecules in oral lichen planus', *Oral Diseases,* 2(3), pp. 188-192.

Raulf, M. (2019) 'T cell: Primary culture from peripheral blood', *Allergy*: Springer, pp. 17-31.

Read, K. A., Powell, M. D., Sreekumar, B. K. and Oestreich, K. J. (2019) 'In vitro differentiation of effector CD4+ T helper cell subsets', *Mouse Models of Innate Immunity*: Springer, pp. 75-84.

Repnik, U., Knezevic, M. and Jeras, M. (2003) 'Simple and cost-effective isolation of monocytes from buffy coats', *Journal of immunological methods,* 278(1-2), pp. 283-292.

Rheinwald, J. and Green, H. 1975a. Serial cultivation of strains of human epidermal keratinocytes: the formation of keratinizing colonies from single cells. Cell 6, 331e343.

Rheinwald, J. G. and Green, H. (1975b) 'Formation of a keratinizing epithelium in culture by a cloned cell line derived from a teratoma', *Cell,* 6(3), pp. 317-330.

Rheinwatd, J. G. and Green, H. (1975) 'Seria cultivation of strains of human epidemal keratinocytes: the formation keratinizin colonies from single cell is', *Cell,* 6(3), pp. 331-343.

Rhodus, N. L., Cheng, B., Myers, S., Bowles, W., Ho, V. and Ondrey, F. (2005) 'A comparison of the pro-inflammatory, NF-κB-dependent cytokines: TNF-alpha, IL-1-alpha, IL-6, and IL-8 in different oral fluids from oral lichen planus patients', *Clinical Immunology,* 114(3), pp. 278-283.

Rhodus, N. L., Cheng, B. and Ondrey, F. (2007) 'Th1/Th2 cytokine ratio in tissue transudates from patients with oral lichen planus', *Mediators of inflammation,* 2007.

Rich, A. M. and Reade, P. (1989) 'A quantitative assessment of Langerhans cells in oral mucosal lichen planus and leukoplakia', *British Journal of Dermatology,* 120(2), pp. 223-228.

Rodrigues Neves, C. T., Spiekstra, S. W., de Graaf, N. P., Rustemeyer, T., Feilzer, A. J., Kleverlaan, C. J. and Gibbs, S. (2020) 'Titanium salts tested in reconstructed human skin with integrated MUTZ-3-derived Langerhans cells show an irritant rather than a sensitizing potential', *Contact dermatitis,* 83(5), pp. 337-346.

Rogge, L., Papi, A., Presky, D. H., Biffi, M., Minetti, L. J., Miotto, D., Agostini, C., Semenzato, G., Fabbri, L. M. and Sinigaglia, F. (1999) 'Antibodies to the IL-12 receptor β2 chain mark human Th1 but not Th2 cells in vitro and in vivo', *The Journal of Immunology,* 162(7), pp. 3926-3932.

Roopashree, M., Gondhalekar, R. V., Shashikanth, M., George, J., Thippeswamy, S. and Shukla, A. (2010) 'Pathogenesis of oral lichen planus–a review', *Journal of Oral Pathology & Medicine,* 39(10), pp. 729-734.

Rosales, C. (2018) 'Neutrophil: a cell with many roles in inflammation or several cell types?', *Frontiers in physiology*, pp. 113.

Rosner, B. A. and Cristofalo, V. J. (1979) 'Hydrocortisone: a specific modulator of in vitro cell proliferation and aging', *Mechanisms of ageing and development,* 9(5-6), pp. 485-496.

Rouabhia, M. and Deslauriers, N. (2002) 'Production and characterization of an in vitro engineered human oral mucosa', *Biochemistry and Cell Biology,* 80(2), pp. 189-195.

Rubaci, A. H., Kazancioglu, H. O., Olgac, V. and Ak, G. (2012) 'The roles of matrix metalloproteinases-2,-7,-10 and tissue inhibitor of metalloproteinase-1 in the pathogenesis of oral lichen planus', *Journal of oral pathology & medicine,* 41(9), pp. 689-696.

Rumsaeng, V., Cruikshank, W. W., Foster, B., Prussin, C., Kirshenbaum, A. S., Davis, T. A., Kornfeld, H., Center, D. M. and Metcalfe, D. D. (1997) 'Human mast cells produce the CD4+ T lymphocyte chemoattractant factor, IL-16', *The Journal of Immunology,* 159(6), pp. 2904-2910.

Russell, J. H. (1983) 'Internal disintegration model of cytotoxic lymphocyte-induced target damage', *Immunological Reviews,* 72(1), pp. 97-118.

Régnier, M., Staquet, M.-J., Schmitt, D. and Schimdt, R. (1997) 'Integration of Langerhans cells into a pigmented reconstructed human epidermis', *Journal of Investigative Dermatology,* 109(4), pp. 510-512.

Saba, I., Barat, C., Chabaud, S., Reyjon, N., Leclerc, M., Jakubowska, W., Orabi, H., Lachhab, A., Pelletier, M. and Tremblay, M. J. (2021) 'Immunocompetent human 3D organ-specific hormone-responding vaginal mucosa model of HIV-1 infection', *Tissue Engineering Part C: Methods,* 27(3), pp. 152-166.

Said, Z., Murdoch, C., Hansen, J., Siim Madsen, L. and Colley, H. E. (2021) 'Corticosteroid delivery using oral mucosa equivalents for the treatment of inflammatory mucosal diseases', *European journal of oral sciences,* 129(2), pp. e12761.

Sallusto, F., Lenig, D., Mackay, C. R. and Lanzavecchia, A. (1998) 'Flexible programs of chemokine receptor expression on human polarized T helper 1 and 2 lymphocytes', *The Journal of experimental medicine,* 187(6), pp. 875-883.

Santoro, A., Majorana, A., Roversi, L., Gentili, F., Marrelli, S., Vermi, W., Bardellini, E., Sapelli, P. and Facchetti, F. (2005) 'Recruitment of dendritic cells in oral lichen planus', *The Journal of Pathology: A Journal of the Pathological Society of Great Britain and Ireland,* 205(4), pp. 426-434.

Schaller, M., Boeld, U., Oberbauer, S., Hamm, G., Hube, B. and Korting, H. C. (2004) 'Polymorphonuclear leukocytes (PMNs) induce protective Th1-type cytokine epithelial responses in an in vitro model of oral candidosis', *Microbiology,* 150(9), pp. 2807-2813.

Schneider, U. and Schwenk, H. (1977) 'Characterization of “T” and “non-T” cell lines established from children with acute lymphoblastic leukemia and non-Hodgkin lymphoma after leukemic transformation', *Immunological Diagnosis of Leukemias and Lymphomas*: Springer, pp. 265-269.

Schneider, U., Schwenk, H. U. and Bornkamm, G. (1977) 'Characterization of EBV-genome negative “null” and “T” cell lines derived from children with acute lymphoblastic leukemia and leukemic transformed non-Hodgkin lymphoma', *International journal of cancer,* 19(5), pp. 621-626.

Schreurs, O., Balta, M. G., Karatsaidis, A. and Schenck, K. (2020) 'Composition of hemidesmosomes in basal keratinocytes of normal buccal mucosa and oral lichen planus', *European journal of oral sciences,* 128(5), pp. 369-378.

Schuler, P. J., Harasymczuk, M., Schilling, B., Lang, S. and Whiteside, T. L. (2011) 'Separation of human CD4+ CD39+ T cells by magnetic beads reveals two phenotypically and functionally different subsets', *Journal of immunological methods,* 369(1-2), pp. 59-68.

Schutyser, E., Struyf, S. and Van Damme, J. (2003) 'The CC chemokine CCL20 and its receptor CCR6', *Cytokine & growth factor reviews,* 14(5), pp. 409-426.

Schwartz, D. M., Burma, A. M., Kitakule, M. M., Luo, Y. and Mehta, N. N. (2020) 'T Cells in Autoimmunity-Associated Cardiovascular Diseases', *Frontiers in Immunology*, pp. 2646.

Scully, C. (2008a) *Oral and Maxillofacial Medicine, the basis of diagnosis and treatment.* 2nd edn.: Churchill livingstone Elsevier.

Scully, C. (2008b) *Oral and maxillofacial medicine: the basis of diagnosis and treatment.* Churchill Livingstone Elsevier.

Scully, C. and Carrozzo, M. (2008) 'Oral mucosal disease: Lichen planus', *British Journal of Oral and Maxillofacial Surgery,* 46(1), pp. 15-21.

Sekiya, T. and Yoshimura, A. (2016) 'In vitro Th differentiation protocol', *TGF-β Signaling*: Springer, pp. 183-191.

Selvaratnam, L., Cruchley, A., Navsaria, H., Wertz, P., Hagi-Pavli, E., Leigh, I., Squier, C. and Williams, D. (2001) 'Permeability barrier properties of oral keratinocyte cultures: a model of intact human oral mucosa', *Oral diseases,* 7(4), pp. 252-258.

Serbina, N. V., Lazarevic, V. and Flynn, J. L. (2001) 'CD4+ T cells are required for the development of cytotoxic CD8+ T cells during Mycobacterium tuberculosis infection', *The Journal of Immunology,* 167(12), pp. 6991-7000.

Shalaby, M., Aggarwal, B., Rinderknecht, E., Svedersky, L., Finkle, B. and Palladino, M. (1985) 'Activation of human polymorphonuclear neutrophil functions by interferon-gamma and tumor necrosis factors', *The Journal of Immunology,* 135(3), pp. 2069-2073.

Shan, J., Li, S., Wang, C., Liu, L., Wang, X., Zhu, D., Fan, Y. and Xu, J. (2019) 'Expression and biological functions of the CCL5-CCR5 axis in oral lichen planus', *Experimental dermatology,* 28(7), pp. 816-821.

Shao, S., Tsoi, L. C., Sarkar, M. K., Xing, X., Xue, K., Uppala, R., Berthier, C. C., Zeng, C., Patrick, M. and Billi, A. C. (2019) 'IFN-γ enhances cell-mediated cytotoxicity against keratinocytes via JAK2/STAT1 in lichen planus', *Science translational medicine,* 11(511).

Sharma, R., Sircar, K., Singh, S. and Rastogi, V. (2011) 'Role of mast cells in pathogenesis of oral lichen planus', *Journal of oral and maxillofacial pathology: JOMFP,* 15(3), pp. 267.

Sheinkopf, L. E., Rafi, A. W., Do, L. T., Katz, R. M. and Klaustermeyer, W. B. 'Efficacy of omalizumab in the treatment of atopic dermatitis: a pilot study'. *Allergy and asthma proceedings*: OceanSide Publications, 530.

Shen, Z., Du, G., Zhou, Z., Liu, W., Shi, L. and Xu, H. (2016) 'Aberrant expression of interleukin-22 and its targeting micro RNA s in oral lichen planus: a preliminary study', *Journal of Oral Pathology & Medicine,* 45(7), pp. 523-527.

Shi, Y., Wu, W., Wan, T., Liu, Y., Peng, G., Chen, Z. and Zhu, H. (2013) 'Impact of polyclonal anti-CD3/CD28-coated magnetic bead expansion methods on T cell proliferation, differentiation and function', *International immunopharmacology,* 15(1), pp. 129-137.

Shimizu, M., Higaki, Y., Higaki, M. and Kawashima, M. (1997) 'The role of granzyme B-expressing CD8-positive T cells in apoptosis of keratinocytes in lichen planus', *Archives of dermatological research,* 289(9), pp. 527-532.

Shin, J. U., Abaci, H. E., Herron, L., Guo, Z., Sallee, B., Pappalardo, A., Jackow, J., Wang, E. H. C., Doucet, Y. and Christiano, A. M. (2020) 'Recapitulating T cell infiltration in 3D psoriatic skin models for patient-specific drug testing', *Scientific reports,* 10(1), pp. 1-12.

Shiohara, T., Moriya, N., Tsuchiya, K., Nagashima, M. and Narimatsu, H. (1986) 'Lichenoid tissue reaction induced by local transfer of Ia-reactive T-cell clones', *Journal of investigative dermatology,* 87(1), pp. 33-38.

Shlomchik, M. J. and Weisel, F. (2012) 'Germinal center selection and the development of memory B and plasma cells', *Immunological reviews,* 247(1), pp. 52-63.

Shruthy, R., Sharada, P., Swaminathan, U. and Nagamalini, B. (2013) 'Immunohistochemical expression of basement membrane laminin in histological grades of oral squamous cell carcinoma: A semiquantitative analysis', *Journal of oral and maxillofacial pathology: JOMFP,* 17(2), pp. 185.

Simark-Mattsson, C., Bergenholtz, G., Jontell, M., Eklund, C., Seymour, G., Sugerman, P., Savage, N. and Dahlgren, U. (1999) 'Distribution of interleukin-2,-4,-10, tumour necrosis factor-α and transforming growth factor-β mRNAs in oral lichen planus', *Archives of oral biology,* 44(6), pp. 499-507.

Simark-Mattsson, C., Bergenholtz, G., Jontell, M., Tarkowski, A. and Dahlgren, U. (1994) 'T cell receptor V-gene usage in oral lichen planus; increased frequency of T cell receptors expressing Vα2 and Vβ3', *Clinical & Experimental Immunology,* 98(3), pp. 503-507.

Simonetti, O., Kempenaar, J., Ponec, M., Hoogstraate, A., Bialik, W., Schrijvers, A. and Boddé, H. (1995) 'Visualization of diffusion pathways across the stratum corneum of native and in-vitro-reconstructed epidermis by confocal laser scanning microscopy', *Archives of dermatological research,* 287(5), pp. 465-473.

Singh, U. P., Venkataraman, C., Singh, R. and Lillard, J. W. (2007) 'CXCR3 axis: role in inflammatory bowel disease and its therapeutic implication', *Endocrine, Metabolic & Immune Disorders-Drug Targets (Formerly Current Drug Targets-Immune, Endocrine & Metabolic Disorders),* 7(2), pp. 111-123.

Skapenko, A., Leipe, J., Lipsky, P. E. and Schulze-Koops, H. (2005) 'The role of the T cell in autoimmune inflammation', *Arthritis research & therapy,* 7(2), pp. 1-11.

Smeltz, R. B., Chen, J., Ehrhardt, R. and Shevach, E. M. (2002) 'Role of IFN-γ in Th1 differentiation: IFN-γ regulates IL-18Rα expression by preventing the negative effects of IL-4 and by inducing/maintaining IL-12 receptor β2 expression', *The Journal of Immunology,* 168(12), pp. 6165-6172.

Smith, A., Watkins, T., Theocharidis, G., Lang, I., Leschinsky, M., Maione, A., Kashpur, O., Raimondo, T., Rahmani, S. and Baskin, J. (2021) 'A novel three-dimensional skin disease model to assess macrophage function in diabetes', *Tissue Engineering Part C: Methods,* 27(2), pp. 49-58.

Sola-Visner, M. and Ramsey, H. (2017) 'Developmental megakaryocytopoiesis', *Fetal and Neonatal Physiology*: Elsevier, pp. 1135-1150. e4.

Sommerhoff, C. and Schaschke, N. (2007) 'Mast cell tryptase β as a target in allergic inflammation: An evolving story', *Current pharmaceutical design,* 13(3), pp. 313-332.

Sousa, F. A. and Rosa, L. E. (2008) 'Oral lichen planus: clinical and histopathological considerations', *Braz J Otorhinolaryngol,* 74(2), pp. 284-92.

Squier, C. (1991) 'The permeability of oral mucosa', *Critical Reviews in Oral Biology & Medicine,* 2(1), pp. 13-32.

Squier, C. A. and Kremer, M. J. (2001) 'Biology of oral mucosa and esophagus', *JNCI Monographs,* 2001(29), pp. 7-15.

Sriram, G., Alberti, M., Dancik, Y., Wu, B., Wu, R., Feng, Z., Ramasamy, S., Bigliardi, P. L., Bigliardi-Qi, M. and Wang, Z. (2018) 'Full-thickness human skin-on-chip with enhanced epidermal morphogenesis and barrier function', *Materials Today,* 21(4), pp. 326-340.

Sriram, G., Bigliardi, P. L. and Bigliardi-Qi, M. (2018) 'Full-Thickness Human Skin Equivalent Models of Atopic Dermatitis'.

Stanbury, R. M. and Graham, E. M. (1998) 'Systemic corticosteroid therapy—side effects and their management', *British Journal of Ophthalmology,* 82(6), pp. 704-708.

Starbeck-Miller, G. R., Xue, H.-H. and Harty, J. T. (2014) 'IL-12 and type I interferon prolong the division of activated CD8 T cells by maintaining high-affinity IL-2 signaling in vivo', *Journal of Experimental Medicine,* 211(1), pp. 105-120.

Stark, H.-J., Baur, M., Breitkreutz, D., Mirancea, N. and Fusenig, N. E. (1999) 'Organotypic keratinocyte cocultures in defined medium with regular epidermal morphogenesis and differentiation', *Journal of Investigative Dermatology,* 112(5), pp. 681-691.

Stark, M. A., Huo, Y., Burcin, T. L., Morris, M. A., Olson, T. S. and Ley, K. (2005) 'Phagocytosis of apoptotic neutrophils regulates granulopoiesis via IL-23 and IL-17', *Immunity,* 22(3), pp. 285-294.

Stockinger, B. (2007) 'Good for Goose, but not for Gander: IL-2 interferes with Th17 differentiation', *Immunity,* 26(3), pp. 278-279.

Suda, T. and Dexter, T. (1981) 'Effect of hydrocortisone on long-term human marrow cultures', *British journal of haematology,* 48(4), pp. 661-664.

Sugerman, P., Satterwhite, K. and Bigby, M. (2000) 'Autocytotoxic T-cell clones in lichen planus', *British Journal of Dermatology,* 142(3), pp. 449-456.

Sugerman, P., Savage, N., Walsh, L., Zhao, Z., Zhou, X., Khan, A., Seymour, G. and Bigby, M. (2002) 'The pathogenesis of oral lichen planus', *Critical Reviews in Oral Biology & Medicine,* 13(4), pp. 350-365.

Sugerman, P. B., Savage, N. W., Zhou, X., Walsh, L. J. and Bigby, M. (2000) 'Oral lichen planus', *Clinics in dermatology,* 18(5), pp. 533-539.

Sun, A., Wang, J., Chia, J. and Chiang, C. (2005) 'Serum interleukin-8 level is a more sensitive marker than serum interleukin-6 level in monitoring the disease activity of oral lichen planus', *British Journal of Dermatology,* 152(6), pp. 1187-1192.

Sutermaster, B. A. and Darling, E. M. (2019) 'Considerations for high-yield, high-throughput cell enrichment: fluorescence versus magnetic sorting', *Scientific reports,* 9(1), pp. 1-9.

Suurmond, J., Stoop, J. N., Rivellese, F., Bakker, A. M., Huizinga, T. W. and Toes, R. E. (2014) 'Activation of human basophils by combined toll-like receptor-and F cε RI-triggering can promote T h2 skewing of naive T helper cells', *European journal of immunology,* 44(2), pp. 386-396.

Szot, C. S., Buchanan, C. F., Freeman, J. W. and Rylander, M. N. (2011) '3D in vitro bioengineered tumors based on collagen I hydrogels', *Biomaterials,* 32(31), pp. 7905-7912.

Takahashi, K., Tanabe, K., Ohnuki, M., Narita, M., Ichisaka, T., Tomoda, K. and Yamanaka, S. (2007) 'Induction of pluripotent stem cells from adult human fibroblasts by defined factors', *cell,* 131(5), pp. 861-872.

Takai, S. and Jin, D. (2022) 'Pathophysiological Role of Chymase-Activated Matrix Metalloproteinase-9', *Biomedicines,* 10(10), pp. 2499.

Takeuchi, O. and Akira, S. (2010) 'Pattern recognition receptors and inflammation', *Cell,* 140(6), pp. 805-820.

Takeuchi, Y., Tohnai, I., Kaneda, T. and Nagura, H. (1988) 'Immunohistochemical analysis of cells in mucosal lesions of oral lichen planus', *Journal of Oral Pathology & Medicine,* 17(8), pp. 367-373.

Tanaka, S., Akaishi, E., Hosaka, K., Okamura, S. and Kubohara, Y. (2005) 'Zinc ions suppress mitogen-activated interleukin-2 production in Jurkat cells', *Biochemical and biophysical research communications,* 335(1), pp. 162-167.

Tao, X. a., Li, C. y., Rhodus, N. L., Xia, J., Yang, X. p. and Cheng, B. (2008) 'Simultaneous detection of IFN-gamma and IL-4 in lesional tissues and whole unstimulated saliva from patients with oral lichen planus', *Journal of oral pathology & medicine,* 37(2), pp. 83-87.

Tao, X. a., Xia, J., Chen, X. b., Wang, H., Dai, Y. h., Rhodus, N. L. and Cheng, B. (2010) 'FOXP3+ T regulatory cells in lesions of oral lichen planus correlated with disease activity', *Oral Diseases,* 16(1), pp. 76-82.

Taub, D., Proost, P., Murphy, W. J., Anver, M., Longo, D., Van Damme, J. and Oppenheim, J. (1995) 'Monocyte chemotactic protein-1 (MCP-1),-2, and-3 are chemotactic for human T lymphocytes', *The Journal of clinical investigation,* 95(3), pp. 1370-1376.

Tavakoli-Saberi, M. R. and Audus, K. L. (1989) 'Cultured buccal epithelium: an in vitro model derived from the hamster pouch for studying drug transport and metabolism', *Pharmaceutical research,* 6(2), pp. 160-166.

Tedesco, S., De Majo, F., Kim, J., Trenti, A., Trevisi, L., Fadini, G. P., Bolego, C., Zandstra, P. W., Cignarella, A. and Vitiello, L. (2018) 'Convenience versus biological significance: are PMA-differentiated THP-1 cells a reliable substitute for blood-derived macrophages when studying in vitro polarization?', *Frontiers in pharmacology,* 9, pp. 71.

Thomas, D. W., Stephens, P., Stephens, M., Patten, D. and Lim, S. (1997) 'T-cell receptor Vβ usage by lesional lymphocytes in oral lichen planus', *Journal of oral pathology & medicine,* 26(3), pp. 105-109.

Thompson, C. B., Lindsten, T., Ledbetter, J. A., Kunkel, S. L., Young, H. A., Emerson, S. G., Leiden, J. M. and June, C. H. (1989) 'CD28 activation pathway regulates the production of multiple T-cell-derived lymphokines/cytokines', *Proceedings of the National Academy of Sciences,* 86(4), pp. 1333-1337.

Thompson, E. B. and Lippman, M. E. (1974) 'Mechanism of action of glucocorticoids', *Metabolism,* 23(2), pp. 159-202.

Thongprasom, K. and Dhanuthai, K. (2008) 'Steriods in the treatment of lichen planus: a review', *Journal of oral science,* 50(4), pp. 377-385.

Thornberry, N. A., Bull, H. G., Calaycay, J. R., Chapman, K. T., Howard, A. D., Kostura, M. J., Miller, D. K., Molineaux, S. M., Weidner, J. R. and Aunins, J. (1992) 'A novel heterodimeric cysteine protease is required for interleukin-1βprocessing in monocytes', *Nature,* 356(6372), pp. 768-774.

Thornhill, M. H., Pemberton, M. N., Simmons, R. K. and Theaker, E. D. (2003) 'Amalgam-contact hypersensitivity lesions and oral lichen planus', *Oral Surgery, Oral Medicine, Oral Pathology, Oral Radiology, and Endodontology,* 95(3), pp. 291-299.

Thornhill, M. H., Sankar, V., Xu, X. J., Barrett, A. W., High, A. S., Odell, E. W., Speight, P. M. and Farthing, P. M. (2006) 'The role of histopathological characteristics in distinguishing amalgam-associated oral lichenoid reactions and oral lichen planus', *Journal of oral pathology & medicine,* 35(4), pp. 233-240.

Tjabringa, G., Bergers, M., van Rens, D., de Boer, R., Lamme, E. and Schalkwijk, J. (2008) 'Development and validation of human psoriatic skin equivalents', *The American journal of pathology,* 173(3), pp. 815-823.

Tobón-Arroyave, S., Villegas-Acosta, F., Ruiz-Restrepo, S., Vieco-Duran, B., Restrepo-Misas, M. and Londoño-López, M. (2004) 'Expression of caspase-3 and structural changes associated with apoptotic cell death of keratinocytes in oral lichen planus', *Oral diseases,* 10(3), pp. 173-178.

Tomakidi, P., Breitkreutz, D., Fusenig, N., Zöller, J., Kohl, A. and Komposch, G. (1998) 'Establishment of oral mucosa phenotype in vitro in correlation to epithelial anchorage', *Cell and tissue research,* 292(2), pp. 355-366.

Trickett, A. and Kwan, Y. L. (2003) 'T cell stimulation and expansion using anti-CD3/CD28 beads', *Journal of immunological methods,* 275(1-2), pp. 251-255.

Tripathi, H., Peng, H., Donahue, R., Chelvarajan, L., Gottipati, A., Levitan, B., Al-Darraji, A., Gao, E., Abdel-Latif, A. and Berron, B. J. (2020) 'Isolation methods for human CD34 subsets using fluorescent and magnetic activated cell sorting: an in vivo comparative study', *Stem cell reviews and reports,* 16(2), pp. 413-423.

Tschachojan, V., Schroer, H., Averbeck, N. and Mueller-Klieser, W. (2014) 'Carbon ions and X-rays induce pro-inflammatory effects in 3D oral mucosa models with and without PBMCs', *Oncology Reports,* 32(5), pp. 1820-1828.

Tyldesley, W. (1974) 'Oral lichen planus', *British Journal of Oral Surgery,* 11(3), pp. 187-206.

Unal, M., Yalcin, B. and Ozturk, O. (2014) 'A Patient Having Recurrent Aphtous Stomatitis After Three Years of Smoking Cessation; A Case Report and Review of Literature', *J Addict Res Ther,* 5(202), pp. 2.

Van Damme, J., Proost, P., Lenaerts, J.-P. and Opdenakker, G. (1992) 'Structural and functional identification of two human, tumor-derived monocyte chemotactic proteins (MCP-2 and MCP-3) belonging to the chemokine family', *The Journal of experimental medicine,* 176(1), pp. 59-65.

Van Den Bogaard, E. H., Tjabringa, G. S., Joosten, I., Vonk-Bergers, M., Van Rijssen, E., Tijssen, H. J., Erkens, M., Schalkwijk, J. and Koenen, H. J. (2014) 'Crosstalk between keratinocytes and T cells in a 3D microenvironment: a model to study inflammatory skin diseases', *Journal of Investigative Dermatology,* 134(3), pp. 719-727.

van den Broek, L. J., Bergers, L. I., Reijnders, C. and Gibbs, S. (2017) 'Progress and future prospectives in skin-on-chip development with emphasis on the use of different cell types and technical challenges', *Stem cell reviews and reports,* 13(3), pp. 418-429.

van der Meij, E. H. and van der Waal, I. (2003) 'Lack of clinicopathologic correlation in the diagnosis of oral lichen planus based on the presently available diagnostic criteria and suggestions for modifications', *J Oral Pathol Med,* 32(9), pp. 507-12.

Varricchi, G., Raap, U., Rivellese, F., Marone, G. and Gibbs, B. F. (2018) 'Human mast cells and basophils—How are they similar how are they different?', *Immunological reviews,* 282(1), pp. 8-34.

Veldhoen, M., Hocking, R. J., Atkins, C. J., Locksley, R. M. and Stockinger, B. (2006) 'TGFβ in the context of an inflammatory cytokine milieu supports de novo differentiation of IL-17-producing T cells', *Immunity,* 24(2), pp. 179-189.

Veldhoen, M., Uyttenhove, C., Van Snick, J., Helmby, H., Westendorf, A., Buer, J., Martin, B., Wilhelm, C. and Stockinger, B. (2008) 'Transforming growth factor-β'reprograms' the differentiation of T helper 2 cells and promotes an interleukin 9–producing subset', *Nature immunology,* 9(12), pp. 1341-1346.

Villa, T. G., Sánchez-Pérez, Á. and Sieiro, C. (2021) 'Oral lichen planus: A microbiologist point of view', *International Microbiology,* 24(3), pp. 275-289.

Vis, M. A., Ito, K. and Hofmann, S. (2020) 'Impact of culture medium on cellular interactions in in vitro co-culture systems', *Frontiers in Bioengineering and Biotechnology*, pp. 911.

Walsh, L., Savage, N., Ishii, T. and Seymour, G. (1990) 'Immunopathogenesis of oral lichen planus', *Journal of Oral Pathology & Medicine,* 19(9), pp. 389-396.

Wang, H., Bai, J., Luo, Z., Fu, J., Wang, H. and Sun, Z. (2017) 'Overexpression and varied clinical significance of Th9 versus Th17 cells in distinct subtypes of oral lichen planus', *Archives of oral biology,* 80, pp. 110-116.

Wang, H., Guan, X., Luo, Z., Liu, Y., Ren, Q. and Zhao, X. (2018) 'The association and potentially destructive role of Th9/IL-9 is synergistic with Th17 cells by elevating MMP9 production in local lesions of oral lichen planus', *Journal of Oral Pathology & Medicine,* 47(4), pp. 425-433.

Wang, H., Zhang, D., Han, Q., Zhao, X., Zeng, X., Xu, Y., Sun, Z. and Chen, Q. (2016) 'Role of distinct CD 4+ T helper subset in pathogenesis of oral lichen planus', *Journal of Oral Pathology & Medicine,* 45(6), pp. 385-393.

Wang, Y., Zhou, J., Fu, S., Wang, C. and Zhou, B. (2015) 'A study of association between oral lichen planus and immune balance of Th1/Th2 cells', *Inflammation,* 38(5), pp. 1874-1879.

Wei, W., Sun, Q., Deng, Y., Wang, Y., Du, G., Song, C., Li, C., Zhu, M., Chen, G. and Tang, G. (2018) 'Mixed and inhomogeneous expression profile of Th1/Th2 related cytokines detected by cytometric bead array in the saliva of patients with oral lichen planus', *Oral surgery, oral medicine, oral pathology and oral radiology,* 126(2), pp. 142-151.

Weiss, A., Imboden, J., Hardy, K., Manger, B., Terhorst, C. and Stobo, J. (1986) 'The role of the T3/antigen receptor complex in T-cell activation', *Annual review of immunology,* 4, pp. 593-619.

Weiss, A. and Imboden, J. B. (1987) 'Cell surface molecules and early events involved in human T lymphocyte activation', *Advances in immunology*: Elsevier, pp. 1-38.

Werner, S. and Smola, H. (2001) 'Paracrine regulation of keratinocyte proliferation and differentiation', *Trends in cell biology,* 11(4), pp. 143-146.

Wildbaum, G., Netzer, N. and Karin, N. (2002) 'Plasmid DNA encoding IFN-γ-inducible protein 10 redirects antigen-specific T cell polarization and suppresses experimental autoimmune encephalomyelitis', *The Journal of Immunology,* 168(11), pp. 5885-5892.

Wilson, E. (1869) 'On lichen planus', *J Cutan Med Dis Skin,* 3, pp. 17-132.

Wingren, A. G., Parra, E., Varga, M., Kalland, T., Sjogren, H.-O., Hedlund, G. and Dohlsten, M. (2017) 'T cell activation pathways: B7, LFA-3, and ICAM-1 shape unique T cell profiles', *Critical Reviews™ in Immunology,* 37(2-6).

Winning, T. A. and Townsend, G. C. (2000) 'Oral mucosal embryology and histology', *Clinics in dermatology,* 18(5), pp. 499-511.

Wolf, K., Alexander, S., Schacht, V., Coussens, L. M., von Andrian, U. H., van Rheenen, J., Deryugina, E. and Friedl, P. 'Collagen-based cell migration models in vitro and in vivo'. *Seminars in cell & developmental biology*: Elsevier, 931-941.

Woo, M., Hakem, R., Soengas, M. S., Duncan, G. S., Shahinian, A., Kägi, D., Hakem, A., McCurrach, M., Khoo, W. and Kaufman, S. A. (1998) 'Essential contribution of caspase 3/CPP32 to apoptosis and its associated nuclear changes', *Genes & development,* 12(6), pp. 806-819.

Wu, C. Y., Warrier, R. R., Carvajal, D. M., Chua, A. O., Minetti, L. J., Chizzonite, R., Mongini, P. K., Stern, A. S., Gubler, U. and Presky, D. H. (1996) 'Biological function and distribution of human interleukin-12 receptor β chain', *European journal of immunology,* 26(2), pp. 345-350.

Wu, T., Du, R., Hong, Y., Jia, L., Zeng, Q. and Cheng, B. (2013) 'IL-1 alpha regulates CXCL1, CXCL10 and ICAM1 in network form in oral keratinocytes', *Clinical laboratory,* 59(9-10), pp. 1105-1111.

Xavier, G. M., Sá, A. R. d., Guimaraes, A. L. S., Silva, T. A. d. and Gomez, R. S. (2007) 'Investigation of functional gene polymorphisms interleukin-1β, interleukin-6, interleukin-10 and tumor necrosis factor in individuals with oral lichen planus', *Journal of Oral Pathology & Medicine,* 36(8), pp. 476-481.

Xie, S., Ding, L., Xiong, Z. and Zhu, S. (2012) 'Implications of Th1 and Th17 cells in pathogenesis of oral lichen planus', *Journal of Huazhong University of Science and Technology [Medical Sciences],* 32(3), pp. 451-457.

Xu, Z., Ho, S., Chang, C.-C., Zhang, Q.-Y., Vasilescu, E.-R., Vlad, G. and Suciu-Foca, N. (2016) 'Molecular and cellular characterization of human CD8 T suppressor cells', *Frontiers in Immunology,* 7, pp. 549.

Yadev, N. P., Murdoch, C., Saville, S. P. and Thornhill, M. H. (2011) 'Evaluation of tissue engineered models of the oral mucosa to investigate oral candidiasis', *Microbial pathogenesis,* 50(6), pp. 278-285.

Yamamoto, T., Nakane, T. and Osaki, T. (2000) 'The mechanism of mononuclear cell infiltration in oral lichen planus: the role of cytokines released from keratinocytes', *Journal of clinical immunology,* 20(4), pp. 294-305.

Yamamoto, T. and Osaki, T. (1995) 'Characteristic cytokines generated by keratinocytes and mononuclear infiltrates in oral lichen planus', *Journal of investigative dermatology,* 104(5), pp. 784-788.

Yamamoto, T., Osaki, T., Yoneda, K. and Ueta, E. (1994) 'Cytokine production by keratinocytes and mononuclear infiltrates in oral lichen planus', *Journal of oral pathology & medicine,* 23(7), pp. 309-315.

Yang, L., Yang, S., Lei, J., Hu, W., Chen, R., Lin, F. and Xu, A. e. (2018) 'Role of chemokines and the corresponding receptors in vitiligo: A pilot study', *The Journal of dermatology,* 45(1), pp. 31-38.

Yokoyama, W. M., Thompson, M. L. and Ehrhardt, R. O. (2012) 'Cryopreservation and thawing of cells', *Current protocols in immunology,* 99(1), pp. A. 3G. 1-A. 3G. 5.

Yoshie, O., Imai, T. and Nomiyama, H. (2001) 'Chemokines in immunity', *Advances in immunology,* 78, pp. 57-110.

Zengel, P., Nguyen-Hoang, A., Schildhammer, C., Zantl, R., Kahl, V. and Horn, E. (2011) 'μ-Slide Chemotaxis: a new chamber for long-term chemotaxis studies', *BMC cell biology,* 12(1), pp. 1-14.

Zhang, C., Yang, M. and Ericsson, A. C. (2021) 'Function of macrophages in disease: Current understanding on molecular mechanisms', *Frontiers in immunology,* 12, pp. 635.

Zhang, J., Zhou, G., Du, G. F., Xu, X. Y. and Zhou, H. M. (2011) 'Biologics, an alternative therapeutic approach for oral lichen planus', *Journal of oral pathology & medicine,* 40(7), pp. 521-524.

Zhang, Z. R., Chen, L. Y., Qi, H. Y. and Sun, S. H. (2018) 'Expression and clinical significance of periostin in oral lichen planus', *Experimental and therapeutic medicine,* 15(6), pp. 5141-5147.

Zhao, Z., Savage, N., Pujic, Z. and Walsh, L. (1997) 'Immunohistochemical localization of mast cells and mast cell-nerve interactions in oral lichen planus', *Oral diseases,* 3(2), pp. 71-76.

Zhao, Z., Sugerman, P., Walsh, L. and Savage, N. (2002) 'Expression of RANTES and CCR1 in oral lichen planus and association with mast cell migration', *Journal of oral pathology & medicine,* 31(3), pp. 158-162.

Zhao, Z., Sugerman, P., Zhou, X., Walsh, L. and Savage, N. (2001) 'Mast cell degranulation and the role of T cell RANTES in oral lichen planus', *Oral diseases,* 7(4), pp. 246-251.

Zhong, E. F., Chang, A., Stucky, A., Chen, X., Mundluru, T., Khalifeh, M. and Sedghizadeh, P. P. (2020) 'Genomic analysis of oral lichen planus and related oral microbiome pathogens', *Pathogens,* 9(11), pp. 952.

Zhou, J., Tang, Z., Gao, S., Li, C., Feng, Y. and Zhou, X. (2020) 'Tumor-associated macrophages: recent insights and therapies', *Frontiers in oncology,* 10, pp. 188.

Zhou, L., Ivanov, I. I., Spolski, R., Min, R., Shenderov, K., Egawa, T., Levy, D. E., Leonard, W. J. and Littman, D. R. (2007) 'IL-6 programs TH-17 cell differentiation by promoting sequential engagement of the IL-21 and IL-23 pathways', *Nature immunology,* 8(9), pp. 967-974.

Zhou, L., Lopes, J. E., Chong, M. M., Ivanov, I. I., Min, R., Victora, G. D., Shen, Y., Du, J., Rubtsov, Y. P. and Rudensky, A. Y. (2008) 'TGF-β-induced Foxp3 inhibits TH17 cell differentiation by antagonizing RORγt function', *Nature,* 453(7192), pp. 236-240.

Zhou, X., Savage, N., Sugerman, P., Walsh, L., Aldred, M. and Seymour, G. (1996) 'TCR Vβ gene expression in lesional T lymphocyte cell lines in oral lichen planus', *Oral diseases,* 2(4), pp. 295-298.

Zhou, X. J., Sugerman, P. B., Savage, N. W. and Walsh, L. J. (2001) 'Matrix metalloproteinases and their inhibitors in oral lichen planus', *Journal of cutaneous pathology,* 28(2), pp. 72-82.

Zhou, X. J., Sugerman, P. B., Savage, N. W., Walsh, L. J. and Seymour, G. J. (2002) 'Intra-epithelial CD8+ T cells and basement membrane disruption in oral lichen planus', *Journal of oral pathology & medicine,* 31(1), pp. 23-27.

Zhu, J., Jankovic, D., Oler, A. J., Wei, G., Sharma, S., Hu, G., Guo, L., Yagi, R., Yamane, H. and Punkosdy, G. (2012) 'The transcription factor T-bet is induced by multiple pathways and prevents an endogenous Th2 cell program during Th1 cell responses', *Immunity,* 37(4), pp. 660-673.

Zhu, Z.-D., Ren, X.-M., Zhou, M.-M., Chen, Q.-M., Hua, H. and Li, C.-L. (2022) 'Salivary cytokine profile in patients with oral lichen planus', *Journal of Dental Sciences,* 17(1), pp. 100-105.